

Establishing the perineuronal net as a neuroprotective barrier in Parkinson's  
disease

Stuart Dickens

University of Leeds  
School of Biomedical Sciences  
Faculty of Biological Science

Supervisors: Dr. Jessica Kwok and Dr. Ralf Richter

July 2021

The candidate confirms that the work submitted is his own, except where stated below. The contribution of the candidate and the other authors to this work has been explicitly indicated below. The candidate confirms that appropriate credit has been given within the thesis where reference has been made to the work of others.

The surface plasmon resonance experiments in chapter 4 were performed and analysed by Dr. Lynda Djerbal.

This copy has been supplied on the understanding that it is copyright material and that no quotation from the thesis may be published without proper acknowledgement.

The right of Stuart Dickens to be identified as Author of this work has been asserted by him in accordance with the Copyright, Designs and Patents Act 1988.

## Acknowledgements

I would like to take this opportunity to thank all the people that have helped me throughout my PhD. Although there is only one name cited as the author of this thesis it could not have been achieved without the wonderful people I am blessed to have around me.

Firstly, I would like to thank my supervisors Jessica Kwok and Ralf Richter, who have had open doors throughout my PhD and always made time for my questions. I had an uncertain start to my PhD and I am eternally grateful for Jessica for taking a chance on me and taking me on as her student. Thank you for inducting me into the mysterious world of PNNs and allowing me the opportunity to work in your lab. I would like to thank Ralf for taking the time to teach a very wet biologist about biophysics and the value in understanding the size of molecules.

Secondly, I would like to thank everyone in the Kwok & Richter groups for their help and support. I am very grateful for having such a kind group of people around me in the office and the lab. Thank you for making the normal day's fun and the hard days bearable. I would especially like to thank Ashleigh Goodenough, Jan Ng and Lynda Djerbal for being fantastic colleagues and all the laughter.

A PhD is a huge technical challenge and I wouldn't have been able to accomplish it or trust my results without the great training I have received. I would like to thank Andrew Tsatsanis for teaching me cell culture and his unique sense of humour. Again I would like to thank Jessica for passing on her expertise in neuronal culture. Thank you Brian and Laura for all your help in teaching me protein purification and trusting me to use your Äktas. Thank you Lynda for letting me borrow your expertise in SPR and thank you Spring for teaching me QCM-D.

Work is a large part of life but it is not the whole of it. I would like to thank all the friends that have made living in Leeds so fun. Thank you Luke, Gareth, Ash, Chris and Brad for all the hot-dogs and hilarious evenings.

Thank you Sarah for putting up with me as I ground out writing a thesis and your strength and kindness. I am forever thankful for your love, you are an inspiration to me. Thank you for supporting me along this journey. Thank you to my family for all their love and support throughout this.

Lastly, I would like to thank God. Thank you for your daily grace and gifts. The beautiful complexity of this world is yours, thank you for the honour of exploring it.

## Abstract

Parkinson's disease (PD) is a progressive neurodegenerative disorder. Disease progression is mirrored by the appearance of Lewy pathology (LP) in the brain, which contains misfolded  $\alpha$ -synuclein ( $\alpha$ SYN). Transmission of misfolded  $\alpha$ -synuclein between neurons is key to LP spread. Determinants of neuronal vulnerability to  $\alpha$ SYN transmission have been investigated but factors of neuronal resistance have not. One potential factor is the presence of a perineuronal net (PNN). The PNN is a condensed form of extracellular matrix (ECM) that enwraps specific populations of neurons and regulates plasticity. It is an aggregated structure formed of protein and glycosaminoglycans. The PNN forms and condenses on neuronal membranes, creating a dense and polyanionic structure with a reticular morphology, which could block  $\alpha$ SYN transmission. The aim of this thesis is to establish whether the PNN is a neuroprotective barrier conferring resistance to neurons against  $\alpha$ SYN seeding and pathology in PD.

To investigate whether the PNN blocks  $\alpha$ SYN uptake an *in vitro* neuronal PNN culture model was established. This model accurately replicated mature cortical PNNs, both in terms of the heterogeneity in PNN composition and its maturation. PNNs transitioned from an immature punctate morphology to the reticular morphology as observed in the mature CNS. We also observed a small population of PNNs that were mature at an earlier time point and a distinct composition, highlighting further heterogeneity. We have established a primary culture model of PNN of use to the PNN field.

To investigate the barrier function of PNNs to  $\alpha$ SYN, we first purified  $\alpha$ SYN and created two, distinct aggregated  $\alpha$ SYN species: oligomers and preformed fibrils (PFFs). DIV56 neuronal cultures, containing mature PNNs, were treated with either with 7  $\mu$ M Alexa 488 labelled oligomer and uptake measured 24 hours later by immunofluorescence or with PFFs and cultured for a further 21 days. The presence of a PNN reduced the uptake of  $\alpha$ SYN oligomer in neurons by two thirds (Oligomer positive: PNN positive  $15.8 \pm 2.52\%$  versus PNN negative:  $49.9 \pm 2.95\%$ , one-way ANOVA,  $p < 0.05$ ). PNN removal by chondroitinase ABC (ChABC) abolished resistance, significantly increasing oligomer positive neurons (PNN intact:  $53.4 \pm 2.54\%$  vs degraded:  $67.1\%$ , two sample t Test,  $p < 0.05$ ). 70 nM PFF treatment caused progressive accumulation of phosphorylated- $\alpha$ SYN staining over 21 days of treatment, reminiscent of  $\alpha$ SYN pathology. Enzymatic removal of the PNN before PFF treatment significantly increased p- $\alpha$ SYN intensity (D21: PNN intact:  $0.00231 \pm 0.00047$  RFU vs degraded  $0.00141 \pm 0.00047$ , one-way ANOVA,  $p < 0.05$ ). Using surface

plasmon resonance, we have highlighted a potential mechanism for the neuroprotection:  $\alpha$ SYN species were found to bind to PNN glycosaminoglycans-chondroitin sulphate E and heparin sulphate. We investigated whether PNN populations were spared in PD brains to establish the relevance of the neuroprotection mechanism. In all brain regions, PNN densities in PD brains were not significantly different compared to non-demented controls (t test,  $p>0.05$ ). Furthermore, no LP bearing PNN neurons were observed. Together this indicates that PNN populations are unaffected in PD brains, demonstrating that PNN-mediated neuroprotection is relevant in PD. This thesis has established that the PNN is a neuroprotective barrier in PD and protects neurons from developing  $\alpha$ SYN pathology *in vitro* and in PD brains. This opens a new research avenue in pursuit of disease halting therapies in PD.

## Table of contents

<b>Chapter 1 Parkinson's disease</b> .....	<b>1</b>
1.1 Epidemiology.....	1
1.1.1 Symptoms and variability in progression.....	2
1.2 Pathophysiology of Parkinson's disease .....	4
1.2.1 Understanding Lewy pathology in synucleinopathies.....	6
1.3 Treatment of Parkinson's disease .....	7
1.3.1 Pharmacological treatment .....	8
1.3.2 Deep brain stimulation in PD.....	8
1.4 Braak Staging in Parkinson's Disease.....	9
1.4.1 Criticisms of Braak Staging .....	11
1.5 $\alpha$ -synuclein- the major player in PD .....	13
1.5.1 Synucleins and structure.....	13
1.5.2 The pathway of aggregation.....	15
1.5.3 Factors governing aggregation .....	16
1.6 PD as a prion-like disease.....	18
1.7 Function of $\alpha$ SYN .....	20
1.7.1 $\alpha$ SYN, a sensor of high membrane curvature .....	20
1.7.2 $\alpha$ SYN-dependent regulation of synaptic transmission.....	22
1.7.2.1 $\alpha$ SYN: restricting SV motility.....	23
1.7.2.2 $\alpha$ SYN as a regulator of exocytosis .....	25
1.7.2.3 $\alpha$ SYN as a regulator of endocytosis .....	26
1.7.3 $\alpha$ SYN in metal ion binding and mitochondrial dynamics .....	28
1.8 Neuronal susceptibility as a factor governing seeding and LP development.....	29
1.8.1 Synaptic and local spread of $\alpha$ SYN is not sufficient for pathology development.....	29
1.8.2 Selective neuronal susceptibility in PD.....	30
1.8.3 Neuronal resistance in another prion-like disease context ....	30
1.9 The Perineuronal Net (PNN) .....	31
1.9.1 PNN composition .....	32
1.9.2 PNN as a neuroprotective barrier in PD .....	35
1.10 Objectives of this thesis.....	35
<b>Chapter 2 Methods</b> .....	<b>37</b>
2.1 Animals .....	37
2.2 Primary cell culture.....	37

2.2.1	Neuronal culture .....	37
2.2.2	Astrocyte culture .....	38
2.3	Immunocytochemistry.....	38
2.3.1	Neurons .....	38
2.4	Imaging, quantification, and statistics .....	40
<b>Chapter 3 Establishment and characterisation of PNN culture model that replicates PNN maturation and heterogeneity .....</b>		<b>41</b>
3.1	Introduction.....	41
3.1.1	PNN development and maturation .....	42
3.1.1.1	Expression of PNN components.....	42
3.1.1.2	Cellular origin of PNN components.....	42
3.1.1.3	The necessity of PNN components for mature PNN structure .....	43
3.1.1.3.1	Hapln1 is necessary for CSPG recruitment and PNN maturation .....	43
3.1.1.3.2	TnR crosslinks PNN CSPGs, creating a reticular PNN .....	43
3.1.1.3.3	Aggrecan.....	44
3.1.1.3.4	Not all PNN components are necessary for mature PNNs .....	44
3.1.1.4	PNN glycosylation during maturation.....	44
3.1.1.5	Understanding changing PNN morphology through the lens of soft matter physics .....	45
3.1.1.5.1	Mechanisms governing PNN polymer density.....	45
3.1.1.5.2	Mechanisms governing attraction between PNN polymers .....	46
3.1.1.6	Role of neuronal activity in PNN maturation .....	47
3.1.1.7	PNN maturing agents .....	48
3.1.1.8	PNN heterogeneity is widespread throughout the CNS .....	49
3.1.1.9	PNN composition and function .....	51
3.1.2	Chapter aims.....	52
3.2	Methods.....	53
3.2.1	Primary Cell Culture .....	53
3.2.2	Immunocytochemistry .....	53
3.2.3	Microscopy, quantification, and statistics .....	53
3.3	Results .....	54
3.3.1	Formation of PNNs <i>in vitro</i> .....	54
3.3.2	Appearance of PNN components during PNN development .....	56

3.3.3	Two routes of PNN maturation.....	57
3.3.4	The heterogeneity of mature PNNs.....	63
3.3.4.1	Acan, bcan and ncan are found in mature cortical PNNs <i>in vitro</i> .....	63
3.3.4.2	Acan is the predominant PNN CSPG in mature cortical PNNs <i>in vitro</i> .....	63
3.3.4.3	Hapln1 does not segregate with a single CSPG .....	65
3.3.4.4	Tenascin R is a key component of mature PNNs <i>in vitro</i> .....	65
3.4	Discussion.....	68
3.4.1	Summary of results .....	68
3.4.2	Maturation of the PNN <i>in vitro</i> .....	69
3.4.2.1	Identification of an early mature PNN population .....	69
3.4.2.2	PNN maturation correlates with rising acan localisation .....	69
3.4.3	PNN heterogeneity: clues to different functions .....	70
3.4.3.1	A WFA negative PNN population .....	71
3.4.3.2	Heterogeneity in CSPG expression between PNNs .....	72
3.4.3.3	Hapln1 does not segregate with a specific CSPG .....	73
3.4.4	TnR localises to mature PNNs <i>in vitro</i> .....	73
3.4.5	Conclusions and future directions .....	75
<b>Chapter 4 The PNN reduces aggregated <math>\alpha</math>SYN species uptake and p-<math>\alpha</math>SYN pathology development.....</b>		<b>76</b>
4.1	Introduction .....	76
4.1.1	$\alpha$ SYN internalisation and seeding .....	76
4.1.2	The PNN as a barrier preventing $\alpha$ SYN internalisation .....	77
4.1.3	Aims of chapter .....	77
4.2	Methods .....	79
4.2.1	Purification of $\alpha$ -synuclein .....	79
4.2.1.1	Fluorescent labelling of $\alpha$ -synuclein .....	80
4.2.2	Creation of pathogenic species.....	81
4.2.3	Atomic force microscopy .....	81
4.2.4	Quality Control of PFF.....	82
4.2.4.1	Sedimentation assay .....	82
4.2.4.2	Thioflavin T assay.....	83
4.2.5	Cell Culture .....	83
4.2.5.1	PNN-HEK 293T culture .....	83
4.2.5.2	Primary culture .....	83
4.2.6	Cell treatment.....	83

4.2.6.1	Oligomer treatment.....	83
4.2.6.2	Fibril treatment.....	83
4.2.6.3	Chondroitinase ABC treatment.....	84
4.2.7	Immunocytochemistry .....	84
4.2.8	Imaging and analysis .....	84
4.2.9	Surface plasmon resonance.....	84
4.2.10	Quartz crystal microbalance with dissipation .....	85
4.3	Results .....	87
4.3.1	Purification of $\alpha$ -synuclein.....	87
4.3.2	Creation of $\alpha$ -synuclein seeding species.....	89
4.3.3	A PNN cell model resists oligomer induced seeding.....	91
4.3.4	PNN neurons resist $\alpha$ SYN oligomer uptake .....	93
4.3.5	Addition of PFFs lead to the progressive development of p- $\alpha$ SYN pathology in neurons .....	94
4.3.6	Removal of extracellular matrix does not affect the degree of p- $\alpha$ SYN pathology.....	99
4.3.7	CS-E and HS bind $\alpha$ SYN .....	99
4.4	Discussion .....	103
4.4.1	Summary of results .....	103
4.4.2	Structurally diverse $\alpha$ SYN species cause seeding.....	103
4.4.3	The perineuronal net blocks uptake of oligomeric $\alpha$ SYN.....	104
4.4.4	The PNN as a protective structure from $\alpha$ SYN pathology ...	107
4.4.5	Putative mechanism for PNN neuroprotection .....	108
4.4.6	Conclusions and future directions .....	110
<b>Chapter 5 PNN populations are spared and unaffected by Lewy pathology in PD brains .....</b>		<b>111</b>
5.1	Introduction.....	111
5.1.1	Cell autonomous factors in determining neuronal susceptibility 111	
5.1.2	The extracellular matrix as a factor in neuronal susceptibility 112	
5.1.3	The PNN as a resistance factor restricting local $\alpha$ SYN spread 113	
5.1.4	Chapter aims.....	114
5.2	Methods.....	115
5.2.1	Human brain tissue .....	115
5.2.2	Preparation of gelatine coated slides .....	115
5.2.3	Immunohistochemistry .....	115

5.2.4	Imaging and quantification .....	116
5.3	Results .....	117
5.3.1	No correlation between PNN density and post-mortem delay 117	
5.3.2	PNN density is preserved in PD .....	118
5.3.2.1	No Lewy bodies in PNN neurons.....	119
5.3.3	Segregation between ECM rich and LB rich areas .....	122
5.4	Discussion.....	124
5.4.1	Summary.....	124
5.4.2	WFA reactivity not affected by short PMD.....	124
5.4.3	PNN populations in the human brain .....	124
5.4.4	PNN populations spared .....	127
5.4.4.1	Correlating PNN populations and neuronal loss .....	127
5.4.4.2	Other factors are not sufficient to explain PNN population sparing.....	129
5.4.4.3	No Lewy Pathology in PNN neurons .....	129
5.4.5	Segregation of ECM and Lewy pathology .....	130
5.4.6	Conclusions and Further directions.....	131
<b>Chapter 6</b>	<b>General discussion and future perspectives .....</b>	<b>132</b>
6.1	Introduction .....	132
6.2	Establishment of a mature PNN <i>in vitro</i> culture .....	133
6.3	The PNN reduces pathogenic $\alpha$ SYN internalisation and p- $\alpha$ SYN pathology development .....	134
6.4	PNN populations are unaffected in PD .....	136
6.5	Mechanism for PNN neuroprotection in PD.....	137
6.6	Implications and future directions .....	139
<b>Chapter 7</b>	<b>Conclusions.....</b>	<b>143</b>
<b>Chapter 8</b>	<b>References .....</b>	<b>144</b>

## List of figures and tables

### Figures

Figure 1: Symptom progression of Parkinson's disease .....	2
Figure 2: Subtypes of Lewy pathology .....	5
Figure 3: Schematic study of Braak staging .....	3
◀Figure 4 The perineuronal net .....	27
Figure 5: Formation of PNN <i>in vitro</i> .....	47
Figure 6: Development of PNN components <i>in vitro</i> .....	49
Figure 7: PNN morphology transitions from punctate to reticular over time .....	50
Figure 8: Recruitment of ACAN to WFA positive PNN.....	51
Figure 9: Recruitment of PNN markers to hapln1 positive PNNs .....	52
Figure 10: Comparison of WFA and CSPG staining of mature DIV56 <i>in vitro</i> PNNs .....	53
◀Figure 11: Heterogeneity of CSPGs localisation in PNNs.....	55
Figure 12: Mature <i>in vitro</i> PNNs contain hapln1 .....	56
Figure 13: A high proportion of <i>in vitro</i> PNNs contain tenascin R .....	58
Figure 14: Heterogeneity among TnR positive PNNs .....	59
Figure 15: Purification of $\alpha$ SYN .....	80
Figure 16: Characterisation of $\alpha$ SYN species.....	82
Figure 17: PNN-HEK cells are resistant to $\alpha$ -synuclein seeding.....	84
▶Figure 18: PNN neurons resist $\alpha$ -synuclein oligomer uptake.....	87
Figure 19: p- $\alpha$ SYN aggregates accumulate over time in PFF treated neurons.....	89
Figure 20: Effect of ChABC on p129 development .....	90
Figure 21: Quantification of p129 intensity.....	91
Figure 22: $\alpha$ SYN binds to sulphated glycosaminoglycans CS-E and HS .....	92
Figure 23: Confirmation of $\alpha$ SYN/ HS interaction .....	94
Figure 24: PMD is not correlated with altered PNN density .....	110
Figure 25: PNN neuronal density is unaffected in the PD brain .....	111
Figure 26: PNN rich areas segregate from Lewy rich areas in PD amygdala .....	112
Figure 27: PNN neurons co-exist with Lewy bearing neurons in the olfactory bulb .....	113
Figure 28: PNN rich areas segregate from Lewy rich areas in the substantia nigra .....	114

**Figure 29: PNN neurons in the temporal cortex co-exist near to LB-bearing neurons.....115**

**Figure 30: Proposed mechanism of PNN in PD pathophysiology .....131**

**Tables**

**Table 1 Criteria for neuropathological staging of Parkinson’s Disease according to Braak and unified staging system for Lewy body disorders. ....3**

**Table 2 Antibodies used in thesis .....31**

**Table 3: Kinetic constants of GAG/ $\alpha$ SYN interaction .....93**

**Table 4: Human cases used in this study.....107**

**Table 5: PNN Densities in the human brain .....109**

## Abbreviations

Acan: Aggrecan  
AD: Alzheimer's disease  
Am: Amygdala  
AON: Anterior olfactory nucleus  
A $\beta$ : Amyloid-beta  
BBB: Blood brain barrier  
Bcan: Brevican  
BDNF: Brain-derived neurotrophic factor  
CaBP: Calcium binding proteins  
Cmd: Cartilage matrix deficiency  
CNS: Central nervous system  
CP: Critical period  
CS: Chondroitin sulphate  
CSPG: Chondroitin sulphate proteoglycan  
C6ST-1: Chondroitin 6 sulfotransferase-1  
DA: Dopamine/dopaminergic  
DBS: Deep brain stimulation  
DIV: Days *in vitro*  
DLB: dementia with Lewy bodies  
DMV: Dorsal motor vagal nucleus  
DS: Dermatan sulphate  
ECM: Extracellular matrix  
FBS: Foetal bovine serum  
GAG: Glycosaminoglycan  
GCI: Glial cytoplasmic inclusion  
GuHCl: Guanidine hydrochloride  
HA: Hyaluronan  
HapIn: HA and proteoglycan link protein  
HAS: Hyaluronan synthase  
HBS: HEPES buffered-saline  
HBSS-: Hank's buffered salt solution (without ions)  
Hc: Hippocampus  
HNE: 4-hydroxy-2-nonenal

HS: Heparin sulphate  
HSPG: Heparin sulphate proteoglycan  
iLBD: Incidental Lewy body disease  
LB: Lewy body  
LDCV: Large dense core vesicle  
LP: Lewy pathology  
LTP: Long term potentiation  
MAO: Monoamine oxidase  
MMP: Matrix metalloprotease-9  
MPTP: 1-methyl-4- phenyl-1,2,3,6-tetrahydropyridine  
MSA: Multiple systems atrophy  
NARP: Neuronal activity-regulated pentraxin  
NCAP: Non-amyloid plaque component  
Ncan: Neurocan  
NDS: Normal donkey serum  
NPTX2: Neuronal pentraxin 2  
nTg: Non-transgenic  
OB: Olfactory bulb  
p- $\alpha$ SYN: phosphorylated  $\alpha$ SYN (p129)  
PAF: Pure autonomic failure  
PBS: Phosphate buffered-saline  
Pcan: Phosphacan  
PD: Parkinson's Disease  
PDD: PD with dementia  
PFF: Preformed fibrils  
PNN: Perineuronal net  
PMD: Post-mortem delay  
PPN: Pedunculopontine nucleus  
PV: Parvalbumin  
QCM-D: Quartz crystal microbalance with dissonance  
ROS: Reactive oxygen species  
RPTP $\zeta$ : Receptor protein tyrosine phosphatase zeta  
RRP: Rapid releasable pool  
RSBD: REM sleep behaviour disorder  
Sema3A: Semaphorin 3a

SN: Substantia nigra  
SNARE: Soluble N-ethylmaleimide-sensitive factor attachment protein receptor  
SNc: Substantia nigra pars compacta  
SNCA:  $\alpha$ SYN gene  
SNr: Substantia nigra pars reticulata  
SPR: Surface plasmon resonance  
SV: Synaptic vesicles  
TBS: Tris buffered saline  
TBS-T: Tris buffered saline with 0.1% tween-20  
Tc: Temporal cortex  
TKO: Triple knock out  
TnR: Tenascin R  
TNS: Tris non-saline  
UDPRS: Unified Parkinson's disease rating scale  
USSLB: Unified Staging System for Lewy Body disorders  
Vcan: Versican  
VTA: Ventral tegmental area  
 $\alpha$ SYN: Alpha-synuclein  
 $\beta$ SYN: Beta-synuclein  
 $\gamma$ SYN: Gamma-synuclein



# Chapter 1 Parkinson's disease

## 1.1 Epidemiology

Parkinson's disease (PD) is the 2<sup>nd</sup> most common neurodegenerative disorder globally. In the UK, there is a 2.7% lifetime risk of being diagnosed, equivalent to 1 in 37 people being diagnosed with Parkinson's (Parkinson's UK, 2018). Age is the largest risk factor as PD is most prevalent in those over 65, affecting 6% of the demographic. The incidence risk almost doubles every 5 years starting from 45 years of age and peaks at 80 years of age (Parkinson's UK, 2018). This is a cause for concern as in the UK due to our ageing population.

Currently, over 65s are a larger demographic than those under 18 (Office for National Statistics, 2014). By 2039, over 65s are estimated to account for nearly a quarter of the UK population (Storey, 2018). The burden of ageing is set to worsen as by 2050 it is estimated that those over 60 will account for 21% of the world's population (Storey, 2018). The reason for this increase is declining mortality rates (Office for National Statistics, 2014). While this is to be celebrated it should cause concern for governments and health services as currently neurological disorders are the leading cause of disability world-wide. In the UK the cost of PD for a household is estimated at £16,582 per year, with an average loss of income of £10,731 and an average health and social care cost of £5,851 (Parkinson's UK, 2017). Furthermore, PD patients are more likely to go into care homes, further placing emotional and financial strain on loved ones (Parashos, *et al.*, 2002). In 2016 they accounted for 276 million disability-adjusted life years (DALYs). The DALY is a metric which accounts for overall disease burden, incorporating years lived with the disability and years of life lost. PD accounted for 4 million DALYs (Feigin, *et al.*, 2019). The prevalence of PD has increased dramatically with a 144% gross increase from 1990. Even when standardised for age it had still increased by 22% (Feigin, *et al.*, 2019).

While PD is not a direct cause of death, PD patients have a higher risk of emergency hospital admission and are 2-3 x more likely to die in hospital (Parashos, *et al.*, 2002; Low, *et al.*, 2015). The cost in the UK of the non-elective admissions was £777 million in 2015. Compared to non-PD patients, PD patients are twice as likely to extend their hospital stay to over three months (Low, *et al.*, 2015). The World Health Organisation has warned that we are heading towards a crisis with PD and other age-related disorders placing unbearable strain on health care and social institutions across the world (WHO, 2011; Alamri, 2015).

### 1.1.1 Symptoms and variability in progression

It was the resting tremor, rigid stoop and slow movement (bradykinesia) that was first identified by James Parkinson in 1817 (Goetz, 2011). In the 200 years since its discovery, these symptoms still form the largest part of the public's image of a Parkinson's patient. However, by themselves these symptoms are not indicative of Parkinson's disease but of a Parkinsonian syndrome. According to the criteria of the UK PD brain bank, diagnosis of this syndrome requires the bradykinesia and at least either: tremor, muscle rigidity or postural instability. For a diagnosis of PD, other causes must then be ruled out e.g., history of repeated head injury or stroke. Step 3 is the identification of at least 3 supportive conditions, these include: unilateral onset of tremor and L-dopa responsiveness (Hughes, *et al.*, 1992). However it has become apparent that these symptoms only comprise a part of an ensemble of symptoms that PD patients present with (Kalia and Lang, 2015). These symptoms can be divided into motor and non-motor symptoms and their progression is summarised in figure 1.

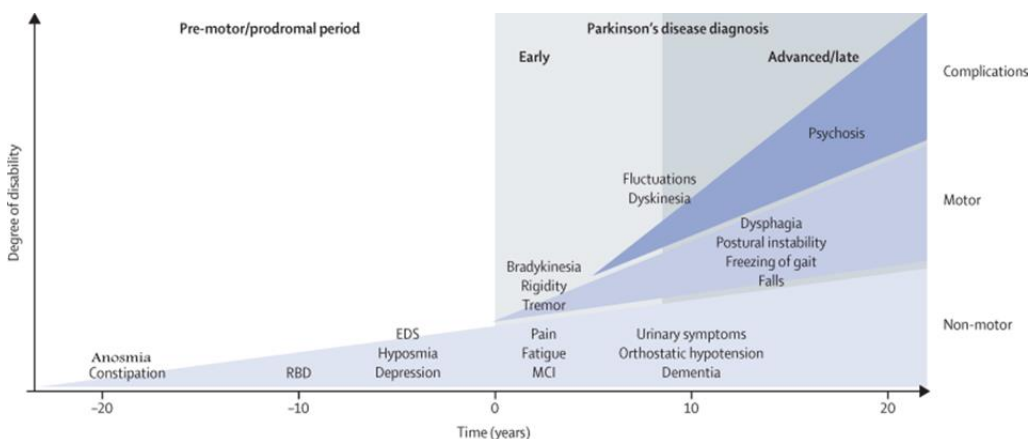


**Figure 1: Symptom progression of Parkinson's disease**

As seen above the non-motor symptoms precede the motor symptoms by 20 years. Current diagnosis rests on the appearance of the motor symptoms, which may prove too late to reverse the disease. As the disease progresses the deficits grow more pronounced and other symptoms appear. Modified from (Kalia and Long, 2015).

As mentioned, the classic motor symptom seen in PD patients is the 'pill rolling' tremor seen in patient's hands. 80% of patients present with tremor, most commonly in the upper limb (Jankovic, 2008). Several years after onset 25-60% patients often exhibit movement freezing (Virmani, *et al.*, 2015). Postural instability leads to falls, a leading cause of hospital admissions in PD patients (Sveinbjörnsdóttir, 2016; Low, *et al.*, 2015). Patients often exhibit with dystonia which can precede PD diagnosis by several years or be brought on by the treatment L-DOPA itself (Fahn, 2008; Sveinbjörnsdóttir, 2016). Oral motor

symptoms, such as drooling, are also a component of PD and can have major impact of quality of life indicators (Rajiah, *et al.*, 2017).

The non-motor symptoms are varied and have received growing attention in the last 20 years as they can precede the onset of the motor symptoms by several decades (Schrag, *et al.*, 2015; Hickey, *et al.*, 2007; Pont-Sunyer, *et al.*, 2015). The non-motor component encompasses gastrointestinal dysfunction, mental health, sensory and psychiatric problems and can become more troublesome than the motor (Sveinbjörnsdóttir, 2016). 80% of PD patients present with anosmia, which can precede motor symptom onset by 5 years (Doty, *et al.*, 1988; Schrag, *et al.*, 2015). Constipation is also highly prevalent in PD, with 80% of patients exhibiting symptoms (Jost and Eckardt, 2003). Constipation is also the earliest presenting symptom prior to diagnosis, having a higher prevalence in PD patients from 10 years prior to motor symptom onset (Schrag, *et al.*, 2015). Sleep disorders, in particular REM sleep behaviour disorder (RSBD), are also prevalent in PD patients (Sveinbjörnsdóttir, 2016). Patients with RSBD act out in their sleep, lashing out with limbs, it has been reported to present in around a third of cases and can precede motor symptoms (Monderer and Thorpy, 2009). The acknowledgement of the non-motor symptoms and a growing understanding of a pre-motor aspect of the disease has led to the staging of early PD (PD prior to onset of repeated falls and hallucinations) by the international Parkinson and Movement Disorder Society. They divided early PD into three stages: *preclinical PD*, where the neurodegenerative processes are at work but yet to result in symptoms; *prodromal PD*, symptoms have developed (often non-motor) but they are insufficient for a diagnosis; and *clinical PD*, where symptoms are sufficient to meet the diagnosis criteria (Kalia and Lang, 2016). While this is important in changing our understanding of the disease it remains an academic distinction due to the lack of established biomarkers and tests that would be able to identify patients in the preclinical phase. There are promising results from measuring the aggregation potential of  $\alpha$ -synuclein ( $\alpha$ SYN) derived from cerebral spinal fluid which shows specificity for PD and RSBD compared to controls. In two studies aggregation of  $\alpha$ SYN was only detected in the PD and RSBD cohort, showing >98% specificity compared to healthy controls (Fairfoul, *et al.*, 2016; Rossi, *et al.*, 2020). However, only 37.4% of RSBD patients go on to develop a synucleinopathy (Iranzo, *et al.*, 2014). Therefore, it must be determined whether the aggregation propensity of  $\alpha$ SYN is a specific feature of RSBD cases fated to develop a synucleinopathy or of RSBD generally. A larger, longitudinal study of RSBD patients could answer this.

PD is a variable disease, in part due to the wide variety of symptoms patients present with and the incomplete penetrance of these symptoms. PD can be sub-divided into tremor-dominant PD and non-tremor dominant (postural instability and bradykinesia are principal symptoms) (Kalia and Lang, 2015). A third, rapid progression, sub-group can be identified. These patients have older disease onset and faster disease course, with worse motor and cognitive deficits (Graham and Sagar, 1999; Halliday, *et al.*, 2008; Howlett, *et al.*, 2015; Van de Berg, *et al.*, 2012; Lewis, *et al.*, 2005). Idiopathic patients can be diagnosed anywhere between 24 and 80 years of age. Typically, in idiopathic cases the earlier the onset the slower the progression (Jankovic, *et al.*, 1990; Kempster, *et al.*, 2010). The passing of several key PD milestones (e.g. frequent falling, cognitive impairment) doesn't vary with age of onset or death but usually precedes death by 5 years (Kempster, *et al.*, 2010). Genetic mutations in PD have helped shed light on the underlying pathophysiology of PD and can be directly causative or increase risk (Koros, *et al.*, 2017). For an overview of the genetics of PD please refer to Lill (2016). However, even within monogenic autosomal dominant forms there is variability and incomplete penetrance, even within families (Markopoulou, *et al.*, 2008; Koros, *et al.*, 2017). This shows that environmental, epigenetic and genetic variability can influence PD progression.

## **1.2 Pathophysiology of Parkinson's disease**

For a definitive diagnosis of PD, rather than parkinsonism, a post-mortem pathology must be confirmed. The pathology criteria are the loss of pigmentation in the Substantia Nigra pars Compacta (SNc) and the appearance of protein plaques, called Lewy bodies (LBs), in neuronal cell bodies (Poewe, *et al.*, 2017). Both criteria must be fulfilled for a PD diagnosis. LBs are eosinophilic, concentrically ringed inclusions and were first described by Dr. Frederic Lewy in 1912. He first identified them within the dorsal vagal nucleus of a PD patient. They have since been found in various nuclei throughout the brain, with a preference for monoamine nuclei (Ohama and Ikuta, 1976; Adler, *et al.*, 2019). They are intracellular inclusions found in neurons and vary between 4-20  $\mu\text{m}$  in diameter (Kuusisto, *et al.*, 2003). The classic LB is spherical, but this varies upon brain region and whether the cell contains melanin (Fig. 2). Cortical LBs have less defined edges and are less circular (Wakabayashi, *et al.*, 2007). The LB is not the only protein inclusion found within PD. Lewy neurites and pale bodies are also seen, depending on the stain used. Lewy neurites are extrasomal and appear in proximal dendrites (Fig. 2). They are elongated structures which can measure up to 300  $\mu\text{m}$  in length. Pale

bodies are also eosinophilic structures, but they lack the defined, concentric staining of the LB. Together these have been identified as earlier stages in LB development (Fig.2). In culture models of PD, Lewy neurites occur before somal inclusions (Volpicelli-Daley, *et al.*, 2011; Mahul-Mellier, *et al.*, 2020). Pale bodies have been suggested to be an intermediate inclusion which condense into LBs (Kuusisto, *et al.*, 2003).

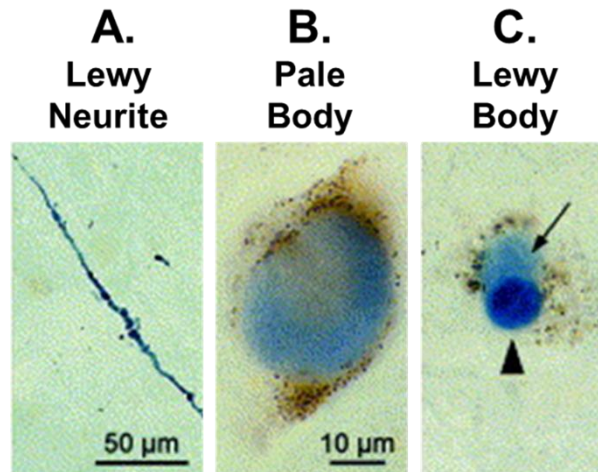


**Figure 2: Subtypes of Lewy pathology**

$\alpha$ SYN immunostaining (blue) from PD post-mortem brain. Brown pigment is neuromelanin. **A.** Lewy neurite, long elongated structures that localise to neuronal projections. **B.** Pale body, diffuse somatic inclusion. **C.** Lewy body (arrowhead), dense circular core surrounded by a diffuse halo (arrow). The halo is not always seen and some LBs have a concentric appearance with a lighter staining in the centre. Images taken from (Braak *et al.* 2004).

LBs contain a large number of different proteins, lipids and organelles, many of which are ubiquitinated (Roy and Wolman, 1969; Kuzuhara, *et al.*, 1988; Wakabayashi, *et al.*, 2007; Shahmoradian, *et al.*, 2019). The core component of the LB is the misfolded  $\alpha$ SYN protein.  $\alpha$ SYN was purified from amyloid plaques from patient brains diagnosed with Alzheimer's disease (AD) and named as the non-amyloid component protein (NACP) (Ueda, *et al.*, 1993; Wakabayashi, *et al.*, 1997). This was then identified as  $\alpha$ SYN, a synaptic protein first isolated from the electric organ of the *Torpedo* ray-fish (Maroteaux, *et al.*, 1988; Jakes, *et al.*, 1994; Spillantini, *et al.*, 1997).  $\alpha$ SYN antibodies detect more Lewy pathology (LP) than other immunohistochemical stains (eosin, ubiquitin or p62 stains). Eosin staining only detected a third of  $\alpha$ SYN-positive LBs and a sixth of pale bodies (Kuusisto, *et al.*, 2003). Lewy neurites can only be detected by  $\alpha$ SYN antibody staining.  $\alpha$ SYN is the essential component of LBs as all alternative LB stains are also positive for  $\alpha$ SYN (Wakabayashi, *et al.*, 1997; Kuusisto, *et al.*, 2003).

There are three members of the synuclein family: alpha, beta and gamma (Surguchov, 2008). Only  $\alpha$ SYN is found in LBs (Spillantini, *et al.*, 1997; Baba, *et al.*, 1998).  $\alpha$ SYN in LBs comes in various forms: full-length, truncated and aggregated forms have all been isolated from patient samples (Baba, *et al.*, 1998; Campbell, *et al.*, 2001). The aggregated  $\alpha$ SYN appears as filaments (Crowther, *et al.*, 2000; Spillantini, *et al.*, 1998b).  $\alpha$ SYN in LBs can also be post-translationally modified.  $\alpha$ SYN can be directly ubiquitinated. This is a pathological phenomenon rather than a queuing up of  $\alpha$ SYN labelled for proteasomal degradation as unmodified  $\alpha$ SYN can be directly degraded by the proteasome (Tofaris, *et al.*, 2001). The predominant pathological  $\alpha$ SYN modification is phosphorylation at serine residue 129 (p- $\alpha$ SYN) (Fujiwara, *et al.*, 2002; Hasegawa, *et al.*, 2002; Anderson, *et al.*, 2006). This modification is specific to LBs and p- $\alpha$ SYN antibodies are used by pathologists in post-mortem diagnosis of synucleinopathies (Adler, *et al.*, 2019).

As mentioned, the LB is made up of a variety of components. In 2007, over 70 different protein components had been isolated from LBs (Wakabayashi, *et al.*, 2007). Neurofilaments are another key LB component and are present with a disorganised phenotype within inclusions (Shahmoradian, *et al.*, 2019; Mahul-Mellier, *et al.*, 2020). Together, with the accumulation of lipids and organelles, the Lewy body could be best understood as a cellular traffic jam around an aggregated  $\alpha$ SYN core (Roy and Wolman, 1969; Shahmoradian, *et al.*, 2019).

### **1.2.1 Understanding Lewy pathology in synucleinopathies**

The LB is a cardinal and essential hallmark of PD. However, it is not unique to PD.  $\alpha$ SYN inclusions are also hallmark for several disorders, collectively called synucleinopathies. A sub-group of these are LB diseases. They are incidental LB disease (iLBD), PD, PD with dementia (PDD), dementia with Lewy bodies (DLB), multiple systems atrophy (MSA) and pure autonomic failure (PAF). iLBD is diagnosed when LBs are found in non-symptomatic patient brains. MSA and PAF are distinct from the others as the inclusions are found in different cell types other than neurons. In PAF, the LBs are found in peripheral neurons rather than the central nervous system (CNS) (Brown, 2017). The key pathological hallmark of MSA are glial cytoplasmic inclusions (GCIs) rather than LBs. They are  $\alpha$ SYN containing inclusions but are found in glia rather than neurons (Spillantini, *et al.*, 1998). The other 4 synucleinopathies can be interpreted as a spectrum of disease (Walker, *et al.*, 2019).

There is a question as to whether PDD and DLB are distinct diseases or different presentations of the same disease as there is very little to differentiate them neuropathologically (Jellinger, 2018; Tsuboi, *et al.*, 2007). Clinically the

different diagnoses are determined by the timing of dementia onset. If it is in an established PD setting (PD for at least one year prior), then it is PDD. If the dementia precedes the motor symptoms by at least a year or occurs within the same year as motor symptom onset, then it is DLB. This '1 year rule' has been criticised as arbitrary but is useful clinically as it recognises that DLB generally follows a more severe and aggressive time course than PDD. The LB disease spectrum (iLBD<PD<PDD<DLB) traverses a symptomatic axis, with cognitive symptoms becoming more prevalent the further along the axis. As discussed, while PD patients exhibit cognitive impairment; it is the degree of the impairment that would distinguish between PDD and PD. Halliday and colleagues followed a PD cohort longitudinally and found that after 20 years of PD all patients had dementia (2008). PD and DLB can be differentiated pathologically by the degree of striatal loss and neocortical LB load. PD shows greater striatal loss and DLB higher cortical LB load. PDD bridges both phenotypes (Jellinger, 2018; Walker, *et al.*, 2019). These correlations can be drawn together to link symptoms to LP load in brain regions. For example, a higher cortical LP load would increase the probability of psychiatric symptoms while LP in the olfactory bulb (OB) would increase the likelihood of anosmia. It should be noted that while LB diseases are distinct clinically the picture is often murkier pathologically. Other neurodegenerative disease pathology can often occur concurrently with LP. For example, in LB diseases with more cognitive impairment (i.e. PDD and DLB) amyloid plaques are often found. The load of mixed pathologies is a good indicator for rate of disease progression, with a higher load predicting a faster progression (Howlett, *et al.*, 2015). Reconciling the synucleinopathies into a spectrum is intellectually appealing but the complexity of pathological evidence so far stops us short of proving this assertion (Halliday, *et al.*, 2008; Beach, *et al.*, 2009). However, the spectrum framework of synucleinopathies is useful in understanding them and demonstrates the importance of understanding LP development and spread.

### **1.3 Treatment of Parkinson's disease**

There is no disease-modifying treatment for PD. The current treatments available can only relieve symptoms and are not without side-effects (Dexter and Jenner, 2013). The treatments can be divided into drug-based or device-based. The drug-based treatments are used early in early PD while the device-based treatments are used later in the disease course after the drugs have lost efficacy (Dietrichs and Odin, 2017).

### 1.3.1 Pharmacological treatment

The drug-based treatments aim to relieve the motor symptoms by replacing the lost dopamine. This can be done by inhibiting dopamine breakdown, directly replacing the dopamine or by using dopamine agonists. Monoamine oxidase (MAO) inhibitors, specifically MAO-B inhibitors, are often prescribed first as they avoid the side-effects of L-DOPA treatment. They raise striatal dopamine (DA) by inhibiting DA breakdown. Furthermore, they have been posited to slow disease progression as they can reduce oxidative stress in DA neurons but a meta-analysis found no strong association between MAO administration and disease progression (Olanow, 1996; Turnbull, *et al.*, 2005).

L-DOPA, commonly known as levodopa, is a precursor of dopamine. It is the mainstay of PD pharmacological treatment (Fahn, 2008). The advantage of L-DOPA over dopamine is that it can cross the blood-brain barrier while dopamine cannot. It is given orally in high doses and is given concurrently with a peripheral DOPA-decarboxylase inhibitor, such as carbidopa or benserazide, to block peripheral conversion of L-DOPA. Remission of akinesia and postural rigidity are well-documented in PD patients after L-DOPA treatment (Fahn, 2008). More variable is the effect on tremor, with some patients seeing some effect while in others the tremor was resistant to treatment (Dietrichs and Odin, 2017).

### 1.3.2 Deep brain stimulation in PD

As PD advances pharmacological treatments lose efficacy or treatment-related side-effects worsen to the point where they can no longer be tolerated. Deep brain stimulation (DBS) has been used in PD for the past 30 years and shows great efficacy in targeting motor and non-motor symptoms (Kalia and Lang, 2015; Zahed, *et al.*, 2021). DBS treatment has been shown to reduce unified Parkinson's disease rating scale (UDPRS) score by an average of 45%, significantly improving patient symptoms. For example, DBS reduced the mean UDPRS tremor score from 4.61, indicating a marked tremor present for the majority of the time, to 1.22, a slight tremor which is only infrequently present (Gervais-Bernard, *et al.*, 2009). A bilateral electrode is implanted into the subthalamic nucleus (STN) or the globus pallidus interna (GPi) and stimulates the region. Current evidence indicates STN implantation results in the best treatment outcomes (Odekerken, *et al.*, 2013). The pattern of stimulation can be tailored to the patient to ensure the best reduction of symptoms, though the precise mechanism for improvement is poorly understood (Kalia and Lang, 2015). DBS shows higher improvement on quality of life and daily living scores

than late-stage pharmacological treatments but has a 4 times higher risk of adverse events. This arises from the requirement of surgery for DBS implementation (Nijhuis, *et al.*, 2021). As with pharmacological treatments, DBS does not alter disease progression and loses efficacy over time (Poewe, *et al.*, 2017).

## 1.4 Braak Staging in Parkinson's Disease

LP is found throughout the brain, affecting higher and lower brain regions as well as being detected in the spinal cord and peripheral nervous system (Rajput and Rozdilsky, 1976; Parkkinen, *et al.*, 2008). Braak and colleagues investigated how this pathology appears. Does it develop simultaneously in all regions, or does it appear in some brain regions before others? They stained 41 PD patients and 61 asymptomatic, LP positive patients and found a hierarchical spread of pathology. This hierarchy could be divided into 6 stages in which stage built on the last, these are summarised in table 1.

The mildest affected cases (stage 1) only exhibited LP in the dorsal motor nucleus (DMV) and OB. In their cohort the DMV was always affected. In the 2<sup>nd</sup> stage pathology is noted in the raphe nuclei and locus coeruleus. The 3<sup>rd</sup> stage is when pathology is first noted in the midbrain, most notably the substantia nigra pars compacta (SNc). Stage 4 presents with limbic (amygdala), trans entorhinal, and allocortex (CA2) involvement. The pathology begins to appear in the neocortex at stage 5 and progresses into the higher regions of the neocortex (primary and first order areas) in stage 6. A clinical PD diagnosis did not appear in the cohort until stages 3/4. This follows the appearance of SNc pathology and strengthens the case that the motor symptoms are Lewy-related (Braak, *et al.*, 2003).

Based on the staging they split the stages into presymptomatic (1-3) and symptomatic (4-6). According to these stages the pathology ascended through the brain in a caudorostral manner (Fig. 3). Due to the 100% involvement of the DMV in all cases they suggested it as an induction site (Braak, *et al.*, 2006). The LP severity varied between individuals and areas. However it did correlate with the stage, with higher pathology load associating with later stages (Braak, *et al.*, 2003). The key finding was the sequential anatomical progression of the pathology. In a follow-up paper they linked the disease stage to cognitive impairment, showing a negative correlation of cognitive faculties and PD stage (Braak, *et al.*, 2005).

**Table 1 Criteria for neuropathological staging of Parkinson's Disease according to Braak and unified staging system for Lewy body disorders.**

Braak Staging		Regions Involved	Unified Staging System for Lewy Body Disorders	
Stage	Pathology		Pathology	Stage
1	Olfactory bulb and tract or dorsal motor vagal nucleus	Olfactory system	Olfactory bulb	1
2	Locus coeruleus, raphe nuclei	Brainstem	Brainstem predominant e.g. dorsal motor vagal nucleus, locus coeruleus, substantia nigra,	2a
3	Pedunclopontine nucleus, substantia nigra, amygdala (central subnucleus)	Limbic system	Limbic predominant Amygdala & cingulate cortex	2b
4	Further amygdala involvement, hippocampus, temporal cortex	Neo cortical	Strong involvement of both brainstem and Limbic regions	3
5	Limbic system, CA2 region of hippocampus, further amygdala involvement		middle temporal and frontal gyri and inferior parietal lobule	4
6	Multiple cortical regions			

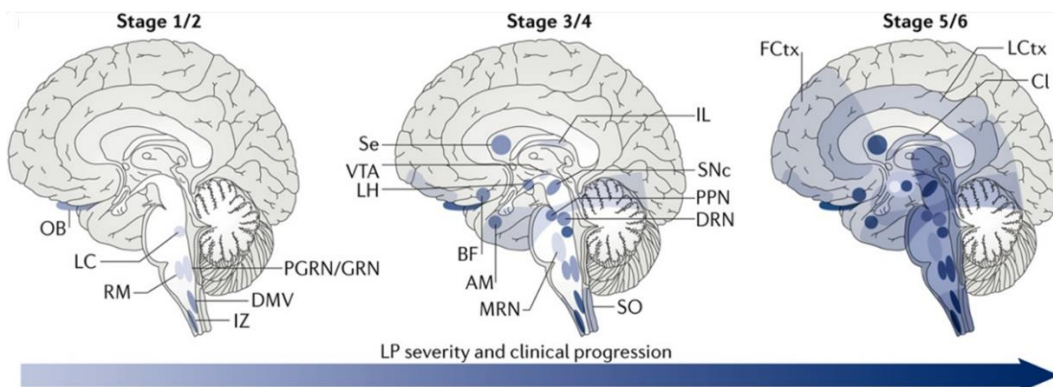


**Figure 3: Schematic study of Braak staging**

Lewy pathology generally ascends through the brain in a caudal-rostral manner. Severity of LP in an area is signified by the darkening hue. Braak staging correlates with clinical progression and LP severity. Abbreviations: AM, amygdala; BF, mangnocellular nuclei of the basal forebrain; CL, claustrum; DMV, dorsal motor vagal nucleus; DRN, dorsal raphe nucleus; FCtx, frontal cortex; IZ, intermediate reticular zone; IL, intralaminar nuclei of the thalamus; LC, locus coeruleus; LCtx, limbic cortex; LH, lateral hypothalamus; MRN, median raphe nucleus; OB, olfactory bulb; PGRN/GRN, paragigantocellular and gigantocellular reticular nucleus; PPN pedunclopontine nucleus; RM, raphe mangus; Se, septum; SO, superior olive; VTA, ventral tegmental area. Image taken from (Surmeier et al. 2017).

### 1.4.1 Criticisms of Braak Staging

It has been nearly twenty years since the Braak PD staging has been proposed and criticisms have arisen during this time. Criticism has condensed around several points: the DMV as the induction point, the caudorostral progression and the correlation of pathology and symptom severity.

The DMV was posited as an induction point because it was the lowest brain region investigated and provided the first step for misfolded  $\alpha$ SYN to enter from the periphery e.g., from the gut. Investigation of PD gut samples found p- $\alpha$ SYN positive inclusions, reminiscent of Lewy neurites, in gastric neurons (Lebouvier, *et al.*, 2008). These p- $\alpha$ SYN inclusions can be detected in gastric biopsy's from PD patients up to 20 years before disease onset and strengthens the case  $\alpha$ SYN aggregation originates in the periphery and is linked to an environmental trigger (Stokholm, *et al.*, 2016). Two groups have both found a proportion of PD cases (7% and 8.3%) that showed no LP in the DMV despite significant pathology elsewhere (Kalaitzakis, *et al.*, 2008; Attems and Jellinger, 2008). Both groups state that the neuronal population was well-preserved, and that extensive neuronal death was not the reason for lack of LP. In DMV negative cases pathology was detected in the OB, indicating this could be another induction site (Van de Berg, *et al.*, 2012). The OB transmitted pathogenic  $\alpha$ SYN to PD-related areas in a mouse model, demonstrating proof of principle (Rey, *et al.*, 2016; Rey, *et al.*, 2019; Bantle, *et al.*, 2019). The original Braak cohort did not contain olfactory only cases, demonstrating the need for large cohorts examining multiple brain regions (Adler, *et al.*, 2019).

The Braak staging hypothesis predicts that as the disease worsens and the pathology spreads, earlier brain regions will exhibit higher LP loads. This trend can be observed in the 2003 cohort (Braak, *et al.*, 2003). However this trend did not hold up to testing as no significant correlation between brainstem pathology and cortical pathology severity has been found, i.e. it was not unusual to see higher levels of pathology in cortical areas than in lower brain regions (Kingsbury, *et al.*, 2010; Dickson, *et al.*, 2010). LP may also be found in non-symptomatic elderly patients, designated as iLBD (Parkkinen, *et al.*, 2005; Zaccai, *et al.*, 2008). A comparison between iLBD and PD, found non-symptomatic iLBD patients with equal pathology loads to PD patients (Zaccai, *et al.*, 2008). So while a link between pathology load and disease duration is apparent in some individuals it is not universally true for PD indicating other factors are at play (Kalaitzakis, *et al.*, 2008). Also, the Braak staging procedure cannot answer this question as it merely judges whether a region has pathology rather than the degree of pathology, so instead groups have taken a semi-quantitative approach. There was a significant correlation between pathology

severity and the severity of motor symptoms and dementia (Wakisaka, *et al.*, 2003; Parkkinen, *et al.*, 2005). While a link between pathology load and symptom severity has been found, a correlation between pathology load and Braak staging has not been established.

Braak staging is suited to classifying idiopathic PD but is poor at classifying LP in other contexts (Braak, *et al.*, 2003; Dickson, *et al.*, 2010; Kingsbury, *et al.*, 2010; Geut, *et al.*, 2020). However there are a significant number of PD cases that do not follow the caudorostral pattern and instead pass over some brain regions and so cannot be classified (Van de Berg, *et al.*, 2012; Adler, *et al.*, 2019). Also, it does not account for pathology severity and is an imperfect predictor of symptoms (Dickson, *et al.*, 2010; Kingsbury, *et al.*, 2010; Parkkinen, *et al.*, 2008). Therefore, a second pathological staging system was developed that would unify synucleinopathies- the Unified Staging System for LB disorders (USSLB) (Beach, *et al.*, 2009). This system adapted both the DLB consortium criteria and the Braak staging to create the following staging method set out in table 1. Stage 1 has LP in the OB only as it is the most frequently affected area in iLBD and Alzheimer's with LB (Beach, *et al.*, 2009). Stage II is when the pathology is found in the brainstem and limbic system, it is split into IIa and IIb according to which area is dominant. IIb recognises the vulnerability of the amygdala to LP (Parkkinen, *et al.*, 2003; Zaccai, *et al.*, 2008; Van de Berg, *et al.*, 2012). When both areas are affected equally it is classified as stage III. Once moderate pathology is detected in the neocortical regions then it is classified as stage IV. If no LP is detected, then it is classified as USSLB stage 0. Using the USSLB 100% of a mixed cohort of iLBD, AD with LB, PD, PDD and DLB (280 cases) could be classified, whereas 25% were unclassifiable using Braak staging (Adler, *et al.*, 2019). This system shows that synucleinopathies follow conserved spreading patterns with some variation between diseases (PD vs DLB).

PD is one of several synucleinopathies in which  $\alpha$ SYN positive inclusions develop and spread through the CNS in a conserved and sequential manner. In PD the spread is from lower brain regions to upper and is caudorostral in manner. The appearance of LP is correlated with neuronal death and symptom progression. It is a complex disease arising from the interaction of many factors and variables such as genetics, age and environment (Surmeier, *et al.*, 2017a). It is these interactions that contribute to the heterogeneity of the disease phenotype and progression, such that it can be classified into several sub-types. However, despite this one factor is preeminent. Mutations and multiplications of the  $\alpha$ SYN gene (SNCA) causes early onset PD and its protein

product is the key component of LP. This factor is the  $\alpha$ SYN protein. In the next section, I will discuss the physiology of  $\alpha$ SYN.

## 1.5 $\alpha$ -synuclein- the major player in PD

### 1.5.1 Synucleins and structure

The synucleins are a three-member family of proteins that are highly dynamic, with no fixed secondary structure (Weinreb, *et al.*, 1996; Jain, *et al.*, 2018).  $\alpha$ SYN was the first member discovered and was found to localise to the nuclear envelope and pre-synaptic terminals of neurons, leading to the name synuclein (Maroteaux, *et al.*, 1988). Originally found in the *Torpedo* ray, it was then found to have a homologous gene family (>50%) in rat, songbird and human (Maroteaux and Scheller, 1991; Jakes, *et al.*, 1994; George, *et al.*, 1995). Interestingly it is only expressed in vertebrates (Sulzer and Edwards, 2019).  $\alpha$ SYN is the largest member (140aa, 14.46 kDa), then  $\beta$ SYN (134aa) and  $\gamma$ SYN (127aa) (Surguchov, 2008). All members are highly expressed in the brain (Maroteaux and Scheller, 1991; Jakes, *et al.*, 1994; Ninkina, *et al.*, 2003; Robertson, *et al.*, 2004). There are family-member specific expression differences though.  $\beta$ SYN is expressed solely in the brain (Human protein atlas).  $\alpha$ SYN is also expressed in erythrocytes and bone marrow (Fauvet, *et al.*, 2012).  $\gamma$ SYN was isolated independently by several groups working on breast cancer. It is expressed in the brain, but similar levels of expression are found in adipose and adrenal tissue (Human protein atlas).

The synucleins are well-conserved in evolution, there is above 60% homology between family members (Surguchov, 2008). Phylogenetic analysis shows  $\alpha$ SYN and  $\beta$ SYN are more closely related than  $\gamma$ SYN (Yang, *et al.*, 1999). Interestingly, the *Torpedo* synuclein is more closely related to  $\gamma$ SYN than the other synucleins (Yang, *et al.*, 1999). The synuclein sequence can be divided into three domains: an amphipathic, basic N-terminal (1-60 aa), the non-amyloid component (61-95aa) and an acidic C terminal domain (95-140 aa), the amino acid numbers refer to the  $\alpha$ SYN sequence. The greatest degree of homology is in the N-terminal region ( $\alpha$ SYN 1-60), which has >80% homology between  $\alpha$ SYN and  $\beta$ SYN (Jakes, *et al.*, 1994). The synuclein family contain seven degenerate 11 aa repeats located in the N terminal and NAC domains. The repeats are reminiscent of the  $\alpha$ -helical sequences in apolipoproteins. These repeats are conserved in all family members, although  $\beta$ SYN lacks the last repeat. The 11 aa periodicity is only broken once in all species and is broken at the same point by the same linker, between the 4<sup>th</sup> and 5<sup>th</sup> sequence by a 4 uncharged amino acid sequence (George, *et al.*, 1995). These repeats are

conserved throughout the phyla. Together this points to a key functional role of the synucleins. Within this 11 aa repeat is a semi-conserved 6aa sequence, KTKEGV. The sequence degenerates as it progresses through the sequence. The 11 aa sequences allow the synucleins to form  $\alpha$ -helices. Only a small proportion (3%) exist with  $\alpha$ -helices in isolation. This proportion is dramatically increased (80%) when synucleins are exposed to vesicles (Davidson, *et al.*, 1998). The N-terminal domain is highly conserved and amphipathic. It is within this region that all PD disease mutations occur (Lill, 2016). Five of the seven 11 aa repeats are in the N terminal domain (Ueda, *et al.*, 1993). It is also the site of  $\alpha$ SYN acetylation (Duce, *et al.*, 2017).

The NAC domain is responsible for the ability of  $\alpha$ SYN and  $\gamma$ SYN to aggregate (Jain, *et al.*, 2018). When purified alone it shows faster aggregation kinetics and forms a  $\beta$ -sheet (Han, *et al.*, 1995). Its importance in  $\alpha$ SYN aggregation is underscored by its presence in the fibril core in all isolated fibril polymorphs (Guerrero-Ferreira, *et al.*, 2019). The presence of NAC aggregates can seed the aggregation of monomeric  $\alpha$ SYN and halves their nucleation time (Han, *et al.*, 1995). The pro-aggregation properties of the NAC domain stem from a 17 aa stretch of hydrophobic residues (66-82 aa) in  $\alpha$ SYN and  $\gamma$ SYN. The precise sequence is not conserved between the two synucleins, with the  $\gamma$ SYN being less hydrophobic due to a basic aa in the sequence (Jain, *et al.*, 2018). This leads to a lower aggregation propensity of  $\gamma$ SYN compared to  $\alpha$ SYN and an inability to form fibrils (Du, *et al.*, 2003). This segment is deleted in  $\beta$ SYN, which cannot aggregate as a result (Giasson, *et al.*, 2001). Disruption of this hydrophobic stretch by the addition a hydrophilic residue reduces  $\alpha$ SYNs aggregation propensity (Giasson, *et al.*, 2001). Part of this sequence is conserved (>60%) between other aggregating proteins, amyloid- $\beta$  (A $\beta$ ) and prion protein (residues 66-73) (Han, *et al.*, 1995). Due to this conservation  $\alpha$ SYN can also seed the aggregation of these proteins as well as naïve  $\alpha$ SYN (Yoshimoto, *et al.*, 1995; Han, *et al.*, 1995).

The acidic C-terminal domain of the synucleins is the least conserved (Yang, *et al.*, 1999). The acidic nature of the domain is the main determinant for the low isoelectric point of  $\alpha$ SYN (pI 4.1). It is also the location of two phosphorylation sites (Y125 and S129). As previously mentioned, p129 is of pathological significance as it is a sensitive marker for LP. Structurally the C-terminal is more disordered than the rest of the protein (Jain, *et al.*, 2018). The domain is sensitive to divalent cations and has a putative metal binding site (Lautenschläger, *et al.*, 2018; González, *et al.*, 2019). The C-terminal inhibits aggregation as deletion enhances aggregation propensity (Crowther, *et al.*, 1998; Sorrentino, *et al.*, 2018). This is underscored by the isolation of C-

terminal truncated forms of  $\alpha$ SYN from LBs (Baba, *et al.*, 1998; Campbell, *et al.*, 2001).

### 1.5.2 The pathway of aggregation

Aggregation is the process by which misfolded or intrinsically disordered proteins cluster together to form multimers. Aggregated  $\alpha$ SYN is the essential constituent of LB, where they exist as fibrils (Shahmoradian, *et al.*, 2019; Roy and Wolman, 1969). This places aggregation at the heart of PD.  $\alpha$ SYN is an intrinsically disordered protein and therefore prone to aggregation; aggregates form spontaneously when the purified protein is left at high concentration for any length of time (Jain, *et al.*, 2018; Ray, *et al.*, 2020). However, the pathway from monomer to fibril is not linear or direct, instead  $\alpha$ SYN can aggregate into many distinct structural species by aggregating along several different aggregation pathways (Alam, *et al.*, 2019). Some intermediate species can interconvert while others are stable.  $\alpha$ SYN can be pictured as a marble at the top of an undulating hill with many different routes down. The altitude represents the aggregation potential. At the top of the hill (the monomeric state),  $\alpha$ SYN has the highest aggregation potential and has the lowest stability. As the marble rolls down the hill it can come to rest at local plateaus (which represent different species) or change paths at certain points (interconversion) (Danzer, *et al.*, 2009; Lorenzen, *et al.*, 2014). As it travels down some paths it will no longer be able to access other routes (some species preclude the creation of other species). The lowest elevation is the fibrillar state of  $\alpha$ SYN. It is the most stable species, so over time  $\alpha$ SYN will tend towards fibril creation, but there are some dead-end intermediates that preclude the formation of fibrils (Smith, *et al.*, 2008).

$\alpha$ SYN aggregates can be broadly defined as either fibrils or oligomers. Fibrils are highly organised around a rich  $\beta$ -sheet core (Guerrero-Ferreira, *et al.*, 2018). Fibrils are the largest  $\alpha$ SYN aggregates, consisting of hundreds of individual monomers and measuring several hundred nanometres in length (Bousset, *et al.*, 2013). They are linear and composed of two protofilaments running in a parallel orientation (Guerrero-Ferreira, *et al.*, 2018; Guerrero-Ferreira, *et al.*, 2019). The individual monomers are stacked on top of one another, with the topmost molecule acting as a recruiting interface for fibrillar growth (Spillantini, *et al.*, 1998; Buell *et al.*, 2014). Several different fibrillar isoforms have been identified, differing in which residues form the  $\beta$ -sheet core (Guerrero-Ferreira, *et al.*, 2018; Guerrero-Ferreira, *et al.*, 2019). Oligomers are a heterogeneous class, comprised of smaller aggregates with a generally ill-defined structure. They can be  $\beta$ -sheet rich or contain  $\alpha$ -helices (Pieri, *et al.*,

2016; Cappai, *et al.*, 2005). Oligomers vary in structure from amorphous aggregates to annular structures (Lashuel, *et al.*, 2002; Danzer, *et al.*, 2007). Oligomers can be sub-divided into on or off-pathway oligomers, depending on whether they are intermediates on route to fibril creation (Lashuel and Grillo-Bosch, 2005; Celej, *et al.*, 2012; Pieri, *et al.*, 2016). Their structure remains ill-defined because they are often structurally unstable and transient. Different aggregation conditions can favour different oligomer creation, which begs the question as to which condition is most physiologically relevant in disease.

### 1.5.3 Factors governing aggregation

A wide variety of  $\alpha$ SYN species have been characterised, the majority of these isolated under *in vitro* conditions. This shows that  $\alpha$ SYN is an aggregation-prone protein, with the precise aggregation pathway taken is determined by external factors. However, a high concentration of  $\alpha$ SYN is necessary for aggregation, as it increases the likelihood of intramolecular interactions. No aggregation is seen at concentrations below 0.5  $\mu$ M (Iljina, *et al.*, 2016; Afitska, *et al.*, 2019). Analysis of the composition of rat synapses estimated endogenous  $\alpha/\beta$ -synuclein concentration at 44  $\mu$ M, indicating aggregation could occur intracellularly (Wilhelm, *et al.*, 2014). Generally in producing  $\alpha$ SYN aggregates, a concentration between 300-800  $\mu$ M is used, though aggregation at a lower concentration can be achieved through the addition of dehydrating agents such as ethanol (Danzer, *et al.*, 2007; Jain, *et al.*, 2018). High concentrations result in  $\beta$ -sheet rich oligomers which have a higher membrane permeability (Fusco, *et al.*, 2017). High temperature and agitation enhance the rate of aggregation by increasing the energy of the molecules (Ikenoue, *et al.*, 2014; Jain, *et al.*, 2018). The composition of the aggregation buffer also plays a role as pH and salt concentration will favour some  $\alpha$ SYN conformations over others- creating different aggregate species (Bousset, *et al.*, 2013; Makky, *et al.*, 2016). Lower salt concentrations lead to wide, flat 'ribbon' fibrils rather than the classic, narrow, 'rod' fibril (Bousset, *et al.*, 2013). Raising or increasing the pH change fibril leads to a twisted periodicity in the fibril chain that is not seen at physiological pH (Makky, *et al.*, 2016). Acidic conditions increases the frequency of secondary nucleation events as the monomer uses the fibril as a surface on which to aggregate (Buell, *et al.*, 2014; Gaspar, *et al.*, 2017). This indicates that aggregation could occur in low pH environments in the cell, e.g., the endo-lysosomal compartment. Both endo-lysosomal associated and cytoplasmic aggregation are observed when cells are challenged with fibrils, indicating that there are several locations for  $\alpha$ SYN aggregation inside the cell (Jiang, *et al.*, 2017). The flatter ribbon species have been amplified from PD patient brains (Van der Perren, *et al.*, 2020)

The presence of other buffer components can also affect the rate of aggregation and the type of aggregates produced. The addition of metal ions dramatically enhances fibril creation, reducing the lag time from 2 weeks to 1 day (Uversky, *et al.*, 2001). At the high concentrations, the metals used can directly interact with  $\alpha$ SYN, biasing it toward fibrillar conformations (Binolfi, *et al.*, 2006). The presence of lipid vesicles might be expected to reduce aggregation as they engender an  $\alpha$ -helical conformation of  $\alpha$ SYN rather than a  $\beta$ -sheet (Davidson, *et al.*, 1998). However, results conflict on this point. The addition of lipid vesicles enhanced aggregation as the vesicles provided a platform on which  $\alpha$ SYN can build to high concentrations, inducing aggregation (Perrin, *et al.*, 2001; Galvagnion, *et al.*, 2015; Ray, *et al.*, 2020). Lipid-dependent aggregation results in a distinct strain of annular protofibrils that are not seen in LB, indicating this might be a minor aggregation pathway (Ding, *et al.*, 2002; Shahmoradian, *et al.*, 2019).

Modification of  $\alpha$ SYN also alters the resultant aggregates. Dopamine can auto-oxidise and the resulting DA-quinone can form adducts with  $\alpha$ SYN. The presence of dopamine creates distinct non-amyloidogenic oligomers, that are SDS-stable (Cappai, *et al.*, 2005). These oligomers are small, amorphous species which can be categorised as off-pathway as dopamine addition precludes fibril formation (Cappai, *et al.*, 2005; Pieri, *et al.*, 2016). DA is a dominant regulator of aggregation as its presence inhibits iron-induced fibrillar species production (Cappai, *et al.*, 2005). 4-hydroxy-2-nonenal (HNE) modification of  $\alpha$ SYN also produces distinct oligomeric species (Näsström, *et al.*, 2011). Not all modification favours off-pathway aggregation. The PD disease mutants and p129 modification all accelerate the production of on-pathway fibrils (Conway, *et al.*, 1998; Wood, *et al.*, 1999; Conway, *et al.*, 2000; Filsy, *et al.*, 2016). The nature of the PD mutation will also affect the nature of the oligomers produced; A30P favoured the creation of annular over tubular species while A53T  $\alpha$ SYN produced both (Lashuel, *et al.*, 2002). C-terminal truncation, a physiological form of  $\alpha$ SYN also favours fibril production (Crowther, *et al.*, 1998; Li, *et al.*, 2005).

The presence of an initial aggregate has a dominant effect on  $\alpha$ SYN aggregation. The initial aggregate not only accelerates aggregation by reducing the lag period, but it can also form a template for the monomeric protein (Wood, *et al.*, 1999; Van der Perren, *et al.*, 2020). This process is called seeding. The presence of a seed eliminates the requirement for primary nucleation. The presence of a fibril accelerates aggregation as the fibril directly recruits monomers into the fibril, elongating the fibril (Buell, *et al.*, 2014). The fibril can also act as a surface for the monomer to aggregate- a process called secondary

nucleation (Gaspar, *et al.*, 2017).  $\alpha$ SYN aggregates extracted from PD brains can also seed recombinant  $\alpha$ SYN (Van der Perren, *et al.*, 2020). This provides the mechanism by which LP can progress through the CNS in a sequential manner as transmission of aggregated  $\alpha$ SYN seeds further aggregation, resulting in pathology. However, as discussed there is wide heterogeneity in  $\alpha$ SYN aggregates. Which species are relevant to PD pathophysiology and which ones are responsible for seeding pathology progression?

## 1.6 PD as a prion-like disease

Both USSLB and Braak staging indicate that Lewy pathology spreads through the brain via conserved pathways in a sequential manner. Lower brain regions are affected before higher brain regions with the initial areas having connections to the periphery. This implies the transmission of a pathogenic agent through the brain areas. One example of this is the progressive development of LBs within embryonic neural tissue transplanted in PD patients. PD patients can undergo surgery to transplant embryonic mesencephalic tissue into the midbrain, leading to significant, but temporary, motor symptom improvement. For example, one patient needed less PD medication to control her symptoms after surgery. However the symptoms worsened at 10 years post-transplantation (Kordower, *et al.*, 2008). Post-mortem analysis has discovered these grafts present with LP, with the degree of pathology correlating with time after transplantation with a 4 year old transplant showing occasional  $\alpha$ SYN positive inclusions while older transplants (12-16 years) showed numerous LBs (Li, *et al.*, 2008; Kordower, *et al.*, 2008). This provided the first evidence that PD pathology could propagate to new brain areas, even those with a different genetic background and age. While this implied the pathology spread between areas rather than arising from independent aggregation events it was not direct proof. Desplats *et al.* (2009) addressed this in a mouse model. GFP labelled mouse cortical neuronal stem cells (GFP-MCNSCs) were implanted into the hippocampus of an overexpressing human  $\alpha$ SYN mouse. After 1 week the GFP-MCNSCs showed human  $\alpha$ SYN immunoreactivity. After 4 weeks a proportion of the cells presented with spherical inclusion bodies positive for human  $\alpha$ SYN. This highlighted was the first *in vivo* evidence that  $\alpha$ SYN could transmit between neurons and cause inclusions. This demonstrated that LP is more likely to arise through the spreading of an agent rather than independent aggregation events. Since this initial study, a large body of confirmatory evidence has accumulated (Shimozawa, *et al.*, 2017; Sacino, *et al.*, 2014; Volpicelli-Daley, *et al.*, 2011; Taylor-Whiteley, *et al.*, 2019; Peelaerts, *et al.*,

2015; Gribaudo, *et al.*, 2019; Luk, *et al.*, 2012; Rey, *et al.*, 2016; Lohmann, *et al.*, 2019; Thakur, *et al.*, 2017).

Misfolded  $\alpha$ SYN fits the role of the pathogenic agent in PD: it is the main constituent of LP; it induces aggregation of endogenous  $\alpha$ SYN and can be released and internalised by neurons (Wakabayashi, *et al.*, 1997; Conway, *et al.*, 2000; Lee, *et al.*, 2005; Lee, *et al.*, 2008a). Several mechanisms for  $\alpha$ SYN transmission between cells have been established.  $\alpha$ SYN is secreted by neurons and cells as a free protein or in exosomes (Lee, *et al.*, 2005; Delenclos, *et al.*, 2017). Misfolded  $\alpha$ SYN can then be internalised by neurons through a receptor mediated process. It should be noted that the use of the receptor is not meant to imply a physiological process rather the misfolded  $\alpha$ SYN is promiscuously binding to a membrane protein that is then internalised; the protein is acting as a receptor. Several receptors have been identified for misfolded  $\alpha$ SYN, which will be expanded upon in chapter 4 (Mao, *et al.*, 2016; Hudák, *et al.*, 2019; Stopschinski, *et al.*, 2018a; Aulić, *et al.*, 2017).  $\alpha$ SYN species can be transported both retrogradely and anterogradely in neurons (Bieri, *et al.*, 2017). Once inside the cell the pathogenic  $\alpha$ SYN can seed cytoplasmic inclusions by recruiting endogenous  $\alpha$ SYN (Danzer, *et al.*, 2007).

The transmissibility of  $\alpha$ SYN has been established *in vivo*. Injection of pathogenic  $\alpha$ SYN into rodent brains leads to development of Lewy-like pathology at the injection site and in connected areas (Peelaerts, *et al.*, 2015). The location of the injection site dictates the spread of the pathology (Luk, *et al.*, 2012; Masuda-Suzukake, *et al.*, 2014; Henderson, *et al.*, 2019). This is further evidence that misfolded  $\alpha$ SYN is the agent rather than independent, sequential aggregation events in linked brain areas and instead shows that spread is dictated by anatomical connections and vulnerability. Injection of  $\alpha$ SYN fibrils leads to LP and dopaminergic cell death, causing a DA deficit reminiscent of that seen in PD patients (Thakur, *et al.*, 2017). This ability is not just an artefact of administration as BSA injection failed to spread beyond the site of administration and only showed diffuse staining (Rey, *et al.*, 2013).

As mentioned, the injection location dictates which brain regions are affected. Braak staging and USSLB of PD patients shows that lower brain regions (i.e. the DMV and OB) are affected first in prodromal patients (Braak and Del Tredici, 2017; Adler, *et al.*, 2019). This has led several groups to model this through peripheral administration of fibrillar  $\alpha$ SYN. Injection into the gut of an  $\alpha$ SYN over-expressing mouse leads to lower brain regions being affected, in accord with Braak staging, the DMV and locus coeruleus are heavily affected (Van Den Berge, *et al.*, 2019). Braak staging can also be recreated in non-transgenic (nTg) animals. Injection into the OB leads to pathology (p129

immunoreactivity) in several connected brain areas that are all affected in PD patients, such as the anterior olfactory nucleus (AON), amygdala and entorhinal cortex, (Rey, *et al.*, 2019). Misfolded  $\alpha$ SYN species can cross the blood brain barrier (BBB) and be internalised by spinal cord and cortical neurons (Peelaerts, *et al.*, 2015). BBB permeability can be enhanced by co-administration of fibrillar  $\alpha$ SYN with a modified rabies virus glycoprotein (RVG9R). A one-off tail vein injection of fibrillar  $\alpha$ SYN:RVG9R complex led to neuronal loss in the DMV, SNc and LC, all areas affected in early Braak staging (Kuan, *et al.*, 2019). p- $\alpha$ SYN was detected in the duodenum but not the OB, indicating that there are specific routes  $\alpha$ SYN can spread along in the CNS.

## 1.7 Function of $\alpha$ SYN

### 1.7.1 $\alpha$ SYN, a sensor of high membrane curvature

It is well established that  $\alpha$ SYN binds to small, negatively charged vesicles and has been labelled as a curvature sensing protein (Pranke, *et al.*, 2011). It can bind to vesicles through its positive N-terminus (Zarbiv, *et al.*, 2014). Upon binding the 11 aa imperfect repeats in the N-terminal domain form extended  $\alpha$ -helices. The positively charged lysine residues are arranged on the outside of the helix and bind to the anionic lipids (Pranke, *et al.*, 2011). Around 20 surface accessible lipids form the binding site (~40 lipids in the bilayer), this is consistent with the theoretical minimum number needed for binding to an extended  $\alpha$ -helix (Middleton and Rhoades, 2010). Disruption of the helices reduce synaptic vesicle (SV) binding (Busch, *et al.*, 2014). Due to the small linker region between the  $\alpha$ -helical stretches, one  $\alpha$ SYN molecule can bind two vesicles independently, in a double-anchor mechanism (Fusco, *et al.*, 2016).  $\alpha$ SYN preferentially binds to highly curved, small vesicles, such as SV and at packing defects in the lipid bilayer (Middleton and Rhoades, 2010). Packing defects are where there is space between the lipids, due to poor fitting between lipid tails, , a kinked unsaturated tail poorly fits in with surrounding saturated lipid tails, creating space in the lipid bilayer. Packing defects occur in lipid raft domains and in highly curved vesicles.  $\alpha$ SYN interdigitates into the head-group layer, causing lipid lateral expansion and membrane thinning (Ouberai, *et al.*, 2013; Braun, *et al.*, 2012).  $\alpha$ SYN binding to highly curved lipids therefore deforms highly curved vesicles. This reduces stress arising from high curvature and modulates the fusion propensity of SV (Ulmer, *et al.*, 2005; Ouberai, *et al.*, 2013).  $\alpha$ SYN can also induce membrane curvature, leading some to call it a curvature creating protein (Braun, *et al.*, 2012).

The ability of  $\alpha$ SYN to preferentially bind to highly curved, small vesicles arises from the poor hydrophobicity on the non-polar face of its  $\alpha$ -helices. Increasing the hydrophobicity through amino acid substitution allows  $\alpha$ SYN to bind to all vesicles, regardless of size and negative charge (Pranke, *et al.*, 2011). Although size, anionic charge and packing defects are semi-interdependent factors they can be arranged in degree of importance. Curvature is the main determinant of  $\alpha$ SYN binding, followed by anionic charge and packing defects, as the requirement of anionic lipids decreases dramatically when the radii of the vesicles are reduced (Pranke, *et al.*, 2011; Middleton and Rhoades, 2010).

The post-translational modification can affect  $\alpha$ SYN lipid binding. Physiological  $\alpha$ SYN is constitutively acetylated at its N-terminal (Duce, *et al.*, 2017). The introduction of an acetyl group doubles the vesicle binding affinity of the protein (Maltsev, *et al.*, 2012; Kang, *et al.*, 2012). It does this through enhancing the propensity to form  $\alpha$ -helical structures, this acts to prime  $\alpha$ SYN for vesicle binding by creating a docking motif. Once attached to the membrane the other  $\alpha$ -helices then form (Maltsev, *et al.*, 2012; Runfola, *et al.*, 2020).

Phosphorylation at aa 129 has also been investigated. It did not affect vesicle affinity of the wild-type protein but did alter mutant affinities. Interestingly p129 led to greater permeabilization and rupture of membranes by  $\alpha$ SYN fibrils (Filsy, *et al.*, 2016). Why phosphorylation leads to greater penetration of lipid bilayers by fibrils has not yet been elucidated. The presence of calcium can also affect lipid binding by masking the acidic residues in the C-terminal. The calcium-dependent lipid binding occurs at physiologically relevant  $\text{Ca}^{2+}$  concentrations for neurons at rest ( $K_D=21 \mu\text{M}$ ), as neuronal  $\text{Ca}^{2+}$  concentrations can reach up to hundreds of micromolar. This can enable to  $\alpha$ SYN to bind up to three different lipid membranes, which could tether up to two SV to the plasma membrane (Lautenschläger, *et al.*, 2018).

$\alpha$ SYN is intrinsically a membrane binding protein, with a preference for high curvature and can induce curvature on membranes (Braun, *et al.*, 2014). The physiological role of  $\alpha$ SYN in the cell is less well-defined. In part this is due to a lack of research, as most of the literature has focussed upon  $\alpha$ SYN's pathological function, as is the case for other neurodegenerative prion-like proteins. The investigation is made more difficult by the presence of the synuclein isoforms, beta and gamma, which can perform redundant and compensatory functions. Also, the classical way of investigating protein function via over-expression of the protein of interest is fraught with difficulty as it can induce a gain of function effect rather than replicate a physiological role for  $\alpha$ SYN. This gain of function can manifest through  $\alpha$ SYN aggregation or aberrant membrane binding. Therefore, in order to determine a physiological role for

$\alpha$ SYN there must be continuity between  $\alpha$ SYN expression level and the function. In the next section this criterion will be employed as a role for  $\alpha$ SYN in synaptic transmission is discussed.

### 1.7.2 $\alpha$ SYN-dependent regulation of synaptic transmission

Synaptic transmission is the means by which neurons communicate. For the majority of synapses, the electrical signal coming from presynaptic neuron is converted into a chemical signal in order to cross the synaptic cleft and so communicate with the other cell. The wave of electrical depolarisation enters the pre-synaptic bouton causing an influx of calcium ions. This mobilises SV, driving their fusion with the plasma membrane. There are two types of SV that can be differentiated by morphology, small clear-core vesicles, which contain small-molecule neurotransmitters such as glutamate, and large dense core-vesicles, which contain larger molecules such as brain-derived neurotrophic factor (BDNF).

From the cellular localisation of  $\alpha$ SYN in nerve terminals and *in vitro* evidence that  $\alpha$ SYN preferentially binds to small vesicles it could be hypothesised that  $\alpha$ SYN binds to SV, and therefore has a role in synaptic transmission (Maroteaux, *et al.*, 1988). However initial attempts at isolating SV bound  $\alpha$ SYN by differential centrifugation or gradient fractionation met with failure. This is because  $\alpha$ SYN dissociates from vesicles in low ionic strength conditions (Sulzer and Edwards, 2019). Electron microscopy of pre-synaptic terminals have demonstrated a predominantly SV localisation for  $\alpha$ SYN in non-transgenic animals. 74% of  $\alpha$ SYN localised to SV in the pre-synapse and 11.6% on the plasma membrane. This is comparable to the SV protein synaptobrevin-2 (VAMP2) which had 82% SV localisation/12% plasma membrane (Vargas, *et al.*, 2017). As  $\alpha$ SYN can bind to VAMP2 it could be that this high proportion of SV localisation in the pre-synapse is due to protein-protein binding rather than direct SV membrane binding (Burré, *et al.*, 2010). In agreement with its affinity for packing defects  $\alpha$ SYN can be found associated with lipid rafts when isolated from mouse brain (Fortin, *et al.*, 2004). Furthermore, the A30P mutant, which has disrupted  $\alpha$ -helices, cannot be isolated from lipid rafts, indicating this is a direct interaction of  $\alpha$ SYN with membranes *in vivo* (Fortin, *et al.*, 2004). One group have found that  $\alpha$ SYN is preferentially bound to SV that are docked to the plasma membrane rather than the free synaptic pool (Burré, *et al.*, 2014).  $\alpha$ SYN is likely acting as a negative regulator of SV docking as triple knock out of the synucleins increased SV docking to the PM (Vargas, *et al.*, 2017).

The precise physiological role of  $\alpha$ SYN in synaptic transmission is unclear. Several different functions have been proposed and will be discussed in this

section (Burré, *et al.*, 2010; Vargas, *et al.*, 2014; Logan, *et al.*, 2017). The reason for this murkiness is because of the potentially confounding gain of function effects caused by  $\alpha$ SYN overexpression. Overexpression alters  $\alpha$ SYN intracellular dynamics, pushing it towards a diffuse cytoplasmic staining rather than vesicular, pre-synaptic localisation (Fortin, *et al.*, 2004; Sulzer and Edwards, 2019). This can lead to aggregation, sequestration of molecular partners, cellular toxicity, and aberrant membrane binding, all of which will mask  $\alpha$ SYNs physiological function (Busch, *et al.*, 2014). To validate a proposed  $\alpha$ SYN physiological function there should be a correlation between  $\alpha$ SYN expression and magnitude of function. Therefore, it should be tested in a knock-out, endogenous and overexpression conditions. If the results are consistent with expression level, then the function can be acknowledged as a physiological function rather than an artefact of expression.

While several distinct functions in synaptic transmission have been proposed for  $\alpha$ SYN, these roles are not unique to  $\alpha$ SYN as deficits observed under  $\alpha$ SYN knock-out conditions can be rescued by the over-expression of the other synuclein family members (Vargas, *et al.*, 2014; Logan, *et al.*, 2017; Vargas, *et al.*, 2017).  $\alpha$ SYN has been proposed to have a roles in: SV organisation, exocytosis and endocytosis (Lautenschläger, *et al.*, 2017; Huang, *et al.*, 2019). These roles can be classified as requiring both lipid and protein binding (SV organisation), and as lipid independent (exocytosis and endocytosis). As mentioned, there is little agreement within this field and much controversy. The aim of this section is not to give a definitive role to  $\alpha$ SYN but to give an overview of the literature.

#### **1.7.2.1 $\alpha$ SYN: restricting SV motility**

SVs are organised into three distinct pools in the presynaptic terminal. Those that are docked on the membrane, and thus primed for subsequent release, are dubbed the rapid releasable pool (RRP). This pool is replenished by those SV in the recycling pool. These SV are located between 45-250 nm from the PM, though in some neurons they are closer to membrane. The third pool, the reserve pool, is not thought to be involved in basal synaptic transmission but can be mobilised for release upon high frequency or prolonged stimulation. Knock-out of  $\alpha$ SYN leads to a reduction in the reserve pool in hippocampal neurons, indicating a role of  $\alpha$ SYN as regulator of SV clustering (Murphy, *et al.*, 2000; Cabin, *et al.*, 2002). However conflicting results were found in a triple knock out (TKO) animal where an increase in distal pool clustering was noted. This is likely a compensation effect driven by upregulation of synapsin when all synuclein expression is ablated (Vargas, *et al.*, 2017). Over-expression of  $\alpha$ SYN

in yeast induces clustering of trans-golgi vesicles (Pranke, *et al.*, 2011). Over-expression in neurons resulted in an increased distal pool, and reduced motility of the pool (Nemani, *et al.*, 2010; Wang, *et al.*, 2014; Scott and Roy, 2012). Together this shows continuity with expression level and as a positive regulator of distal pool size.

*In vitro* experiments have demonstrated that  $\alpha$ SYN can cluster SV through directly binding separate SVs via its broken  $\alpha$ -helix or through its C-terminal in a calcium dependent mechanism (Fusco, *et al.*, 2016; Lautenschläger, *et al.*, 2018). It can also cluster SV through binding to the proteins associated with SV e.g. VAMP2 (Diao, *et al.*, 2013). The question remains if both mechanisms of vesicle interaction are physiologically relevant. Clustering in the distal pool is dependent on  $\alpha$ SYN directly interacting with SV lipids as  $\alpha$ -helix impaired mutants were unable to induce clustering (Wang *et al.*, 2014). It has yet to be established if  $\alpha$ SYN does this as a monomer or multimer. Other interacting partners have been identified for  $\alpha$ SYN that could help mediate SV clustering. VAMP2 and the synapsins.  $\alpha$ SYN interacts with VAMP2 through a 15aa sequence (96-110 aa) in the C terminal domain inducing SV clustering (Diao, *et al.*, 2013). Mutation of this sequence prevents  $\alpha$ SYN from interacting with VAMP2 and prevented distal pool clustering *in vitro* (Sun, *et al.*, 2019). The synapsins are a class of proteins with established roles in SV clustering and mobilisation. Silencing of the synapsins prevents  $\alpha$ SYN induced clustering and can restore it upon synapsin addition (Atias, *et al.*, 2019). This indicates that while  $\alpha$ SYN has a role in SV clustering it is dependent on synapsin (Hoffmann, *et al.*, 2021).

SV mobility is negatively correlated with  $\alpha$ SYN expression level as it leads to higher clustering in the distal pool, preventing mobilisation (Scott and Roy, 2012). Reduced SV mobility leads to slower recycling and RRP replenishment, resulting in a reduction in exocytosis events (Nemani, *et al.*, 2010). This can be reversed through removal of VAMP2 or synapsin (Atias *et al.*, 2019, Sun *et al.*, 2019). The enhanced clustering and reduced mobility of distal pool leads to a reduction in exocytosis upon  $\alpha$ SYN over-expression (Cabin, *et al.*, 2002; Larsen, *et al.*, 2006; Nemani, *et al.*, 2010; Wang, *et al.*, 2014; Logan, *et al.*, 2017). Upon knock-out of  $\alpha$ SYN the cell compensates via upregulation of synapsins, which can control distal pool clustering (Vargas, *et al.*, 2017). Synapsin-mediated distal pool clustering can be overcome through high intracellular calcium. In  $\alpha$ SYN knock-out cultures there is a shift to a lower calcium sensitivity, most likely due to the higher dependence on synapsin-mediated clustering (Cabin, *et al.*, 2002).

Together this places  $\alpha$ SYN as a coordinator of SV clustering, interacting both directly with SV and via SV related proteins.  $\alpha$ SYN can directly cluster SV through either a protein dependent mechanism, via VAMP2, or by directly binding lipids of different SV. This ability could be enhanced by the formation of  $\alpha$ SYN multimers (Wang, *et al.*, 2014; Burré, *et al.*, 2014).  $\alpha$ SYN requires synapsin for clustering. Together this allows  $\alpha$ SYN to cluster SV in the distal pool and reduce their motility.

### **1.7.2.2 $\alpha$ SYN as a regulator of exocytosis**

Exocytosis is the process of SV fusion to the plasma membrane to enable neurotransmitter release and neuronal communication. It is triggered by depolarisation of the presynaptic terminal, causing a calcium influx which triggers soluble N-ethylmaleimide-sensitive factor attachment protein receptor (SNARE) complex to fully assemble and the SV to fuse with the plasma membrane, releasing its contents into the synaptic cleft, enabling synaptic transmission. Not all SV fully fuse into the plasma membrane instead some reclose and detach, in what is called a 'kiss-and-run' event (Alabi and Tsien, 2013). The synucleins have been proposed to modulate exocytosis in several distinct mechanisms: reduction in the number of exocytotic events (as discussed); enhancement of SNARE complex assembly and plasma membrane docking; and promotion of full SV fusion (Larsen, *et al.*, 2006; Burré, *et al.*, 2010; Logan, *et al.*, 2017). The literature behind these roles will be explained.

Overexpression of  $\alpha$ SYN causes a reduction in the total number of exocytotic events. This has been shown in adrenal chromaffin cells and primary neurons (Larsen, *et al.*, 2006; Nemani, *et al.*, 2010; Logan, *et al.*, 2017; Sun, *et al.*, 2019; Atias, *et al.*, 2019). The quanta size per release event remained unchanged, ruling out an effect on SV loading. The decrease is not due to alteration in fusion dynamics as the phenotype could not be replicated by slowing down SV fusion (Nemani, *et al.*, 2010). Instead  $\alpha$ SYN diminishes the rapid releasable pool by reduction of the parent recycling pool (Nemani, *et al.*, 2010).  $\alpha$ SYN over-expression increases the distal pool, and attenuates its cycling (Nemani, *et al.*, 2010; Wang, *et al.*, 2014). Anchoring of SV in the distal pool ultimately then leads to a reduction in the number of exocytosis events.

$\alpha$ SYN can interact with the N-terminal of VAMP2 through its C-terminus. This interaction facilitates SNARE formation in a  $\alpha$ SYN concentration dependent manner, acting as a catalyst (Burré, *et al.*, 2010). A follow-up study suggested that this function may be driven by  $\alpha$ SYN membrane bound multimers (Burré, *et al.*, 2014). Removal of the synucleins reduces the rate of SNARE complex formation, leading to a deficit in SV release upon prolonged stimulation (Burré,

*et al.*, 2010).  $\alpha$ SYN is thought to act as a non-classical chaperone of SNARE assembly. Knock-out of the SNARE chaperone cysteine string protein- $\alpha$  (CSP $\alpha$ ) and the SNARE formation deficit can be rescued by  $\alpha$ SYN over-expression, indicating an overlapping role (Chandra, *et al.*, 2005; Sharma, *et al.*, 2011). However, its role as a SNARE chaperone is controversial, as one group found that  $\alpha$ SYN inhibited SNARE complex formation in a dose dependent manner (Darios, *et al.*, 2010). This discrepancy may have been the lack of liposomes in their conditions, which is a necessary component for  $\alpha$ SYN-mediated SNARE assembly (Burré, *et al.*, 2014).

As mentioned, not all SV fusion events result in complete fusion. These 'kiss and run' events are transient and only allow release of smaller cargo, such as glutamate, while retaining larger cargo, e.g. peptides such as BDNF (Jackson, *et al.*, 2015). Synucleins inhibit kiss-and-run events, preventing pore closure and enhancing dilation, leading to full vesicular fusion and accelerated release of larger cargo (Logan, *et al.*, 2017). While other groups have failed to show a clear effect of  $\alpha$ SYN in exocytosis this is most likely to differences in the tools used (Vargas, *et al.*, 2014; Xu, *et al.*, 2016). Logan *et al.* (2017) only investigated peptide transmission using BDNF-pHluorin while other groups measured quenching of vGlut-pHluorin (Vargas, *et al.*, 2014; Alabi and Tsien, 2013).

### **1.7.2.3 $\alpha$ SYN as a regulator of endocytosis**

Sustaining high rates of neurotransmission necessitate high rates of endocytosis or else the synapse will be depleted. Endocytosis and recovery of synaptic vesicles can occur through several distinct mechanisms which can be categorised by time frame. The slowest is bulk endocytosis (5s<) where large portions of the PM are internalised as endosomes. Next is the poorly defined ultrafast endocytosis (Lautenschläger, *et al.*, 2017). Clathrin mediated endocytosis (10-20s) is the best characterised process. 'Kiss and run' endocytosis occurs <1s and is when the SV fails to fully fuse with the PM but instead reseals and stays in the cytoplasm. It is thought that a mixture of these endocytic processes are at play in neurons with the precise ratios varying between neuron sub-types (Alabi and Tsien, 2013).

As a membrane curvature creating/sensing protein it is feasible that  $\alpha$ SYN may have a role in endocytosis through aiding SV invagination and budding. Synuclein knock-out results in a reduction in the rate of endocytosis, implicating  $\alpha$ SYN in clathrin-mediated endocytosis (Vargas *et al.*, 2014). However, there is no clear expression-function relationship as overexpression models also slow clathrin-mediated endocytosis (Xu *et al.*, 2016; Busch *et al.*, 2014; Medeiros *et*

al., 2017). Electron microscopy reveals that over-expression of  $\alpha$ SYN into the synapse results in a build-up of chaperone mediated endocytosis (CME) intermediates and large invaginations of the membrane (Busch, *et al.*, 2014). This is likely an aberrant phenotype rather than an amplification of a physiological role, as it can result from promiscuous binding of overexpressed  $\alpha$ SYN to the membrane, obstructing normal CME. Therefore, a lipid dependent role for  $\alpha$ SYN in endocytosis that is consistent with expression level cannot yet be established.

A negative regulatory role in 'kiss and run' endocytosis was first hypothesised by Lautenschläger *et al.*, (2017).  $\alpha$ SYN was posited to promote 'kiss and run' by stabilising the SV curvature during a fusion event, making full fusion less likely. Logan *et al.*, (2017) investigated this. Single synaptic fusion events are difficult to detect via imaging, so they instead opted to measure large dense core vesicles (LDCVs) instead due to their larger size (70-200nm). 'Kiss and run' events were measured through dispersion of large LDCV cargo (BDNF, and neuropeptide Y). Contrary to the hypothesis,  $\alpha$ SYN expression level negatively correlated with 'kiss and run' fusion. TKO increased the number of closure events in neurons while overexpression reduced it. Inhibition of 'kiss and run' events directly enhanced release of large cargo.  $\alpha$ SYN enhanced pore dilation, promoting full membrane fusion and slowing endocytosis by preventing kiss and run fusion events. However, LDCV 'kiss and run' events only account for a small amount (<10%) of hippocampal neuron transmission giving  $\alpha$ SYN a limited role in endocytosis (Logan, *et al.*, 2017). Two outstanding questions need to be answered to determine the degree of physiological relevance. Is 'kiss and run' endocytosis relevant for SV fusion in dopaminergic neurons? And does  $\alpha$ SYN also promote pore dilation of dopaminergic neuron SV? 'Kiss and run' endocytosis has been observed for dopamine release from midbrain neurons (Staal, *et al.*, 2004). The later question has not been directly addressed. SNCA<sup>-/-</sup> neurons do not show any difference in the amount of extracellular DA released but did show reduced paired pulse depression. This is partially consistent with a role for  $\alpha$ SYN in 'kiss and run' endocytosis as in knock-out conditions higher levels of 'kiss and run' endocytosis would result in less paired pulse depression (Abeliovich, *et al.*, 2000). However, with this a lower extracellular DA release would also be expected. To resolve the question DA release should be investigated in TKO neurons to remove any confounding compensation effect of other synucleins.

### 1.7.3 $\alpha$ SYN in metal ion binding and mitochondrial dynamics

Roles in the nucleus, mitochondria and metal binding have been posited for  $\alpha$ SYN. Over-expression of  $\alpha$ SYN leads to mitochondrial and nuclear localisation. This leads to mitochondrial fission through a dynamin-related protein 1 independent mechanism and aberrant gene transcription (Nakamura, *et al.*, 2011). Both phenotypes can be exacerbated when tested on a background of cellular stress. These studies rely on overexpression of  $\alpha$ SYN, which can reveal a pathological function but is limited in establishing a physiological role. Many of these studies fail to investigate whether there is a corresponding effect upon  $\alpha$ SYN KO. Nakamura *et al.* (2011) found that there was no corresponding effect on mitochondria morphology in TKO midbrain neurons. The effect on mitochondria was only present in an overexpression conditions, indicating an aberrant gain of function rather than a physiological role.

$\alpha$ SYN has been shown to interact with divalent ions. Interactions between  $\alpha$ SYN and iron, magnesium, copper, calcium, zinc, cobalt and nickel have been described, with a focus on their effects on aggregation propensity (González, *et al.*, 2019). However these initial studies used millimolar concentrations of the ions, far in excess of physiological tissue concentrations (Uversky, *et al.*, 2001). When tested at physiologically relevant concentrations only calcium and copper have been found to interact with  $\alpha$ SYN (Binolfi, *et al.*, 2006; Lautenschläger, *et al.*, 2018). Some have suggested a physiological role for copper in modulating  $\alpha$ SYN/lipid binding. Copper interacts with  $\alpha$ SYN at two binding sites; a high affinity site in the N-terminus and a low affinity binding site at histidine 50, an important residue as H50Q is a PD causing mutation (Mason, *et al.*, 2016). Both copper redox states enhance the  $\alpha$ -helical content of both acetylated and non-acetylated  $\alpha$ SYN, enhancing lipid binding (Miotto, *et al.*, 2015; Miotto, *et al.*, 2017; Lucas and Lee, 2011). It can also bind to membrane bound  $\alpha$ SYN. This interaction is conserved between synucleins as  $\text{Cu}^{1+}$  also promoted  $\alpha$ -helical content in  $\beta$ SYN (Miotto, *et al.*, 2017).  $\text{Cu}^{1+}$  is the predominant ion and is particularly enriched in SV, where it reached 290  $\mu\text{M}$  compared to 16  $\mu\text{M}$  in the cytoplasm (Scheiber, *et al.*, 2014). This indicates a functional relevance of  $\alpha$ SYN copper binding.

## 1.8 Neuronal susceptibility as a factor governing seeding and LP development

### 1.8.1 Synaptic and local spread of $\alpha$ SYN is not sufficient for pathology development

Prion-like spreading conjures a picture of an indiscriminate wave of seeding and propagation, infecting all cells, causing a tsunami of cell dysfunction and death. This does not align with the picture of PD neuropathologically; LP appearance is discrete and patchy. Braak staging itself demonstrates the selectivity of spread with specific nuclei and regions being affected. Prion-like spreading can occur through the connectome, via synaptic connections, and through local diffusion.  $\alpha$ SYN can be transported both retrogradely and anterogradely in neurons but  $\alpha$ SYN transmission favours anterograde transport, in agreement with the caudorostral spread of LP (Mezias, *et al.*, 2020). The strength of connections does not predict spread as linked regions do always develop pathology proportionate to the strength of the connections (Henrich, *et al.*, 2020). This demonstrates while the connectome is necessary for  $\alpha$ SYN spread it is not sufficient and other factors regulate pathology development (Oliveira, *et al.*, 2019; Henderson, *et al.*, 2019).

Mechanisms for connectome-independent, local  $\alpha$ SYN spread have been demonstrated *in vitro*.  $\alpha$ SYN can be transferred between neurons via tunnelling nanotubes, an overflow mechanism to reduce  $\alpha$ SYN load on the neurons degradation machinery (Lee, *et al.*, 2013; Abounit, *et al.*, 2016). Similarly,  $\alpha$ SYN can be released and transmitted via exosomes, another mechanism for local transmission (Lee, *et al.*, 2005; Emmanouilidou, *et al.*, 2010; Danzer, *et al.*, 2012; Gustafsson, *et al.*, 2018). Free  $\alpha$ SYN can also be internalised by cells through endocytosis or through direct membrane penetration. Pathogenic  $\alpha$ SYN can rupture membranes, this ability not only potentiates its seeding capacity, allowing escape from the endo-lysosomal compartment, but also allows it to escape apoptotic bodies and directly penetrate the plasma membrane (Jiang, *et al.*, 2017). However, despite the plethora of mechanisms for local  $\alpha$ SYN transmission only a subset of neurons within a nuclei develop pathology (Kingsbury, *et al.*, 2010; Henrich, *et al.*, 2020). The mechanisms for synaptic spread and local spread of  $\alpha$ SYN exist but evidence for their widespread implementation in post-mortem patient brains is lacking, indicating other factors must regulate  $\alpha$ SYN spread.

### 1.8.2 Selective neuronal susceptibility in PD

The selectivity of  $\alpha$ SYN seeding and LP development in PD depends on the neuron phenotype. Different neuronal sub-types have differing susceptibilities to  $\alpha$ SYN seeding. DA neurons are particularly vulnerable in PD but there is even variability between DA neuron sub-types (Anderegg, *et al.*, 2015; Pacelli, *et al.*, 2015). GABAergic neurons in the DMV and pedunclopontine nucleus (PPN) never develop LP while this resistance is not seen for striatal GABAergic neurons (Mori, *et al.*, 2008). The lack of a conserved susceptibility among neuronal sub-types indicates that neuronal susceptibility to LP is determined by a constellation of factors not neurotransmitter expression alone. Factors identified are:  $\alpha$ SYN expression, neurotransmitter expression, autophagic capacity, calcium binding protein expression (CaBP), arborisation, neuronal firing, reliance on oxidative phosphorylation and amount of mitochondrial DNA deletions (Mosharov, *et al.*, 2009; Elstner, *et al.*, 2011; Pacelli, *et al.*, 2015; Flores-Cuadrado, *et al.*, 2016; Rendón-Ochoa, *et al.*, 2018; Erskine, *et al.*, 2018; Courte, *et al.*, 2020). These will be expanded on in chapter 5. These cell-autonomous factors improve our understanding of neuron susceptibility but are only one part of the equation, that of neuronal vulnerability. Factors of neuronal resistance must also be considered if we are to fully understand neuronal susceptibility and how it relates to the selective spread of LP.

### 1.8.3 Neuronal resistance in another prion-like disease context

Like PD, AD is a neurodegenerative disease with prion like components and selective neuronal susceptibility. In AD, the prion-like agents are amyloid- $\beta$  ( $A\beta$ ) and hyperphosphorylated tau. The extracellular matrix (ECM) is an overlooked factor in neurodegenerative disease. The ECM occupies the space between cells and plays an essential role in many CNS functions, e.g. neuronal migration and synaptic signalling (Dityatev and Rusakov, 2011; El Ayachi, *et al.*, 2011). It is formed of glycosaminoglycans (GAGs) and proteins and alters the diffusion of molecules through it (Syková, *et al.*, 2005; Zamecnik, *et al.*, 2012; Soria, *et al.*, 2020). There is a specialised form of the ECM, called the perineuronal net (PNN) that enwraps specific neurons, creating a dense pericellular coat (Fawcett, *et al.*, 2019). The PNN has been established as a neuroprotective factor against oxidative stress and prion-like seeding (Suttkus, *et al.*, 2016a).

Investigation of PNN neurons in AD has discovered that the numbers of PNN neurons are unchanged between AD patients and age-matched controls (Morawski, *et al.*, 2010a). Neurofibrillary tangles (intraneuronal plaques of hyperphosphorylated tau) were never found in PNN-bearing neurons, except in

rare circumstances (3 out of 700 PNN positive neurons) (Brückner, *et al.*, 1999). This effect was conserved between cortical and sub-cortical regions and between PNN positive neuron sub-types (pyramidal and non-pyramidal) (Brückner, *et al.*, 1999; Morawski, *et al.*, 2010a). Gross examination found a segregation between tangle rich and PNN rich areas, indicating a resistance phenotype (Brückner *et al.*, 1999). In an oligomeric-tau transmission model, around 40% of PNN-negative neurons internalised tau-oligomers compared to 10% of PNN neurons (Suttkus, *et al.*, 2016b). This demonstrates that PNN neurons were 4 times less likely to internalise extracellular pathogenic seeds, leading to PNN rich areas showing little tangle presence. There was partial overlap between PNN areas and those containing A $\beta$  plaques, with PNN neurons co-existing in plaque heavy regions (Yasuhara, *et al.*, 1994; Brückner, *et al.*, 1999). Quantification of PNN neurons in an AD mouse model demonstrated that the PNN population was unaffected by A $\beta$  plaque development (Morawski, *et al.*, 2010b). Neurons with an extracellular CSPG-coat were fourfold less vulnerable to A $\beta$ -induced toxicity than those without. This protection was dependent on the PNN-like coat as its digestion ablated the resistance phenotype (Miyata, *et al.*, 2007). Together this establishes that the PNN is a neuroprotective structure in AD. As PD and AD both share a prion-like component it can be hypothesised that the PNN is also a neuroprotective structure in PD. The testing of this hypothesis is the aim of this thesis.

## 1.9 The Perineuronal Net (PNN)

A subset of neurons in the CNS are wrapped by a specialised structure called the PNN, a compound structure of protein and sugar. The PNN coats the soma and the proximal dendrites of neurons and has a reticular morphology. It coats a variety of different neuron subtypes. The largest subgroup is the parvalbumin (PV) positive interneurons. 40-80% of PV neurons are wrapped by PNNs (Ueno, *et al.*, 2017a; Yamada and Jinno, 2017; Ueno, *et al.*, 2018a). Excitatory and motor neurons also express PNNs. PNNs are highly expressed in multiple brain regions. Further notable populations are: the CA2 region of the hippocampus; Golgi and large excitatory deep cerebellar neurons in the cerebellum and around motoneurons in the spinal cord (Yamada and Jinno, 2017; Carulli, *et al.*, 2006; Carulli, *et al.*, 2007; Galtrey and Fawcett, 2007; Irvine and Kwok, 2018). The PNN primarily functions as a restrictor of plasticity and regulator of synapse stabilisation (Frischknecht, *et al.*, 2009; Schweitzer, *et al.*, 2017; Favuzzi, *et al.*, 2017; Fawcett, *et al.*, 2019). Its removal re-opens plasticity and alters the excitatory: inhibitory synapse input onto PNN neurons (Geissler, *et al.*, 2013; Donato, *et al.*, 2013; Favuzzi, *et al.*, 2017; Edamatsu, *et al.*, 2018;

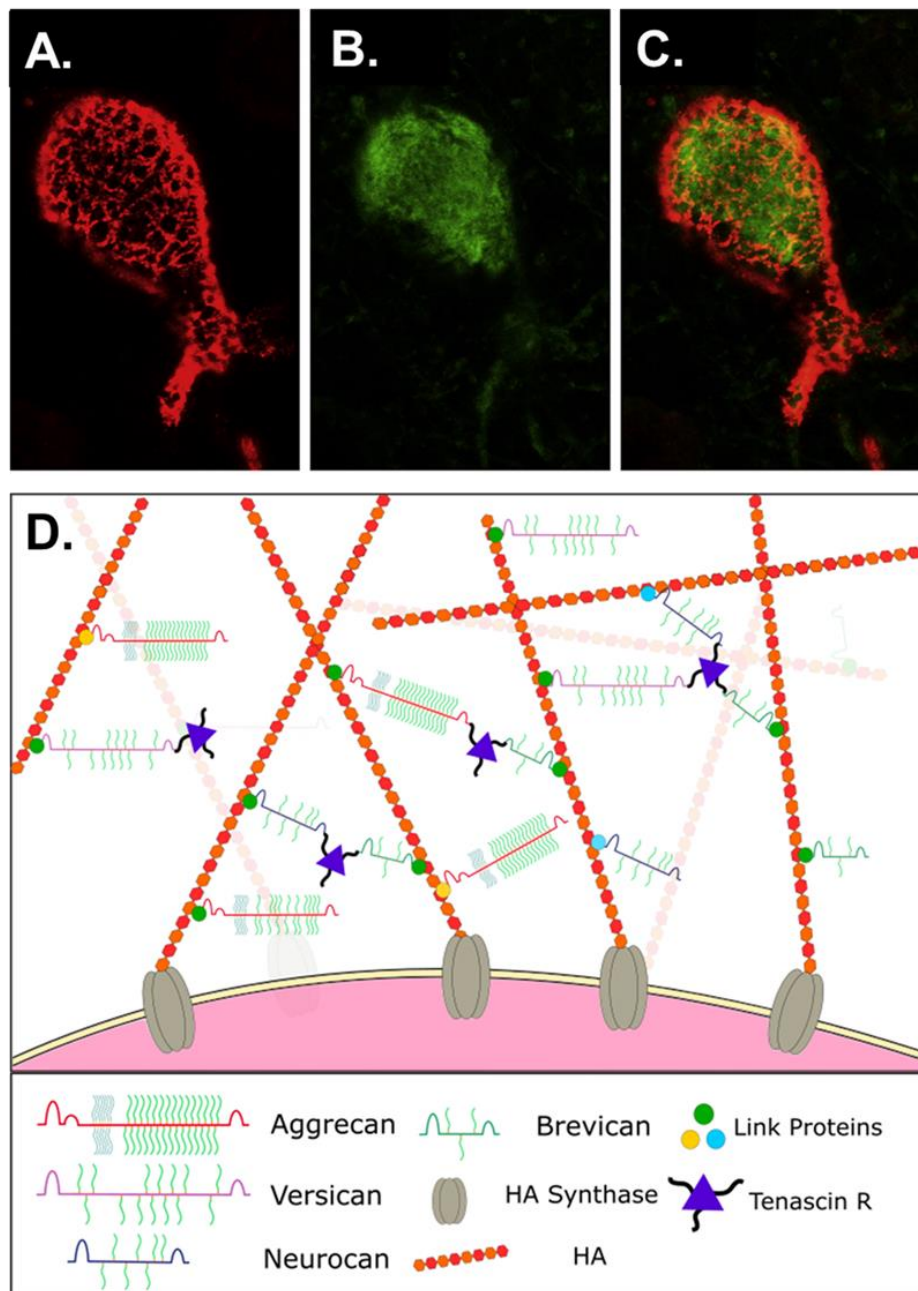
Gottschling, *et al.*, 2019). It is highly negatively charged which allows it to act as an ion sink (Morawski, *et al.*, 2015). This enables PNN neurons to sustain long trains of action potentials (Balmer, 2016). The classic mature PNN morphology, found on cortical PV neurons, is a honey-comb structure that extends over the cell body and the proximal dendrites. The holes are filled by synapses, which are stabilised by the PNN (Dityatev, *et al.*, 2007; Carulli, *et al.*, 2020). Other PNN morphologies exist, i.e. motoneurons present with a thick perisomatic PNN as shown by CSPG staining (Smith, *et al.*, 2015). The reason for this structural variety is unknown but most arises from a different component composition. PNN development and maturation will be expanded on in chapter 3.

### 1.9.1 PNN composition

The PNN is an assembly of protein and sugar wrapping around a neuron (Fig. 4). PNN components can be broken down into 4 categories: the hyaluronan (HA) scaffold, the HA and proteoglycan link proteins (hapln); proteoglycans; and crosslinkers and signalling molecules (Sorg, *et al.*, 2016). Each class comprises of several different members. The reasons for this variety and apparent redundancy are currently unresolved. All PNN components associate onto a megadalton hyaluronan scaffold. The HA backbone is synthesised by the PNN bearing neurons (Carulli, *et al.*, 2007; Kwok, *et al.*, 2010). The proteoglycans bind to the HA and the binding is stabilised by the addition of a hapln (Kwok, *et al.*, 2010). The cross-linkers and signalling molecules either bind to the HA backbone or the proteoglycan. The addition of hapln proteins and cross-linking molecules condense the PNN structure, creating a dense barrier (Kwok, *et al.*, 2010; Morawski, *et al.*, 2014).

The PNN is a negatively charged structure which allows it to repel negatively charged reactive oxygen species (ROS) (Cabungcal, *et al.*, 2013). Its polyanionic nature arise from the high density of negatively charged GAGs located within it. The GAGs are: HA, chondroitin sulphate (CS), dermatan sulphate (DS) and heparin sulphate (HS). Of the sulphated GAGs, CS and HS are the most abundant within the PNN and both can be differentially sulphated (Deepa, *et al.*, 2006). Except for HA, these GAGs are conjugated on proteoglycans anchored to the PNN. A proteoglycan is a protein with multiple GAG chains covalently attached to the protein core. They can be further categorised depending on the underlying protein structure and the type of GAGs attached. The CS proteoglycans (CSPGs) are the most well studied in the PNN compared to HS proteoglycans (HSPGs). Five PNN CSPGs have been identified: phosphacan (pcan) and the four members of the lectican family, aggrecan (acan), brevican (bcan), neurocan (ncan) and versican (vcan). Pcan is

the soluble form of receptor protein tyrosine phosphatase zeta (RPTP $\zeta$ ). The number of glycosylation sites differs between the CSPGs. Aggrecan is the most glycosylated (~120) and brevican is the least (~3) (Yamaguchi, 2000). On lecticans, the predominant PNN CSPGs, the CS chains are tens of kilodaltons long and are bound to the middle domain of the elongated CSPG, creating a bottlebrush-like structure. There may also be heterogeneity in the degree of glycosylation and the GAG composition of the PNN but this has not yet been directly investigated.



#### ◀Figure 4 The perineuronal net

A-C. Mature cortical PNN as stained by *Wisteria floribunda* agglutinin (WFA, red) surrounding a parvalbumin positive interneuron (PV, green). The reticular morphology extends around the soma and cortical dendrites. Images are adapted from (Vo *et al.* 2013). D Hyaluronan (HA) synthases on the cell membrane extrude HA into the extracellular matrix. They act as both a receptor and an enzyme. A variety of chondroitin sulphate proteoglycans (CSPGs), the bottlebrush structures, bind the HA. This interaction is stabilised by link proteins (haplins). Tenascin R can interact with up to three C-terminals of CSPGs and may act as a cross linker between them. Together the link proteins and the tenascins condense the PNN into a dense structure. The chondroitin sulphate (CS), shown in green on the CSPGs, are highly negative and contribute to the polyanionic environment of the PNN which allows the sequestration of ions. Image taken from (Warren *et al.* 2018).

### 1.9.2 PNN as a neuroprotective barrier in PD

Based on this evidence, it is feasible that the PNN is a factor of neuronal resistance in PD. The case is strengthened by comparing PNN populations to the pattern of LP spread. Areas of high PNN density, e.g. the red nucleus and substantia nigra pars reticulata (SNr) both fail to develop LP and are spared from neuronal loss (Hardman, *et al.*, 1996; Brückner, *et al.*, 2008; Rácz, *et al.*, 2016; Surmeier, *et al.*, 2017b). Both mechanisms of neuroprotection could play a role in PD, by denying  $\alpha$ SYN membrane access and protecting the neurons from ROS produced by microglia. Therefore, the aim of this thesis will be to investigate if the PNN plays a neuroprotective role in PD

### 1.10 Objectives of this thesis

In this chapter we have introduced PD and the key role of  $\alpha$ SYN seeding in driving LP spread. We have shown that LP spread is selective and specific, following a conserved pathway through the brain. This pattern cannot be solely explained by the connectome, selective neuronal susceptibility also plays a role in dictating LP spread. Previous work examining neuronal susceptibility in PD has focussed on factors underlying neuronal vulnerability, neglecting potential factors of neuronal resistance. The PNN is a pericellular barrier that plays a neuroprotective role in AD, a disease with a similar prion-like mechanism. We posit that the PNN could play a similar neuroprotective role in PD by restricting  $\alpha$ SYN seeding. The overarching objective of this thesis is to establish a neuroprotective role for the PNN in PD. This will be done use of  $\alpha$ SYN seeding paradigms on *in vitro* PNN cell culture model and confirming the validity of these results through examining PNN populations in post-mortem PD brains.

The explicit aims of this study are:

1. To establish a cortical PNN cell culture which accurately models *in vivo* cortical PNNs.
  - a. Demonstrate that this PNN culture replicates the reticular morphology of mature PNNs as they would appear within the mature CNS.
  - b. Characterise the *in vitro* PNN population for: identity, composition, and heterogeneity. The PNN population will be quantified to give a population overview.
  - c. Track the development of the PNN in culture and determine if it resembles development *in vivo*.
  
2. To investigate whether the presence of a PNN reduces the internalisation of pathogenic  $\alpha$ SYN and seeding *in vitro*.
  - a. Create and characterise monomeric, oligomeric and fibrillar  $\alpha$ SYN.
  - b. Investigate the ability of the PNN to reduce seeding in a PNN-HEK model.
  - c. Determine if the PNN reduces internalisation of  $\alpha$ SYN oligomers.
  - d. Determine if the PNN reduces the development of p- $\alpha$ SYN pathology development.
  - e. Is this neuroprotective effect of PNN incidental to a broader PNN neuron phenotype or integral to it?
  
3. To investigate if PNN populations are affected in late-stage post-mortem PD brains.
  - a. Examine PNN densities in LP affected brain regions.
  - b. Examine the propensity of PNN neurons develop LP.
  - c. Determine if there is segregation between PNN rich and LP rich areas.

## Chapter 2 Methods

### 2.1 Animals

E19 pregnant adult, female and pre-weaners (P0-6) Wistar rats were used. All animals were housed in standard housing conditions with a 12 hour light / dark cycle with food *ad libitum*. The time mated pregnant females were singly housed. The work was performed under the regulations of the Animals Scientific Procedures Act 1986 and covered by the Home Office project license (#70/8085) and PIL for Stuart Dickens (#I9C757118).

### 2.2 Primary cell culture

#### 2.2.1 Neuronal culture

E18, cortical cultures were created from Wistar rats. The pregnant female was euthanised with CO<sub>2</sub> and decapitated, the pups were decapitated and the heads cooled to 4°C on ice. The cortices were dissected out and suspended in cold Hank's buffered salt solution, without ions (HBSS-) (ThermoFisher #11590466). The media was then aspirated and the cortices digested with filter-sterilised papain (2 mg/ml in HBSS-, Lorne Laboratories #LS003119) for 6 min at 37 °C. Filter-sterilisation was done here and in the following cases using a 0.22 µm filter (Merck-Millipore #10596512) To degrade released DNA, DNase I was added to a final concentration of 50 µg/ml (Sigma #DN25). The cell containing supernatant was then taken and centrifuged at 100 x g, 2 min, RT. The cells were resuspended in Neurobasal with 2% B27, 0.4 mM Glutamax and 0.1% antibiotic-antimycotic (ThermoFisher #21103049, #17504044, #35050038, #15240062). An aliquot was taken, diluted 1:1 with trypan blue (ThermoFisher #15250061) and manually counted with a haematocytometer. Cells were plated at 100,000 cells/well in a 24 well plate containing 40 µg/mL poly-D-lysine treated coverslips. The 24-well plate contained isolated chimney wells and sterile H<sub>2</sub>O was added in between to reduce evaporation and improve even heating. The coverslips (SLS #MICC3336) were boric acid washed and etched with sodium hydroxide, washed in H<sub>2</sub>O and autoclaved. Before plating they were incubated with 40 µg/ml of poly-D-lysine (Sigma #P0899) in water for 2 hrs at RT. They were then washed three times with sterile PBS before left to warm in the incubator with media.

After plating, half the neuronal media volume was replaced twice a week. For the first 7 days the neurons were fed with Neurobasal with additives. From 7-14 day *in vitro* (DIV) the media was replaced with BrainPhys media with 2% SM1 and antibiotic-antimycotic (StemCell Technologies #5792). From 14 DIV, the

media was replaced with 1:1 BrainPhys with SM1 and astrocyte conditioned BrainPhys.

### **2.2.2 Astrocyte culture**

Astrocytes from P0-6 Wistar rats were harvested in accordance with the UK Home Office guidelines. The pups were decapitated, and the brains dissected out. The cortices were then removed and manually dissociated with a sterile blade. The mixture was then digested for 20 min with a 0.1% filter-sterilised trypsin solution (Sigma #T0303) at 37 °C. DNase I was added as before. The cell containing solution was then centrifuged at 100 x g, 5 min, RT. The pellet was then resuspended in DMEM + 10% foetal bovine serum (FBS) with antibiotic-antimycotic (Lonza #12-707F, ThermoFisher #15240062). The cells were then titrated with fire polished glass pipettes with different apertures. The cells were then plated in 40 µg/mL poly-L-lysine coated culture flasks. The media was then replaced the following day and every three days hence. Once the flasks were confluent the cell population was enriched for astrocytes using differential adhesion. The flasks were shaken at 125 rpm overnight to remove contaminating cells. The astrocytes were then split and upscaled into larger flasks. Once the cultures reached 70-100% confluent the media was replaced with BrainPhys with additives for 48 hrs. The conditioned media was then centrifuged to remove contaminating cells and filter sterilised.

## **2.3 Immunocytochemistry**

### **2.3.1 Neurons**

Neurons were fixed at room temperature in 4% paraformaldehyde, 3% sucrose solution for 10 minutes. The cells were then washed in 3% sucrose then permeabilised with 0.01% triton x-100 for 10 minutes. Non-specific binding sites were blocked by incubation with 3% normal donkey serum (Sigma #D9663) in Tris buffered saline (TBS) for 1 hr at room temperature. The neurons were then incubated with primary antibodies (see table 2), diluted in blocking solution, overnight at 4 °C. The following day the neurons were then washed with TBS and incubated with the appropriate secondary antibodies, diluted in blocking solution, for 2 hours at room temperature. They were then washed in TBS and mounted onto SuperFrost microscope slides (Fisher Scientific Ltd #10149870) using Fluorsave (Merck #345789).

**Table 2 Antibodies used in thesis**

Antibody	Species Origin	Dilution	Working concentration (µg/mL)	Company (Product no.)
<b>1° antibodies</b>				
Anti-aggrecan	Rabbit	1:250	2	Millipore (AB1031)
Anti-αSYN	Mouse	1:250	4	Sigma (S5566)
Anti-β <sub>3</sub> Tubulin	Chicken	1:500	0.6	Abcam (ab41489)
Anti-β <sub>3</sub> Tubulin	Mouse	1:500	4	Abcam (ab6267)
Anti-brevican	Sheep	1:250	0.8	R&D Systems (AF4009)
Biotinylated-HABP <sup>1</sup>	-	1:250	1	AMS Bio (AMS.HKD.B141)
Anti-HAPLN1	Goat	1:250	4	R&D Systems (AF2608)
Anti-HAPLN2	Rabbit	1:100	0.5	Novus Biologicals (NBP1-91977)
Anti-HAPLN4	Goat	1:100	10	Novus Biologicals (AF4085)
Anti-NeuN	Guinea-pig	1:500	2	Synaptic Systems (266004)
Anti-neurocan	Mouse	1:50	7.38	DSHB <sup>2</sup> (1F6)
Anti-parvalbumin	Mouse	1:500	2	Novus Biologicals (NBP2-50038SS)
Anti-phosphacan	Mouse	1:50	3.3	DSHB <sup>2</sup> (3F8)
Anti-p129 αSYN	Rabbit	1:500	2	Abcam (ab51253)
Anti-tenascin-R	Goat	1:250	4	R&D Systems (AF3865)
Anti-versican	Mouse	1:100	1.69	DSHB <sup>2</sup> (12C5)
Biotinylated-WFA	-	1:300	6.6	Sigma (L1516)
<b>2° antibodies</b>				
Hoechst	-	1:30,000	0.33	Invitrogen (H3570)
CF <sup>TM</sup> 405 M anti-guinea-pig	Donkey	1:500	4	Sigma (SAB4600468)
AF <sup>1</sup> 405 anti-goat	Donkey	1:500	4	Abcam (Ab175664)
Pacific blue streptavidin	-	1:500	4	Invitrogen (S11222)
AF <sup>1</sup> 488 anti-rabbit	Donkey	1:500	4	Invitrogen (A21206)
AF <sup>1</sup> 488 streptavidin	-	1:500	4	Invitrogen (S32354)
AF <sup>1</sup> 568 anti-goat	Donkey	1:500	4	Invitrogen (A11057)
AF <sup>1</sup> 568 anti-mouse	Donkey	1:500	4	Invitrogen (A10037)
AF <sup>1</sup> 568 anti-rabbit	Donkey	1:500	4	Invitrogen (A10042)
AF <sup>1</sup> 568 streptavidin	-	1:500	4	Invitrogen (S11226)
640/660 Neurotrace <sup>TM</sup>	-	1:150	-	Invitrogen (N21483)
AF <sup>1</sup> 647 anti-IgY chicken	Goat	1:500	4	Invitrogen (A21449)
AF <sup>1</sup> 647 anti-mouse	Donkey	1:500	4	Invitrogen (A31571)

1 HABP: Hyaluronan binding protein

2 DSHB: Developmental studies hybridoma bank

3 AF: Alexa Fluor

## 2.4 Imaging, quantification, and statistics

Imaging was performed either using a LSM880 confocal microscope (Zeiss) with 20x and 63x objectives or a AxioScan Z.1 Slidescanner (Zeiss) with a 20x objective. The Slidescanner was operated by the Bioimaging facility. For confocal, coverslips were imaged with 20x objective and tile-scanning for quantification. High resolution images were created by z-stack imaging with 63x objective. A projection image was then created using max intensity plugin on ImageJ. For the Slidescanner, tile images with 20x objective were taken and stitched to provide entire coverslip image. Filters were set to ensure no overlap between channels. For quantification regions of interest were imaged and PNNs were identified and counted based on morphology. OriginPro 2019b was used in graph creation and statistical analysis. Tests for significance ( $p < 0.05$ ) were performed using either: one-way analysis of variance (ANOVA) with Tukey's post hoc test or two-way Student's t-test.

## Chapter 3 Establishment and characterisation of PNN culture model that replicates PNN maturation and heterogeneity

### 3.1 Introduction

During postnatal development there are periods of heightened plasticity where experience drives organisation of neural circuitry, this allows individuals to adapt behaviours to their environment. These windows are called critical periods (CPs) and are conserved across species (Reha, *et al.*, 2020). They are most clearly observed in the development of sensory processes e.g. vision and auditory organisation. An example of a conserved CP is the acquisition of language in humans and of song in songbirds (Cornez, *et al.*, 2018). The classical example of CP development is the monocular deprivation paradigm in the visual cortex. Occlusion of one eye causes cortical neurons to favour input from the non-deprived eye, creating a bias. If the occlusion is removed before CP closes then the bias disappears, if the occlusion is removed after CP closure then the bias persists, indicating neural wiring has solidified (Pizzorusso, *et al.*, 2002). CP closure is linked to the maturation of inhibitory, parvalbumin positive neurons. Timely PNN development around PV neurons is required for their maturation (Ye and Miao, 2013). Therefore, CP opening, and closure depends in part on the PNN. Degradation of the PNN is sufficient to reopen a CP (Pizzorusso, *et al.*, 2002; McRae, *et al.*, 2007; Popelář, *et al.*, 2017).

The PNN is a key regulator of plasticity and are conserved across species (Lander, *et al.*, 1997; Adams, *et al.*, 2001; Matthews, *et al.*, 2002; Cornez, *et al.*, 2018; Edwards, *et al.*, 2020). It stabilises existing synapses and restricts new synapses onto the enwrapped neurons (Geissler, *et al.*, 2013; Gottschling, *et al.*, 2019). Prolonging the CP via monocular deprivation, delays PNN development (Guimarães, *et al.*, 1990). PNN attenuation, through component knock out, prevents CP closure (Carulli, *et al.*, 2010). Continued CP closure depends on the PNN as degradation reawakens experience-dependent plasticity (Pizzorusso, *et al.*, 2006). Reawakening latent CNS plasticity has great utility in disease treatment, e.g. spinal cord injury (Siebert, *et al.*, 2011). Reawakening juvenile plasticity through PNN manipulation holds great hopes for treating spinal cord injury and stroke. Currently the only way to manipulate the PNN is through the generalised destruction of the ECM by enzymatic degradation (Fawcett, *et al.*, 2019). This can lead to maladaptive plasticity (Rankin-Gee, *et al.*, 2015). Improving understanding of PNN development and how it exerts its function is key to finer manipulation of plasticity.

### 3.1.1 PNN development and maturation

#### 3.1.1.1 Expression of PNN components

PNN structures develop postnatally between P7 and 56 in the rodent and between 1 month to 20 years of age in humans, coinciding with CP development (Carulli, *et al.*, 2006; Mauney, *et al.*, 2013; Rogers, *et al.*, 2018). The precise timing of PNN development varies between brain regions (del Rio, *et al.*, 1994; Köppe, *et al.*, 1997; Brückner, *et al.*, 2000). This variation reflects the staggered timing of CPs in the CNS, with lower CNS regions preceding higher regions. As the PNN matures it transitions from a punctate morphology to a contiguous, reticular structure (Ueno, *et al.*, 2017b; Lipachev, *et al.*, 2019; Sigal, *et al.*, 2019). The punctate morphology represents an immature PNN phenotype as it is linked to persistent juvenile plasticity (Bukalo, *et al.*, 2001; Brückner, *et al.*, 2000; Carulli, *et al.*, 2010; Rowlands, *et al.*, 2018; Eill, *et al.*, 2020). During PNN development, the mRNA expression of PNN components rise and peak. Peak timing varies between component and region (Hirakawa, *et al.*, 2000; Carulli, *et al.*, 2007; Galtrey, *et al.*, 2008; Gao, *et al.*, 2018). For example, in the cerebellum, *ncan* mRNA expression peaks between P3-7 while *acan* mRNA peaks later, between P14-21 (Carulli, *et al.*, 2007). The peak of a component even differs between brain areas; the *Ncan* peak occurs later in the cortex (P10) and spinal cord (P14-P21) (Galtrey, *et al.*, 2008; Gao, *et al.*, 2018). The peak timing corresponds with PNN formation and the staggered maturation of CNS regions but a direct relationship between a single PNN component and PNN maturation has not been identified (Köppe, *et al.*, 1997).

#### 3.1.1.2 Cellular origin of PNN components

The PNN is an extracellular structure and components originate from both the host neuron and other sources (Carulli, *et al.*, 2006; Galtrey, *et al.*, 2008; Giamanco and Matthews, 2012; Geissler, *et al.*, 2013). The surface anchors for the PNN must, by necessity, come from the neuron. HA chains are directly extruded from HA synthases (HAS) expressed by the PNN neuron (Itano, *et al.*, 1999; Carulli, *et al.*, 2006; Carulli, *et al.*, 2007; Galtrey, *et al.*, 2008). Until recently, HAS was the only known cellular anchor for the PNN. RPTP $\zeta$  has been identified as a PNN anchor for *acan*, stabilising it to the PNN via a TnR-dependent mechanism (Eill, *et al.*, 2020). This research also hinted at another, yet unknown, PNN anchor. The PNN link proteins and TnR are both expressed by the PNN-bearing neurons (Bekku, *et al.*, 2003; Carulli, *et al.*, 2006; Geissler, *et al.*, 2013). CSPG origin is mixed and depends on the CSPG. *ncan* and *acan* both originate from the PNN-neurons themselves, while *bcn* in the PNN comes

from both astrocytes and neurons (Carulli, *et al.*, 2006; Geissler, *et al.*, 2013; Favuzzi, *et al.*, 2017). The PNN binding molecules semaphorin 3a (sema3A) and neuronal activity-regulated pentraxin, a PNN binding molecules, both originate from presynaptic neurons (Chang, *et al.*, 2010; Carulli, *et al.*, 2013).

### **3.1.1.3 The necessity of PNN components for mature PNN structure**

#### **3.1.1.3.1 Hapln1 is necessary for CSPG recruitment and PNN maturation**

PNN knock-out animals have shown that specific components are required for maturation of the PNN structure. *Hapln1*<sup>-/-</sup> animals have persistent visual plasticity and present with weak, diffuse PNNs that cover less area, reminiscent of an immature PNN phenotype (Carulli, *et al.*, 2010; Sigal, *et al.*, 2019).

Removal of hapln1 from the PNN ablates ncan, bcan, vcan staining in the PNN and reduced acan and pcan staining (Carulli, *et al.*, 2010). As acan and pcan staining was partially preserved this indicates their localisation to PNN is partly through another mechanism e.g. another hapln or RPTPζ (Bekku, *et al.*, 2012; Eill, *et al.*, 2020). Why does *Hapln1*<sup>-/-</sup> knock-out arrest the PNN in the punctate morphology? Link proteins are necessary for stabilisation of HA/CSPG binding (unpublished data) and their expression causes a condensation of diffuse PNNs (Kwok, *et al.*, 2010). Link protein removal leads to a reduction in CSPG binding to the PNN (Carulli, *et al.*, 2010; Bekku, *et al.*, 2012). If the PNN transition is caused by crossing a concentration threshold of PNN components then hapln1 KO would prevent maturation by reducing component concentration (Richter, *et al.*, 2018).

#### **3.1.1.3.2 TnR crosslinks PNN CSPGs, creating a reticular PNN**

PNNs in *TnR*<sup>-/-</sup> animals exhibit a punctate morphology and show impaired long term potentiation (LTP) (Bukalo, *et al.*, 2001). It should, however, be noted that the impaired LTP could be independent of the punctate PNNs as TnR is also expressed in the loose ECM. TnR binds to the G3 domain of CSPGs and can bind up to three lecticans (Milev, *et al.*, 1998; Aspberg, 1995; Aspberg, *et al.*, 1997; Lundell, *et al.*, 2004). *TnR*<sup>-/-</sup> PNNs are arrested in the punctate state, indicating TnR is necessary for PNN maturation. TnR could be responsible for PNN maturation through crosslinking CSPGs. This would condense the PNN, linking unconnected puncta, and transforming the PNN into the contiguous, reticular morphology. Supplementation of TnR in a *TnR*<sup>-/-</sup> cultures partially restores a reticular phenotype (Morawski, *et al.*, 2014). However, in a mouse model lacking 4 ECM components, including TnR, mature, reticular PNNs were still observed in the hippocampus (Rauch, *et al.*, 2005). This indicates TnR-dependent crosslinking is necessary but not essential for reticular PNNs.

### 3.1.1.3.3 Aggrecan

Two *Aggrecan*<sup>-/-</sup> mouse models have been created: an organism wide knock-out, cartilage matrix deficiency (*cmd*) and a brain specific knock-out created through Cre-lox (*Aggrecan-loxP/Cre*). The *cmd* mouse model is embryonic lethal in the homozygous due to the essential role of acan in alveoli function (Watanabe, *et al.*, 1997). However, the homozygous KO can be studied *in vitro* through organotypic slice or dissociated neuronal cultures from mouse embryos (Giamanco, *et al.*, 2010). Acan knock-out ablated PNN staining as detected by acan and WFA but spared hapln1 and TnR PNN localisation (Giamanco, *et al.*, 2010). This contrasted with the brain-specific KO where both hapln1 and TnR staining were ablated (Rowlands, *et al.*, 2018). The brain-specific KO posits a master role for acan in PNN structure while the *cmd* model suggests a more limited role.

### 3.1.1.3.4 Not all PNN components are necessary for mature PNNs

Not all PNN components alter PNN structure: cortical PNNs in *neurocan*<sup>-/-</sup>, *bcan*<sup>-/-</sup> and *hapln4*<sup>-/-</sup> animals remained intact (Zhou, *et al.*, 2001; Brakebusch, *et al.*, 2002a; Bekku, *et al.*, 2012). Impaired PNNs were discovered in the trapezoid body and cerebellum, in *neurocan*<sup>-/-</sup> and *hapln4*<sup>-/-</sup> animals respectively (Bekku, *et al.*, 2012; Schmidt, *et al.*, 2020). Study of PNN knock out animals has given us great insight into how the PNN is constructed in different CNS regions. While the heterogeneity has been identified, the functional effects have not.

### 3.1.1.4 PNN glycosylation during maturation

CS chains decorate the CSPGs found in the PNN and loose ECM (Yamaguchi, 2000). CS can be sulphated at several different positions, creating different subtypes (Mikami and Kitagawa, 2013). Of the different types, sulfation at the 4 or 6 position on the N-acetyl galactosamine are the most common and are termed CS-A or CS-C. CS-A is inhibitory for neurite outgrowth while CS-C is permissive (Wang, *et al.*, 2008). During embryonic development CS-C predominates but slowly diminishes while CS-A increases in proportion until they both account for ~40% of total CS at E17 (Kitagawa, *et al.*, 1997). This trend continues postnatally. In the adult, CS-A accounts for between 80-90% of total CS while the CS-C proportion is between 2-5% (Deepa *et al.*, 2006). The increase in the 4S:6S ratio creates a more inhibitory CNS environment. PNN sulfation continues to change in ageing as the 4S:6S ratio specifically increases in the PNN (Foscarin, *et al.*, 2017). This makes the mature PNN an inhibitory structure, discouraging new synapse formation on the enwrapped neuron. Overexpression of chondroitin 6 sulfotransferase-1 (C6ST-1) impairs PNN formation; reducing acan PNN localisation through negatively regulating its half-

life in the PNN (Miyata, *et al.*, 2012; Miyata and Kitagawa, 2016). The C6ST-1 animal also presents with persistent plasticity, reminiscent of the phenotype seen in PNN KO animals, indicating a CP closure failure (Miyata, *et al.*, 2012). In a similar vein, juvenile plasticity can be reawakened by masking the inhibitory CS-A via antibody binding (Yang, *et al.*, 2017). The disulphated 4S,6S subunit, termed CS-E, has been shown to have important roles in PNN molecule binding (Gama, *et al.*, 2006; Dick, *et al.*, 2013; Bernard and Prochiantz, 2016; Van't Spijker, *et al.*, 2019).

### **3.1.1.5 Understanding changing PNN morphology through the lens of soft matter physics**

The morphology of a film is governed by two factors: the interaction of polymer density and the attractive forces between polymer chains. We can understand the PNN as a film where the polymers are the HA and CSPGs and the attractive forces are cross-linkers (Richter, *et al.*, 2018). As grafting density increases (i.e., the concentration of HA or CSPGs in the PNN) the film will transition from a punctate, granular film to a continuous film. If the attractive forces between polymers are increased, then this will rearrange a continuous film into a disrupted film as the polymers compact. In a sufficiently dense film the energetically favourable state will be a reticular morphology as the development of circular holes minimises the phase boundaries (Richter, *et al.*, 2018). In our PNN model and *in vivo* we see a transition from a punctate, discontinuous phase to a reticular phase as the PNN matures. This indicates changes in component density and/or changes in compaction due to the appearance of cross-linkers.

#### **3.1.1.5.1 Mechanisms governing PNN polymer density**

The morphology of the PNN is directly linked to plasticity as arresting PNNs in a punctate state maturation, through PNN component knock-out, causes persistence of a juvenile state of plasticity (Carulli, *et al.*, 2010; Rowlands, *et al.*, 2018; Eill, *et al.*, 2020). Changes in PNN polymer density can be driven by changes in CSPG and HAS expression. As discussed, CSPG expression rises and peaks during development, this can directly affect their density in the PNN. PNN CSPG density also depends on link protein expression as knock-out of *Hapln1* or *Hapln4* leads to smaller PNNs and a reduction in CSPG PNN localisation (Carulli, *et al.*, 2010; Bekku, *et al.*, 2012). Overexpression of *Hapln1* leads to a condensation of acan positive pericellular coats (Kwok, *et al.*, 2010). PNN maturation could be controlled by a *Hapln* dependent rise in CSPG density.

There is variation between which PNN maturation mechanisms are at play. For example, while Carulli *et al.* (2010) showed an upregulation of the acan in the visual cortex. This upregulation was not due to increased transcription as mRNA expression decreased in the same period. The other factor governing CSPG density on the PNN is their turnover rate, reducing degradation will increase the lifespan on the PNN and therefore their density. This can be controlled by the glycosylation state of the PNN itself. Overexpression of C6ST-1 leads to an upregulation of the 6S moiety in the PNN and persistent plasticity (Miyata, *et al.*, 2012; Miyata and Kitagawa, 2016). This upregulation led to a selective reduction of acan in PNN by increasing turnover by matrix proteases (Miyata and Kitagawa, 2016). In the course of normal PNN maturation there is a reduction of 6S and an increase of the 4S moiety (Kitagawa, *et al.*, 1997). This reduction would lead to decreased degradation of acan and a rise in acan levels within the PNN. This could account for the acan increases observed within our culture and *in vivo*.

HAS mRNA expression also changes during PNN development. All HAS isoforms showed a transient increase at early time points, although the precise timing of the peak differed between isoforms and the CNS region investigated (Carulli, *et al.*, 2007; Galtrey, *et al.*, 2008). Changes in HAS expression provides another mechanism to modulate PNN morphology. A decrease in HAS expression would lead to a decrease in HA density on the cell surface, reducing the number of binding sites for PNN components and changing PNN morphology.

#### **3.1.1.5.2 Mechanisms governing attraction between PNN polymers**

Another mechanism driving the change in PNN morphology is to alter the forces of attraction between polymers through the addition of crosslinkers. This is seen in other extracellular matrices (Richter, *et al.*, 2018). Several PNN cross-linkers have been identified but the extent of their contributions within the PNN has yet to be resolved. These are TnR and sema3A (Morawski, *et al.*, 2014; Djerbal, *et al.*, 2019). A single TnR molecule can bind to the G3 domain of three separate CSPGs (Aspberg, *et al.*, 1997; Milev, *et al.*, 1998; Lundell, *et al.*, 2004). It is widely expressed in cortical PNNs and PNNs in *TnR*<sup>-/-</sup> animals present with punctate PNNs (Celio and Chiquet-Ehrismann, 1993; Weber, *et al.*, 1999; Haunsoø, *et al.*, 2000). Re-addition of TnR to *tnr*<sup>-/-</sup> PNN neurons leads to partial recovery of the reticular morphology showing that TnR is responsible for maintenance of the reticular morphology of PNNs (Morawski, *et al.*, 2014). It has recently been shown that TnR could also increase the density of acan and

other CSPGs in the PNN by working in tandem with RPTP $\zeta$ /phosphacan to anchor acan to the cell surface (Eill, *et al.*, 2020).

Sema3A is a secreted chemorepulsive molecule that negatively regulates axon growth (Zimmer, *et al.*, 2010). While TnR crosslinks the CSPGs core protein, sema3A could crosslink the PNN via a different mechanism- binding the GAG moieties themselves (Dick, *et al.*, 2013; Djerbal, *et al.*, 2019). It is expressed as a dimer and localises to the PNN via specific CS-E binding (Dick, *et al.*, 2013; Vo, *et al.*, 2013). As a dimer it could feasibly bind to two CS-E chains from different CSPGs, collapsing and rigidifying the PNN matrix into a reticular morphology (Richter, *et al.*, 2018; Djerbal, *et al.*, 2019). Sema3A delivery to PNNs can be synapse dependent. Purkinje cells express sema3A mRNA and synapse with DCN PNN positive neurons (Carulli, *et al.*, 2013). Severing the connection between DCN PNN positive neurons and Purkinje cells reduced Sema3a binding to the PNN. Concomitant with this was a significant reduction in the number of holes seen in the PNNs and a shift towards a punctate morphology. This opens the possibility that PNN maturation is a reversible and dynamic process dependent on synaptic activity. Indeed, inhibition of neuronal firing reduces PNN intensity (Pizzorusso, *et al.*, 2002; Dityatev, *et al.*, 2007).

### **3.1.1.6 Role of neuronal activity in PNN maturation**

As discussed, knock-out of PNN components arrests the PNN in a punctate morphology, indicating they are necessary for maturation to the reticular morphology (Haunso $\ddot{o}$ , *et al.*, 2000; Br $\ddot{u}$ ckner, *et al.*, 2000; Eill, *et al.*, 2020). The monocular deprivation paradigm demonstrates that neuron activation is also necessary for PNN development and maturation (Pizzorusso, *et al.*, 2002; Ueno, *et al.*, 2017b; Sigal, *et al.*, 2019). Silencing of neuronal activity *in vivo* reduces PNN intensity (Kalb and Hockfield, 1990; Yamada, *et al.*, 2017). The dependence of neural activity has been shown directly *in vitro*. Application of tetrodotoxin to block synaptic transmission suppressed PNN formation and the only PNNs observed exhibited a punctate morphology (Kalb and Hockfield, 1990; Dityatev, *et al.*, 2007). Treatment with potentiators of GABAergic transmission can also accelerate PNN maturation, cementing the importance of synaptic transmission in PNN maturation and tying PNN maturation to maturation of GABAergic neurons (Dityatev, *et al.*, 2007; Hou, *et al.*, 2017). However, the relationship between synaptic transmission and the PNN is bidirectional. PNN appearance precedes that of synapse formation and is needed for synapse stabilisation (Dino, *et al.*, 2006; Geissler, *et al.*, 2013; Gottschling, *et al.*, 2019). Mechanistically the PNN achieves this both through the individual functions of its components and emergent function from the

aggregate structure. Individual lecticans may be responsible for stabilisation of synapse subtypes. Bcan has been shown to specifically stabilise excitatory synapses on PNN positive PV neurons (Favuzzi, *et al.*, 2017). While knock-out of ncan leads to a reduction in inhibitory synapse contacts (Geissler, *et al.*, 2013; Schmidt, *et al.*, 2020). *Tnr<sup>-/-</sup>* also led to a specific reduction in perisomatic synapses (Saghatelyan, *et al.*, 2001; Nikonenko, *et al.*, 2003). Furthermore, the both the ECM and PNN can restrict the diffusion of synaptic machinery, such as the AMPA and NMDA receptors (Frischknecht, *et al.*, 2009; Schweitzer, *et al.*, 2017). This corralling of post-synaptic machinery improves synaptic transmission and creates putative sites for new synapses. Neuronal activity also modulates the mature PNN, though to a lesser degree than during CPs. Severing efferent connections to PNN neurons causes a reduction in PNN intensity (Carulli, *et al.*, 2013; Faralli, *et al.*, 2016). Interestingly, enriched environment exposure also causes a similar decrease through increased matrix metalloprotease-9 (MMP-9) activity. If MMP-9 is knocked out then PNN intensity increases, demonstrating the complex regulation of the PNN and plasticity (Stamenkovic, *et al.*, 2017). This shows neuronal activity plays a key role both in PNN development and its maintenance. It is likely that neuronal activity drives the transcription of PNN molecules through NMDA receptor-mediated calcium influx though this has yet to be demonstrated.

### **3.1.1.7 PNN maturing agents**

Alongside neuronal activity, several molecules have been implicated in PNN maturation. Hapln1 and TnR are integral PNN components and have already been discussed, the other class are PNN binding molecules which bind through CS-E. CS-E is a highly enriched subtype within the PNN that increases during PNN development and binds to several key molecules involved in CP maintenance: brain-derived neurotrophic factor (BDNF), Sema3a, Otx2, NARP and neuronal pentraxin 2 (NPTX2) (Huang, *et al.*, 1999; Sugiyama, *et al.*, 2008; Gu, *et al.*, 2013; de Winter, *et al.*, 2016; Van't Spijker and Kwok, 2017). BDNF is released by excitatory neurons during development and governs PV maturation. Infusion or overexpression accelerates PV maturation, bringing the CP forward (Huang, *et al.*, 1999). BDNF has been shown to bind to CS-E and, to a lesser extent, CS-A (Gama, *et al.*, 2006). While the link between BDNF and the PNN has not been investigated, CS-E and CS-A both become enriched during PNN maturation, creating a positive feedback loop where increasing PNN maturation would amplify BDNF binding, driving PV maturation. Like BDNF, Sema3A is also released by excitatory neurons, i.e., Purkinje cells in the cerebellum. Purkinje cells synapse with PNN-bearing deep cerebellar neurons. Severance of these connections led to a reversal in PNN morphology towards a punctate

phenotype (Carulli, *et al.*, 2013). This provides a transcription independent mechanism for neuronal activity in PNN maintenance. Denervation also led to a marked reduction in sema3A localisation to the PNN, correlating with the morphology reversal. The homeoprotein Otx2 is produced by the choroid plexus cells and diffuses through the ECM and drives PV maturation (Bernard and Prochiantz, 2016). As with BDNF, Otx2 infusion precipitates a precocious CP, shifting it to an earlier time point. Otx2 is specifically recruited onto PV neurons by the PNN through binding to CS-E (Beurdeley, *et al.*, 2012). Interestingly, Otx2 infusion circumvents the requirement of neuronal activity as it can induce PV and PNN maturation in dark reared animals (Sugiyama, *et al.*, 2008). Otx2 tone remains constant in adulthood and its disruption precipitates a precocious CP and concurrent PNN reduction (Beurdeley, *et al.*, 2012; Spatazza, *et al.*, 2013). Otx2-dependent maturation of the PNN and PV neurons can only occur if it can bind to the PNN. Reduction of PNN CS, through enzyme knock-out, reduces Otx2 internalisation in PV neurons and corresponding deficit in PNN and PV maturation. This kept the CNS in a persistent high plasticity state, similar to those seen with other PNN impairment models (Hou, *et al.*, 2017). It is likely there are several, overlapping mechanisms for PNN maturation and which work in concert. How these mechanisms interact, their timing in PNN maturation, or if there is a master regulator, has not yet been resolved. For example, does TnR and hapln1 localisation occur after Otx2 binding or occur independently? An *in vitro* model of PNN maturation would provide a firm foundation from which to answer this and other questions. A higher temporal resolution can be achieved with less cost than with animal models. Also, multiple factors, e.g. neural activity and treatment application, can be concomitantly measured and manipulated. Therefore, the establishment of an *in vitro* PNN maturation model would be of great advantage for the study of the PNN and neuroplasticity.

### **3.1.1.8 PNN heterogeneity is widespread throughout the CNS**

As discussed, the PNN is a critical structure in controlling neuronal plasticity and is found throughout the CNS. The mature PNN presents as a reticular structure but the extent of coverage differs between brain areas. PNNs in the telencephalon extend over the proximal dendrites while PNNs in lower brain regions only cover the soma (Carulli, *et al.*, 2006; Horii-Hayashi, *et al.*, 2015; Irvine and Kwok, 2018). PNN thickness also differs between regions; PNNs in the spinal cord and cerebellum are thicker than their cortical counterparts (Smith, *et al.*, 2015). The functional differences arising from the different coverage and thickness has not been elucidated. Thicker PNNs could act as larger ionic sinks, encouraging prolonged neuronal firing (Balmer, 2016).

WFA has commonly been used as a pan-PNN maker but pairing with PNN component antibodies has revealed that WFA does not stain all PNNs (Irvine and Kwok, 2018; Ueno, *et al.*, 2018b). In the spinal cord a significant proportion of PNNs are WFA-, between 10-30% depending on which CSPG is used as a counterstain. Bcan and ncan revealed the highest proportion of WFA negative PNNs indicating they are less likely to carry the WFA epitope compared to acan, vcan or pcan (Irvine and Kwok, 2018). Whether these CSPGs colocalised within the PNN was not investigated. Determining colocalization between CSPGs is important for characterisation of PNN subtypes. PNN glycosylation changes during development but is not uniform in the mature CNS. This is shown by the high proportion of WFA negative PNNs and by analysis of acan glycoforms. Different glycoforms of acan recognised partially overlapping populations of PNNs and even segregate within the PNN (Matthews, *et al.*, 2002; Miyata, *et al.*, 2018). CA1 PNN positive, pyramidal cells either contained all glycoforms, a combination of two or just one glycoform (Matthews, *et al.*, 2002; Yamada and Jinno, 2017). It is possible variation in glycosylation is incidental and irrelevant to PNN function and arises from the vagaries of cellular glycosylation and GAG digestion. However as discussed, it has been shown that some CS subtypes are necessary for PNN function, e.g. 4S:6S ratio and CS-E, indicating this heterogeneity cannot be completely incidental.

The entire lectican family and pcan/RPTP $\zeta$  localise to the PNN (Fawcett, *et al.*, 2019). Acan is the predominant CSPG in mature PNNs and is widespread throughout the CNS. The other CSPGs show more specific expression. For example in the red nucleus, ncan positive PNNs are only found in the parvocellular region while acan is found throughout (Rácz, *et al.*, 2016). In the prelimbic cortex ncan only/WFA positive PNNs were identified; while in the primary motor cortex PNNs contained all CSPGs (Ueno, *et al.*, 2017a). Bcan and vcan are found in PNNs throughout the CNS but are also enriched in the perinodal ECM (Bekku, *et al.*, 2012; Ueno, *et al.*, 2017a; Irvine and Kwok, 2018; Bekku, *et al.*, 2009; Dours-Zimmermann, *et al.*, 2009). The perinodal ECM condenses around the nodes of Ranvier and aids axonal conductance. The perinodal net lacks acan but contains the other lecticans (Bekku, *et al.*, 2009; Dours-Zimmermann, *et al.*, 2009; Bekku and Oohashi, 2011). It is beyond the scope of this work but is reviewed by Fawcett and colleagues (2019). Bcan also plays a specific role in the synaptic ECM of the calyx of Held, another form of ECM that lacks acan (Blosa, *et al.*, 2013).

As discussed, the link proteins, hapln1 and hapln4, are essential in stabilising CSPGs to the PNN. Hapln1 is expressed in PNNs throughout the CNS (Carulli, *et al.*, 2007; Galtrey, *et al.*, 2008; Carulli, *et al.*, 2010). Hapln4 shows more

selective expression. It is found in PNNs in the mid and hindbrain and is a core component of the perinodal net (Bekku, *et al.*, 2003; Bekku, *et al.*, 2010).

There is heterogeneity in PNN composition throughout the CNS, both within and between CNS regions. The concentration of components in the PNN also varies, as shown by differing intensities (Blosa, *et al.*, 2013; Ueno, *et al.*, 2017a). PNN intensity is dynamic, varying during learning tasks (Banerjee, *et al.*, 2017; Carulli, *et al.*, 2020). The widespread heterogeneity in PNN composition is at odds with the PNN's role in restricting plasticity and is unlikely to be completely incidental, as demonstrated by KO animals. This complexity and variety instead might reflect different functions of the PNN which have yet to be identified.

### 3.1.1.9 PNN composition and function

The minimum necessary components for a PNN are HA, a CSPG and a link protein (Kwok, *et al.*, 2010). This is sufficient to create a dense, detergent resistant barrier that can inhibit neurite outgrowth (Yang, *et al.*, 2017). However, as highlighted, there is significant variety in PNN composition between brain regions. It is unlikely this heterogeneity is redundant but instead reflects differences in PNN function.

CSPGs are an important component of the PNN and have glycan dependent and independent roles (Beurdeley, *et al.*, 2012; Dick, *et al.*, 2013; Chang, *et al.*, 2010; Favuzzi, *et al.*, 2017). Bcan has been shown to stabilise excitatory synapses in PV neurons. Bcan stabilises AMPA receptors and potassium channels on the cell surface (Favuzzi, *et al.*, 2017). Bcan KO leads to a reduction in excitatory synapses and plasticity deficit (Brakebusch, *et al.*, 2002; Favuzzi *et al.*, 2017). Bcan knock-out also disrupts synaptic transmission in the calyx of Held, in accord with its enrichment in these synapses (Blosa, *et al.*, 2015). Ncan KO leads to a reduction in inhibitory synapses and LTP deficit, hinting at a corresponding role in inhibitory synapse stabilisation, although the precise molecular mechanism has yet to be resolved (Zhou, *et al.*, 2001; Schmidt, *et al.*, 2020). However, while a specific role for bcan has been identified; the specific roles for other CSPGs have yet to be determined. If these can be resolved, then the reasons for PNN heterogeneity can be properly understood.

There is genetic linkage between the four link protein family members and lecticans: hapln1/vcan, hapln2/bcan, hapln3/acan, hapln4/ncan (Spicer, *et al.*, 2003). This raises the possibility of preferential binding between haplins and CSPGs. However, hapln/CSPG binding interactions have not been systematically tested and knock-out animal data does not neatly fit with this

hypothesis. All haplins are expressed in the brain but only hapln1 and hapln4 have been shown to localise to the PNN (Spicer, *et al.*, 2003; Carulli, *et al.*, 2010). Hapln2 localises to the perinodal net where it interacts with vcan (Oohashi, *et al.*, 2002). Hapln1 is a key CSPG stabiliser in PNNs as knock-down leads to the loss of several lecticans from the PNN in the cortex (Carulli, *et al.*, 2010; Kwok, *et al.*, 2010). This role is not conserved in the lower brain regions where it is restricted to acan stabilization (Bekku, *et al.*, 2012). Hapln4 is found in cortical PNNs but KO does not produce a cortical PNN deficit (Bekku, *et al.*, 2012; Rowlands, *et al.*, 2018). Hapln4 is indispensable for bcan PNN localisation in the hindbrain and in the calyx of Held (Bekku, *et al.*, 2012; Popelář, *et al.*, 2017). Hapln4 KO also caused a reduction in pcan and ncan PNN staining in the hindbrain. Functionally hapln4 KO decreased GABAergic synapse stabilisation in the DCN (Edamatsu, *et al.*, 2018). However, CSPG staining was not investigated by Edamatsu *et al.* (2018) so it is not known how hapln4 KO led to the synaptic deficit. Together, this hints at a regional dominance of haplins, hapln1 in the cortex and hapln4 in the hindbrain.

An *in vitro* neuronal PNN model would provide a platform to investigate the effect of PNN components on function. There are several advantages to PNN culture model: cost, time, ease of manipulation through genetic manipulation. While the effect on behaviour cannot be investigated it would allow the molecular mechanisms to be determined with high resolution. Previous *in vitro* PNN cultures have established the contribution of glia and neuronal activity to PNN formation (Dityatev, *et al.*, 2007; Giamanco and Matthews, 2012; Geissler, *et al.*, 2013). Some of the cultures have exhibited reticular morphologies but many have presented with punctate PNNs. A prerequisite of this model would be the replication of mature PNN heterogeneity. Once established it could also be used to investigate the role of the PNN in PD disease mechanisms.

### **3.1.2 Chapter aims**

The aim of this chapter is to establish and characterise a mature, reticular PNN culture. Cortical neurons will be used as cortical PNNs have been well-characterised *in vitro*. I will determine when the PNN develops and matures *in vitro* and when key PNN components, hapln1 and acan, localise to the PNN. I will then correlate this with PNN morphology as revealed by these stains and WFA. Once a reticular culture has been established then the mature culture will be characterised and the CSPG composition will be determined. Whether these CSPGs segregate with TnR and Hapln proteins will also be investigated. Establishing a mature PNN culture will be of great benefit to the PNN field and will allow investigation of the role of the PNN in  $\alpha$ SYN seeding.

## **3.2 Methods**

### **3.2.1 Primary Cell Culture**

For protocols on primary neuron and astrocyte culture please refer to section 2.2.

### **3.2.2 Immunocytochemistry**

Neurons were fixed at room temperature in 4% PFA, 3% sucrose solution for 10 minutes. The cells were then washed in 3% sucrose then permeabilised with 0.01% triton x-100 for 10 minutes. Non-specific binding sites were blocked by incubation with 3% normal donkey serum (Sigma #D9663) in Tris buffered saline (TBS) for 1hr at room temperature. The neurons were then incubated with primary antibodies (table 2), diluted in blocking solution, overnight at 4°C. The following day the neurons were then washed with TBS and incubated with the appropriate secondary antibodies, diluted in blocking solution, for 2 hours at room temperature. They were then washed in TBS and mounted onto SuperFrost microscope slides (Fisher Scientific Ltd #10149870) using Fluorsave (Merck #345789).

### **3.2.3 Microscopy, quantification, and statistics**

Coverslips were imaged on either LSM880 confocal microscope (Zeiss) with 20x and 63x objectives or AxioScan Z.1 Slidescanner (Zeiss) with a 20x objective. The Slidescanner was operated by the Bioimaging facility. For confocal, coverslips were imaged with 20x objective and tile-scanning for quantification of PNN morphology and components. High resolution images were created by z-stack imaging with 63x objective. A projection image was then created using max intensity plugin on ImageJ. For the slidescanner, tile images with 20x objective were taken and stitched to provide entire coverslip image. Filters were set to ensure no overlap between channels. PNNs were identified and counted based on morphology. Coverslips are from two rats, some coverslips were excluded due to poor viability. Total PNNs per coverslip were calculated. Punctate and reticular PNNs were classified by morphology by the observer. Data are mean of coverslips with standard error of the mean used. OriginPro 2019b was used in graph creation and statistical analysis. Tests for significance ( $p < 0.05$ ) were performed using one-way analysis of variance (ANOVA) with Tukey's post hoc test.

## 3.3 Results

### 3.3.1 Formation of PNNs *in vitro*

Previous studies have shown that it is possible to culture PNN neurons *in vitro* from rodent embryos (Miyata, *et al.*, 2005; Dityatev, *et al.*, 2007; Geissler, *et al.*, 2013). Therefore, we aimed to establish an *in vitro* PNN culture to test whether the PNN conferred resistance against  $\alpha$ SYN seeding.

We first investigated the morphology of PNNs formed in the long-term neuronal culture model. One key limitation in previous cultures is that the PNNs only developed a punctate morphology; this does not replicate the reticular structure seen *in vivo* (Miyata, *et al.*, 2005; Dino, *et al.*, 2006). We have previously hypothesised that the punctate morphology represented an immature PNN phenotype and that they would develop into the 'mature' reticular phenotype over time (Richter, *et al.*, 2018).

We thus cultured the neurons for up to 56 DIV allowing the development of potential mature morphology. We stained the rat neuronal culture with WFA at several different time points to track PNN development. At DIV14, not shown, some weak punctate staining was seen on a few neurons. However, at DIV21, WFA positive puncta became more common and resembled the punctate PNNs seen elsewhere (Miyata, *et al.*, 2005). This staining grew in intensity and coalesced into a mature, reticular PNN morphology as the culture aged (Fig. 5A). At DIV35 the PNN morphology transitioned from an immature to a mature phenotype. By DIV55 mature, reticular PNNs were the majority morphology. This supports the hypothesis that PNNs develop from an immature, punctate morphology to a reticular morphology (Richter, *et al.*, 2018).

Characterisation of the culture revealed that only  $7.6 \pm 1.1\%$  of neurons had reticular PNNs at DIV56 (Fig.5B). This is comparable to the proportion of PNN neurons in the cortex *in vivo* (4-10%) (Brückner, *et al.*, 1999; Mueller, *et al.*, 2016). In our culture, parvalbumin positive neurons were the predominant subpopulation of PNN ensheathed neurons (PV positive PNN neurons:  $62.5 \pm 0.075\%$ ), accounting for roughly two thirds of the PNN population (Fig.5C). Again this is comparable with the population of PNN neurons in the frontal cortex (Ueno, *et al.*, 2017a). Together this demonstrates we have established a PNN culture model that accurately replicates the cortical PNN population seen *in vivo*. Furthermore, this model provides a platform from which to observe PNN maturation.

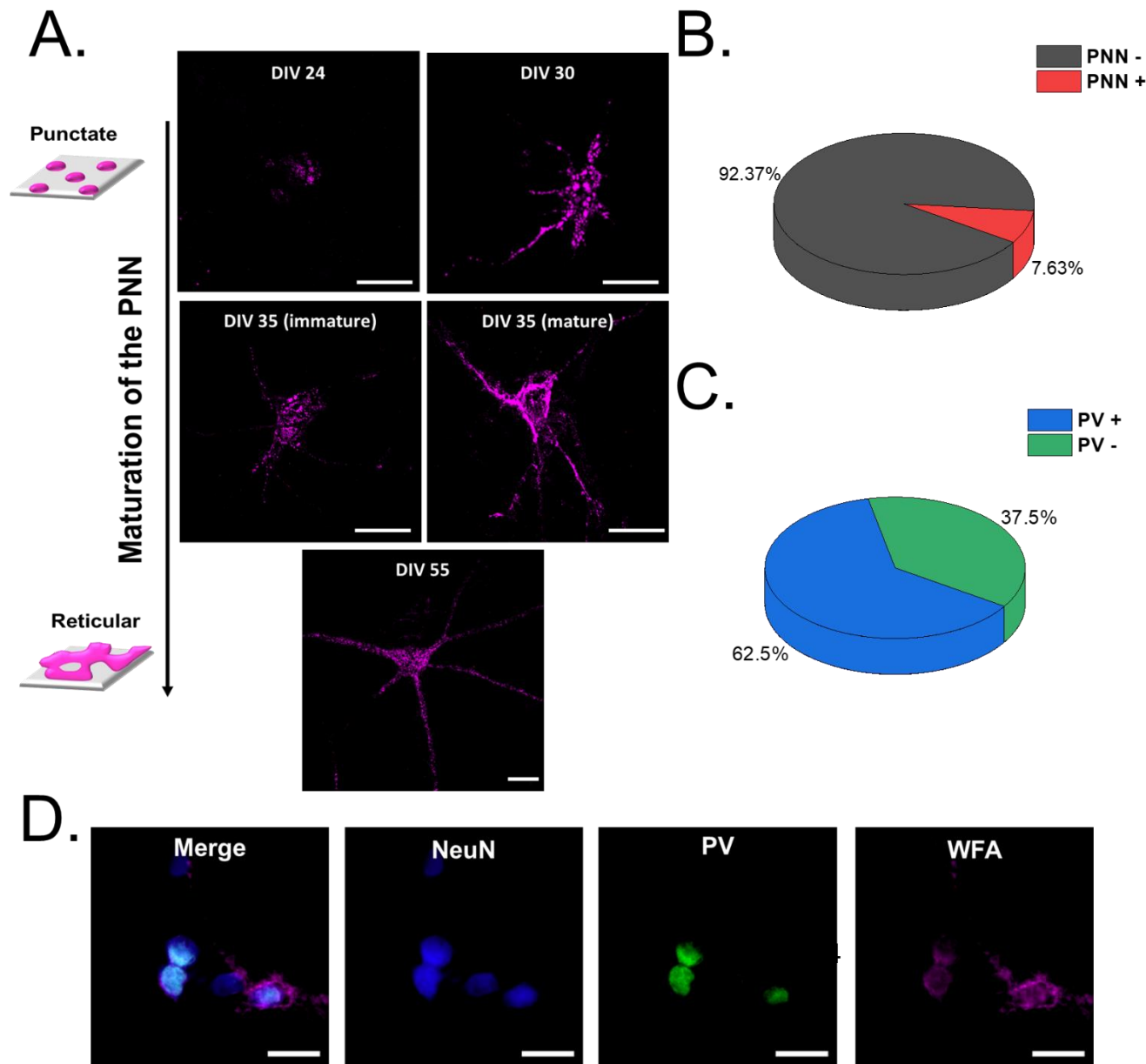


**Figure 5: Formation of PNN *in vitro***

**A.** Representative images of WFA reactive PNNs across several time points in rat neuronal culture. PNNs began to appear at DIV30 with a punctate appearance. The WFA staining began to coalesce at DIV35 to a reticular morphology. By DIV56 the PNNs showed the mature reticular morphology seen *in vivo*. Scale bar is 20  $\mu\text{m}$ . **B.** Quantification of neuronal culture. Neurons were counted and the proportion of WFA positive neurons (PNN positive) was determined for N= 3 rats, n= 3534 neurons. **C.** The perineuronal neurons were quantified to determine what proportion were parvalbumin positive neurons, around 60% of PNN neurons are parvalbumin neurons. **D.** Representative image of parvalbumin positive neurons at DIV42. Scale bar is 20  $\mu\text{m}$ .

### 3.3.2 Appearance of PNN components during PNN development

We have established an *in vitro* cortical PNN model which also models PNN development. The PNN is a composite structure, containing several different classes of molecules. Previously in our group we have created an *in vitro* PNN model using HEK cells and have shown that hapln1, acan and HA are sufficient to create a PNN-like structure (Kwok, *et al.*, 2010). Furthermore, hapln1 and acan are major PNN components in the cortex as knock out animals show cortical PNN deficits (Rowlands, *et al.*, 2018; Carulli, *et al.*, 2010). Therefore, we wanted to define when hapln1 and acan appeared during PNN development. The components were stained for at different time points during *in vitro* PNN development. Staining for the protein would also reveal what morphology it manifested as and at what time points, furthering our knowledge of PNN maturation.

WFA stained a consistent proportion of PNNs across all time points, showing no significant differences between proportion of PNNs stained (WFA positive neurons: DIV21:  $71.3 \pm 9.8\%$ , DIV28:  $58.4 \pm 9.4\%$ , DIV35:  $71.2 \pm 13.2\%$ , DIV56:  $86.9 \pm 8.8\%$ ) (Fig. 6A). This indicates that, in contrast to other PNN glycan epitopes, the glycosylation pattern detected by WFA is conserved across PNN development (Kitagawa, *et al.*, 1997; Foscarin, *et al.*, 2017; Nadanaka, *et al.*, 2020). While acan positive PNNs were detected at DIV21 they were the minority ( $19.1 \pm 11.9\%$ ). The number of acan positive PNNs significantly increased by DIV28, more than doubling to account for  $52.5 \pm 5.6\%$  of all PNNs (Fig. 6B). The proportion of acan positive PNNs was significantly higher at DIV56, where acan stained the majority ( $94.3 \pm 6.5\%$ ). Interestingly, the WFA positive PNN proportion was much higher than the acan proportion at earlier time points indicating that WFA epitope was not carried by glycosylated acan as has been previously suggested but by a different CSPG (Fig. 6A vs. B) (Miyata, *et al.*, 2018). The proportion of PNNs positive for hapln1 remained consistent for the first 35 days of culture, accounting for  $29.2 \pm 9.8\%$  of PNNs (Fig. 6C). By DIV56 the proportion of PNNs positive for hapln1 had significantly increased, more than doubling, accounting for  $77.4 \pm 15.7\%$  of PNNs. It is unknown what triggers this rise. The *Haplns* are a core component of PNNs and knock out of *Hapln1* or *Hapln4* leads to impaired PNNs in the brain (Carulli, *et al.*, 2010; Bekku, *et al.*, 2012). It is therefore unlikely that the PNNs in our culture lack any *Hapln* protein, therefore it is possible that up to DIV56 another *Hapln* is predominant in the PNN before a transcriptional switch to hapln1.

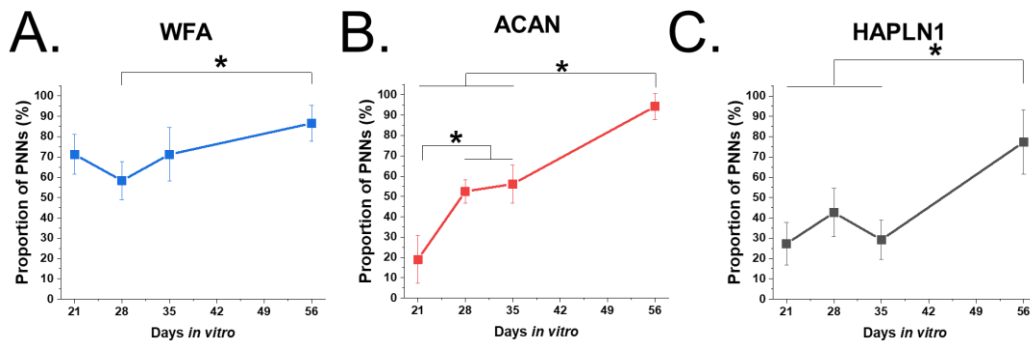


**Figure 6: Development of PNN components *in vitro***

Quantification of *in vitro* PNNs positive for components (HAPLN1, ACAN and WFA) across different time points as determined by immunofluorescence. Data are mean with SEM, N= 5 cultures from 3 rats. Number of neurons counted for each time point: DIV21= 882, DIV28= 496, DIV35= 433. Significance was determined by one-way ANOVA ( $p < 0.05$ ). **A.** Quantification of WFA positive PNNs during culture development. WFA staining accounts for a consistently high proportion of PNNs at all-time points. **B.** Quantification of ACAN positive PNNs during culture development. ACAN positive PNNs increase as the culture ages. ACAN localises to a minority of PNNs at DIV 21 but significantly increases by DIV28. ACAN positive PNNs account for 94% of PNNs at DIV56. **C.** Quantification of HAPLN positive PNNs during culture development. For the first 35 days of culture the proportion of HAPLN1 positive PNNs remain consistent at roughly a third of the total PNN population. However, at DIV56, when the PNNs are mature, the population significantly rises to 75% of PNNs.

### 3.3.3 Two routes of PNN maturation

In our *in vitro* PNN culture we have identified two PNN morphologies: punctate and reticular. We quantified the proportions of each morphology at the different time points and which component stain manifested as each morphology. The punctate morphology accounted for the majority of WFA positive PNNs at DIV21 ( $78 \pm 2.0\%$ ). The proportion of punctate PNNs consistently dropped over the following time points, only accounting for 14% of PNNs at DIV56 (Fig. 7A). A similar trend was seen for acan (Fig. 7B). This clear morphology transition provides further evidence for the PNN maturation hypothesis, where an immature punctate morphology coalesces to a mature reticular phenotype.

Interestingly, hapln1 positive PNNs were seen at all-time points but they exhibited a reticular morphology throughout (Fig. 9). This was in direct contrast to acan and WFA which appeared punctate at earlier time points. At the earliest time point these reticular PNNs were negative for WFA and acan. While the punctate PNNs were invariably negative for hapln1 (Fig. 8). This reveals that there is a subset of PNNs that present with a mature morphology at a much earlier time point and have a different composition. These PNNs shall be

referred to early mature PNNs. It is possible that these PNNs form on a different neuronal subtype. 37.5% of PNNs in our culture were not reactive for parvalbumin (Fig. 5C). This fraction is the similar size to the proportion of early mature PNNs

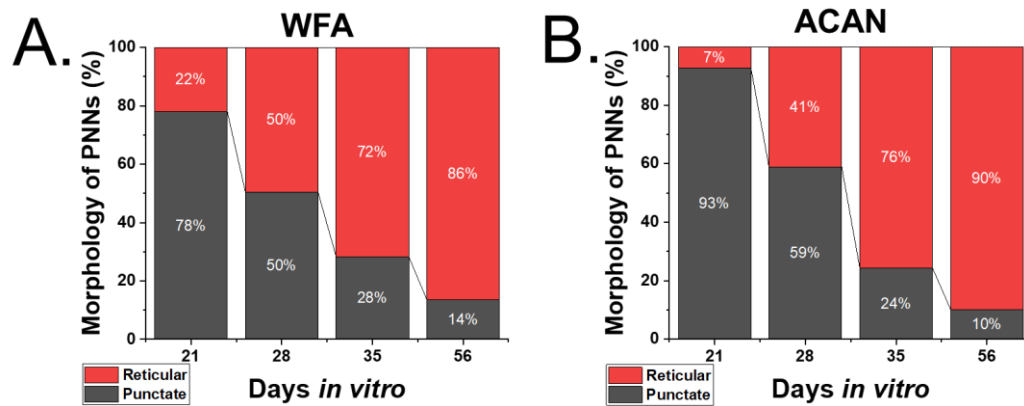


**Figure 7: PNN morphology transitions from punctate to reticular over time**

**A.** Quantification of WFA PNN morphology at different time points in neuronal culture. The organisation of WFA staining changes from a majority discrete, punctate staining at DIV21 to a majority of contiguous, reticular staining as the culture at DIV56. Data are mean with SEM, N= 5 cultures from 3 rats. Number of neurons counted for each time point: DIV21= 616, DIV28= 285, DIV35= 319, DIV56= 391 **B.** Quantification of ACAN morphology at different time points in neuronal culture. The transition mirrors that of WFA. Data are mean with SEM, N= 5 cultures from 3 rats. Number of neurons counted for each time point: DIV21= 67, DIV28= 237, DIV35= 233, DIV56= 434.

and could therefore be the early mature PNN neurons. This would indicate that PNNs on different neuronal subtypes mature at different rates.

Punctate PNNs were only WFA positive at DIV21. Acan commonly localised to the punctate PNNs at DIV28, where it then partially colocalised with WFA staining (Fig. 8). By DIV35, both acan and WFA signal and colocalization had increased, though it remained punctate in ~25% of PNNs (Fig. 7). This increase in colocalization indicates a CSPG transition for acan to become the predominant source for WFA signal in the PNN during maturation. For early mature PNNs, acan staining also began to appear at DIV28 (Fig. 9). This was accompanied by WFA and was reticular in nature. The intensity and extent of staining increased as the culture aged (Fig. 8). The distinct recruitment of acan and WFA to hapln1 positive or negative PNNs raises the question of whether there are two routes of PNN maturation: (1) the appearance of 'nascent' punctate PNNs followed by their subsequent maturation and; (2) a transition in component expression in pre-existing, hapln1 positive PNNs. It could also be that the maturation switch we observe could be due to the pruning of existing

punctate, WFA positive PNNs as the culture ages rather than their development into mature, reticular PNNs. To resolve this the PNN population percentage should be determined against the total neuronal population. If a percentage decrease is seen as the PNN matures it would suggest pruning of PNNs.

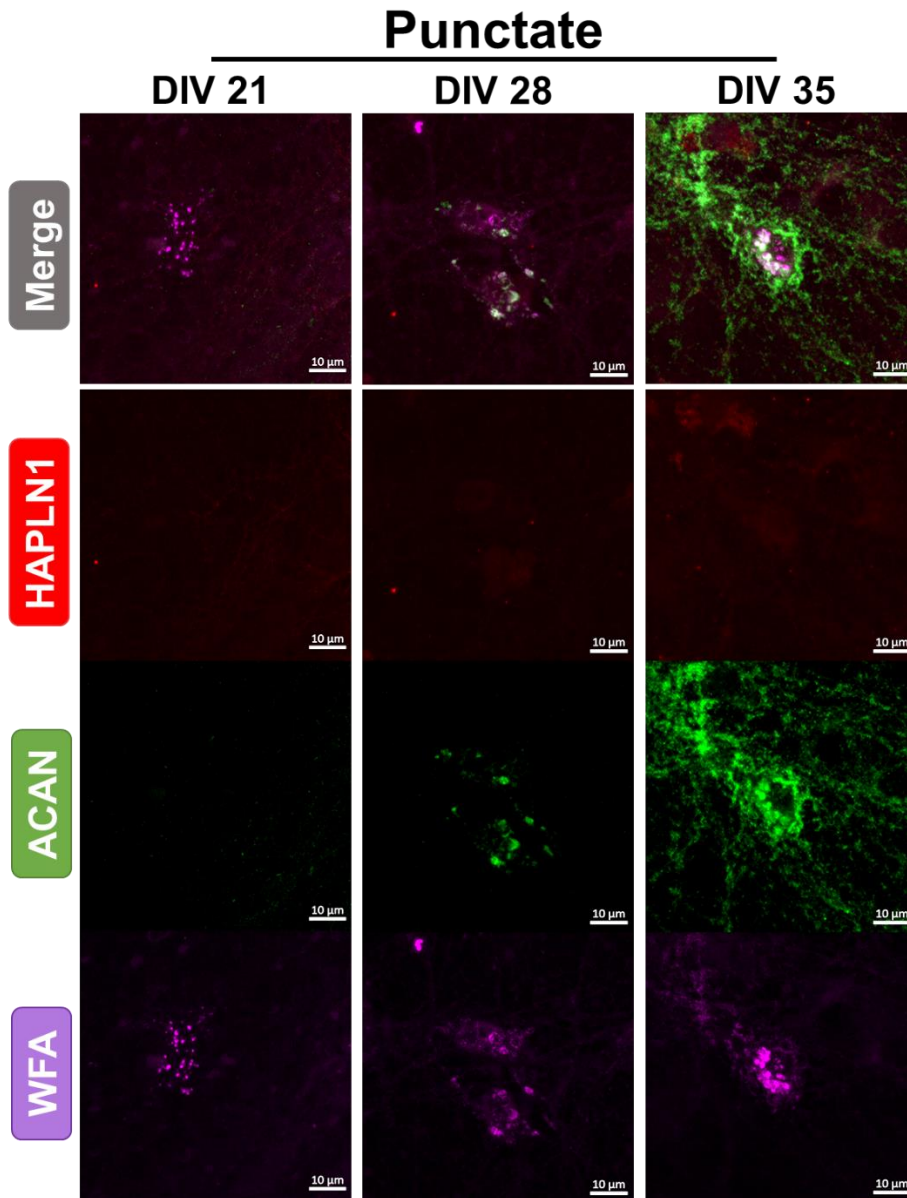


**Figure 8: Recruitment of ACAN to WFA positive PNN**

Representative immunofluorescence images of rat cortical *in vitro* PNN neurons across several time points. At DIV21 PNN first forms as small WFA positive puncta. At DIV28 the puncta are enlarged and ACAN has started localising to the PNN. At DIV35, the last time point before reticular PNNs become the majority morphology, the staining intensity has increased and the number of puncta has increased.

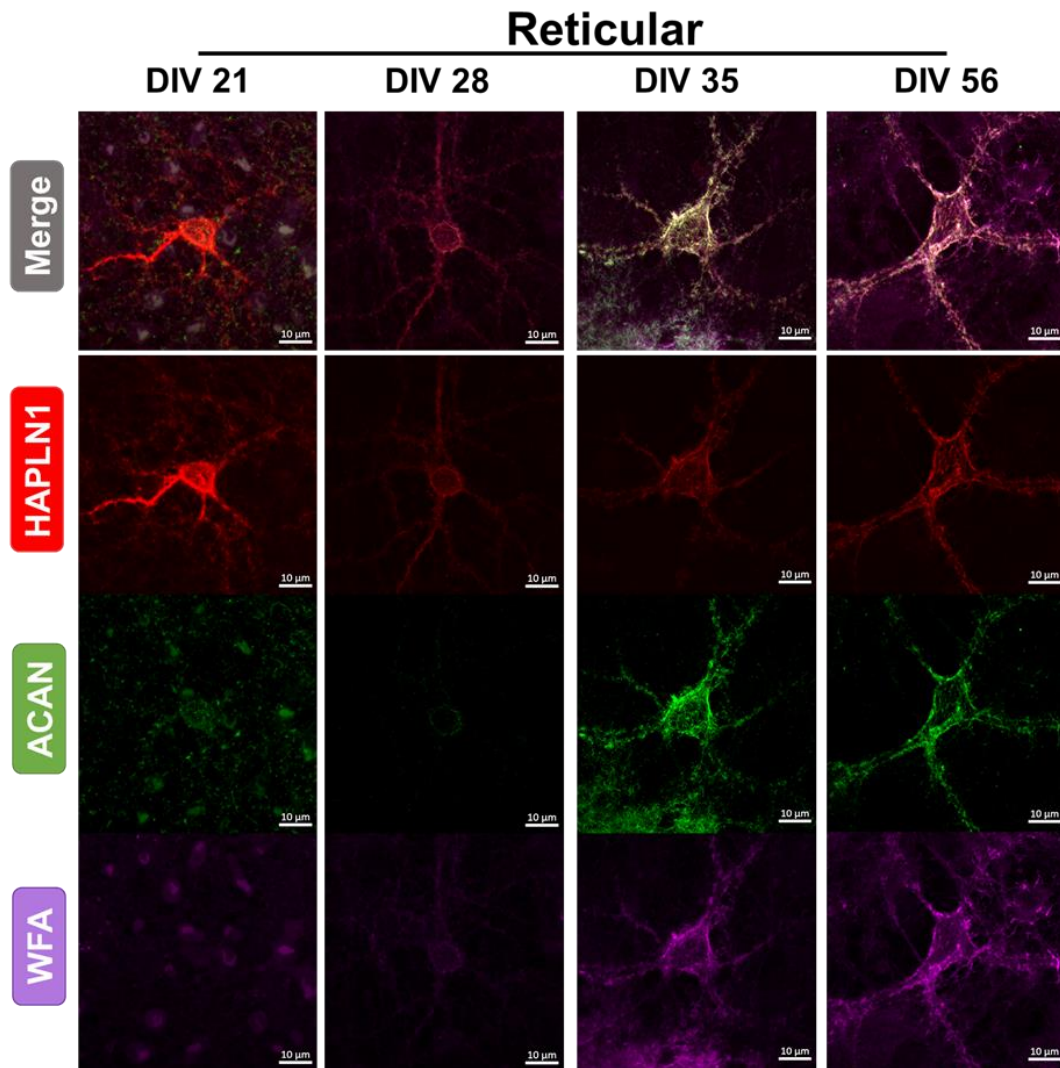


**Figure 9: Recruitment of PNN markers to hapln1 positive PNNs**

Representative immunofluorescence images of rat cortical *in vitro* PNN neurons across several time points. At DIV21 the only reticular PNNs found are only positive for HAPLN1. By DIV28 weak ACAN and WFA reticular staining can be seen. The intensity of WFA and ACAN increases as the culture ages. At DIV56 the PNN staining has fully condensed and mature, reticular PNNs are the majority morphology.

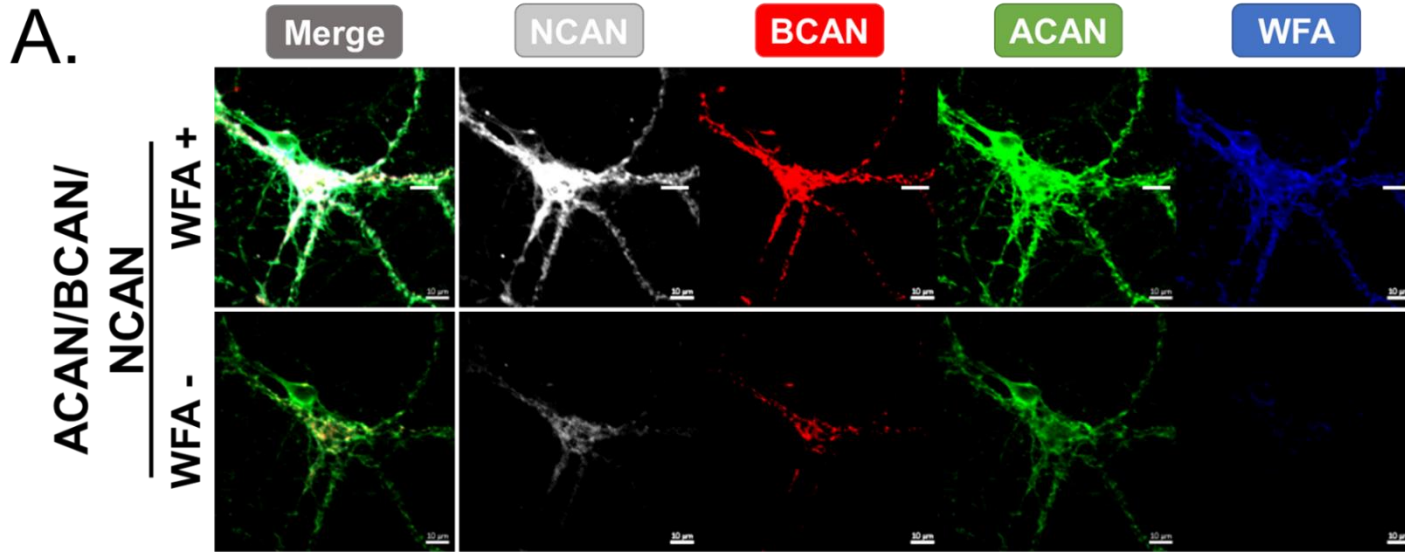
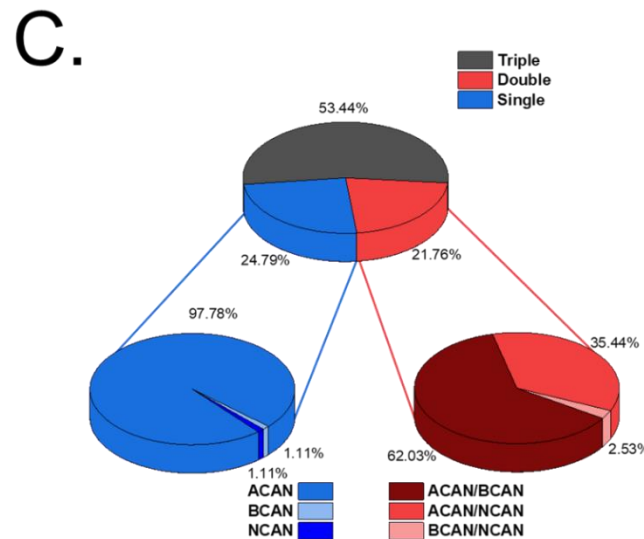
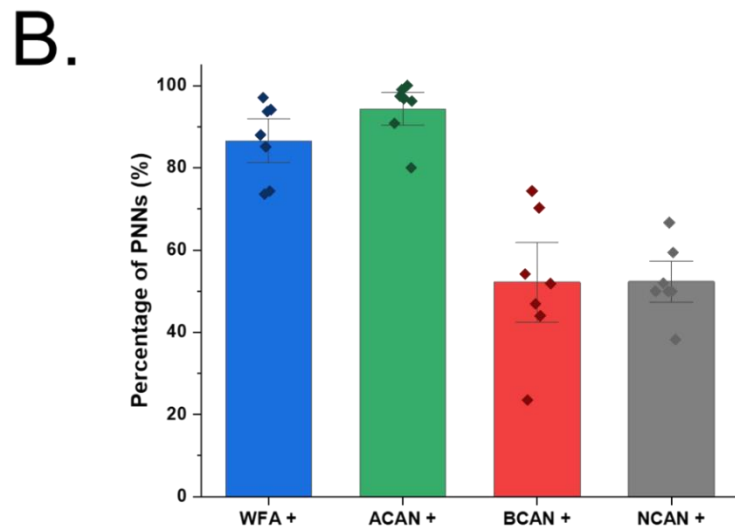
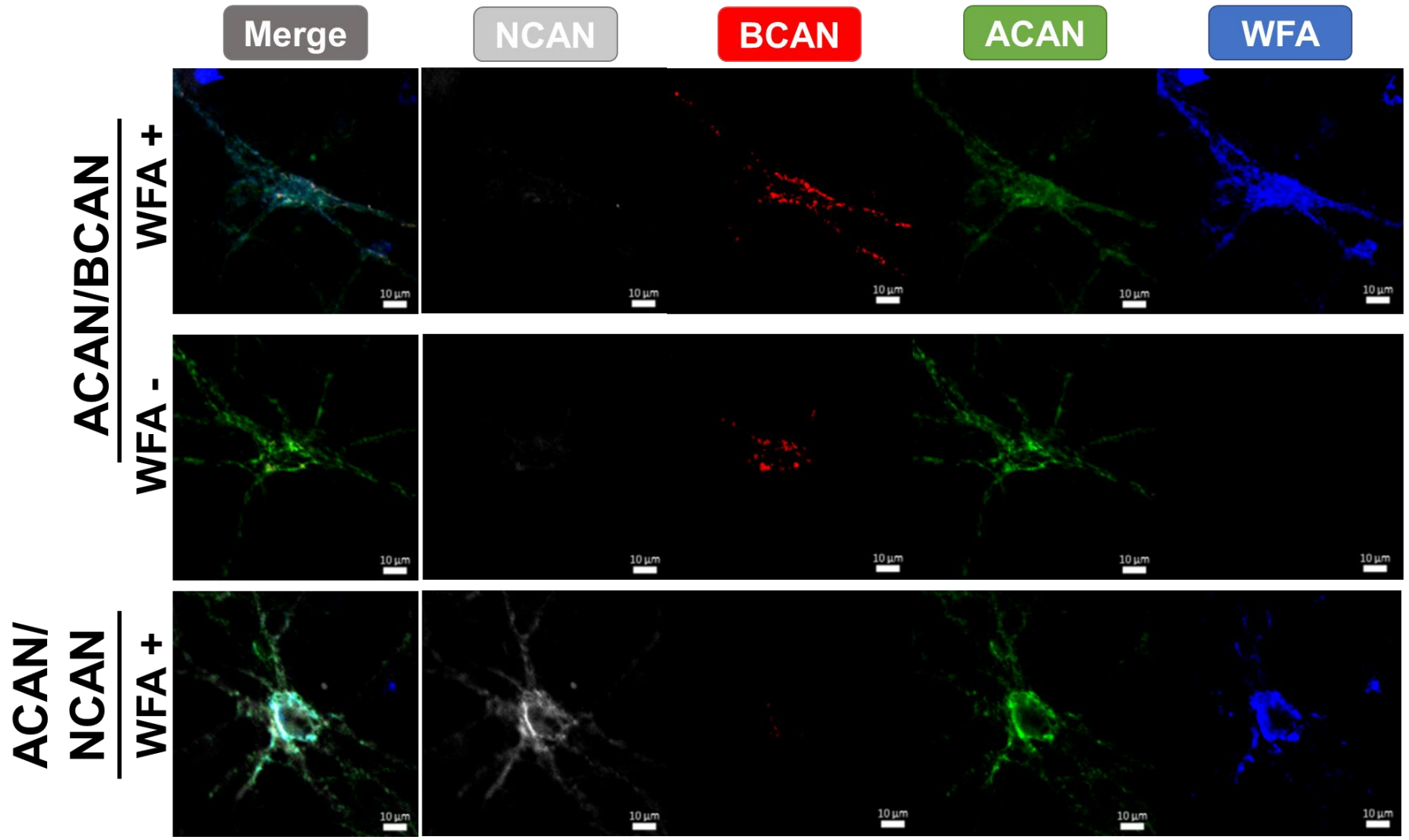


**Figure 10: Comparison of WFA and CSPG staining of mature DIV56 *in vitro* PNNs**

**A.** Mature *in vitro* PNNs display multiple CSPG reactivities. ACAN, BCAN and NCAN were found to localise to the same PNNs. The majority of these PNNs were also reactive for WFA but a minority showed no WFA reactivity, indicating altered glycosylation. Representative immunofluorescence images show PNNs at DIV56 that are reactive for all CSPGs but have different WFA reactivity. **B.**



**B.** Quantification of PNN components at DIV56. WFA and ACAN account for the majority of PNNs. ACAN and WFA accounted for significantly more PNNs than BCAN or NCAN as determined by one-way ANOVA ( $p < 0.05$ ). Data bars are mean of coverslip percentages with SEM. Data points are PNN percentages for individual coverslips of 3 rats. **C.** Breakdown of WFA positive PNNs by CSPG reactivity. The majority of WFA positive PNNs are positive for all CSPGs however a proportion are only reactive for one or two CSPGs. Almost all single CSPG PNNs were ACAN positive. For PNNs that were positive for two CSPGs ACAN/BCAN was the most common pairing. Data are mean percentage of N=3 rats, n=457.



### ◀Figure 11: Heterogeneity of CSPGs localisation in PNNs

Representative immunofluorescence images of PNNs at DIV56 in rat cortical neuronal culture. Arrow heads indicate PNNs of interest. **A.** ACAN and BCAN positive PNN. The majority of ACAN/BCAN PNNs are also reactive for WFA. However, a minority do not present with WFA signal, indicating an altered glycosylation profile. **B.** ACAN and NCAN positive PNNs. ACAN and NCAN also colocalise to PNNs without BCAN. They formed a small minority of mature PNNs at DIV56 and were all reactive for WFA. Scale bar is 50  $\mu$ m.

### 3.3.4 The heterogeneity of mature PNNs

#### 3.3.4.1 Acan, bcan and ncan are found in mature cortical PNNs *in vitro*

After establishing a mature PNN culture model which replicates the reticular PNN morphology observed in the CNS, we wanted to determine if the mature PNNs replicated the diversity of PNN composition seen *in vivo*. This would determine how accurate the *in vitro* PNN culture was to *in vivo* PNNs. We stained mature DIV56 cultures for the CSPGs: bcan, ncan and vcan (Fig.10). We did not detect vcan in our culture but bcan and ncan were detected. HABP was also used to stain for the presence of HA in the PNN. HABP was found on PNNs in our culture and was also reticular in nature at DIV56. Bcan and ncan both showed a reticular morphology and colocalised with acan and WFA positive PNNs. While the majority of PNNs were positive for all components a significant proportion lacked one or more of the components. WFA stained for the majority of PNNs but  $13.4 \pm 3.6\%$  of PNNs lacked WFA staining, indicating variability in PNN glycosylation (Fig.10b). Furthermore, among WFA positive PNNs,  $47.6 \pm 6.1\%$  lacked one or more of the CSPGs, resulting in double or single CSPG positive PNNs (Fig.10C). This heterogeneity is replicated in WFA negative neurons (Fig.11). The heterogeneity among CSPG expression in PNNs replicates what is seen *in vivo* (Ueno, *et al.*, 2018a; Irvine and Kwok, 2018). Heterogeneity was also seen when CSPGs were co-stained for with TnR but not with hapln1 (Fig.12 and Fig. 13). The reason for this heterogeneity and its functional implications are yet unresolved. This model replicates PNN heterogeneity and therefore provides a platform from which to approach this question.

#### 3.3.4.2 Acan is the predominant PNN CSPG in mature cortical PNNs *in vitro*

Quantification of the number of PNNs positive for CSPGs and WFA revealed that WFA and acan stained the highest proportion of PNNs ( $86.6 \pm 9.5\%$  and  $94.3 \pm 7$ ). They stained for a significantly higher proportion of PNNs than bcan

and ncan, which were only found in ~50% of PNNs (Fig. 10B). Acan accounted for the majority of double and single CSPG PNNs (Fig. 10C). Acan negative PNNs accounted for less than 1% of WFA positive PNNs and less than 4% of WFA negative PNNs, further indicating that acan is a key PNN component in our culture. As less than 1% of WFA positive PNNs were negative for acan it strongly indicates that acan is the main bearer of the WFA epitope in mature cortical PNNs. This is in agreement with *in vivo* data (Ueno, *et al.*, 2017b). However, as shown in the previous section, this is not the case during PNN development where an unknown CSPG carried the WFA epitope. This data shows that acan is the predominant PNN CSPG and is therefore the best pan-PNN marker for this culture. However, the acan positive PNN proportion is not significantly higher than the WFA positive proportion, indicating that both can be used as PNN markers. This is in contrast to the spinal cord where a significantly higher proportion of PNNs were identified with acan than WFA (Irvine and Kwok, 2018). This further demonstrates the heterogeneity of PNNs across the CNS and care should be used when choosing which markers to analyse PNN populations.

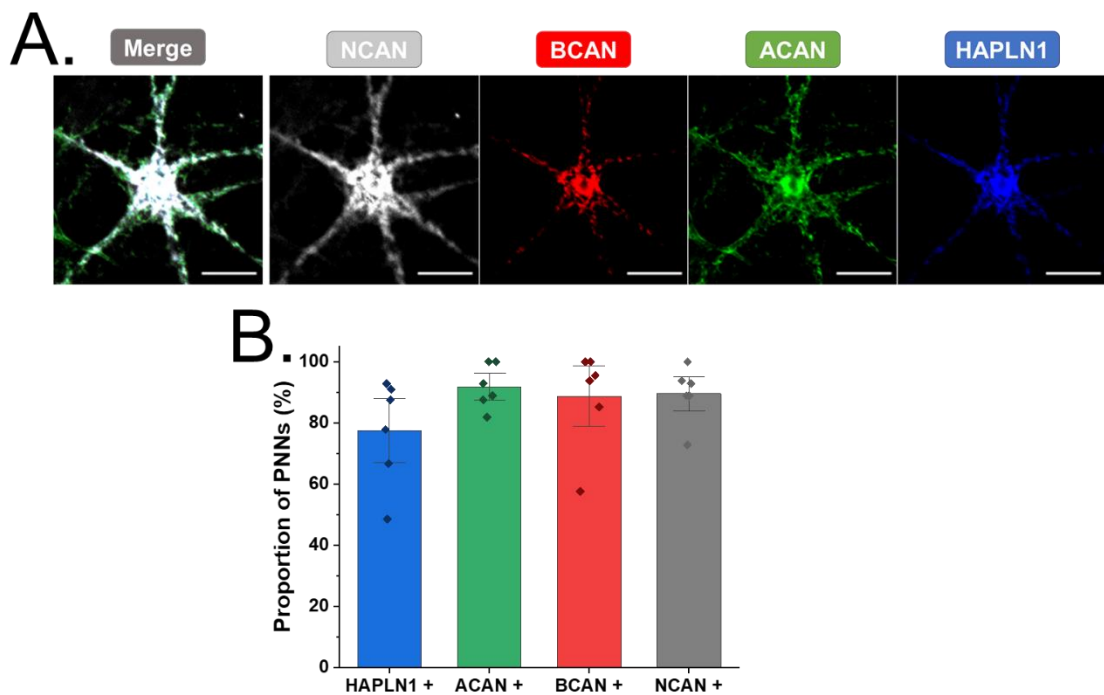


**Figure 12: Mature in vitro PNNs contain hapln1**

**A.** Representative immunofluorescence images of PNNs at DIV56 in rat cortical neuronal culture. HAPLN1 staining colocalised with all CSPGs antibodies. Scale bar is 50  $\mu$ m **B.** Quantification of PNNs. Data are means with SEM. Data points are percentages of PNNs counted per coverslip. N=6 coverslips, representing two rats, n=121 neurons.

### 3.3.4.3 Hapln1 does not segregate with a single CSPG

Hapln1 is a key component of cortical PNNs *in vivo* as knock-out animals show disturbed PNNs with diminished acan and WFA staining (Carulli, *et al.*, 2010). Interestingly, the knockout of the related hapln4 does not lead to acan reduction in the brainstem or cortex despite disruption of other PNN components (Bekku, *et al.*, 2012). This indicates that hapln1 may have a specific role in stabilising acan to the PNN and would help explain PNN heterogeneity as its presence would determine acan localisation. If this is the case, then we should observe a strong colocalization between acan and hapln1 and the acan only positive PNNs observed should be hapln1 positive. However, we did not see this segregation of hapln1 with acan. While hapln1 showed a strong reticular morphology in mature PNNs (Fig. 12A) it did not segregate with acan or any other CSPG (Fig. 12B). No significant differences between the percentage of PNNs detected by PNN markers was observed. A higher proportion of BCAN and NCAN positive PNNs was observed in Fig. 10B compared to Fig. 12B this is due to the different denominator and method of imaging as the hapln1 stain was used to guide the imaging. All hapln1 positive PNNs observed were positive for all CSPGs, no single and double CSPG PNNs were observed as with WFA staining. In our culture hapln1 does not segregate with any single CSPG and is only found in complex PNNs containing all CSPGs.

### 3.3.4.4 Tenascin R is a key component of mature PNNs *in vitro*

The precise role of TnR in the PNN has yet to be fully elucidated. It has roles in PNN-mediated synaptic plasticity and is a putative PNN cross-linker (Bukalo, *et al.*, 2001; Morawski, *et al.*, 2014). Therefore, we wished to determine whether our *in vitro* PNN model contained TnR. If it was shown to be present, then our model could be used to investigate the function of TnR in the PNN. As with hapln1, we also wished to determine if TnR segregated with a specific CSPG as this would improve our understanding of the molecular underpinnings of PNN heterogeneity. We stained mature PNNs at DIV56 for TnR and the CSPGs then imaged and quantified the number of PNNs. TnR staining was used to guide imaging. TnR was found in  $80.6 \pm 3.7\%$  of PNNs but a proportion of PNNs were TnR negative (Fig. 13A and B). Unlike hapln1, a proportion of TnR positive PNNs were not positive for all CSPGs (Fig. 13C and Fig. 14). Ncan only/TnR positive PNNs were not observed in the culture (Fig. 13C). Ncan also recognised a significantly smaller proportion of PNNs than acan or bcan (Fig. 13B). Together this may indicate a preference of TnR for acan and bcan or a lack of interaction with ncan. This is in contrast to the biochemical data where TnR has been shown to interact with all PNN CSPGs (Aspberg, *et al.*, 1997;

Milev, *et al.*, 1998). In summary we have shown that TnR is a major component of mature PNNs in our model. TnR has been posited as a putative PNN cross-linker and as such could drive the transition between punctate and reticular PNNs. Therefore, in future our model should be used to determine when TnR expression starts and if its appearance coincides with PNN maturation.

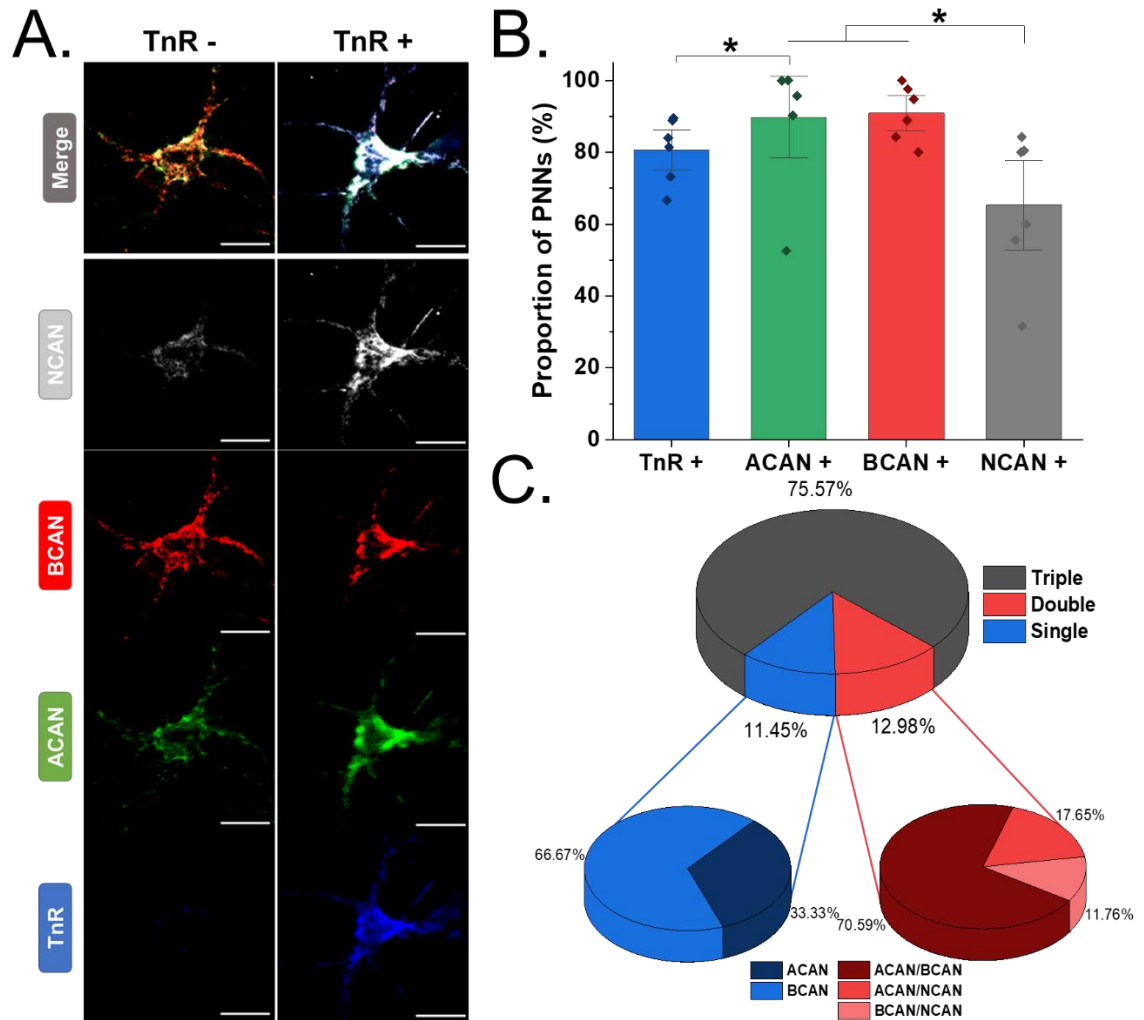


**Figure 13: A high proportion of in vitro PNNs contain tenascin R**

**A.** Representative immunofluorescence images of PNNs at DIV56 in rat cortical neuronal culture. Both TnR positive and negative PNNs were found in the culture. Tenascin R colocalised with all CSPG staining. Scale bar is 50  $\mu\text{m}$ . **B.** Quantification of mature PNNs at DIV56. Data are means with SEM. Data points are sum of PNNs counted per coverslip. N=6 coverslips, representing two rats, n= 169 neurons. **C.** Pie chart breakdown of TnR positive PNNs. The majority of TnR positive PNNs contained all CSPGs. For single or double CSPG PNNs TnR segregated with BCAN. Data are sum of all PNNs counted across 6 coverslips (3 per rat).

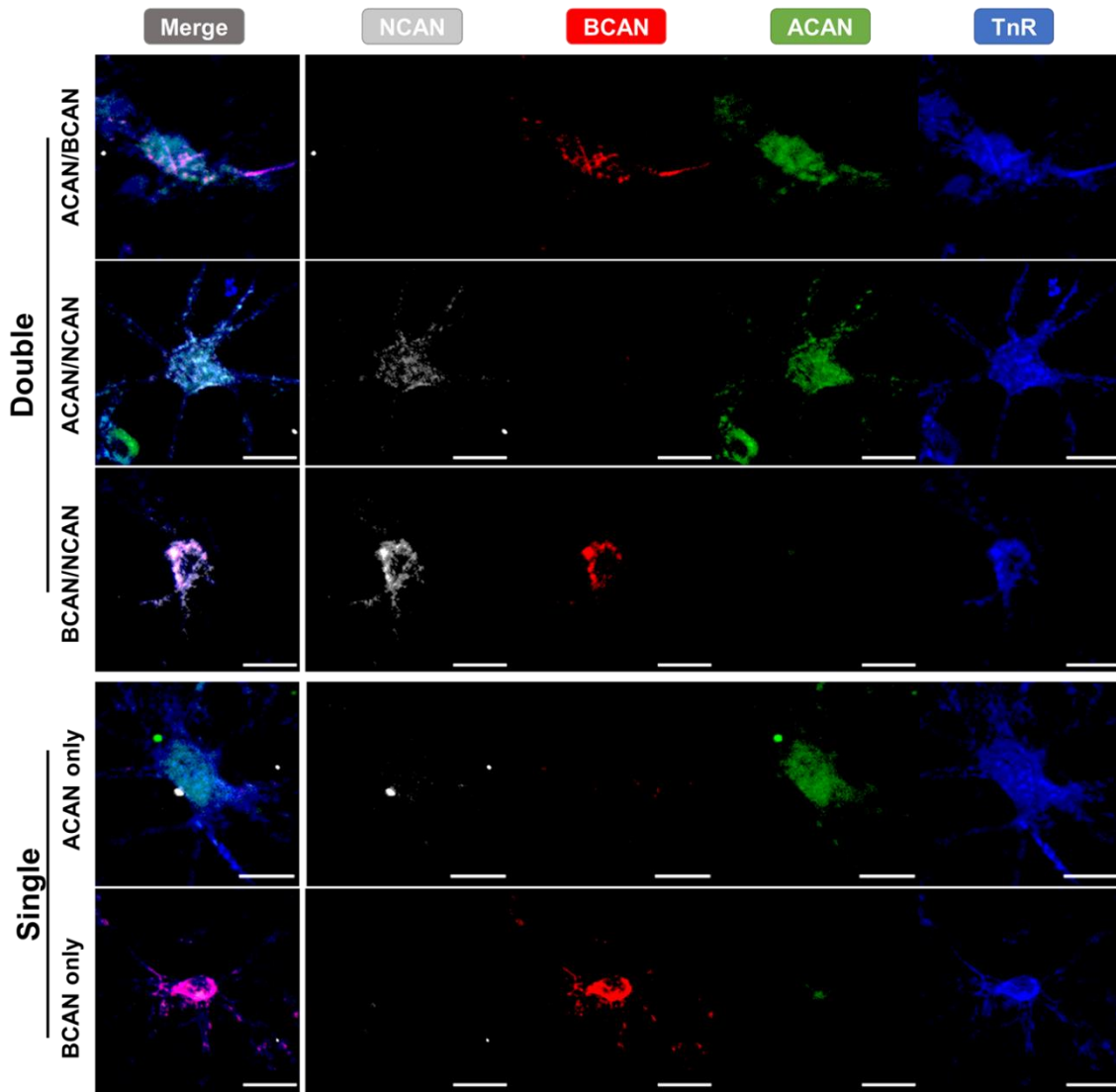


**Figure 14: Heterogeneity among TnR positive PNNs**

Representative images of PNNs from DIV56 rat neuronal cortical culture. Scale bar is 50  $\mu\text{m}$  **A.** Double CSPG PNNs are also positive for TnR. **C.** Single CSPG PNNs are positive for TnR.

## 3.4 Discussion

### 3.4.1 Summary of results

We have developed an *in vitro* neuronal culture which develops mature cortical PNNs. WFA reactive PNNs appear around DIV21 and are punctate in nature. Between DIV28-35, the staining coalesces as the culture ages into a mature, reticular morphology. By DIV56 the reticular morphology is the predominant population, accounting for 90% of PNNs, and replicates PNN morphology in the mature CNS. We have shown that WFA is the best marker for tracking PNN development as it stains the majority of PNNs at all-time points. Acan, the predominant CSPG found in cortical PNNs, appears later in PNN development than WFA and hapln1, but localises to the majority of mature PNNs. We have identified two distinct populations of PNNs during development; punctate, WFA positive PNNs (immature) and reticular, hapln1 positive PNNs (early mature). This distinction disappears as the culture matures and shows not all PNNs mature at the same rate. We characterised the composition of mature PNNs at DIV56. We found they contained hapln1, TnR and a variety of CSPGs. Vcan and pcan were not detected in our culture at DIV56 but bcan, acan and ncan were identified.

There are conflicting reports regarding pcan and vcan expression in the PNN *in vitro*. Vcan PNN expression was identified in rat hippocampal neurons at DIV21, while we did not observe it our cortical culture at DIV56 (John, *et al.*, 2006). Pcan PNN expression was not found at DIV30 in rat cortical cultures while it has been identified at DIV21 by a different group (Miyata, *et al.*, 2005; Giamanco, *et al.*, 2010). These discrepancies can be explained by temporal and spatial heterogeneity. Vcan PNN expression varies between brain region, with higher expression in the hippocampus than the parietal cortex (Ueno, *et al.*, 2017a; Gao, *et al.*, 2018). Temporal variation in expression has been demonstrated in this culture and elsewhere. Pcan PNN expression has been shown early in PNN development (Hayashi, *et al.*, 2005; Galtrey, *et al.*, 2008). It is likely both CSPGs are present within our culture but at an earlier time point.

We found there was considerable heterogeneity within the PNN population regarding WFA reactivity, the CSPGs they contained and whether they contained TnR. In summary we have established a PNN culture model that accurately replicates the PNN heterogeneity and complexity seen in the cortex. We observed the progressive maturation of PNNs in culture and thus have established a platform that PNN maturation can be studied and manipulated.

### **3.4.2 Maturation of the PNN *in vitro***

#### **3.4.2.1 Identification of an early mature PNN population**

WFA reactivity started appearing at DIV21 in our culture and was punctate in appearance, accounting for roughly  $71.3 \pm 4.9\%$  of PNNs. A hapln1 positive reticular PNN population was also observed which accounted for the remaining PNNs. They are distinct populations due to the minimal overlap between the staining (hapln positive/WFA positive:  $3.38 \pm 2.2\%$ , WFA positive/hapln positive:  $8.0 \pm 3.1\%$ ) compared to the proportion of WFA positive PNNs that were acan positive at DIV21. As the culture matured the colocalization of acan, hapln1 and WFA significantly increased. The identity of this population was not resolved during this project but is likely that they are non-PV neurons as the proportion of PNN neurons that were not PV neurons was also around 30%. In the cortex the other population of PNN neurons are pyramidal neurons (Brückner, *et al.*, 2004). Reticular PNNs have been shown to form on cortical pyramidal neurons *in vivo* (Hausen, *et al.*, 1996; Wegner, *et al.*, 2003; Alpár, *et al.*, 2006). Excitatory circuits typically mature before their inhibitory counterparts and help drive their maturation in the cortex (Lodato, *et al.*, 2011). The earlier maturation of excitatory neurons could therefore explain the early appearance of mature PNNs.

#### **3.4.2.2 PNN maturation correlates with rising acan localisation**

During development, the PNN transitions from a punctate to a reticular morphology (Ueno, *et al.*, 2017b; Richter, *et al.*, 2018; Rogers, *et al.*, 2018). In our culture we can observe PNN maturation as a punctate morphology gives way to a reticular. The punctate form has also been shown in other neuronal cell culture models at similar time points *in vitro*, but this is the first time the transition to a reticular morphology has been shown (Miyata, *et al.*, 2005; Dityatev, *et al.*, 2007; Van't Spijker, *et al.*, 2019). We observed that PNN maturation enters a key point between DIV28-35 as this is when the PNN population switches from the immature state to the mature. In our culture we see acan signal increases during maturation, indicating a role in maturation. This mirrors what is seen *in vivo*. mRNA expression of *Aggrecan* also increases during PNN maturation in several CNS regions, including the parietal cortex (Carulli, *et al.*, 2007; Galtrey, *et al.*, 2008; Gao, *et al.*, 2018). While HA was identified on PNNs in our model we did not investigate the expression of HAS isoforms during development. This should be investigated and HAS expression manipulated to determine whether HAS overexpression would lead to the development of a continuous PNN film.

There are multiple pathways for PNN maturation. A reticular film arises from the interaction between polymer density and attraction and therefore the morphology can be achieved through different contributions of either. It is most likely that the maturation process is caused by multiple mechanisms working in concert. The degree of contribution by each mechanism may change with CNS region and the PNN neuron subtype. For example, in our culture we observed a small proportion of reticular PNNs at DIV21 that were hapln1 positive/WFA-. This early mature population must therefore be maturing at a different rate, hinting at a distinct maturation mechanism from other cortical PNNs and that hapln1 expression is linked to morphology maturation. The advantage of our *in vitro* culture is that it models the maturation of PNN closely and provides a platform from which these questions can be resolved. This is because *in vitro* culture models allow for the fine manipulation of PNN components through silencing or addition of the components. This can be achieved with a higher temporal resolution than *in vivo* models. For example, while TnR expression was shown in PNNs at DIV56, its expression during maturation was not investigated. Determining when TnR expression begins and whether it only appears on reticular PNNs will help resolve if TnR is involved in PNN maturation. Furthermore, we can investigate if PNN maturation can be accelerated by the addition of putative maturing agents (i.e., TnR or Sema3A) or through neuronal activity (e.g., plating on multiple electrode arrays). Improving our understanding of PNN maturation will inform our understanding of why PNN formation fails in developmental disorders (e.g., schizophrenia and epilepsy) and provide avenues by which to correct the deficit. It will also provide us the tools by which to reopen plasticity in the CNS. This could have huge implications for conditions such as spinal cord injury or stroke.

### **3.4.3 PNN heterogeneity: clues to different functions**

To create a PNN only three classes of components are needed: membrane bound hyaluronan, a link protein and a CSPG (Kwok, *et al.*, 2010). However, there is redundancy within the classes as multiple HAS isoforms, link proteins and CSPGs have been found in the PNN *in vivo*. PNN binding molecules such as TnR, Sema3A, pentraxin 2 and others have also been identified and their removal affects PNN structure (Fawcett, *et al.*, 2019). What effect this heterogeneity has on PNN function is unresolved. Currently the best way to address this question is through the creation and study of PNN component knock-out animals. This is a costly and intensive process. Also it may have unanticipated effects beyond the PNN as many of the PNN components, while enriched in the PNN, are found throughout the CNS and beyond and have PNN-independent roles (Deepa, *et al.*, 2006; Xu, *et al.*, 2014). An accurate *in*

*in vitro* PNN model several advantages of: reduced costs, easy, transient genetic manipulation, and circumvent the risk of confounding non-PNN related effects. However, as with any model, the reductive nature of an *in vitro* PNN model could remove the very complexity that was to be studied. Therefore, we needed to establish that our *in vitro* PNN model could replicate *in vivo* PNN heterogeneity. We have shown that our model contains PNN heterogeneity in CSPG and TnR localisation and glycosylation state.

### 3.4.3.1 A WFA negative PNN population

The PNN marker WFA stained the majority of mature PNNs but a significant proportion of PNNs were WFA-. This shows variation in PNN glycosylation in culture. The glycosylation of the PNN, or GAG code, has been shown to have important effects on PNN function. The 6S:4S ratio modulates the inhibitory nature of PNN (Dou and Levine, 1995; Loers, *et al.*, 2019). 4S rises through development and is inhibitory while 6S is permissive (Kitagawa, *et al.*, 1997). The WFA lectin has been shown to bind to unsulphated chondroitin and CS-E, which are both enriched in the PNN (Deepa *et al.*, 2006; Nadanaka *et al.*, 2020, *unpublished data*). CS-E is important for BDNF, Otx2 and Sema3A (Gama, *et al.*, 2006; Beurdeley, *et al.*, 2012; Dick, *et al.*, 2013). WFA has been regarded as the pan-PNN marker though our data and recent literature has shown that it is not universal (Irvine and Kwok, 2018; Ueno, *et al.*, 2018). The existence of WFA negative PNNs therefore posits a PNN population lacking CS-E and therefore unable to bind several molecules important for PNN function (e.g., Sema3A, Otx2). This hints at both an altered function and a different maturation mechanism for this population of PNN neurons and warrants further investigation.

The CSPG acan has been shown to be the main bearer of the WFA epitope in the mature CNS (Irvine and Kwok, 2018; Miyata, *et al.*, 2018). Our model replicates this as acan is the predominant CSPG in WFA positive PNNs. Interestingly, we have found that this is not the case during PNN development. While WFA stains a consistent proportion of PNNs throughout development; the proportion of PNNs that are acan positive is much lower. Furthermore, at earlier time points we observed segregation between acan and WFA within the PNN, this segregation disappeared by DIV56. This indicates another CSPG bears the WFA epitope early in PNN development. There is then a transition as acan expression rises as the PNN matures, seen by the increased colocalization of the acan and WFA PNN populations. The identity of this CSPG was not resolved in this study but previous work has shown that ncan and pcan expression peaks early in PNN development and could bear the WFA epitope

(Hayashi, *et al.*, 2005; Miyata, *et al.*, 2005; Dino, *et al.*, 2006; Galtrey, *et al.*, 2008; Gao, *et al.*, 2018). Therefore, WFA colocalization with other CSPGs should be investigated.

### 3.4.3.2 Heterogeneity in CSPG expression between PNNs

Multiple CSPGs have been identified in the PNN and CSPG expression is not uniform across the PNN population in the CNS (Irvine and Kwok, 2018; Ueno, *et al.*, 2017a). This was replicated in our culture: 50% of PNNs only expressed one or two of the CSPGs stained for and only 50% of PNNs contained bcan or ncan; while the majority of mature PNNs contained acan. Furthermore, CSPG expression changed during development as acan expression rose indicating temporal heterogeneity. Why does such spatial and temporal heterogeneity exist?

If the sole function of the PNN is to provide an inhibitory barrier to plasticity then the role of CSPGs is to bear inhibitory GAG chains. The number of GAG attachment sites vary between CSPGs. Acan has 120 GAG attachment sites while ncan and bcan have 7 and 3 respectively (Yamaguchi, 2000). This could then explain the increase in acan in maturation as it would increase the GAG capacity of the PNN. This, coupled with the rise in 4S, would create a more inhibitory PNN as is seen *in vivo* (Foscarin, *et al.*, 2017). However, this assumes the core protein of the CSPG is incidental beyond providing GAG attachment sites. CSPG knock-out animals challenge this assumption and indicate a specific role for CSPGs which require the core protein. Favuzzi *et al.* (2017) established that bcan specifically stabilises excitatory synapses on PNN-bearing PV neurons. Ncan may play a similar stabilisation role for inhibitory synapses; knock out in the medial nucleus of the trapezoid body led to a selective decrease in inhibitory synapses and altered synaptic transmission (Schmidt, *et al.*, 2020). This highlights a specific role for individual CSPGs in the PNN, although whether it is mediated by the protein core or the GAG chains has yet to be resolved.

Interestingly, CSPGs may regulate PNN development through regulation of the mRNA of other PNN components. In the *ncan*<sup>-/-</sup> animal *hapln1* and *bcan* mRNA levels were reduced while *acan* was spared. Similarly, in an *acan*<sup>-/-</sup> animal led to a reduction in other PNN component expression (Rowlands, *et al.*, 2018). However, in neuronal cultures from the *cmd* animal *hapln1* PNN staining was preserved indicating variability between models. PNN component expression was not tested in the *bcan*<sup>-/-</sup> animal so it is not known whether it also exerts a regulatory effect. How CSPGs may regulate the expression of other PNN components has not yet been explored. This could be easily tested in our

culture through transient CSPG silencing and mRNA analysis at different time points in the culture.

### 3.4.3.3 Hapln1 does not segregate with a specific CSPG

When the *hapln* family were first identified it was noted that each member showed genetic linkage to a lectican gene (Spicer, *et al.*, 2003). This led to the hypothesis that each hapln protein had a preferential CSPG partner. This hypothesis would offer a neat explanation to the apparent redundancy within the *hapln* family but has yet to be proved. Data from *hapln* knock-out animals is conflicted. *Hapln1*<sup>-/-</sup> resulted in the loss of all CSPGs from cortical PNNs, despite the fact hapln4 is also found in cortical PNNs (Bekku, *et al.*, 2003; Carulli, *et al.*, 2010; Rowlands, *et al.*, 2018). The protein expression of the CSPGs was conserved in the knock-out, indicating it was the structure the components bound to rather than the components themselves that was lost (Carulli, *et al.*, 2010). This would indicate there is no specific hapln/CSPG pairing. However, in the *hapln4*<sup>-/-</sup> animal bcan expression was completely lost from cerebellar PNNs, while hapln1/acan localisation was unaffected. Also, ncan was only partially affected (Bekku, *et al.*, 2012). This indicates a preferential pairing between hapln1, ncan and acan. This would indicate a specific pairing between hapln4/bcan in the cerebellum but it is in contrast to the visual cortex where *hapln1*<sup>-/-</sup> caused ablation of bcan localisation to the PNN (Carulli, *et al.*, 2010). In our cortical culture we saw no segregation of hapln1 with a single CSPG. Instead, it was only found in PNNs with all three CSPGs. This agrees with the *hapln1*<sup>-/-</sup> mouse model which also showed no preference. This shows that there is no specific pairing of hapln1 with a CSPG in the cortex. However, this does not reconcile with what is seen in cerebellar PNNs which indicates organisational differences between PNNs in different CNS regions. To resolve this the biophysical interactions between haplins and CSPGs should be systematically screened. This would resolve whether there is specific hapln/CSPG pairing.

### 3.4.4 TnR localises to mature PNNs *in vitro*

TnR is a necessary component of PNNs as its removal leads to punctate and reduced PNNs (Brückner, *et al.*, 2000; Haunsoø, *et al.*, 2000; Morawski, *et al.*, 2014). This is reminiscent of the immature punctate PNNs seen in our culture and *in vivo*. TnR stained a high proportion of PNNs and seemed to segregate from ncan as no TnR positive/ncan only PNNs were identified. This is interesting as an interaction between ncan and TnR has been demonstrated (Aspberg, *et al.*, 1997). Further contributors to PNN/CSPG diversity is the existence of CSPG splice variant and post-translational cleavage products. The

segregation between ncan and TnR may arise from ncan lacking the requisite G3 domain. This can be investigated via Western blot of PNN ncan (Deepa, *et al.*, 2006)

We did not investigate the expression of TnR during development in our culture. TnR expression during development has been investigated in both the cerebellum and spinal cord. In both CNS regions expression peaked during development before decreasing as the animal reaches adulthood (Carulli, *et al.*, 2007; Galtrey, *et al.*, 2008). However, it has not been investigated in the cortex and due to the established heterogeneity between PNN populations this should be investigated. Our culture provides the opportunity to investigate TnR expression during cortical PNN maturation and answer the question whether a TnR expression peak coincides with the switch from punctate to reticular PNNs. If TnR is expressed at DIV21 in the early mature PNN population but not the punctate population then it would provide strong evidence that TnR catalyses cortical PNN maturation.

### 3.4.5 Conclusions and future directions

The aim of this chapter was to establish an *in vitro* PNN culture model that accurately modelled mature PNNs as they are seen *in vivo*. We have succeeded in this aim. The PNNs in this culture replicate the mature, reticular morphology seen in the mature CNS. We have also shown that the PNNs contain the PNN components seen in the cortex: the CSPGs, acan, bcan and ncan, hapln1 and TnR. The *in vivo* PNN heterogeneity is also replicated. The reasons underlying this heterogeneity are unresolved but our culture provides a platform from which to investigate this question through transient knock-down of components of interest. During the culture we observed PNN maturation. The PNN coalesced from a faint punctate morphology to the mature, reticular morphology seen in the adult CNS. Concomitant with this transition is a rise in acan staining. Interestingly, we have found a PNN population that was reticular at an earlier time point, indicating different maturation timeframes between PNNs. What underlies the transition in PNN morphology is unknown but the *in vitro* model can be used to answer this question as *in vitro* cultures can be observed at granular detail and putative maturing agents can be used (TnR, Sema3A, neuronal activity). Establishing a culture model which accurately replicates PNN development and heterogeneity has great utility in PNN research. It can provide answers on PNN biology as well as provide a platform to investigate the role of PNNs in disease. I will use this model to examine if the PNN is a protective against  $\alpha$ -synuclein seeding in Parkinson's disease.

## Chapter 4 The PNN reduces aggregated $\alpha$ SYN species uptake and p- $\alpha$ SYN pathology development

### 4.1 Introduction

Parkinson's disease (PD) is a progressive, age-related neurodegenerative condition that is estimated to affect over 10 million people world-wide (Tysnes and Storstein, 2017). As discussed in chapter 1, due to the lack of disease halting treatments and rising life expectancy, PD is set to become a modern epidemic. Symptom appearance and progression can be linked to the appearance of protein inclusions, called LP, in linked brain areas. This has led to the staging of PD by Braak and colleagues (2004). The majority of sporadic PD cases can be classified by this staging, although there are now a unified classification system for all Lewy diseases (Dickson, *et al.*, 2010; Adler, *et al.*, 2019). The main constituent of LP is misfolded  $\alpha$ -synuclein ( $\alpha$ SYN) (Wakabayashi, *et al.*, 1997; Spillantini, *et al.*, 1997; Shahmoradian, *et al.*, 2019). Mutations and multiplications in the  $\alpha$ SYN gene (SNCA) are causative for PD, demonstrating the central role of  $\alpha$ SYN in PD (Koros, *et al.*, 2017).

#### 4.1.1 $\alpha$ SYN internalisation and seeding

Misfolded  $\alpha$ SYN can act as a prion-like agent and spread between neurons and brain regions seeding further pathology, as demonstrated in patient grafts and animal injection models (Kordower, *et al.*, 2008; Li, *et al.*, 2008; Desplats, *et al.*, 2009; Rey, *et al.*, 2016; Kuan, *et al.*, 2019). Seeding is the ability of specific misfolded  $\alpha$ SYN species to catalyse the transformation of naïve  $\alpha$ SYN to a misfolded species, with the misfolded protein acting as a template. For seeding to occur pathogenic  $\alpha$ SYN species must be transmitted into naïve neurons and come into contact with the naïve  $\alpha$ SYN. This requires the pathogenic species to be internalised by the neuron. Several transmission mechanisms have been identified: neuron to neuron trafficking, either through synaptic connections or tunnelling nanotubes; or by travel through the extracellular matrix (ECM), as free  $\alpha$ SYN or within exosomes (Danzer, *et al.*, 2012; Masuda-Suzukake, *et al.*, 2014; Abounit, *et al.*, 2016; Jiang, *et al.*, 2017). Pathogenic  $\alpha$ SYN is internalised via RAB5a-mediated endocytosis (Sung, *et al.*, 2001; Lee, *et al.*, 2008b; Desplats, *et al.*, 2009; Bieri, *et al.*, 2017). Several cellular receptors have been identified; lymphocyte activated gene 3 (LAG3), neurexins, syndecans and Cx32 (Shrivastava, *et al.*, 2015; Mao, *et al.*, 2016; Reyes, *et al.*, 2019). Receptor-mediated endocytosis results in  $\alpha$ SYN in the endosomal-lysosomal system where the majority is then degraded (Lee, *et al.*, 2008a). However, a

proportion of it escapes into the cytoplasm where it seeds  $\alpha$ SYN aggregation (Freeman, *et al.*, 2013; Flavin, *et al.*, 2017; Jiang, *et al.*, 2017; Karpowicz, *et al.*, 2017). Many different species of  $\alpha$ SYN aggregates that have been identified and several distinct species have demonstrated seeding ability (Danzer, *et al.*, 2007; Bousset, *et al.*, 2013; Peelaerts, *et al.*, 2015). It is not yet resolved if there is a single species responsible for seeding in PD or whether it is a mixture. The blocking of transmission and seeding of  $\alpha$ SYN has great therapeutic potential as it targets disease progression rather than temporarily alleviating symptoms.

#### **4.1.2 The PNN as a barrier preventing $\alpha$ SYN internalisation**

The spread of LP is specific and conserved, indicating that specific factors must regulate progression (Braak, *et al.*, 2004). The connectome is one such factor and can explain how LP moves from one brain region to another, but it is not sufficient (Rey, *et al.*, 2013; Oliveira, *et al.*, 2019; Henrich, *et al.*, 2020). Cellular susceptibility is another factor which can predict pathology development (Alegre-Abarategui, *et al.*, 2019). We are investigating what factors make neurons resistant to  $\alpha$ SYN seeding and LP development. In Alzheimer's disease, which also features prion-like seeding, the presence of a perineuronal net (PNN) protects the neurons from  $\beta$ -amyloid toxicity and tau seeding (Brückner *et al.*, 1999; Miyata *et al.*, 2007; Suttikus *et al.*, 2016). The PNN is a dense form of ECM that forms around specific neuron populations. It is a composite structure of GAGs and proteins, which together make a dense and negatively charged structure that covers the neuronal soma and proximal dendrites (Fawcett, *et al.*, 2019). Its main function is to restrict plasticity in the adult brain but a secondary function in neuroprotection has been elucidated (Suttikus *et al.*, 2016; Fawcett *et al.*, 2019). The presence of a PNN protects neurons from oxidative stress, iron toxicity and protein seeding (Miyata *et al.*, 2007; Cabungcal *et al.*, 2013; Suttikus *et al.*, 2014; Suttikus *et al.*, 2016). These processes have been identified in Parkinson's disease (Belaidi and Bush, 2016; Surmeier, *et al.*, 2017a). The PNN could directly block  $\alpha$ SYN seeding by denying  $\alpha$ SYN access to the cell membrane, a pre-requisite for its internalisation. Therefore, the PNN will be investigated as a potential factor for neuronal resistance in PD.

#### **4.1.3 Aims of chapter**

As shown in the last chapter, we have established the first *in vitro* rat neuronal culture that develops mature, reticular PNNs. A weakness of previous *in vitro* PNN cultures is they have used punctate, immature PNNs (Miyata, *et al.*, 2007; Dityatev, *et al.*, 2007). While this has not prevented a protective effect from

being identified, it is not modelling the PNNs as they appear in the aged brain (Ueno, *et al.*, 2018a; Rogers, *et al.*, 2018). This culture, therefore, provides the first time that the role of the PNN in  $\alpha$ SYN transmission can be tested. The aim of this chapter is to investigate if the PNN is a neuroprotective structure in PD. This will be investigated in cell culture: first by using a PNN-HEK cell model and then validating the results in primary neuronal culture. Two established and distinct seeding species will be used as the main pathophysiological species has not been resolved. The two species used will be: the seeding oligomer and sonicated preformed fibrils (PFF) (Danzer, *et al.*, 2007; Volpicelli-Daley, *et al.*, 2011). These structurally distinct species both induce seeding. The ability of PNNs to block  $\alpha$ SYN uptake and pathology development will be examined. Together this work will determine if the PNN is a neuroprotective barrier in PD.

## 4.2 Methods

### 4.2.1 Purification of $\alpha$ -synuclein

All purification was done in and with the kind support of the Leeds Protein Production Facility. The pET-23a\_ $\alpha$ SYN was a kind gift from David P. Smith from Sheffield Hallam University. The human  $\alpha$ -synuclein sequence was subcloned into pOPINS3C using the complimentary In-Fusion™ primers, where the end of each sequence is complimentary to the empty pOPINS3C vector (F: AAGTTCTGTTTCAGGGTCCCATGGATGTCTTCATG AAAGG, R: CTGGTCTAGAAAGCTTTTACGCTTCTGGTTCGTAG). The pOPINS3C vector contains: an N-terminal SUMO and 6 histidine tag to aid solubility and purification. The tag can be cleaved from the protein of interest by a 3C cleavage site (Fig. 15A). The PCR (NEB Q5 polymerase 2,000 U/mL, dNTPs, Q5 enhancer, Q5 reaction buffer, NEB #M0491) was performed using the following conditions: 35 cycles of 10s 98 °C, 20s 70 °C, 15s 72 °C then the product ran on and excised from an agarose gel. The product was then ligated into pOPINS3C vector using the NEBuilder HiFi DNA assembly, following manufacturer's instructions and at a 1:2 vector: insert ratio. The completed reaction mixture was cleaned via incubation with 20 U Dpn1, transformed into DH5- $\alpha$  *E.Coli* and plated on 100  $\mu$ g/mL ampicillin, 20  $\mu$ g/mL X-Gal. Successful white colonies were then picked and grown in liquid overnight. A restriction digest PCR of the clones was then performed as a quality control step before they were sent off for sequencing (Eurofins).

The vector was then transformed into multiple bacteria strains to determine which strain would give the highest yield. Bacterial strains (and antibiotics) used were: Arctic (50  $\mu$ g/mL gentamycin), Rosetta (50  $\mu$ g/mL chloramphenicol), Rosetta2 (50  $\mu$ g/mL chloramphenicol), Rosetta-Gami2 (50  $\mu$ g/mL chloramphenicol and 25  $\mu$ g/mL streptomycin), Shuffle-T7 Express (50  $\mu$ g/mL spectinomycin) and Lemo21 (50  $\mu$ g/mL chloramphenicol). They were all grown under ampicillin for selection of the plasmid. For the conditions for Lemo21 several L-Rhannose conditions were used (500, 1000, 1500, 2000  $\mu$ M). The strains were grown to OD600: 0.4-0.5 then induced with 0.1 mM IPTG and grown at either 18 °C or 25 °C overnight. The next day the protein was harvested using MangeHis purification on a MicroLab Star liquid handling system (Hamilton). The Rosetta 2 strain, grown at 25 °C, gave the highest yield.

For large scale purification the protocol was scaled up. The resulting bacteria were resuspended in cold low salt his buffer (20 mM Tris-HCl, pH7.6, 300 mM NaCl, 20 mM Imidazole, 5% glycerol, 0.075%  $\beta$ -mercaptoethanol) with protease

inhibitor (400 µl per litre of culture of Proteoloc, Expedeon #44204) and lysed using a cell disruptor (15,000 psi). Debris were removed via centrifugation (6,000 x g, 15min, 4 °C). The pellet was then clarified of DNA (35,000 x g, 40 min). Unwanted protein contaminants were then precipitated by boiling (85 °C, 10 min) and removed by centrifugation at 16,000 x g, 20 min, 4 °C.  $\alpha$ -synuclein is an intrinsically disordered protein and so sample heating has no effect on structure or  $\alpha$ -synuclein produces the highest yield compared to other methods (Coelho-Cerqueira, *et al.*, 2013).

Purification of  $\alpha$ -synuclein was performed on the Äkta Pure (Cytiva) at 4 °C in a cool cabinet. Initial purification was done using a Nickel column (5 mL Fast flow HisTrap column, GE #GE17-5255-01) and elution with imidazole. Low salt his, high salt his (with 500 mM NaCl) and elution (300 mM NaCl, 400 mM Imidazole) buffers were used. The fractions were then probed for  $\alpha$ -synuclein via gel staining (Instant Blue protein stain, Stratech #ISB1L-EXP-1L). Briefly, fractions were diluted 1:2 with SDS loading buffer (Laemmli buffer with 5%  $\beta$ -mercaptoethanol), boiled for 3 minutes at 95 °C and loaded onto 4-20% Tris-glycine gels (BioRad #4561096) then run at 200 V constant until sufficient resolution was achieved. To determine protein size estimates, a prestained protein ladder was run alongside (NEB #P7719).

The sample was then dialyzed (3 MWCO, Pierce #66130) against low salt his buffer at 4 °C, overnight to remove excess imidazole. It was at this step the N-terminal tag was removed using an in-house 3C protease (1:100, enzyme: protein ratio). The sample was then purified using another nickel purification step, using the same buffers. Fractions from the flow-through were then collected and probed for  $\alpha$ -synuclein. Positive fractions were then concentrated using a 3K MWCO concentrator (Pierce #88514 or #88526) and centrifugation (4,000G, 4 °C). The sample was concentrated to 2.5 mL and gel filtration performed. Gel filtration of the sample was done using a 16/600 75 superdex column (GE healthcare #GE28-9893-33) and 100 mM ammonium acetate buffer, pH 7.0. Fractions of interest were then pooled and the concentration determined by A280 measurement. The  $\alpha$ -synuclein was then aliquoted and lyophilized. Aliquots were stored at -80 °C.

#### **4.2.1.1 Fluorescent labelling of $\alpha$ -synuclein**

$\alpha$ -synuclein was fluorescently labelled using Alexa Fluor™ 488 NHS Ester (Succinimidyl Ester) (ThermoFisher #A20000). The monomeric protein was resuspended to 5 mg/mL in 0.1 M sodium bicarbonate buffer, pH 8.3. It was then centrifuged at 10,000 x g, 4 °C for 10 minutes to remove any pre-existing aggregates. 100 µg of the dye was added (10 mg/mL in DMSO) and the sample

gently shaken for 1 hour, 200 rpm, in dark. Excess dye was then removed by dialysis against 0.5 L sodium bicarbonate buffer, in dark at room temperature for 4 hours. Samples were dialyzed using a 0.1 mL 2K MWCO slide-a-lyzer cassette (ThermoFisher #11717539). The labelled protein was then recovered and either subjected to aggregation or snap frozen and stored at -80 °C until use.

#### 4.2.2 Creation of pathogenic species

Before aggregating the  $\alpha$ -synuclein, the monomer, once reconstituted, was centrifuged at 10,000 x *g*, 4 °C for 10 minutes to remove pre-existing aggregates. Seeding oligomers were created according to the Smith group protocol (Taylor-Whiteley, *et al.*, 2019). In brief, monomeric  $\alpha$ -synuclein was reconstituted to 0.1 mg/mL (7  $\mu$ M) in aggregation buffer 1 (50 mM phosphate buffer, pH 7.0, 20% EtOH), then shaken overnight at 1200 rpm, 21 °C. The following day the oligomer was concentrated 10-fold using a 30K MWCO, 0.5 mL concentrator (Microcon #MRCF0R030), to remove monomeric protein. The sample was centrifuged at 3,000 x *g* for 10-minute intervals. The concentrated oligomer was then diluted to 0.01 mg/mL in media and added to the cells. This was performed on the same day as concentrating. For fluorescently labelled oligomers, Alexa-488 tagged  $\alpha$ -synuclein monomer was used as starting material and the oligomer covered to prevent bleaching.

For the creation of PFF, the protocol established by Volpicelli-Daley Group was used (Patterson, *et al.*, 2019).  $\alpha$ SYN was reconstituted to 5 mg/mL in Dulbecco's PBS containing antibiotic-antimycotic (ThermoFisher # 15240062), to prevent contamination. The sample was then shaken at 1000 rpm for seven days at 37 °C. After this time the solution became cloudy- indicating fibrillization had occurred. For fluorescently labelled PFFs, 10% of the monomer was labelled with Alexa-488. After confirmation of fibrillization (sedimentation and thioflavin T assays, and AUC) the PFFs were aliquoted, snap frozen, and stored at -80 °C until use. Immediately prior to neuronal treatment the PFF was thawed, diluted to 0.1 mg/mL in sterile PBS with antibiotic-antimycotic, and sonicated to produce smaller fibrils. PFFs were sonicated on ice for 1 min, 30% amplitude, 1s on, 1s off (Fisher-Scientific #FB120, 2mm tip # 12921181).

#### 4.2.3 Atomic force microscopy

Sample preparation was performed at room temperature. Monomer and oligomer samples were diluted to 1  $\mu$ M in 20  $\mu$ L in respective buffers and then applied to freshly cleaved mica substrate for 1 min. 200  $\mu$ L of ultrapure H<sub>2</sub>O was added and the surface was washed through 10x serial ultrapure H<sub>2</sub>O washes

(½ volume changed each time). The sample was then blown dry with N<sub>2</sub> (g) and stored in an air tight container. Samples were imaged with tapping mode on a Multi-Mode 8 atomic force microscope (Bruker) using FESPA-V2 tips (Bruker) (nominal resonance frequency  $f_0 = 50\text{-}100$  kHz, nominal spring constant  $K = 1\text{-}5$  N/m).

#### 4.2.4 Quality Control of PFF

To confirm that the PFF protocol was successful and fibrillar species were created two quality control assays were performed: sedimentation assay and Thioflavin T aggregation assay. The assay protocols were taken from Patterson *et al.* (2019).

##### 4.2.4.1 Sedimentation assay

If the creation of PFFs had been successful, then they should sediment at lower speeds than the monomer. Alongside the PFF and oligomer, a monomer sample was run as a control. 5 mg/mL PFF was diluted 1:10 in PBS. The samples were then centrifuged at 10,000 x g for 30 min at RT then the supernatant transferred to a fresh microcentrifuge tube. The pellet was then resuspended in fresh PBS- to the same volume as the supernatant. 4x Laemmli buffer was then added to the samples, both pellet and supernatant. The samples were then boiled at 95 °C for 10 min. They were then loaded on a 4-20% Tris-glycine gel (BioRad # 4561096) and ran at 120 V until adequately resolved. An AccuMarQ molecular weight marker was run alongside (Bradilla #A010-601). The proteins were then transferred onto 0.45 µm PVDF membrane (ThermoFisher #LC2005) using the wet transfer method (120 V, 75 minutes, 4 °C). After transfer the membrane was fixed with 0.4% PFA in PBS for 10minutes. This fixes  $\alpha$ -synuclein and other low weight proteins on the membrane, aiding visualisation (Lee and Kamitani, 2011). The membrane was washed here and in all subsequent steps with Tris buffered-saline with 0.1% tween-20 (TBS-T). TBS: 20 mM Tris, pH 7.6, 130 mM NaCl. The membrane was then blocked in 5% skimmed milk in TBS-T for 1 hour at room temperature and incubated with 1:1000 anti- $\alpha$ SYN antibody (Sigma #S5566) overnight at 4°C in blocking solution. The next day the membrane was washed 3x 10 minutes at room temperature and incubated with 2° antibodies in blocking solution (1:5000, VectorLabs #PI-2000). The membrane was then washed again and incubated with ECL (ThermoFisher #10005943) and imaged at -30 °C using an intelligent dark box (FujiFilm, #Y515-Di). The proportion of  $\alpha$ SYN in each fraction was calculated using densitometry (ImageJ).

#### 4.2.4.2 Thioflavin T assay

Compared to the monomer, PFFs are  $\beta$ -sheet rich structures and can therefore react with amyloid dyes. This differential binding can be used in a fluorescence assay to determine if the PFFs were created. Samples were diluted 1:50 in Dulbecco's PBS and then mixed 1:1 with fresh, filtered Thioflavin T buffer (25  $\mu$ M thioflavin T, 100 mM glycine, 1% Triton X-100, pH8.5). The samples were then pipetted into a 96 well plate as 3 replicates and incubated in the dark for 1 hour. After this the wells were read on OmegaSTAR plate reader using 440,520 band-pass filters (BMG LabTech).

#### 4.2.5 Cell Culture

##### 4.2.5.1 PNN-HEK 293T culture

HEK 293T and PNN HEK 293T cells were maintained at 37°C, 5% CO<sub>2</sub> in high glucose DMEM (Gibco) supplemented with 5% foetal bovine serum (BioSera) (Kwok, *et al.*, 2010). All plasticware and glass was pre-treated with 0.01% poly-L-lysine (Sigma #P4832) for 30 minutes and washed twice with dH<sub>2</sub>O prior to plating. Cells were plated at 25,000/coverslip and left to adhere overnight before treatment.

##### 4.2.5.2 Primary culture

The protocols for primary neuronal and astrocyte culture were set out in 2.1. Neuronal cultures were maintained to 56DIV before treatment.

#### 4.2.6 Cell treatment

##### 4.2.6.1 Oligomer treatment

Alexa-488 oligomer or monomer stock (1 mg/mL, with respect to monomer) was diluted 1:100 in culture media and added to cells (final concentration: 0.01 mg/mL) for twenty-four hours before fixation and staining. Neurons were treated at DIV 56.

##### 4.2.6.2 Fibril treatment

Neurons were treated at DIV 56. The PFF were sonicated prior to cell treatment and diluted in cell media, 1:100, to final concentration 70 nM (with respect to starting monomer concentration). Neurons were then fixed at 7, 14 and 21 days after treatment. Monomeric  $\alpha$ SYN was also used at 70 nM. For untreated neurons they were treated with equal volumes of PBS.

#### 4.2.6.3 Chondroitinase ABC treatment

For the PNN and ECM digested condition neurons were treated with ChABC. Prior to  $\alpha$ SYN treatment neurons, PNNs were digested with chondroitinase ABC from *Proteus vulgaris* (Sigma #C2905). Neurons were treated for 30 minutes with 200 mU/ml ChABC, with 50 mM sodium acetate in media. The neurons were then washed with neuronal media and then treated with  $\alpha$ SYN.

#### 4.2.7 Immunocytochemistry

The protocol and antibodies used to stain the cells used in this chapter are set out in section 2.2. The following adaptations were implemented for the staining of the HEK cell lines. They were fixed in 4% PFA in PBS at room temperature for 10 minutes. The incubation steps for blocking and antibodies were shortened: blocking, 30 minutes; antibodies, 2 hours.

#### 4.2.8 Imaging and analysis

Please refer to section 2.3 for more detail. The confocal microscope was used to image the experiments using the oligomer. The Slidescanner was used to image the PFF experiment. Images were analysed using Cell Profiler 3.1.9 software to measure no. of cells (NeuN or Hoechst), PNN positive cells (WFA positive NeuN/Hoechst positive), cellular puncta (colocalisation of NeuN/488-oligomer or HEK cytoplasm/488-oligomer or  $\alpha$ SYN puncta), or p- $\alpha$ SYN staining intensity normalised to  $\beta_3$  tubulin staining. Significance was then tested for using OriginPro. The specific test used are specified in figure legends.

#### 4.2.9 Surface plasmon resonance

$\alpha$ SYN/GAG interaction assays were performed using surface plasmon resonance (SPR) by Dr. Lynda Djerbal. Analysis was performed using a Biacore SPR (T3000) on CM4 sensor chips (GE healthcare). All solutions were filtered and degassed before use (0.22  $\mu$ m). Running buffer was HBS-P (10 mM HEPES pH 7.4, 150 mM NaCl and 0.005% v/v surfactant P). Dextran was activated with equal volumes of 100 mM N-hydroxysuccinimide and 400 mM N-ethyl-N'-(diethylaminopropyl)-carbodiimide. Activated dextran was covalently coupled with 80  $\mu$ g/ml streptavidin (Sigma #S0677) in 10 mM sodium acetate buffer, pH 4.2. This resulted in ~1000 resonance units (RU) of streptavidin immobilised per chamber. The remaining activated groups on the dextran were blocked by the addition of 50  $\mu$ l of 1 M ethanolamine hydrochloride-NaOH, pH 8.5.

Biotinylated GAGs (CS-D, CS-E or HS) at 5 µg/ml in 10 mM HEPES, 0.3 M NaCl, pH 7.4 were captured to the surface to ~60 RU level per chamber. Flow chamber 1 (FC1): CS-D, FC2: CS-E, FC3: HS, FC4: streptavidin control. Before protein injection, the surface was washed twice with high salt HBS (2 M NaCl). Protein was injected for 5 min (association phase) and washed for 5 min with HBS (dissociation phase). Surface was regenerated using high salt HBS at 60 µl/min. The streptavidin chamber sensorgram was used to subtract background from the GAG chamber sensorgrams. Data analysis and graph creation was performed using Biaeval 3.1 software. Data was fitted using the 1:1 Langmuir model to determine binding kinetics. This assumes a one to one relationship between the ligand and receptor (αSYN and GAG) and that each binding site is equal and independent from the others (Hodnik and Anderluh, 2010).

#### **4.2.10 Quartz crystal microbalance with dissipation**

αSYN/GAG interactions were confirmed using quartz crystal microbalance with dissipation monitoring (QCM-D). For this, a Q-Sense E4 system, with four flow chambers (FCs) in conjunction with QSoft 401 software at 23°C (Biolin Scientific). Before use 4 SiO<sub>2</sub> sensors (QSX303, Biolin Scientific) were cleaned using 2% SDS in ultrapure H<sub>2</sub>O for 30 minutes, rinsed with ultrapure H<sub>2</sub>O and 100% ethanol and then blow-dried using nitrogen gas. Sensors were then treated in a UV/ozone chamber for 30 minutes to render the surface hydrophilic. Sensors were placed in normal volume FCs (1 per chamber) which were connected to inlet and outlet tubing. The outlet tubing was then connected to 20 ml syringes in the syringe puller (Midland Scientific #KD 78-8212) with 1 syringe per chamber. Inlet tubing was placed in aliquots of the running buffer (HBS). Chambers were placed under a continuous flow at 20 µl/min for a minimum of 30 minutes to ensure a stable baseline. The 20 µl/min was used for all subsequent steps except the washing when a 200 µl/min flow rate was used. Before starting all resonances for each sensor were searched for and checked using the software. After a stable baseline was ensured the GAG layer was then created. All buffers were degassed before use.

The first step in creating a GAG layer is to create a biotin-displaying supported lipid bilayer. For the creation of this layer, sonicated unilamellar vesicles made from DOPC lipids and DOPE-CAP-biotin lipids (at a molar ratio of 99.5 to 0.5) were used at 50 µg/ml for 15 min. The layer was then washed for 10 minutes with HBS to remove loose liposomes. Streptavidin was then flowed over the surface for 15min at 20 µg/ml. The surface was then washed with HBS until the baseline was stable for a minimum of 10min (~ -40 Hz). 10 µg/ml biotinylated HS was then flowed over the surface until the baseline stabilised (~ -50 Hz). HS

from porcine intestinal mucosa (Celsus Laboratories) was used and was biotinylated at the reducing end via oxime ligation (Thakar, *et al.*, 2014). The chambers were then washed with the respective protein buffers for 10 min to remove lipids and biotinylated HS from the solution phase and to test the stability of the surface. . Dulbecco's PBS was the buffer for the monomer and sonicated PFF. The oligomer was in aggregation buffer (see 4.22). The chambers were as follows: FC1: GAG control, FC2: monomer, FC3: oligomer, FC4: PFF. FC1 was also washed with Dulbecco's PBS. Protein was then flown across the surface at 125 µg/ml until a binding equilibrium was attained. An exception to this was the sonicated PFF chamber, in which the protein sample ran out before the trace stabilised. After binding equilibrium was attained, or protein sample ran out, the surfaces were washed with their respective buffers. The GAG surface was regenerated using 6 M guanidine hydrochloride for 20 min then placed back to buffers.

Chambers were cleaned using 2% SDS and 100% EtOH, 10 min wash step each, with 5 min wash steps with dH<sub>2</sub>O in between. After the final dH<sub>2</sub>O wash step a 5 min air step was performed. The sensors, chambers and tubing were then disassembled and blow dried with nitrogen gas. The Q-Tools software was used to create the graphs using the 5<sup>th</sup> overtone, the other overtones would have provided comparable results. Frequency shifts were normalised automatically by the QTools software.

## 4.3 Results

### 4.3.1 Purification of $\alpha$ -synuclein

To express recombinant  $\alpha$ SYN we opted to do so as a tagged protein. In our initial experiments we determined that the SUMO tag enabled greater  $\alpha$ SYN expression. The SNCA gene was subcloned from the pET-23a vector into pOPINS3C using complimentary In-Fusion™ primers. The pOPINS vector contains an N-terminal 6-histidine sequence fused to a SUMO tag. These are located at the N-terminal of  $\alpha$ -synuclein and could be removed by cleavage of the 3SC site that separates the tags from the protein of interest (Fig. 15A). The vector was transformed into Rosetta2 (DE3) *E. coli* strain. Protein expression was induced with IPTG at 25 °C as this gave the largest yield (data not shown).  $\alpha$ -synuclein was purified using a three-step method. The capture step was performed using nickel-affinity chromatography. The His-SUMO- $\alpha$ SYN fusion protein ran at 34 kDa on a gel (Fig. 15B). The tag size is 13.2 kDa and  $\alpha$ SYN is 14 kDa, together coming to 27.2 kDa. However,  $\alpha$ SYN runs higher than its native 14 kDa, at 17 kDa (Fig. 15C). This is thought to be due to poor interaction between the SDS molecules and the basic N-terminal tail (Huang, *et al.*, 2005). This may explain why the fusion protein band runs higher than predicted. With 5 L of starter culture the amount of protein overwhelmed the HisTrap column capacity as the  $\alpha$ SYN fusion protein can be seen in the flow through and salt washes. The protein was eluted easily from the column at 60 mM imidazole. Boiling of the sample reduced high MW contaminants but saw the appearance of lower weight contaminants, which could be degradation products. While boiling has no effect on  $\alpha$ SYN, it may lead to SUMO degradation (Coelho-Cerqueira, *et al.*, 2013). This is of small consequence as the protein is already purified at this point, so the SUMO-tag has served its purpose. The fusion protein accounts for 53% of the total eluted protein. This is higher than other protocols and may either be due to the differences in protein expression (bacterial cell line or tagged vs untagged) or cell disruption (high pressure homogenisation vs sonication).

Having expressed and captured sufficient tagged  $\alpha$ SYN, we then cleaved the tag to produce pure untagged  $\alpha$ SYN, suitable for aggregation. The tag was cleaved overnight using an in-house recombinant 3SC protease. The untagged  $\alpha$ SYN was purified through an intermediate purification step where it was flowed over the HisTrap column again. The now untagged  $\alpha$ SYN flowed over the column and did not bind while the Ni-binding contaminants and His-SUMO tag both bound. This step increased the relative purity to 95% as determined by

densitometry. In a final polishing step to remove the high MW contaminants the  $\alpha$ SYN was purified by gel chromatography and the  $\alpha$ SYN containing fractions taken (Fig. 15D). This resulted in 99% purity. We have successfully expressed and purified monomeric  $\alpha$ SYN in amounts sufficient for our experiments (~2.5 mg/L of culture).

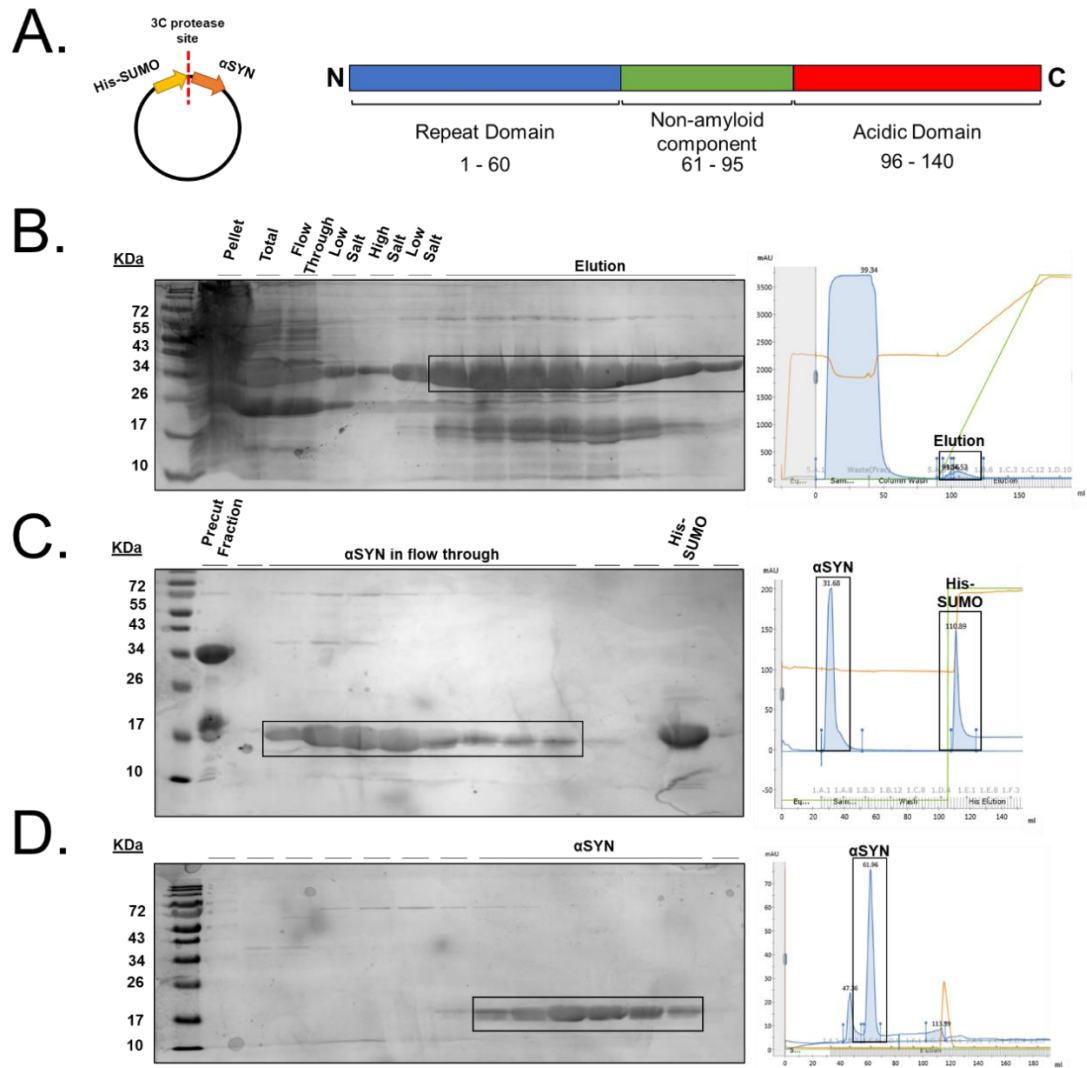


**Figure 15: Purification of  $\alpha$ SYN**

**A.** Schematic of pOPINS3C and  $\alpha$ SYN. **B.** HisTrap purification of His-SUMO- $\alpha$ SYN. Boiled, clarified lysate was passed over a 5 ml FastFlow HisTrap column. The column was washed with low and high salt washes before being eluted with imidazole. Tagged protein exceeded column binding capacity. Purified fractions were then pooled and cleaved and dialysed overnight with a SUMO 3C protease. **C.** After overnight dialysis and SUMO tag cleavage, the sample was passed back over the HisTrap column. Freshly untagged  $\alpha$ SYN then passed over the column and appeared in the flow through. Positive fractions were then taken and pooled **D.** Pooled and concentrated fractions were then passed over a HiLoad 16/600 Superdex 75 column and eluted in 0.1 M  $\text{NH}_3\text{Ac}$ .  $\alpha$ SYN fractions were then pooled and lyophilized.

### 4.3.2 Creation of $\alpha$ -synuclein seeding species

To test if the PNN blocked  $\alpha$ SYN seeding it necessitated the creation of  $\alpha$ SYN species capable of seeding. Both oligomeric and fibrillar forms of  $\alpha$ SYN have been shown to cause seeding in cells. However, it is not yet known which form is responsible for seeding in the disease pathology. Therefore, we decided to create both and test their seeding capability in PNN neurons. The seeding oligomer (B1) created by Danzer, *et al.* (2007) was chosen for two reasons: it demonstrated high seeding efficiency and it could be created using low starting concentrations of monomeric  $\alpha$ SYN. The Smith adaption of the seeding oligomer protocol was chosen as it simplified the original protocol while maintaining seeding efficacy (Taylor-Whiteley, *et al.*, 2019). The morphology and size of the oligomer preparations were measured using atomic force microscopy.

The created oligomers were measuring  $12.4 \pm 4.0$  nm in height and a radius of  $154 \pm 53$  nm ( $n = 11$ ) (Fig. 16A.). No large aggregates were observed in the monomeric preparation and the tallest structure measured 3 nm in height. This is consistent with monomeric  $\alpha$ SYN. The results are morphologically consistent with the literature which reported seeding oligomers are large amorphous aggregates measuring between 10-20 nm in height. Assuming a Kuhn model chain and an unstructured protein of 140aa, it is assumed that it will behave as a random coil, creating a structure between 2 and 7 nm in size, depending whether a globular chain model (in which the chain is not solvated) or real chain model (in which the chain is well solvated) is used (Rubinstein and Colby, 2003). The samples were air-dried so thus will be dehydrated, this would collapse the random coil to a smaller size and the 3 nm recorded height is consistent with this.

Creation of the fibril species is well-established in the literature with several quality control experiments that can be performed to confirm successful creation. The PFF protocol set out by Volpicelli-Daley and colleagues (2014) was followed as described in the methods. Conversion to a fibrillar state was confirmed by sedimentation assay and the thioflavin T aggregation assay. The majority of the fibril sample was found in the pellet fraction, indicating conversion to large species (soluble: 23% vs pellet: 73%) (Fig. 16B). The opposite was true for the monomer, indicating that it had remained mostly monomeric (soluble: 81% vs pellet: 19%). A  $\alpha$ SYN positive band at 35 kDa was seen in the fibril pellet sample. This has been observed by other groups but it's

structure has not been resolved (Lee, *et al.*, 2008a; Patterson, *et al.*, 2019). The oligomer was intermediate between the monomer and the fibril (soluble: 63% vs pellet: 37%), indicating a poorer conversion to sedimentable species. The fibrils were beta-sheet rich as they alone possessed thioflavin T reactivity (Fig. 16C). In conclusion both the oligomer and fibril species were successfully created and verified to be distinct species.

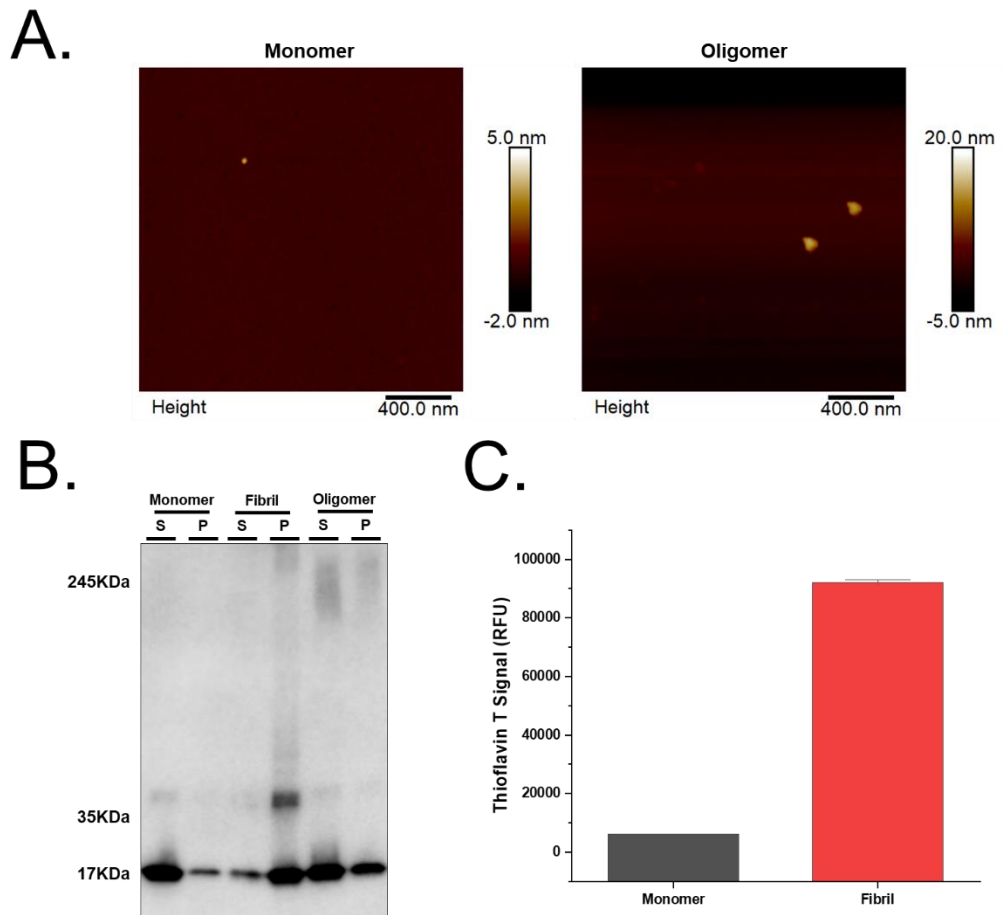


**Figure 16: Characterisation of  $\alpha$ SYN species**

**A.** AFM topography comparison of monomer and oligomer. **B.** Sedimentation assay for pelletable  $\alpha$ SYN (10,000x g, 30min). S: soluble fraction, P: resuspended pellet fraction. **C.** Thioflavin T assay. Signal is expressed as relative fluorescent units (RFU).

### 4.3.3 A PNN cell model resists oligomer induced seeding

Due to the novel nature of this work, an exploratory experiment was first designed and performed to determine whether the hypothesis, *does the PNN block  $\alpha$ SYN seeding*, warranted further exploration. Our lab has previously created a simplified model of the PNN using 3 PNN components and a HEK cell line host, creating a stably expressing PNN-HEK cell line (Kwok, *et al.*, 2010). These cells have a high growth rate and low maintenance cost. The PNN-HEK and untransfected HEK cell lines were treated with the Alexa-488 labelled oligomer or monomer for 24 hours and then fixed and imaged to determine uptake and seeding of the  $\alpha$ SYN species.

Treatment with the monomer did not result in measurable uptake at 24 hours in either cell line as no Alexa-488 signal was detected (Fig. 17A). It also did not result in seeding and recruitment of the endogenous  $\alpha$ SYN as no  $\alpha$ SYN puncta were detected. Treatment with the oligomer resulted in measurable uptake of the oligomer at 24 hours and seeding of endogenous  $\alpha$ SYN in both the PNN-HEK and HEK cell lines. However, the PNN-HEK cells showed significantly lower number of puncta-positive cells ( $22.3 \pm 10.3\%$  in PNN-HEK vs  $48 \pm 4.36\%$  in HEK,  $p < 0.01$ ) (Fig. 17B), indicating that the PNN-HEK cells were resistant to oligomer induced seeding. However, amongst the cells that developed puncta, the mean number of  $\alpha$ SYN puncta was not significantly different between the two cell lines (Fig. 17C). This is important as the degree of recruitment of endogenous  $\alpha$ SYN is correlated with the expression level of  $\alpha$ SYN in a cell. If the number of cellular puncta were reduced in the PNN-HEK cell line it would raise the possibility that the endogenous levels of  $\alpha$ SYN may have been lowered by the transfection process. However, there was no significant difference, indicating that the underlying process of and capacity for seeding was unchanged between the two cell lines. Rather, it is the presence of the PNN which reduces the uptake of oligomeric  $\alpha$ SYN, leading to less cells undergoing the seeding process.

In conclusion, the presence of a PNN like coating bestows resistance to oligomer induced seeding, making the cells twice as resistant to oligomer uptake and the associated seeding. Therefore, the initial hypothesis, *does the PNN block  $\alpha$ SYN seeding*, appears true and warrants further investigation in a more physiological model.

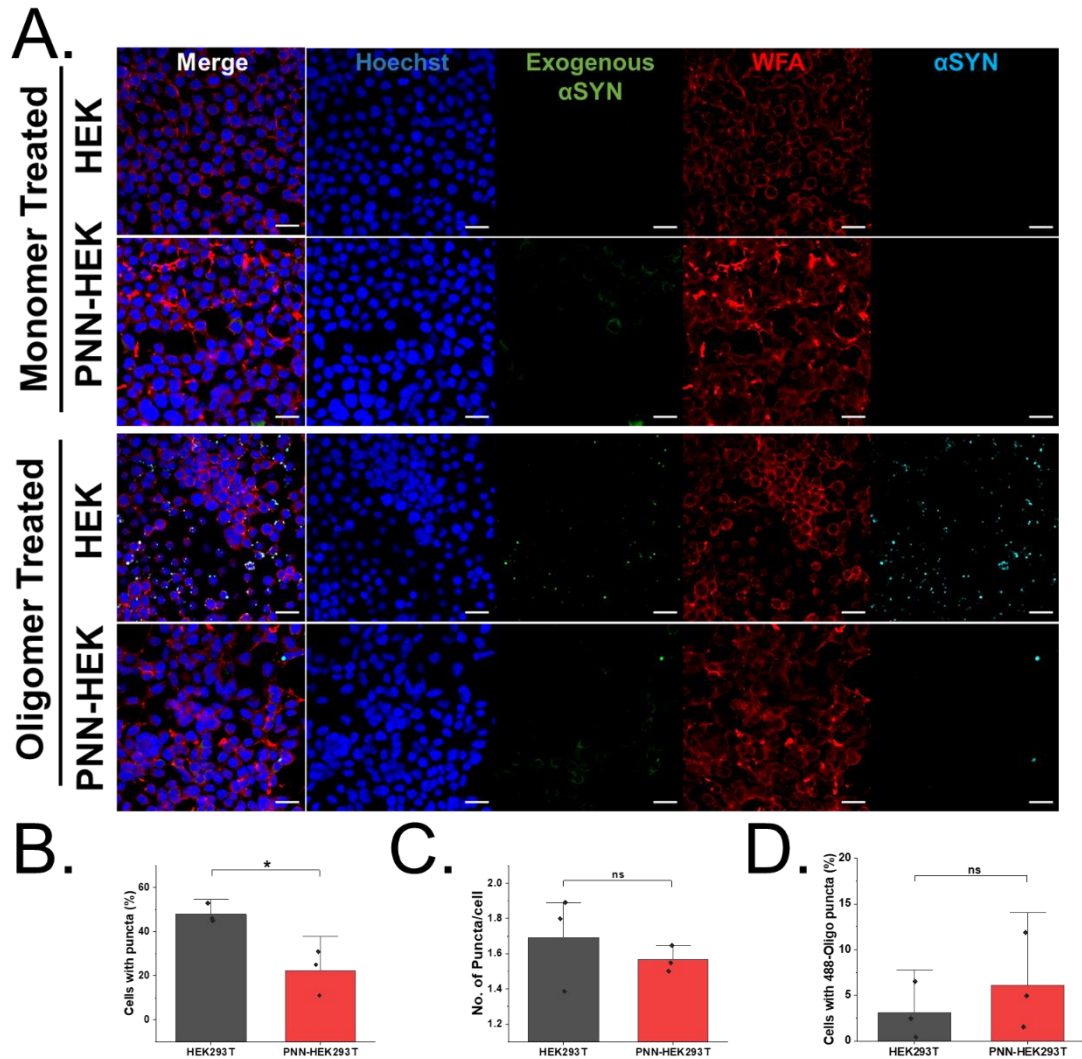


**Figure 17: PNN-HEK cells are resistant to  $\alpha$ -synuclein seeding**

**A.** Cells were treated with 0.01 mg/mL Alexa 488 conjugated monomeric or oligomeric  $\alpha$ SYN for 24 hours. Only oligomeric  $\alpha$ SYN persisted in the cells after 24 hours. Oligomer treatment caused endogenous  $\alpha$ SYN puncta to form ( $\alpha$ SYN, teal). This was more marked in the HEK cells compared to the PNN-HEK. Scale bar is 20  $\mu$ m. **B.** Quantification of percentage of puncta positive cells in the two cell lines. PNN-HEK cells were twice as resistant to  $\alpha$ SYN puncta formation (22% vs 48%). **C.** Quantification of cellular  $\alpha$ SYN puncta number. Data shown are averages of 3 different experiments. **D.** Quantification of oligomer puncta. There was no significant difference found between the two cell lines. Data shown was averages 3 different experiments. Error bars are standard deviation. Significance (\*) is  $p < 0.05$  and was detected by unpaired Student's t-test. An average of 1500 cells were counted for each experiment.

#### 4.3.4 PNN neurons resist $\alpha$ SYN oligomer uptake

The internalisation of pathogenic  $\alpha$ SYN by neurons is a necessary step before inclusion formation and cellular toxicity. The PNN is an extracellular barrier and could prevent the uptake of pathogenic  $\alpha$ SYN by denying membrane access. We have shown that the presence of a PNN-like coat makes HEK cells twice as resistant to  $\alpha$ SYN oligomer uptake (Figure 17B), indicating the PNN could act as a protective barrier. Having established a mature PNN model in chapter 3, we continued this study by incubating the neuronal culture with fluorescently labelled  $\alpha$ SYN oligomer. 24 hours after incubation there was widespread uptake of the oligomer by the neurons, with somatic and dendritic labelling observed (Fig. 18A). Interestingly, the PNN neurons showed little to no colocalization of the oligomer, indicating that they did not internalise it. Quantification of the somatic inclusions was performed in the neuronal cultures, it showed that PNN neurons were more around two thirds more resistant to oligomer uptake than their unsheathed counterparts (Oligomer positive: PNN positive  $15.8 \pm 2.5\%$  vs PNN negative  $49.9 \pm 3.0\%$ , Fig. 18B). The magnitude of this marked resistance compares with the resistance observed in the PNN-HEK cell line (Fig. 18B). This indicates that the PNN neurons are twice as resistant to oligomer uptake compared to their unsheathed counterparts.

To determine whether the resistance was due to the PNN or other cell-intrinsic factors, we digested the PNN with chondroitinase ABC. This enzyme completely digested the PNNs, entirely ablating WFA staining (Fig. 18A). The ChABC treated culture showed significantly higher oligomer internalisation (Fig. 18C). For both rats the proportion of oligomer positive neurons went up 14% ( $53.4 \pm 6.2\%$  vs  $67.1 \pm 6.8\%$ ,  $p < 0.05$ ). Though this was not significant the size of the increase corresponds to the proportion of PNN positive neurons in our cultures (10%) (Fig. 18B). Therefore, it is likely that it is the PNN itself that is blocking oligomer internalisation rather than any PV interneuron-specific effect.

ChABC has been shown to degrade both CS-GAGs and HA at different pH *in vitro*. It is possible that the ChABC treatment was only degrading CS-GAGs, denuding the PNN but leaving it intact. If this was the case, then it would reveal that the CS-GAGs are the neuroprotective agents in the PNN. However, unpublished results from our group have shown that ChABC has a dual mechanism at physiological pH. It degrades both the CS-GAGs and the HA backbone. This means in our experimental paradigm the PNN is most likely being fully degraded rather than denuded. Future work should determine if a specific component is responsible for the resistance or if it is an emergent function of the PNN.

We have shown that the presence of a PNN reduces pathogenic oligomer internalisation. Digestion of the PNN ablates this resistance. This establishes the PNN as a neuroprotective structure against pathogenic species internalisation.

#### **4.3.5 Addition of PFFs lead to the progressive development of p- $\alpha$ SYN pathology in neurons**

Several pathogenic  $\alpha$ SYN species can cause seeding. Having established that the PNN is a neuroprotective structure against seeding from  $\alpha$ SYN oligomers we then determined if this phenomenon was species specific or a part of a wider neuroprotection against  $\alpha$ SYN seeding species. Therefore, we investigated whether the presence of a PNN could protect neurons from fibrillar  $\alpha$ SYN induced seeding.

The pathogenicity of PFFs is well-established. Exposure of cells and animals to PFFs results in phosphorylated  $\alpha$ SYN pathology, reminiscent of PD pathology, and can induce cellular/animal deficits and toxicity. Fibrillar species have also been isolated from LP and these patient derived species also have seeding potential, therefore we elected to use PFFs on our culture.

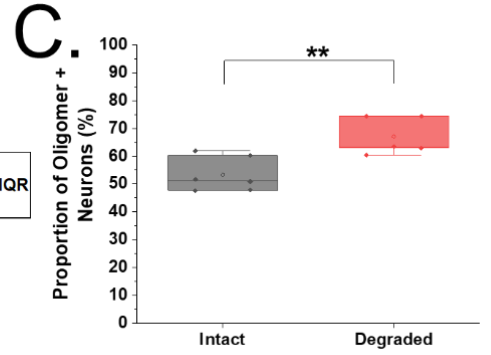
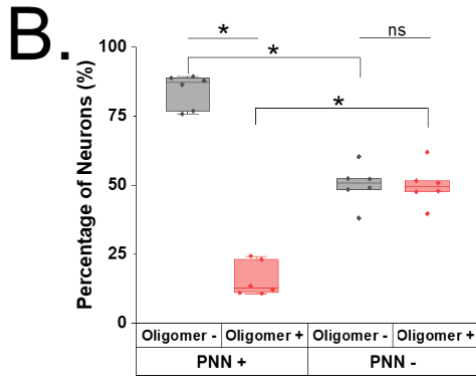
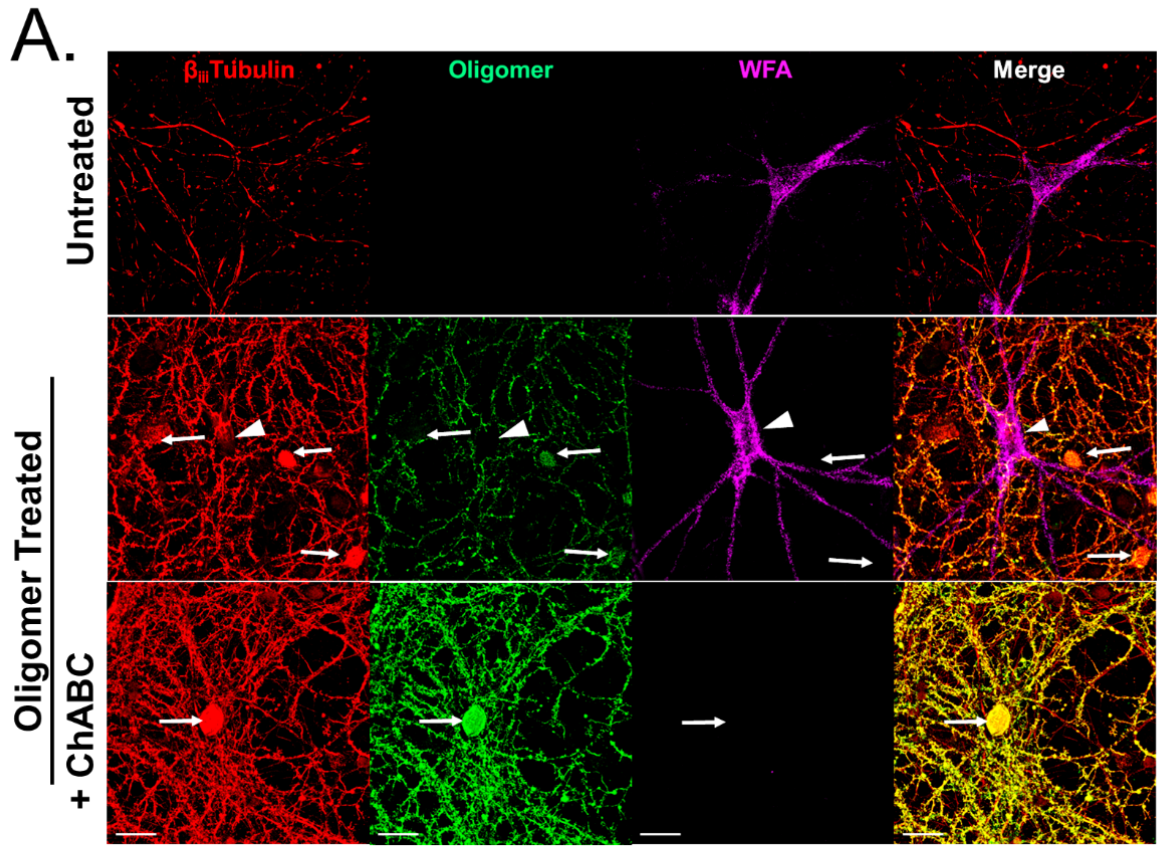
Mature neuronal cultures were exposed to PFF for up to 21 days before fixation. Other groups have shown that p- $\alpha$ SYN pathology takes time to develop and progresses from dendritic inclusions to somatic (Volpicelli-Daley, *et al.*, 2014; Mahul-Mellier, *et al.*, 2020). Therefore, a long incubation period was chosen to allow maximal pathology to develop and allow somatic inclusions to develop. The development of somatic inclusions is critical to determining whether PNN neurons are resistant as the PNN only covers the soma and proximal neurites. Tracing distal dendrites back to their parent neuron to determine whether they are PNN positive would involve high magnification, whole coverslip imaging and be computationally intensive. Somatic inclusions allow for simpler testing of the PNN neuroprotection hypothesis. Somatic inclusions are also critical in PD pathology and are linked to neuronal death.

DIV56 neurons were treated with PFFs and fixed at days: 7, 14 and 21 post-treatment. p- $\alpha$ SYN signal progressively developed over this time with no staining detected in untreated controls at 21 days post treatment (Fig. 19 and Fig. 21). The intensity of the p- $\alpha$ SYN staining (relative to  $\beta_3$ -tubulin staining) was significantly higher at 21 days than at 7 days treated neurons ( $0.372 \pm 0.009$  vs  $0.0048 \pm 0.002$ ) (Fig. 21). The pathology was localised predominantly to the neurites with small numbers of neurons presenting with somatic inclusions. PNN neurons were detected at all time points. However, the small

numbers of somatic inclusions and PNN neurons made it unfeasible to determine if PNN neurons were significantly resistant compared to unsheathed neurons.

► **Figure 18: PNN neurons resist  $\alpha$ -synuclein oligomer uptake**

**A.** DIV56 neurons were treated with 0.01 mg/ml Alexa 488 labelled oligomer for 24hrs. PNN neurons (WFA, purple, arrows) were less likely to colocalise with  $\alpha$ SYN oligomer staining than those without (arrowheads). This resistance was removed with PNN digestion with ChABC. Scale bar is 20  $\mu$ m. **B.** Quantification of oligomer treated neurons. Only a third of PNN ensheathed neurons were positive for the oligomer while half of PNN-negative neurons colocalised with the oligomer. Data point shown are the averages 3 different rats. Total neurons for each category are shown (PNN+: Oligomer - = 261, Oligomer + = 47, PNN-: Oligomer - = 1671, Oligomer + = 1863). Error bars are standard deviation. Significance is  $p < 0.05$  (\*) was detected within the PNN populations and oligomer subgroups and was detected by one-Way ANOVA. **C.** ChABC treatment abolished staining perineuronal nets and resistance of these neurons. Box plots show that ChABC treatment significantly increased the number of neurons positive for oligomer puncta, this increase is from the PNN-degraded population. Significance (\*) is  $p < 0.05$  and was detected by unpaired Student's t-test, N= 6 coverslips from 2 rats, total neurons counted for each category: intact= 1850 neurons, degraded= 1754.



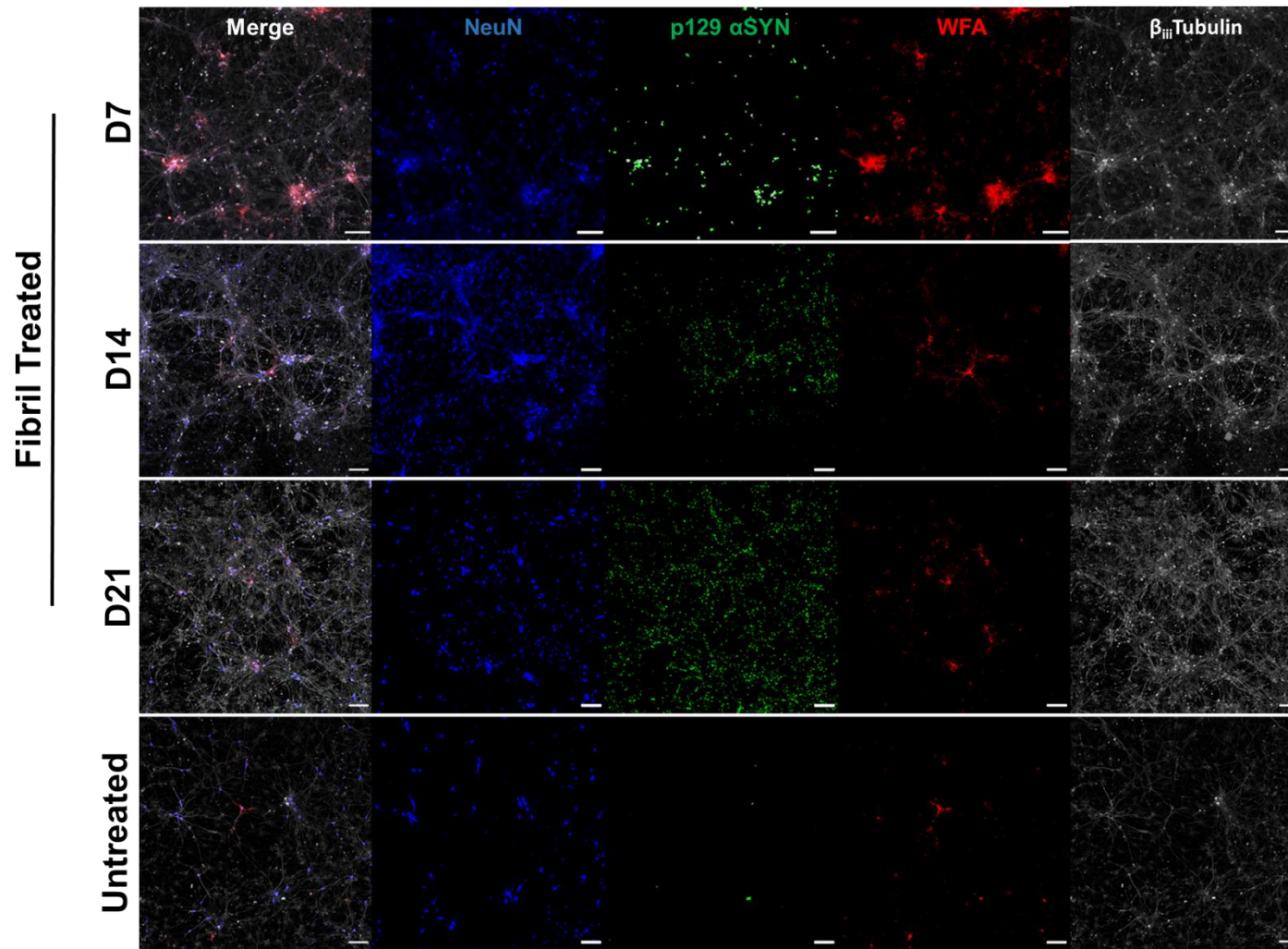


**Figure 19: p- $\alpha$ SYN aggregates accumulate over time in PFF treated neurons**

DIV56 neurons were treated with 70 nM sonicated fibrils. After treatment, p129  $\alpha$ SYN began to appear from day 7 post treatment. p129  $\alpha$ SYN staining became more prolific in the culture over time. No staining was detected in the untreated cultures by day 21. p129  $\alpha$ SYN staining localised to primarily to neurites ( $\beta_{III}$  Tubulin, white) compared to soma (NeuN, blue). PNN neurons persisted in fibril treated cultures. Scale bar is 100  $\mu$ m.

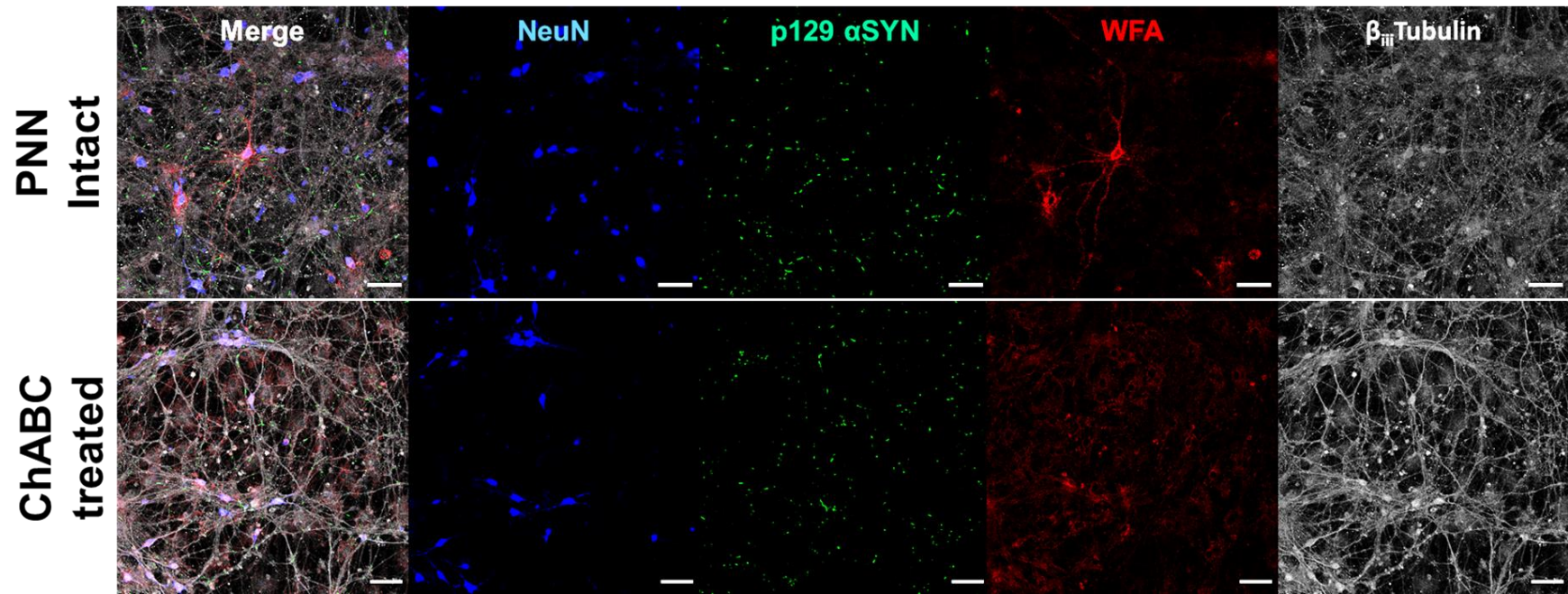


**Figure 20: Effect of ChABC on p129 development**

Representative images of DIV77 neuronal cultures. Cultures were treated with PFF at DIV56 neurons following ChABC pretreatment. PNNs had not recovered after 21 days. Scale bar is 100  $\mu$ m.

#### 4.3.6 Removal of extracellular matrix does not affect the degree of p- $\alpha$ SYN pathology

Since we could not directly determine if PNN neurons developed p- $\alpha$ SYN pathology, we decided to determine if the global level p- $\alpha$ SYN staining was significantly altered by removing of the ECM with ChABC treatment. ChABC treatment digests the CS and HA in both the PNN and the loose extracellular matrix and so may affect the magnitude of pathology developed. Similar to previous experiments, ChABC treatment removed the extracellular matrix, as determined by reduction in WFA signal (Fig. 20). p- $\alpha$ SYN signal intensity significantly increased after ChABC treatment (Fig. 21). This indicates that the ECM negatively regulates the development and degree of p- $\alpha$ SYN pathology caused by PFF treatment.

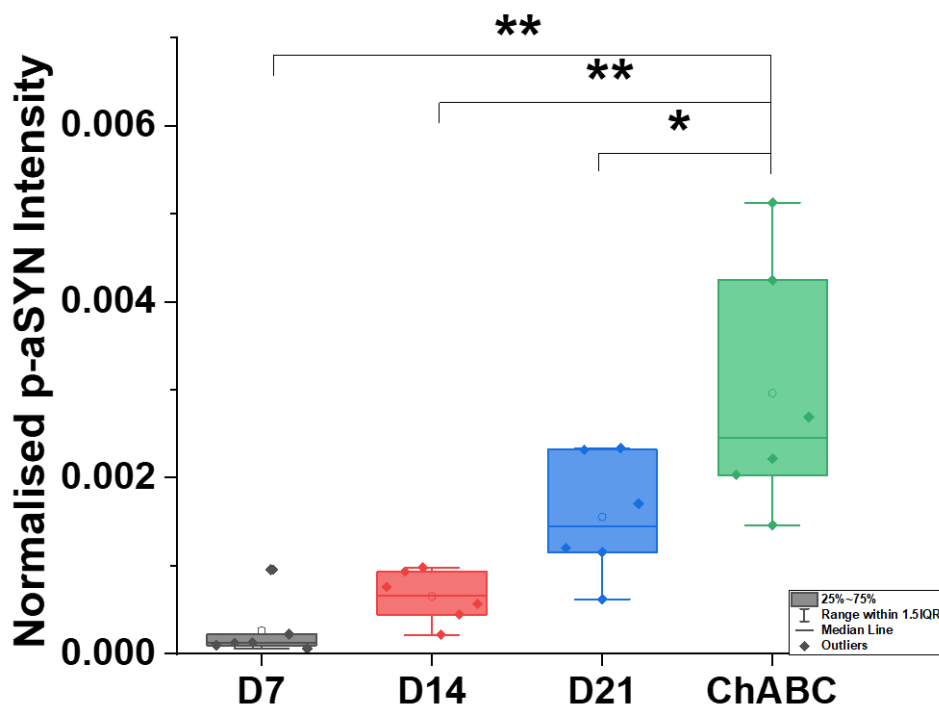


**Figure 21: Quantification of p129 intensity**

Quantification of p- $\alpha$ SYN intensity, normalized to  $\beta_3$ Tubulin integrated intensity. p- $\alpha$ SYN intensity has significantly increased from D7 to D21 as determined by One-way ANOVA with Tukey's post hoc test ( $p > 0.05$ ). Data points are average intensity of a coverslip, N= 6 coverslips from 2 rats.

#### 4.3.7 CS-E and HS bind $\alpha$ SYN

The presence of a PNN reduces neuronal uptake of oligomeric  $\alpha$ SYN and p- $\alpha$ SYN pathology development. How does the PNN mediate this effect?  $\alpha$ SYN has been shown to bind to HS. Highly sulphated HS is enriched in the PNN, making the PNN a possible chelator of  $\alpha$ SYN (Deepa, *et al.*, 2006). The PNN could deny  $\alpha$ SYN membrane access by trapping it via binding. We tested this

hypothesis through investigating whether  $\alpha$ SYN species interacted with PNN GAGs using SPR. CS-E and HS were tested in this experiment. CS-E has previously been shown to bind to PNN effector molecules (e.g. sema3A and Otx2) and HS is the second most abundant GAGs in the PNNs (Deepa, *et al.*, 2006; Beurdeley, *et al.*, 2012; Dick, *et al.*, 2013). Both monomeric and oligomeric  $\alpha$ SYN bound to CS-E and HS in a concentration dependent manner (Fig. 22). This interaction was specific as neither species interacted with CS-D, another CS GAGs which same charge-over-mass ratio but with the sulphation at different carbons than in CS-E (Fig. 22). The  $K_D$  of  $\alpha$ SYN/GAG interaction for all species and GAGs was in the micromolar range. However, the similar  $K_D$  was determined by different association and dissociation rates for each  $\alpha$ SYN species. The monomer showed an overall lower binding response and a slower association and disassociation. In comparison the oligomer showed a stronger binding response but a rapid association and dissociation (Fig. 22B). This may be due to a diffusion effect, with the smaller monomer diffusing into the glycan matrix (Schuck and Zhao, 2001). Unexpectedly, we could not detect any binding between the GAGs and PFF. This was unexpected as it has been shown in the literature (Holmes, *et al.*, 2013; Stopschinski, *et al.*, 2018b).

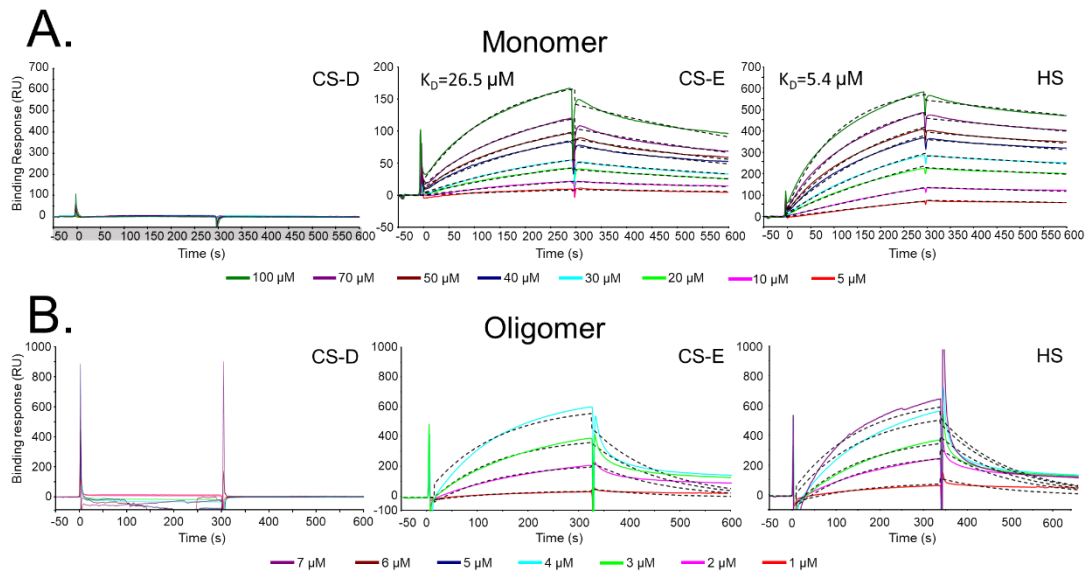


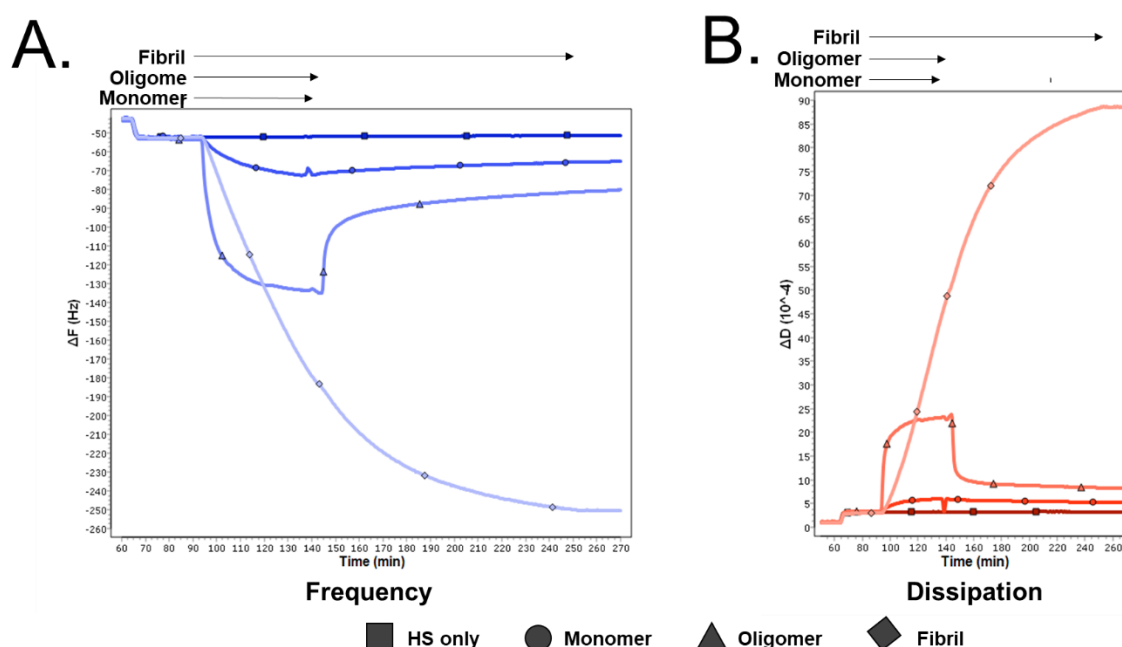
**Figure 22:  $\alpha$ SYN binds to sulphated glycosaminoglycans CS-E and HS**

**A.** Monomeric  $\alpha$ -synuclein was injected over CS-D, CS-E and CS-D (left to right). A range of concentrations were injected (100  $\mu\text{M}$   $\alpha$ -synuclein selectively bound to CS-E and HS, but not to CS-D. Data was fitted with a 1:1 Langmuir binding model (dotted lines). **B.** Oligomeric  $\alpha$ -synuclein was injected over CS-D, CS-E and CS-D at a range of concentrations (left to right). Results shown are from one experiment. The experiments were performed twice.

To verify the binding, we used QCM-D, which can simultaneously detect the potential interaction between  $\alpha$ SYN and GAGs, and measure changes in the organisation of surface bound GAG induced by  $\alpha$ SYN binding. Sema3A, another GAG binding protein, has previously been shown to crosslink GAG chains and rigidify the GAG film (Djerbal, *et al.*, 2019). This change can be detected with QCM-D by measuring a decrease in dissipation ( $\Delta D$ ).  $\alpha$ SYN fibrils and oligomers are built from multiple monomers so could potentially crosslink GAGs through binding multiple GAG chains. QCM-D confirmed the interaction between PNN GAGs and monomeric and oligomeric  $\alpha$ SYN. The profile of binding for both species mirrored that seen by SPR, providing further confirmation of the interaction. In contrast to our SPR results we did detect PFF binding to HS as shown by a decrease in frequency (Fig. 23). The binding profile for PFF was unusual, as it did not plateau or dissociate. The magnitude of binding was much larger than the oligomer or monomer ( $\Delta F$ : PFF: -250, oligomer: -134, monomer: -71.1). The absence of a plateau may be a result of self-aggregation of PFF material on the GAG layer. For the oligomer and monomer, we observed some dissociation, but it did not return to baseline after protein addition was halted and the surface washed. The PFF showed no dissociation during washing. Addition of GuHCl was able to fully regenerate baseline as detected by a return to pre-protein addition frequency and dissipation baselines, showing the proteins could be fully removed and the GAG layer had not undergone an irreversible transformation. The lipid only control was not included so we cannot rule out a lipid interaction with PFF, the dependence of lipids in QCM-D may explain the discrepancy between the two biophysical techniques. We did not detect crosslinking for any of the  $\alpha$ SYN species as  $\Delta D$  was positive in all cases (Fig. 23B). Through biophysical techniques we have demonstrated that  $\alpha$ SYN species bind to CS-E and HS, the two major GAGs in the PNNs. This provides a putative link underlying the neuroprotective role of the PNN against  $\alpha$ SYN seeding.

**Table 3: Kinetic constants of GAG/ $\alpha$ SYN interaction**

		Ka (1/Ms)		Kd ( $10^{-3} \text{ s}^{-1}$ )		Kd ( $\mu\text{M}$ )		Chi2
Monomer	CS-E	64	72.1	1.4	1.30	22	18.0	3.92
			55.6				1.48	
	HS	91	95.7	0.45	0.437	5.5	5.56	38.9
					86.7			0.467
Oligomer	CS-E	223	44	9.6	7.97	105	181	501
			402				11.20	
	HS	88	17.7	6.93	7.28	128	212	2080
					158			6.58

**Figure 23: Confirmation of  $\alpha$ SYN/ HS interaction**

QCM-D  $\Delta F$  and  $\Delta D$  traces of HS/ $\alpha$ SYN interactions. Arrows indicate how long a protein was flown over the surface before changing back to buffer. Traces represent 4 different chambers containing a HS-lipid surface **A**. Frequency shift as  $\alpha$ SYN begins to bind. The monomer showed the lowest shift with a slow association and dissociation (plateaued at 139 minutes, -71.1 Hz). Oligomer showed a larger shift with a rapid association and dissociation (plateaued at 142 minutes, -134 Hz). Fibril showed large increase which began to slow before addition was stopped (250min, -250 Hz). All proteins stabilised above the GAG baseline, indicating continued binding. This was regenerated with GuHCl. **B**. Corresponding dissipation traces for A. All traces mirrored  $\Delta F$  and increased, demonstrating the surface was becoming softer. Monomer: 142min,  $4.93 \times 10^6$ . Oligomer: 142 minutes,  $23.5 \times 10^6$ . Fibril: 250 minutes,  $88.5 \times 10^6$ .

## 4.4 Discussion

### 4.4.1 Summary of results

We have successfully purified  $\alpha$ SYN monomer and created two pathogenic  $\alpha$ SYN species with seeding capabilities: oligomers and fibrils. The oligomer was internalised by both the HEK cell line and primary neurons. In HEK cells it led to the endogenous  $\alpha$ SYN forming puncta. PFF treatment in primary neurons resulted in phosphorylated  $\alpha$ SYN pathology which progressively spread in the culture over time. We have then established that a PNN can block  $\alpha$ SYN uptake and seeding in a PNN-HEK cell line and in primary neurons. The resistance is PNN dependent as PNN removal through enzymatic digestion removed the protection. The low level of somatic inclusion formation in the PFF treated neurons prevented testing of the neuroprotection hypothesis, although the number of PNN neurons were unaltered upon PFF treatment. Together this establishes the PNN as a neuroprotective structure against  $\alpha$ SYN induced seeding.

### 4.4.2 Structurally diverse $\alpha$ SYN species cause seeding

We have successfully created oligomeric and fibrillar  $\alpha$ SYN species which are both capable of seeding endogenous  $\alpha$ SYN aggregation. Despite this shared ability they are structurally distinct species. Another group has shown the seeding oligomer preparation contains  $\alpha$ SYN multimers, with up to hexamers being detected (Illes-Toth, *et al.*, 2015). However, we have detected large aggregates using AFM ( $154 \pm 53$  nm) which are larger than an estimated hexamer size. The oligomeric species is smaller than the mature fibril, which extends over 500 nm in length (Spillantini, *et al.*, 1998b; Bousset, *et al.*, 2013). The average PFF length is 52.1 nm, which is smaller than the oligomer in size (Patterson, *et al.*, 2019). However, while the fibril is elongated, the oligomer is amorphous. The oligomer is also twice the height of the fibril (12.4 vs 6.0 nm) (Makky, *et al.*, 2016). Illes-Toth *et al.* (2015) determined that the structure of the oligomer was closer to that of a compact ring rather than an elongated fibril through collision cross-sectional analysis, further demonstrating that the oligomer has a distinct structure from the fibril. In addition, epitope mapping of oligomers and fibrils has shown that the species have different reactivity to antibodies indicating different residues are exposed in the structures (Illes-Toth, *et al.*, 2015).

In our sedimentation assay we have shown that a large proportion of the oligomer do not form sedimentable species (Fig. 16B). This either indicates that

they are either lower order multimers or dynamically revert to the monomeric state. Danzer *et al.* (2007) showed that 80% of the oligomer preparation formed small oligomers as detected by fluorescence-intensity distribution analysis, demonstrating lower order oligomers do exist in the preparation. This is a more sensitive technique than the sedimentation assay as it directly measures the fluorescence intensity of particles in their native solution to determine size, allowing segregation of components into different size categories. The sedimentation assay is binary, assuming that all higher order species will sediment, ignoring lower order species, i.e., dimers, which instead remain soluble. Furthermore, the use of a denaturing SDS-PAGE, while allowing determination of conversion rate, disrupts the assemblies and so prevents an entire population view of the sample. Some oligomer preparations form a dynamic equilibrium, where the oligomer can convert back into monomer (Danzer, *et al.*, 2007). It cannot be ruled out that the seeding oligomer also forms a dynamic equilibrium and so converts back into a monomeric fraction post filtration. However previous investigation of the oligomer preparation also favours a heterogeneous mixture (Illes-Toth, *et al.*, 2015). The seeding oligomers are poorly characterised when compared to the fibril and other oligomer classes. It is not yet known whether they are on or off-pathway oligomers. Longer term aggregation studies need to be performed to determine if the preparation tends towards fibrils, as with the Danzer toxic oligomer, or a stable off-pathway oligomer (Danzer, *et al.*, 2007). Analytical ultracentrifugation and size exclusion chromatography (SEC) are other techniques that should be employed to determine the proportion of different multimers in the oligomer preparation. SEC would also then purify the different multimers. If stable they could then be individually tested for seeding activity. Despite the heterogeneity of the oligomer sample, it was still able to reproducibly seed cellular  $\alpha$ SYN aggregation and was therefore used in the study.

#### **4.4.3 The perineuronal net blocks uptake of oligomeric $\alpha$ SYN**

For seeding to occur the pathogenic  $\alpha$ SYN species must first be internalised by the cell. Diverse mechanisms of internalisation have been identified for  $\alpha$ SYN, as discussed in the introduction. After internalisation the pathogenic  $\alpha$ SYN is localised to the late-endosomal/lysosomal network and degraded unless it ruptures the vesicles and escapes (Freeman, *et al.*, 2013; Jiang, *et al.*, 2017; Flavin, *et al.*, 2017). Then once in the cytoplasm it can then induce aggregation of endogenous  $\alpha$ SYN (Flavin, *et al.*, 2017; Freeman, *et al.*, 2013). For the pathogenic  $\alpha$ SYN to reach its internalisation receptor it must be able to access the cell membrane. We have shown the presence of a perineuronal net reduces

internalisation of oligomeric  $\alpha$ SYN by 50% in primary neurons. We put forward that the interposition of a cellular barrier, the PNN, denies  $\alpha$ SYN membrane access and therefore prevents internalisation. Another explanation for this phenomenon is that PNN-bearing neurons lack the appropriate machinery for  $\alpha$ SYN internalisation, for example the expression of LAG3, a  $\alpha$ SYN fibril receptor, varies between brain regions (Freeze, *et al.*, 2018). This was not directly assessed in the study but is unlikely as: a proportion of PNN-bearing neurons (15.8%) did internalise the oligomer; and PNN removal ablated the resistance phenotype. This indicates that PNN-bearing neurons can internalise pathogenic  $\alpha$ SYN and that the PNN is the significant factor preventing uptake rather than receptor expression.

The PNN can deny membrane access through three potential mechanisms, with two mechanisms depending on if it interacts with  $\alpha$ SYN. The PNN is a charged structure, a property which arises from the negatively charged glycosaminoglycans within it (Morawski, *et al.*, 2005).  $\alpha$ SYN may bind to or be repelled by this negative charge. At physiological pH,  $\alpha$ SYN has a negative charge due to its low isoelectric point which could indicate it is repelled by the PNN (Cabungcal, *et al.*, 2013). However, there are differences between the charge state of  $\alpha$ SYN's domains. The N-terminal contains positively charged lysine residues which allows binding to small negatively charged vesicles (Pranke, *et al.*, 2011). In this case, the N-terminal could allow binding to the GAGs in the PNN on the basis of a charge interaction. This interaction could trap  $\alpha$ SYN species on the PNN preventing or slowing further diffusion as has been shown for ions (Balmer, 2016; Morawski, *et al.*, 2015). We have shown that  $\alpha$ SYN monomers and oligomers both bind to CS-E and HS which are both key PNN glycans (Deepa, *et al.*, 2006; Holmes, *et al.*, 2013; Stopschinski, *et al.*, 2018b).

Membrane bound HS proteoglycans (HSPGs) are a cellular mediator for  $\alpha$ SYN fibril internalisation (Holmes, *et al.*, 2013; Hudák, *et al.*, 2019). The HS chains are the key mediator as their removal reduces  $\alpha$ SYN fibril internalisation (Holmes, *et al.*, 2013; Stopschinski, *et al.*, 2018b). This is further underscored by the ability of extracellular heparin to reduce  $\alpha$ SYN internalisation by competing with membrane HSPGs (Holmes, *et al.*, 2013). We could not confirm if PFFs interacted with HS or CS-E as used in this study. The SPR results indicate a lack of interaction while in QCM-D, any interaction was masked by self-aggregation observed. Not all  $\alpha$ SYN species bind to HS, as non-amyloid oligomers failed to bind (Ihse, *et al.*, 2017). We demonstrated an interaction between oligomers and HS in our study. This discrepancy is due to the different oligomer species used. CS application has been shown to reduce  $\alpha$ SYN

internalisation but to a lesser extent than HS, indicating a potential interaction (Ihse, *et al.*, 2017). Membrane bound CS has no apparent role in internalisation as ChABC treatment does not reduce intake (Holmes, *et al.*, 2013; Ihse, *et al.*, 2017).

The PNN is a physical barrier and can exert a molecular sieving effect which prevent large molecules from reaching the cell surface. Loose pericellular coats, made of hyaluronan and aggrecan, can prevent large particles from reaching the cell surface. 100 nm particles could only diffuse to within 7  $\mu\text{m}$  of the cell surface while 40 nm particles could only diffuse to within 5  $\mu\text{m}$  (Chang, *et al.*, 2016; Scrimgeour, *et al.*, 2017). The PNN is a much denser structure as link proteins cause the coat to condense and the presence of crosslinkers can further reduce the pore size (Kwok, *et al.*, 2010). The fibrils and oligomers used in this study are larger than this, although it has not yet been investigated how an elongated structure will diffuse through pericellular coats. The full length fibril is a rigid structure in the context of the cell, having higher bending rigidity than actin (Knowles, *et al.*, 2007; Makky, *et al.*, 2016). This makes it unlikely for fibrils to easily diffuse through the dense PNN despite their small width.

It is likely that both a molecular interaction and a molecular sieving effect play roles in PNN-mediated inhibition of  $\alpha\text{SYN}$  uptake, with the precise balance between the two depending on the size and structure of the pathogenic species. While internalisation of the oligomer was investigated, the effect of the PNN on fibril internalisation was not directly investigated. This should be rectified through the application of fluorescently tagged fibrils on the neuronal culture. Live-cell imaging should also be used to determine how  $\alpha\text{SYN}$  travels through the PNN and to definitively answer if the PNN blocks internalisation or slows it. Another outstanding question is how can a somatic PNN reduce uptake when it is not covering the dendrites? As this is where both oligomer internalisation and p- $\alpha\text{SYN}$  pathology can occur. One suggestion is that the soma is main location for internalisation for  $\alpha\text{SYN}$ . The presence of a PNN would then reduce uptake to a level where the remaining pathogenic  $\alpha\text{SYN}$  is degraded, preventing it from overwhelming the cell.

Diffusion of free extracellular  $\alpha\text{SYN}$  is not the only method of  $\alpha\text{SYN}$  transmission; exosomal  $\alpha\text{SYN}$  and  $\alpha\text{SYN}$  transmission through synapses, along the connectome, are both well-established methods for  $\alpha\text{SYN}$  seeding and LP spread through the brain (Rey, *et al.*, 2013). Exosomal spread of  $\alpha\text{SYN}$  has a higher efficiency than its free counterpart (Danzer, *et al.*, 2012). While we did not investigate exosomal  $\alpha\text{SYN}$  spreading, we expect the interposition of PNN to still block it due to its dense nature. Synaptic spread, despite its prominence,

is not sufficient to explain pathology spread (Oliveira, *et al.*, 2019; Henrich, *et al.*, 2020). Neuron to neuron transmission of pathogenic  $\alpha$ SYN was not examined in this study but should be investigated in future now that the principle of PNN-mediated neuroprotection has been established in PD.

#### 4.4.4 The PNN as a protective structure from $\alpha$ SYN pathology

Both oligomer and fibril treatment caused seeding of cellular  $\alpha$ SYN seeding. The fibril induced aggregate formation at a 100-fold lower concentration than the oligomer. This may be due to the extended structure of the fibril which allows it to better rupture intracellular vesicles and escape into the cytoplasm, bringing it into contact with naïve  $\alpha$ SYN (Flavin, *et al.*, 2017; Jiang, *et al.*, 2017). Other seeding oligomer species used in the literature are less efficient in pathology development compared to the fibril and even different fibril species show different seeding capabilities (Peelaerts, *et al.*, 2015). However, a direct comparison cannot be drawn in this study as different parameters were used for judging seeding. In HEK cells endogenous  $\alpha$ SYN formed puncta after oligomer exposure. Oligomer induced seeding was not examined in neurons due non-reactivity of the  $\alpha$ SYN antibody to rat  $\alpha$ SYN. In 3D neuronal culture, oligomer exposure leads to the development of somatic Lewy-like inclusions after twenty-four hours. However, the inclusions lacked p129 reactivity at this time point (Taylor-Whiteley, *et al.*, 2019). To address this, neurons should be treated with the oligomer for up to 21 days and the level of p129 inclusions measured. This would then allow comparison of the seeding efficiency of the fibril and oligomer species.

Fibril treatment led to the progressive development of p- $\alpha$ SYN aggregates. These were primarily elongated and localised to the dendrites. The PNN primarily covers the soma and the proximal neurites while the majority of phosphorylated  $\alpha$ SYN aggregates are in the distal neurites at earlier time points. In long-term neuronal culture the neurites form a dense-mesh and can project over a 100  $\mu$ m from the soma. Deconvoluting this dense network to trace projections back to the parent soma is computationally intensive and requires high magnification, whole coverslip imaging. Therefore, the incubation period was extended up to 21 days post exposure as somatic inclusions have been shown to form at this time. The long incubation period was based off the work of Mahul-Mellier *et al.* (2020) who established the importance of time in the development of somatic LB-like inclusions. At 21 days post exposure they found ~22% of neurons developed LB-like inclusions. The appearance of somatic inclusions would allow us to easily determine if PNN neurons developed LB-like pathology after fibril treatment and therefore if the PNN was

protective against  $\alpha$ SYN pathology development. However the number of somatic inclusions detected in our culture was lower than that reported in the literature (Mahul-Mellier, *et al.*, 2020). This may be because human PFF were used on rat neurons. Such cross-seeding has three-fold lower efficiency than homologous seeding (Luk, *et al.*, 2016). Another factor could be the lower plating density used in our culture. The proportion of PNN neurons was unchanged in fibril treated cultures. The low proportions of somatic inclusion bearing neurons and PNN neurons in the culture mean the percentage of inclusion-bearing PNN neurons is heavily subject to variance. However, this study has provided the initial evidence to establish the PNN as a neuroprotective factor in  $\alpha$ SYN seeding. As such the hypothesis warrants further investigation using less reductive models. Therefore, the results found here should be confirmed through the testing in a different paradigm. Injection of fibrillar  $\alpha$ SYN into a PNN rich region of the rodent brain should be performed to adequately test if the PNN protects neurons from developing Lewy-like pathology. Another way of testing the hypothesis would be to investigate whether the PNN population in the human brain presents with LB. This would establish the relevance of the PNN as a neuroprotective factor in PD.

#### **4.4.5 Putative mechanism for PNN neuroprotection**

Using biophysical techniques, we have identified that both monomeric and oligomeric  $\alpha$ SYN bind to the PNN GAGs HS and CS-E. This was a specific interaction as neither species interacted with CS-D. All GAGs used in this study are negatively charged though the charge density differs across the disaccharide sub-unit (Gama, *et al.*, 2006; Djerbal, *et al.*, 2019). Synthetic GAG manufacture is complex so GAGs from biological sources were used, leading to high variability in sub-unit composition. Analysis of the CS-E and CS-D composition (purified from natural source) used in this study has shown that the CS-E preparation contains ~70% CS-E while the CS-D preparation only contains ~30% CS-D, with ~70% being other CS types. (Djerbal, *et al.*, 2019). This raises the possibility that the lack of binding was due to low purity. The sulfation pattern of glycans play a biological role by providing different recognition motifs for proteins, e.g. sema3A, Otx2 (Gama, *et al.*, 2006; Beurdeley, *et al.*, 2012; Vo, *et al.*, 2013). While we have identified an interaction between PNN GAGs and  $\alpha$ SYN we are unable to rule out if this was a GAG specific interaction or an electrostatic interaction.  $\alpha$ SYN has previously been shown to bind to HS, an interaction that depends heavily on the presence of N-sulfation. The dependence on N-sulfation rather than 2 or 6 sulfation demonstrates that the spatial location and charge density of the HS GAG

matters for  $\alpha$ SYN binding, arguing against a simple electrostatic interaction and agrees with our observation that  $\alpha$ SYN binds CS-E but not CS-D (Stopschinski, *et al.*, 2018). The HS interaction is important for  $\alpha$ SYN seeding as HSPGs on the cell-surface provide a vector for  $\alpha$ SYN internalisation (Holmes, *et al.*, 2013). The  $K_D$  calculated for PNN GAG/ $\alpha$ SYN binding was in the micromolar range, which is weaker than other PNN-GAG binding proteins, such as Sema3a (Djerbal, *et al.*, 2017). However, this still has biological relevance; the high GAG density within the PNN make an avidity interaction likely. Other GAG binding proteins rely on an avidity interaction (Maureen, *et al.*, 2015). In our results the smaller monomeric  $\alpha$ SYN showed slow association and dissociation compared to the oligomer. The slow binding hints at diffusion of the monomer into the GAG layer and slow diffusion arising from avidity to glycan chains (Schuck and Zhao, 2001). In accordance with this, the larger size of the oligomer prevents diffusion into the matrix, resulting in a fast association and dissociation. Altering the density of the GAG layer would allow testing of this hypothesis. If the monomer binding profile changes with density it would indicate avidity. GAG density can be finely tuned in QCM-D via adjusting the proportion of streptavidin conjugated lipids.

We had conflicting results regarding GAG binding to PFF. We detected no response for any GAG when using SPR. In QCM-D we observed PFF binding, but it was non-saturable and showed no dissociation. This could reflect self-aggregation of PFF on the QCM-D surface. The surface could be regenerated through GuHCl addition, indicating this binding did not arise from an irreversible change in the GAG matrix. The question is then whether the PFF binding observed in QCM-D was to GAGs or to the underlying lipids or streptavidin. As discussed in chapter 1,  $\alpha$ SYN can bind to lipids and lipids can provide a nucleation surface for  $\alpha$ SYN aggregation (Galvagnion, *et al.*, 2015). Lipid binding is not assured as  $\alpha$ SYN requires anionic lipids and curvature (Perlmutter, *et al.*, 2009). This can be confirmed via the inclusion of a lipid and streptavidin only control. If GAG binding is shown then this raises the possibility that the PNN can provide a nucleation surface for  $\alpha$ SYN, which has implications for PD pathophysiology and creates a more nuanced role for PNN.

The PNN provides a competing pool of HS and CS-E which can chelate  $\alpha$ SYN, reducing the proportion that is available to be internalised, therefore reducing seeding. This provides a putative mechanism for the PNN-mediated neuroprotection we observed. However, while we detected  $\alpha$ SYN/GAG binding in our biophysical experiment we did not observe it in our cell culture. No colocalization was detected between WFA and oligomeric  $\alpha$ SYN. There are several possible explanations that could explain this discrepancy. WFA and

$\alpha$ SYN both bind CS-E (Djeral, *et al.*, 2019; Nandanaka, *et al.*, 2020). The lack of colocalisation might then arise from steric hindrance and competition between WFA and  $\alpha$ SYN for CS-E in the PNN, though this would not account for binding of PNN HS/ $\alpha$ SYN. Another explanation is the time-frame examined. The binding between PNN GAGs and  $\alpha$ SYN was weak, so while  $\alpha$ SYN may initially bind to the PNN it would diffuse away over time. To investigate this shorter time frames, or live-cell imaging should be used.

#### **4.4.6 Conclusions and future directions**

The aim of this chapter was to establish the PNN as a neuroprotective barrier against  $\alpha$ SYN seeding. It is not yet known if there is a dominant seeding species in PD pathophysiology. The fibril is currently favoured as the seeding species, but its efficacy is not proof of pathophysiological relevance. As the question remains open, we elected to test the PNN against both oligomer and fibrillar seeding species. In both cases the presence of a PNN increased the resistance of neurons to oligomer uptake and pathology development. This establishes the PNN as a neuroprotective barrier against  $\alpha$ SYN seeding through reducing uptake. The precise mechanism behind this neuroprotection phenotype has yet to be identified but doing so could open a new therapeutic avenue for PD halting therapies. This chapter has demonstrated that the PNN is a factor that governs  $\alpha$ SYN seeding and pathology development. The discovery of the PNN as a neuroprotective factor in PD could help explain why some neuronal populations do not develop LP while neighbouring populations do. Future work should focus on elucidating the precise mechanism and proving the relevance in more complex models and in different modes of  $\alpha$ SYN transmission.

## Chapter 5 PNN populations are spared and unaffected by Lewy pathology in PD brains

### 5.1 Introduction

PD is a progressive neurodegenerative disease. Symptom development is linked to neuronal loss and the appearance of LP in associated brain regions. Neuronal loss and the appearance of LP are conserved in PD, following a spatio-temporal pattern. This conserved distribution can be classified according to a staging procedure, in which post-mortem PD brains can be indexed into 6 categories depending on where the pathology has reached (Braak, *et al.*, 2003; Adler, *et al.*, 2019). This has led to the hypothesis that LP can spread, in a prion-like manner, through the brain with aggregated  $\alpha$ SYN acting as the prion-like agent. However, a prion-like process does not fit neatly with the specific and conserved spread of LP. Prion-like transmission implies spreading through a 'nearest neighbour' process and/or the connectome.  $\alpha$ SYN transmission has been shown to occur predominantly via the connectome (Henrich, *et al.*, 2020; Mezas, *et al.*, 2020).

#### 5.1.1 Cell autonomous factors in determining neuronal susceptibility

$\alpha$ SYN spread is not dictated purely by connectivity as the strength of synaptic connectivity does not accurately predict pathology development (Surmeier, *et al.*, 2017b; Henderson, *et al.*, 2019; Henrich, *et al.*, 2020). For example, after PFF injection into the PPN the weakly connected central amygdala nucleus exhibited greater pathology than the gigantocellular nucleus, despite the latter possessing threefold higher connections (Henrich, *et al.*, 2020). Furthermore, as mentioned not all neurons within a nucleus develop pathology or are lost in PD (Braak, *et al.*, 1994; Harding, *et al.*, 2002). Therefore, LP spread cannot be purely dictated by the connectome. Differential neuronal susceptibility must also play a role. Cell autonomous factors interact to determine differential neuronal susceptibility to LP. These include: SNCA expression, axonal arborisation, mitochondrial stress, intracellular calcium concentration, autophagic capacity, neurotransmitter expression, intracellular iron concentration (Hirsch, 1992; Mosharov, *et al.*, 2009; Elstner, *et al.*, 2011; Braidy, *et al.*, 2013; Pacelli, *et al.*, 2015; Duda, *et al.*, 2016; Deas, *et al.*, 2016; Do Van, *et al.*, 2016; Volpicelli-Daley, *et al.*, 2016; Courte, *et al.*, 2020). Together these determine how vulnerable a neuron is to LP and death. One example of this is the comparison of DA neurons from the SN with those of the ventral tegmental area (VTA). SN DA neurons are much more vulnerable to LP than their VTA counterparts

despite both containing DA, which can induce  $\alpha$ SYN aggregation (Cappai, *et al.*, 2005). The particular vulnerability of SN DA neurons in PD is well documented, with some studies reported 68% of cells lost (Giguère, *et al.*, 2018). SN DA neurons have a higher degree of axonal arborisation than VTA DA neurons, requiring a higher dependence on mitochondrial oxidative phosphorylation, leading to higher levels of mitochondrial DNA deletions and oxidative stress (Pacelli, *et al.*, 2015). This could explain their differing vulnerability to LP. However, the relationship between arborisation and susceptibility is not clear cut; cholinergic neurons in the striatum show a high degree of arborisation yet develop limited pathology (Zhou, *et al.*, 2002). Neuronal susceptibility is the product of a complex interactions between factors.

### 5.1.2 The extracellular matrix as a factor in neuronal susceptibility

Other factors, beyond the connectome and cell autonomous variables, may dictate neuronal susceptibility and the pattern of LP spreading in PD. One possible factor is the neural extracellular matrix, an overlooked factor in PD. The ECM can be subdivided into the loose ECM and the PNN. The ECM controls extracellular space size and diffusion through it (Zamecnik, *et al.*, 2012; Syková, *et al.*, 2005; Bekku, *et al.*, 2010; Sucha, *et al.*, 2020).  $\alpha$ SYN transmission necessitates travel through the extracellular space and therefore can be regulated by the ECM. In the previous chapter we have shown that GAGs found in the ECM, CS-E and HS, bind to  $\alpha$ SYN. This interaction could slow  $\alpha$ SYN diffusion through ECM rich brain regions, limiting and restricting  $\alpha$ SYN spread and giving rise to the LP pattern seen in PD. The potential of chelating  $\alpha$ SYN in the extracellular space has already been shown to be of great value;  $\alpha$ SYN antibody treatment reduced pathology development through preventing diffusion and uptake, rescuing motor deficits (Tran, *et al.*, 2014). Chelating  $\alpha$ SYN in the ECM reduces neuronal uptake and increases  $\alpha$ SYN degradation by extracellular proteases and microglia (Lee, *et al.*, 2008b; Pampalakis, *et al.*, 2016; Choi, *et al.*, 2020). However, pathogenic  $\alpha$ SYN can also affect the ECM itself. PFF treatment increased nanoscale diffusion and extracellular space size through microglial activation. Microgliosis led to degradation of hyaluronan in the loose ECM, expanding EC space (Soria, *et al.*, 2020). Similarly in AD, another prion-like disease, areas of high ECM density contained  $\beta$ -amyloid plaques (Yasuhara, *et al.*, 1994; Brückner, *et al.*, 1999). While the loose ECM does not restrict prion-like spreading, a neuroprotective role for the PNN has been identified (Brückner, *et al.*, 1999; Morawski, *et al.*, 2010a; Morawski, *et al.*, 2012b; Suttikus, *et al.*, 2016b; Soria, *et al.*, 2020). PNN neurons were unaffected in AD and did not develop neurofibrillary tangles (NFT)

(Brückner, *et al.*, 1999; Morawski, *et al.*, 2010a; Morawski, *et al.*, 2012b). The PNN reduced entry of oligomeric tau into neurons. This was a structure-dependent mechanism as impairment of the dense, cross-linked PNN structure abolished the effect (Suttkus, *et al.*, 2016b). In chapter 4, we have established a similar role for the PNN in  $\alpha$ SYN uptake and seeding. Furthermore, the PNN is resistant to microglial-mediated degradation (Schüppel, *et al.*, 2002; Soria, *et al.*, 2020). This disparity between the PNN and loose ECM is most likely due to the structural organisation. In comparison to the loose ECM, the PNN is a dense, cross-linked structure that resists solubilisation by detergents (Deepa, *et al.*, 2006; Kwok, *et al.*, 2010).

### 5.1.3 The PNN as a resistance factor restricting local $\alpha$ SYN spread

$\alpha$ SYN transmission spreads primarily through the connectome rather than lateral spread despite a mechanism for lateral spread being established. Neuronal death is a hallmark of PD (Giguère, *et al.*, 2018). As neurons die they release  $\alpha$ SYN aggregates into the extracellular space, where they can then be internalised by neighbouring neurons, seeding further pathology (Jiang, *et al.*, 2017). Despite this neighbouring neuron populations are often spared in PD; in the SN, the pars compacta (SNc) region is severely affected but the neighbouring pars reticulata (SNr) shows limited pathology and cell loss (Hardman, *et al.*, 1996). A similar affect is seen in the heterogeneous PPN, as only cholinergic neurons develop LP (Henrich, *et al.*, 2020). Why is lateral spread not common in PD and why are only specific neuronal subtypes affected? Factors governing selective neuronal vulnerability in PD have been highlighted but the factors governing neuronal resistance have not been so robustly investigated. Neuronal resistance turns the paradigm on its head by asking what makes neuronal populations less likely to develop LP. The PNN could be a neuronal resistance factor. As discussed the PNN protects neurons against oxidative and A $\beta$  induced cell death (Miyata, *et al.*, 2007; Morawski, *et al.*, 2010a). It can also reduce entry of pathogenic tau into neurons (Brückner, *et al.*, 1999; Suttkus, *et al.*, 2016a). In the previous chapter we have identified a similar neuroprotective role for the PNN in PD. The PNN reduced uptake of oligomeric  $\alpha$ SYN by two thirds and removal of the PNN and ECM enhanced p- $\alpha$ SYN pathology formation. The mechanism has been established *in vitro* but its disease relevance has yet to be established. The PNN can restrict prion-like spreading and thus determine the pattern of pathology. In AD, areas devoid of PNNs, e.g. locus coeruleus, exhibited high NFT load, while PNN rich areas, e.g. ventral posterior nuclei showed little pathology (Morawski, *et al.*, 2010a). It is possible similar gating and restriction occurs within PD. Therefore, PNN

neurons will be investigated in post-mortem PD brains to determine whether they develop LP and if they are spared. The segregation between PNN rich and Lewy rich areas will be also examined in this study.

#### **5.1.4 Chapter aims**

The aim of this chapter is to investigate PNN populations in post-mortem PD brains and to establish disease relevance for the neuroprotective mechanism identified in chapter 4. To examine whether PNNs are spared in PD, brain regions which contain both PNNs and LP will be investigated. Late-stage PD brains (Braak 6) will be used so to exclude a minor resistance effect. It is possible that the PNN only provides an initial protective effect and PNN neurons develop LP and die later in disease progression. WFA will be used as the PNN marker as it has been predominantly used in the literature to identify PNN populations. This may lead to some PNN populations being missed but it will suffice for this pilot study.

## 5.2 Methods

### 5.2.1 Human brain tissue

The paraffin embedded patient and non-demented control samples were kindly supplied by the Netherlands Brain bank. The profile of the cohort is summarised in table 4. Four out of five of the PD patients were Braak stage 6 with widespread pathology with an average disease duration of 12.2 years ranging from 6-16 years. PD diagnosis was confirmed at post-mortem by a neuropathologist. Non-demented controls had no significant pathology except for 1 which was diagnosed with iLBD. PD cohort had an average age of 77, ranging from 65-86 years of age. The NDC cohort had an average age of 87.8, ranging from 82-96 years of age.

**Table 4: Human cases used in this study**

Case ID	Age	Sex	PMD (hours)	Cause of death	Disease Duration (years) <sup>1</sup>	Braak LB Stage	Brain regions
<b>Non-demented controls</b>							
2011-021	85	F	7:05	Terminal renal insufficiency		0	Hc, OB, Tc
2011-082	84	F	5:55	Respiratory failure by pneumonia		0	Am, Hc, OB, SN, Tc
2014-051	92	M	7:45	Liver cirrhosis ascites and anuria		0	Am, Hc, OB, Tc
2017-003	96	F	6:15	Pneumonia, general deterioration and cachexia		4	Am, Hc, OB, SN, Tc
2017-093	82	M	5:45	Euthanasia		0	Am, Hc, SN, Tc
<b>Parkinson's Disease</b>							
2014-018	86	M	6:15	End stage PD with possible pneumonia	7	6	Am, Hc, OB, SN, Tc
2014-034	72	M	8:45	Atrial fibrillation, Asystole	9	6	Am, Hc, OB, SN, Tc
2014-067	65	F	7:35	Cachexia and dehydration by advanced Parkinson dementia	16	6	OB, Hc, Tc
2015-063	76	M	8:15	Sepsis by urinary tract infection, decompensation cordis, endstage dementia	16	6	Am, Hc, OB, SN, Tc
2015-088	86	F	3:00	Seizure by Midazolam and Morphine	13	4	OB, Hc, Tc

1- As judged by pathologists in conjunction with medical history

### 5.2.2 Preparation of gelatine coated slides

The 1% gelatine solution was prepared by slowly dissolving the gelatine in water, heated to 50 °C. Chromium potassium sulphate (1.7 mM) was added to further aid section attachment. Frosted microscope slides (Dixon #N/A143) were submerged into the solution for several seconds before drying at 37 °C. Slides were stored at 4 °C until use.

### 5.2.3 Immunohistochemistry

The tissue was sectioned using a microtome and 7 µm sections were prepared and mounted on 1% gelatine slides and left to dry overnight at 37 °C. The next day sections were deparaffinised in xylene and brought to dH<sub>2</sub>O using

decreasing concentrations of ethanol (2x 100%, 90%, 70%, 50%) and then dH<sub>2</sub>O. Slides were submerged for 10 minutes at each step. Two types of antigen retrieval were performed in subsequent steps. First the tissue was submerged in 80% formic acid for 30 minutes. Slides were then washed in 3x 5 minutes dH<sub>2</sub>O then submitted to a 2<sup>nd</sup> antigen retrieval step. This consisted of 30 min submersion in a vessel of 10 mM citraconic solution, pH 6 at 85 °C. Then the vessel containing the solution and slides was removed from the water bath and left to cool to room temperature, allowing antigen sites to reform. The slides were then washed 3x 10 min PBS (137 mM NaCl, 2.7 mM KCl, 1.5 mM KH<sub>2</sub>HPO<sub>4</sub>, 10.1 mM Na<sub>2</sub>HPO<sub>4</sub>) and permeabilised for 15 min with PBS containing 0.1% Triton x-100. All the following steps were performed in a moist chamber with parafilm covering the sections to prevent evaporation and photobleaching. Sections were then blocked at room temperature for 1 hour with 10% NDS. Sections were incubated with 1° antibodies overnight at 4 °C. Antibodies were diluted in 5% NDS. The following day, sections underwent 3x 10 minute PBS washing steps before incubation with 2° antibodies (excluding Hoechst and Neurotrace) for 2 hours at room temperature. Sections then were washed twice more with PBS (10 minutes) before incubation with Neurotrace for 20 minutes. Sections were then rinsed twice with PBS before being incubated with Hoechst for 2 hours at room temperature. The length of these wash steps was recommended by the NeuroTrace manufacturer. The Hoechst incubation was combined with a 2 hour wash step. Sections were then washed 2x with PBS and 2x with Tris non-saline (20 mM Tris, pH 7.6). TNS was used to remove high levels of phosphate that would otherwise react with the Fluorsave mounting media. Sections were mounted with Fluorsave and rectangular glass coverslips (Fisher Sci Ltd #15356429).

#### **5.2.4 Imaging and quantification**

Sections were imaged with the AxioScan Z.1 Slidescanner (Zeiss) with a 20x objective. Whole sections were imaged using the tilescan function and stitched together. The filters were set to ensure no overlap between channels. The Slidescanner was operated by the Bioimaging facility. Counting was done manually and data analysis, including graph creation was performed using OriginPro. Two-way t-tests were used to test for significance (<0.05) between PD and NDC brain regions.

## 5.3 Results

### 5.3.1 No correlation between PNN density and post-mortem delay

Extended post mortem delay (PMD) (>24 hr) has been shown to affect the WFA epitope, decreasing staining intensity (Morawski, *et al.*, 2012a). PMD varied between 3-9 hours in our cohort (Fig. 24, Table 3). Although, this was below the 24 hr limit defined in the study; we tested for a potential correlation to exclude PMD as a confounding factor. We correlated the PNN densities of different brain regions with patient PMD. No significant correlation was detected by Spearman's rank test ( $p>0.05$ ) (Fig. 24). Therefore, in this study, we can exclude PMD as a confounding factor on PNN density as detected by WFA.

**Table 5: PNN Densities in the human brain**

Brain Region	Diagnosis	Mean PNN density (mm <sup>2</sup> )	Standard Deviation	Significance (p<0.05)
Amygdala	NDC	30.1	4.26	ns (p=0.663)
	PD	25.2	11.5	
Olfactory Bulb	NDC	12.0	4.48	ns (p=0.987)
	PD	12.0	1.74	
Substantia Nigra	NDC	31.1	11.8	ns (p=0.244)
	PD	17.3	4.03	
Temporal Cortex	NDC	35.0	8.74	ns (p=0.735)
	PD	37.3	9.03	

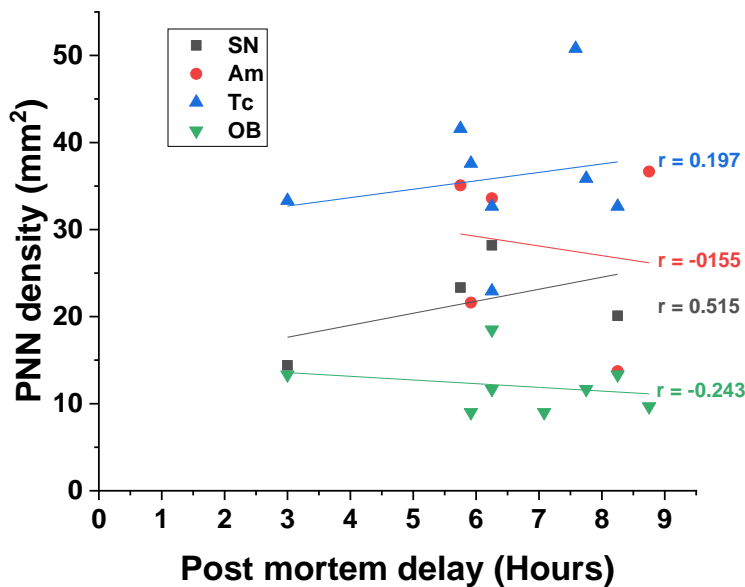


**Figure 24: PMD is not correlated with altered PNN density**

Patient PNN densities from different samples were plotted against post-mortem delay (PMD). PNN density was not correlated with PMD as determined by Spearman's rank ( $p > 0.05$ ). Data are average densities per patient brain region.

### 5.3.2 PNN density is preserved in PD

PNN density was investigated among the five brain regions (Fig. 25, Table 4) to determine if PNN populations were spared in PD. If PNN neurons were affected in PD then we would expect to see a decrease in density as the populations died off (Parkkinen, *et al.*, 2011). PNNs were detected in four of the five brain regions. The TC showed the highest PNN density ( $35 \pm 8.7$  PNNs/mm<sup>2</sup>) and the AON the lowest ( $12 \pm 4.5$  PNNs/mm<sup>2</sup>). Interestingly, no PNNs were detected in the hippocampus in either NDC or PD samples using WFA. The Hc was then excluded from analysis. Likewise, one Am sample (PD 2014-018) was also excluded as neither PNNs nor LB could be detected. In all four brain regions, PNN density was not significantly affected in PD compared to control (Fig. 25 Table 5), (two-way *t* Test,  $p > 0.05$ ). This pilot study indicates that PNN neurons are not lost in PD pathophysiology.

Neuronal density was not examined as the NeuroTrace Nissl was not specific for neurons. Co-staining with Hoechst revealed complete overlap of nuclei stained. The nuclei stained by NeuroTrace Nissl also varied in size. Together, with the Hoechst colocalisation, this indicates that NeuroTrace Nissl likely stains glia as well as neurons. This meant the PNN neurons as a proportion of total neuron population could not be examined.

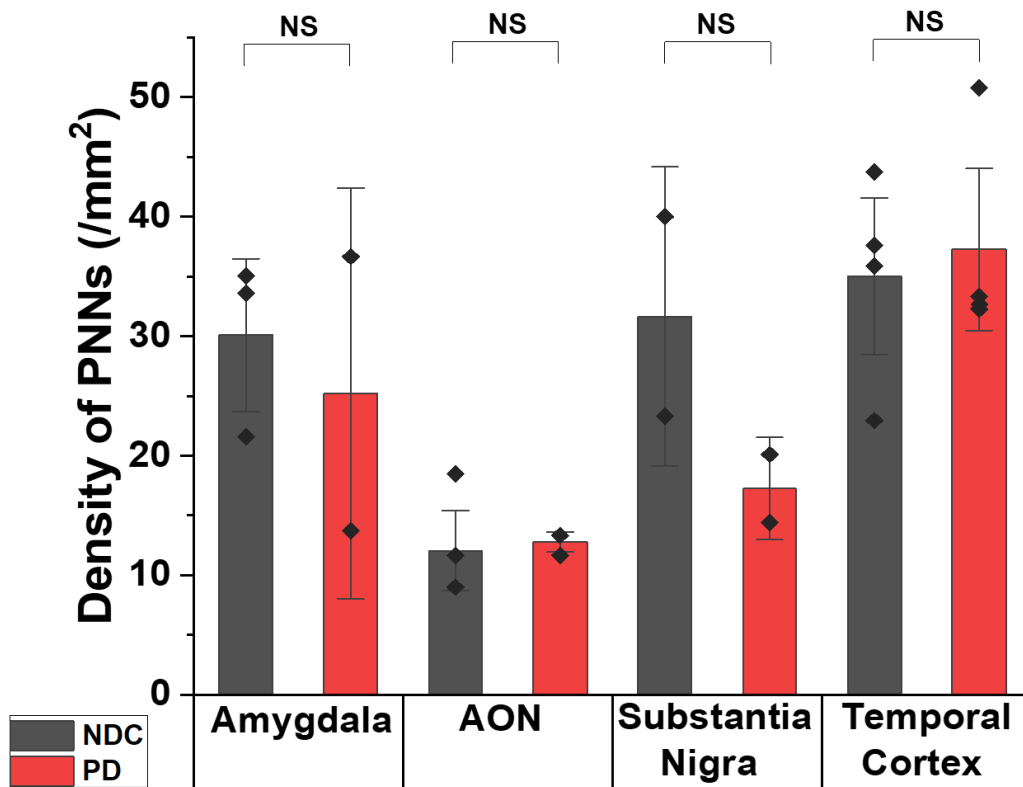


**Figure 25: PNN neuronal density is unaffected in the PD brain**

WFA labelled PNN neurons were counted in multiple brain areas (AON is anterior olfactory nucleus) and normalised to density per mm<sup>2</sup>. Symbols represent individual patients mean PNN density (average of 3 sections). Bars represent mean PNN neuron density for non-demented control (NDC) and Parkinson's disease (PD). Error bars are SEM. No significant differences were found between PNN densities of PD and NDC among any of the brain areas ( $p > 0.05$ ), as determined by a two sample t-Test.

### 5.3.2.1 No Lewy bodies in PNN neurons

In chapter 4, we have shown that PNN neurons resist uptake of aggregated  $\alpha$ SYN and negatively regulate p- $\alpha$ SYN development. Having established this *in vitro* we then sought to establish whether the neuroprotection mechanism is conserved in the human disease condition. If PNN neurons resist aggregate uptake and p- $\alpha$ SYN development, then in the PD brain we would expect to see little colocalization of Lewy pathology in PNN neurons. In the AON and Tc, we observed overlap between areas of PNNs and LP (Fig. 27 and 29). Despite the proximity of LB-containing neurons and PNN neurons we did not observe LBs within PNN neurons. This corresponds to our previous work (Ch. 4) and is consistent that the PNN protects neurons from LB development. A cytoplasmic stain was not employed during this study so we could not determine in PNN neurons had Lewy neurites. Furthermore, no colocalization was seen between

WFA reactive material and LP indicating that Lewy aggregates do not contain WFA reactive CS.

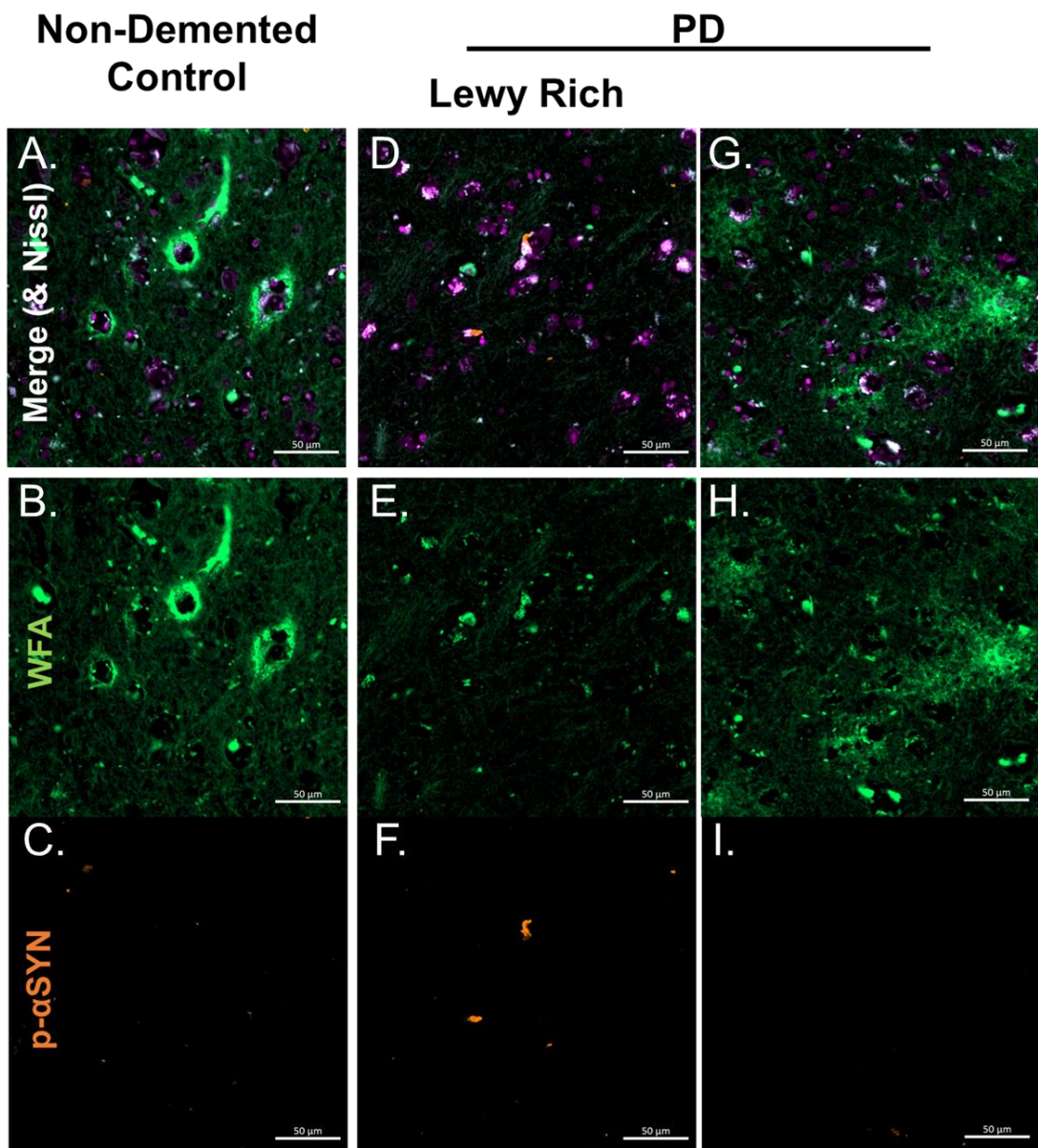


**Figure 26: PNN rich areas segregate from Lewy rich areas in PD amygdala**

Representative immunofluorescence images of human amygdala from non-demented control and Parkinson's disease (PD) patients (7  $\mu$ m sections). PNNs were labelled by WFA (green) and coalesced around a proportion of Nissl-stained neurons (purple). LP was detected by staining for p-129  $\alpha$ SYN (orange). Perinuclear LB aggregates were found in a proportion of neurons.

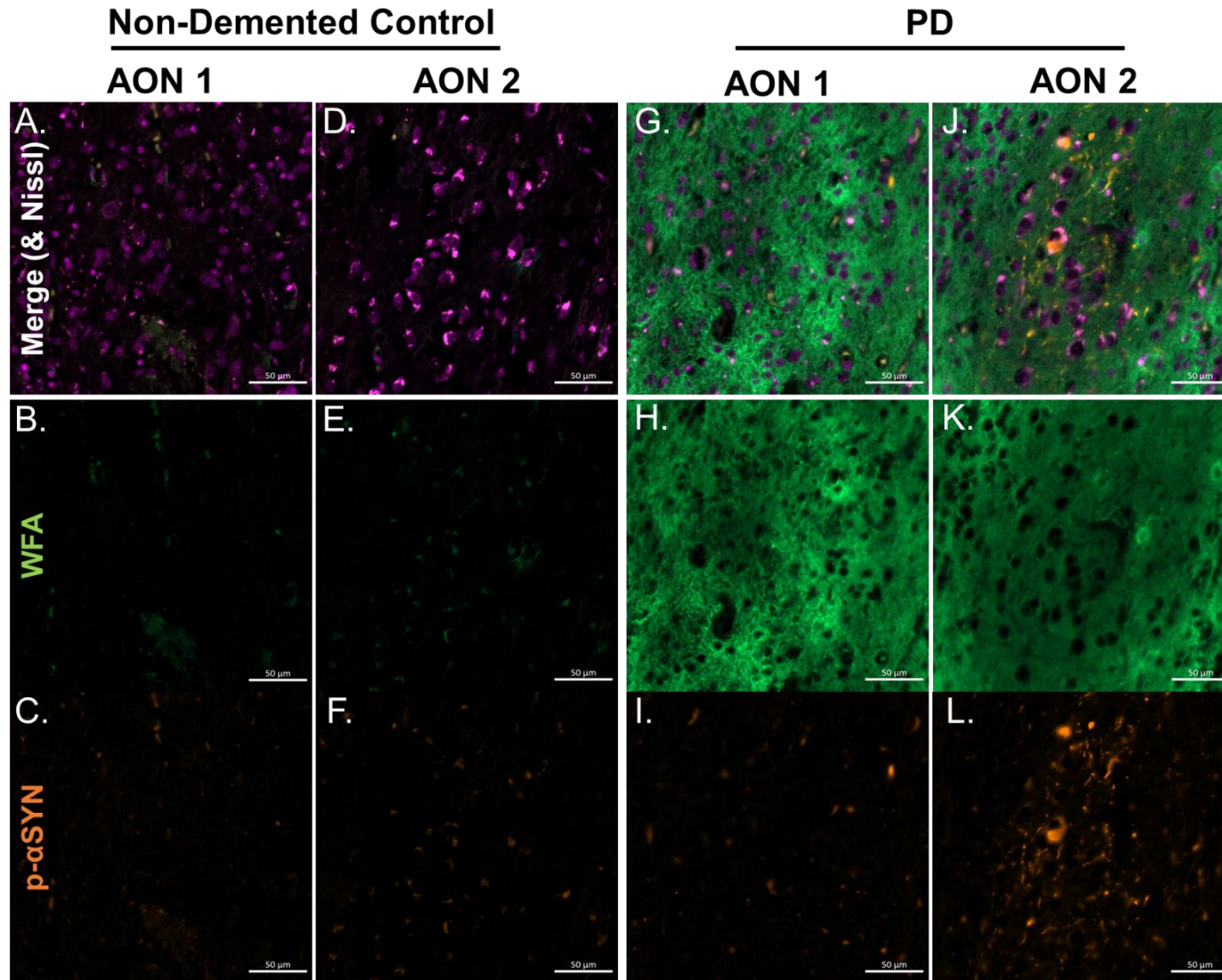


**Figure 27: PNN neurons co-exist with Lewy bearing neurons in the olfactory bulb**

Representative immunofluorescence images of anterior olfactory nuclei (AON) in the human olfactory bulb. Images are shown from non-demented control and Parkinson's disease (PD) patients (7  $\mu$ m sections). PNNs were labelled by WFA (green) and coalesced around a proportion of Nissl-stained neurons (purple). Lewy pathology was detected by p-129  $\alpha$ SYN staining (orange). Lewy pathology was found in AON 1 and AON 2 but was higher in AON 2. PNN neurons appeared unaffected by nearby Lewy pathology and did not present with LBs.

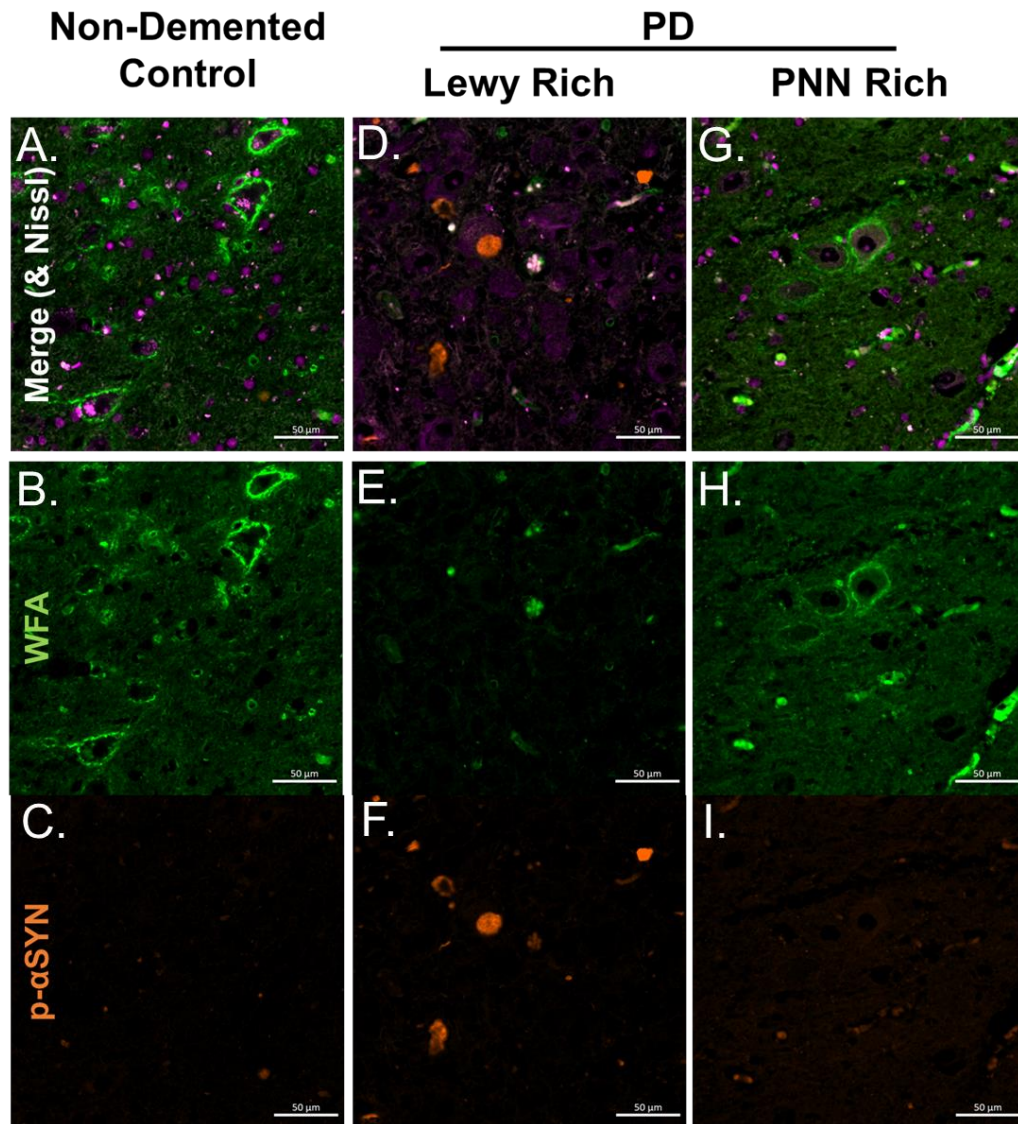


**Figure 28: PNN rich areas segregate from Lewy rich areas in the substantia nigra**

Representative immunofluorescence images of human substantia nigra from non-demented control and Parkinson's disease (PD) patients (7  $\mu$ m sections). PNNs were labelled by WFA (green) and coalesced around a proportion of Nissl-stained neurons (purple). LP was detected by staining for p-129  $\alpha$ SYN (orange). Perinuclear LB aggregates were found in a proportion of neurons. PNN neuronal density was unaffected in PD and no PNN neurons presented with p- $\alpha$ SYN pathology.

### 5.3.3 Segregation between ECM rich and LB rich areas

Regional colocalisation was seen in the AON and some regions of the Tc. However, an inverse relationship was observed elsewhere. Segregation of PNN rich and Lewy rich areas was observed within the SN, Am and some cortical areas and outside of AON, meaning LP and PNNs did not share the same areas (Fig. 26, 27, 28 and 29). In the SN this corresponded to the Lewy rich pars compacta (SNc) and the PNN rich pars reticulata (SNr). In the TC PNNs

were highest in layers III and IV, in agreement with the literature. Cortical LP was highest in deeper cortical layers. This inverse relationship between LP and ECM is reminiscent of that observed in Alzheimer's (Brückner, *et al.*, 1999; Morawski, *et al.*, 2012a).

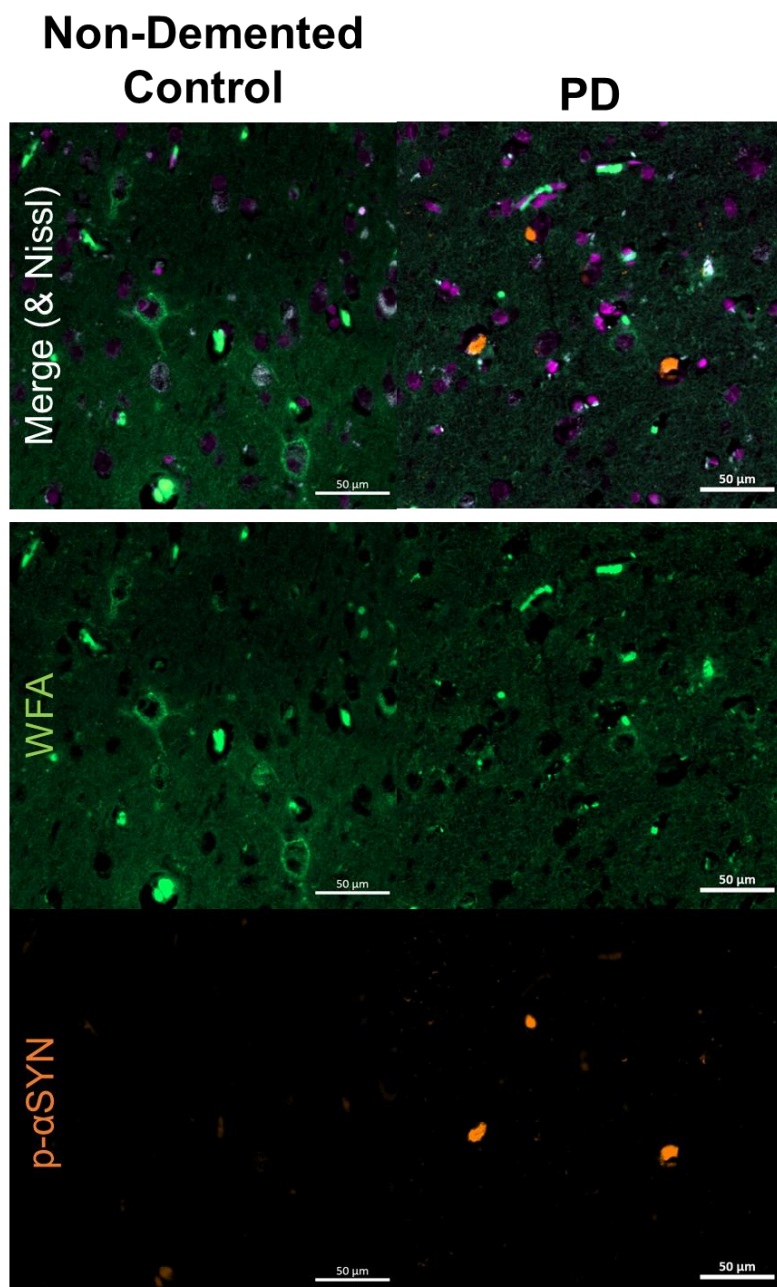


**Figure 29: PNN neurons in the temporal cortex co-exist near to LB-bearing neurons**

Representative immunofluorescence images of human temporal cortex from non-demented control and Parkinson's disease (PD) patients. PNNs were labelled by WFA (green) and coalesced around a proportion of Nissl-stained neurons (purple). LP was detected by staining for p-129 αSYN (orange). Perinuclear LB aggregates were found in a proportion of neurons. While PNN neurons were found in close proximity to affected neurons, no PNN neurons displayed LP.

## 5.4 Discussion

### 5.4.1 Summary

In this chapter, we have demonstrated that PNN enwrapped neurons are spared in PD. We have shown PNN densities are unchanged in PD compared to NDC in multiple brain regions (Am, AON, Tc and SN). The regions chosen all develop LP in PD and contain PNNs; thus were the best choice to test whether PNN neurons were affected in PD. No LB containing PNN neurons were observed in any region. In some brain areas (Am, Tc and SN), segregation was observed between areas of LP and PNN regions. This pilot study provides the first evidence to support the PNN being a factor underlying neuronal resistance in PD.

### 5.4.2 WFA reactivity not affected by short PMD

WFA reactivity has been shown to be negatively affected by extended PMD (>24hours) (Morawski, *et al.*, 2012a). It was shown WFA reactivity in rodent was lost over time, with near complete loss by 24hours and high temperature (37°C) accelerating the decay. Lectin sensitivity has been observed by other groups who, using WFA and VVA, report a loss of PNNs in AD (Kobayashi, *et al.*, 1989; Baig, *et al.*, 2005). In both cases the average PMD exceeded 12 hours, with the mean PMD ranging between 22-39 hours. Similarly in Rogers *et al.* (2018) the mean PMD exceeded 12 hours (17.5 hours). This indicates that a PMD of 12 hours is sufficient to disrupt lectin reactivity. PMD was controlled for in this study and was shown not to negatively affect PNN below 12 hours, in accord with the literature (Morawski, *et al.*, 2012a).

### 5.4.3 PNN populations in the human brain

Populations of PNN neurons are observed throughout the CNS. Their density varies between regions with the cortex showing the highest density of WFA-reactive PNNs (Ueno, *et al.*, 2017a). This was mirrored in our results where the highest density was in the Tc. PNN density shows a laminar distribution with the highest density in layers III and IV (Brückner, *et al.*, 1999; Morawski, *et al.*, 2012a; Mauney, *et al.*, 2013). PNN density varies between cortical regions: density in the occipital cortex was  $65 \pm 3$  cells/mm<sup>2</sup> while in the prefrontal cortex density was much lower,  $1.02 \pm 0.97$  cells/mm<sup>2</sup> (Morawski, *et al.*, 2012a; Mauney, *et al.*, 2013). In this study, PNN density in the Tc was  $35 \pm 8.7$  cells/mm<sup>2</sup>. This is higher than previously published ( $17 \pm 7$  cells/mm<sup>2</sup>).

PNN enwrap PV interneurons in amygdala. There is slight variation between Am nuclei with the lateral nucleus showing the highest density (Pantazopoulos, *et al.*, 2008a). PNN density was not broken down by nuclei in this study due to the anatomical variance within this cohort. In other studies, the whole amygdala is used and the caudorostral location can be controlled. In this study there was significant variation in the caudorostral location of the samples used. This is because the samples were taken and embedded by a variety of neuropathologists and submitted to a brain bank. Both Am nuclei size and PNN density vary greatly depending on the caudorostral location (Harding, *et al.*, 2002; Pantazopoulos, *et al.*, 2008b). This variation prevented subdivision by neuroanatomical nuclei. PNN density in the amygdala is low ( $<10$ ) (Pantazopoulos, *et al.*, 2008a; Pantazopoulos, *et al.*, 2008b). This contrasts with our observations ( $30.1 \pm 4.3$ ). In the human Am a proportion of glia are WFA positive, a proportion that is enriched in schizophrenia (Pantazopoulos, *et al.*, 2008a). The higher density observed in our cohort could be due to contaminating WFA positive glia. As discussed, the neuronal stain used in this study was non-specific. The criteria for PNN identification was for a pericellular, WFA positive ring surrounding the nuclear stain. This does not rule out potential inclusion of WFA positive glia in the PNN density count. It may also explain the higher PNN density in the Tc. The PNN morphology observed in the Am lacked the dendritic stain seen previously (Pantazopoulos, *et al.*, 2008a). This may be due to differences in immunohistochemistry techniques employed. Chromogenic detection methods are more sensitive in detecting low-abundance epitopes and would thus reveal the dendritic PNN. In accordance with this, our study we only detected dendritic PNN staining in one brain region, the cortex. In future, a specific neuronal stain should be included to prevent inclusion of confounding WFA positive glia.

The lowest PNN density was observed in the OB with PNNs observed in AON 1 and 2. In both the rat and human the OB is a site of high ECM staining. In the bulb, PNN staining is rare while the loose ECM shows organised staining. WFA reactivity is highest in glomeruli and external plexiform layer (Hunyadi, *et al.*, 2020). PNN staining was only detected in the mitral cell layer and their scarcity may explain the persistent plasticity seen within the olfactory system (Imai, 2014). Within the rat AON, PNNs have been observed around 20% of small and medium sized neurons. This PNN area is separated from the pial surface by the WFA positive external plexiform layer (Bertolotto, *et al.*, 1996). We observed a similar staining pattern in human although we were not able to determine the PNN population as a proportion of the total neuronal population.

PNN location in the SN is localised to the SNr (Yasuhara, *et al.*, 1994; Bertolotto, *et al.*, 1996; Brückner, *et al.*, 2008). They surround non-pigmented neurons which are most likely PV interneurons (Hardman, *et al.*, 1996; Brückner, *et al.*, 2008). It is likely that the PNN ensheathed neurons we observed in the SN are PV interneurons though this has yet to be confirmed through co-staining. The SNr PV neurons are GABAergic and predominantly project to the motor thalamus. Their activation modulates thalamocortical activation and their hyperactivation could contribute to the motor deficits seen in PD (Hardman, *et al.*, 1996).

We did not detect any PNNs in the human Hc using WFA, in agreement with previous studies (Lendvai, *et al.*, 2013; Rogers, *et al.*, 2018). In the rodent there is a high density of PNNs within the CA2 region. We therefore expected to find a high density of PNNs within the Hc. This was not the case. We failed to detect any PNNs with WFA staining in the human Hc in either NDC or PD samples. This may reflect a species difference between rodent and human or a difference in PNN composition. The PNN is a key structure in plasticity and memory and therefore it would be unusual for PNNs to be absent in the human Hc, a key location in memory formation. More samples, especially the NDC, will provide more information.

Chapter 3 and the literature have established PNN heterogeneity, specifically the existence of WFA negative PNNs (Ueno, *et al.*, 2018b; Miyata, *et al.*, 2018). Therefore, it is likely the failure to detect WFA positive PNNs in the Hc is due to PNN heterogeneity. Acan has been identified as a key component of hippocampal PNNs and been used to identify PNNs in the human Hc previously (Lendvai, *et al.*, 2013; Rogers, *et al.*, 2018). An acan antibody was used as WFA failed to detect hippocampal PNNs; this could be because of the extended PMD of their samples (>12hours) (Rogers, *et al.*, 2018). PMD was controlled for in this study and shown not to correlate with PNN density. We cannot exclude that WFA-reactivity in the Hc is exceptionally sensitive and degraded after a 3 hour PMD. However, we and others have identified a significant proportion of PNNs lack WFA (chapter 3, (Irvine and Kwok, 2018; Ueno, *et al.*, 2018b). Unpublished results from our lab have shown acan detects more PNNs in the rodent Hc than WFA. Therefore, based on our data and the literature, we posit that the discrepancy between acan and WFA PNN staining in the Hc reflects heterogeneity in glycosylation rather than PMD-induced WFA loss.

The aim of this chapter was to demonstrate whether PNN neurons were spared in PD, as such a small pilot study was planned to test this hypothesis. WFA was chosen as WFA reactive PNNs had previously been shown in the regions of

interest while other PNN antibodies had not been extensively tested in human. This study has provided the initial evidence showing that PNN neurons are spared in PD. This encouraging initial result should now be built upon and confirmed using different PNN markers and neuronal stains.

#### **5.4.4 PNN populations spared**

The spread of LP through the CNS is a conserved process and occurs in an ascending manner. The mechanisms underlying this conservation have not been fully elucidated. The spread can in part be understood in terms of neural connections between brain regions. However the connectome is not sufficient to explain the spread of LP (Oliveira, *et al.*, 2019; Henrich, *et al.*, 2020). The strength of neuronal connections does not predict pathology development in the PFF transmission model (Henrich, *et al.*, 2020). PD has been defined as a prion disorder as aggregated  $\alpha$ SYN can propagate itself by recruiting native  $\alpha$ SYN to misfold (Brundin and Melki, 2017). This hypothesis has explanatory power as  $\alpha$ SYN expression level correlates with the vulnerability of brain regions to LP (Erskine, *et al.*, 2018; Henderson, *et al.*, 2019; Courte, *et al.*, 2020). However, vulnerability is modulated by other factors such as cell type, gene expression (e.g. LRRK2, calcium binding proteins), cellular stress and axonal arborisation. The perineuronal net could be another such factor governing neuronal vulnerability, increasing neuronal resistance.

##### **5.4.4.1 Correlating PNN populations and neuronal loss**

Neuronal death is a selective process in PD and is correlated with symptom severity. Cell loss is selective but occurs throughout Lewy affected regions (Hirsch, 1992; Giguère, *et al.*, 2018). Why neuronal loss is selective is due to the differing susceptibility of different neuronal populations. It has not been investigated whether PNN neurons are lost in PD. If PNN neurons were lost in PD then we would expect to see a reduced density. We investigated PNN populations in brain regions affected by LP. In all brain regions PNN density remained unchanged and no PNN neurons contained LBs. This would indicate that the PNN is a factor governing neuronal susceptibility by conferring resistance.

Neuronal loss has been most intensively investigated in the SN (Giguère, *et al.*, 2018). Pigmented, dopaminergic neurons are the most affected, showing a 46% decline in cell density in the SN between Braak stages III-IV (Hirsch, 1992; Dijkstra, *et al.*, 2014). There are conflicting reports about the process of neuronal loss as SN neuronal loss in PD has been shown to occur in both a stage-dependent and a progressive manner, where disease duration correlated

with neuronal loss (Pearce, *et al.*, 1995; Dijkstra, *et al.*, 2014; Giguère, *et al.*, 2018). This conflict may arise from the differing methodological approaches taken by different groups (Giguère, *et al.*, 2018).

Cholinergic neurons are also lost in PD, showing a 50% reduction in the PPN with sparing of neighbouring GABAergic and glutamatergic neurons (Hirsch, *et al.*, 1987). In the PPN, both cholinergic and glutamatergic neurons are devoid of PNNs while neighbouring neurons are clad in PNNs (Bertolotto, *et al.*, 1996; Brückner, *et al.*, 2008). The PPN was not investigated in this study but it is likely PNN populations are also spared there.

Interestingly in PD, a 100% increase in dopaminergic neurons has been observed in the OB. Dopaminergic cells have an inhibitory effect in the OB and may underlie hyposmia in PD (Huisman, *et al.*, 2004; Huisman, *et al.*, 2008; Mundiñano, *et al.*, 2011). However, the bulb is a PNN poor area as shown by the literature and so was not investigated in this study (Bertolotto, *et al.*, 1996). One study has investigated neuronal loss in the AON and reported neuronal loss that correlated with disease duration (Pearce, *et al.*, 1995). However, the subtypes of neurons lost or preserved were not investigated. We have shown PNN neurons are spared in PD and density is unchanged in AON indicating they are spared from the neuronal loss. To build upon this study, the fate of neuronal subtypes in the PD AON should be investigated.

In the Am a 30% reduction in volume was reported. This arose from neuronal loss in the corticomедial nucleus with other nuclei volumes remaining unaffected (Harding, *et al.*, 2002). The corticomедial nucleus is worst affected by LP but has not yet been investigated for PNNs (Braak, *et al.*, 1994; Pantazopoulos, *et al.*, 2008a). Neuronal loss has not yet been shown in the cortex or Hc (Pedersen, *et al.*, 2005; Joelsing, *et al.*, 2006). The lack of neuronal loss could be due to the late development of pathology in these areas compared to lower brain regions. The literature investigating neuronal loss in other brain regions is meagre when compared to the SN, and there is variety in the methods used to identify neurons and quantify loss. A systematic study should be performed so neuronal susceptibility in PD can be compared across brain regions. The neuronal stain used in our study was not specific so neuronal loss could not be estimated. In the next study this should be performed as then the proportion of PNNs can be estimated for each region. If PNN proportions increase in PD then this would confirm that PNN neurons are preserved in regions experiencing neuronal loss.

We have shown that PNN populations are unaltered in PD, even within regions showing severe neuronal loss. This is reminiscent of the protection seen in

Alzheimer's disease. In AD brains, PNN neurons did not internalise misfolded tau or develop neurofibrillary tangles (Brückner, *et al.*, 1999; Morawski, *et al.*, 2012b; Suttkus, *et al.*, 2016b). PNN neurons resisted  $\beta$ -amyloid toxicity *in vitro* and co-existed alongside toxic amyloid plaques (Yasuhara, *et al.*, 1994; Brückner, *et al.*, 1999; Miyata, *et al.*, 2007). Together this suggests that the PNN is neuroprotective in prion-like diseases. However, the neuronal stain used in this study was found to be non-specific. WFA positive glia have been observed in the human amygdala (Pantazopoulos, *et al.*, 2008a). In PD, astrocyte proliferation is absent (Halliday and Stevens, 2011). Therefore, it is unlikely but cannot be discounted that the results observed in this study are due to a rise in confounding glia, masking PNN neuronal loss. To remedy this, a larger study should be performed with a specific neuronal stain. This would serve three purposes: increase the n-number of this pilot study, confirm PNN populations are unchanged and allow neuronal loss to be quantified in each brain region.

#### **5.4.4.2 Other factors are not sufficient to explain PNN population sparing**

Since cell death in PD is selective it raises the question whether the sparing of PNN populations is incidental, arising from other underlying factors such as neuronal subtype. The presence of calcium favours  $\alpha$ SYN aggregation (Lautenschläger, *et al.*, 2018). The high expression of calcium binding proteins, i.e. PV, can thus protect neurons from  $\alpha$ SYN aggregation. Calbindin expressing DA neurons in SN are relatively spared compared to their non-CaBP expressing counterparts (Yamada, *et al.*, 1990). The majority of PNN neurons are PV neurons. In our *in vitro* model in chapter 4 the majority of our PNN neurons were PV positive. We then showed that PNN removal is sufficient to ablate the resistance to oligomer uptake and aggregate development, demonstrating that PV expression was not protective. Furthermore, investigation of PV-mediated resistance *in vivo* and post-mortem tissues has shown PV neurons develop LBs. This was observed in the AON, Hc and Am (Flores-Cuadrado, *et al.*, 2016; Flores-Cuadrado, *et al.*, 2017; Ubeda-Bañon, *et al.*, 2017). The interaction of the PNN and PV has not been investigated in post-mortem tissue. However, our *in vitro* results highlight that the PNN can protect PV neurons. To follow-up this study, PV density should be analysed alongside the PNN population.

#### **5.4.4.3 No Lewy Pathology in PNN neurons**

We have observed that PNN densities are unchanged in PD, even within regions that experience neuronal loss. During this study we did not observe any PNN neurons containing LBs. LB development is a precursor to neuronal death

as the proportion of LB-bearing neurons remains consistent throughout the disease course (Greffard, *et al.*, 2010; Parkkinen, *et al.*, 2011; Osterberg, *et al.*, 2015). Therefore, the lack of LB bearing PNN neurons correlates with the sparing of PNN populations. Furthermore, it correlates with our findings from chapter 4, where PNN positive neurons show lower uptake of  $\alpha$ SYN oligomers. LP develops and matures over time. It starts in the neurites, coalescing in the soma as a pale body before condensing into a mature LB (Kuusisto, *et al.*, 2003; Mahul-Mellier, *et al.*, 2020). It is possible that the PNN does not prevent pathology development in the enwrapped neurons but merely slow it. If this was the case, then PNN neurons may present with Lewy neurites. This was not examined in our study due to the lack of dendritic staining. However, if the PNN only slowed LP development then it would be expected that LBs be found in PNN neurons in regions affected early in PD pathophysiology and PNN loss may be seen, i.e. AON. We have shown PNN populations are spared and did not present with LBs in the AON. This makes the slowing hypothesis less likely.

#### **5.4.5 Segregation of ECM and Lewy pathology**

As mentioned, LP develops along a conserved route. The connectome and  $\alpha$ SYN expression are two major factors that govern the spread but are not the only factors (Surmeier, *et al.*, 2017a). We have shown that PNN populations are spared in PD, indicating they are a factor determining neuronal vulnerability. Mapping of pathology spread from a PFF injection into the PPN revealed differences in vulnerability (Henrich, *et al.*, 2020). The superior colliculus and the substantia nigra reticulata both have similar strength connections to the PPN but showed differences in pathology severity. The superior colliculus showed severe p- $\alpha$ SYN staining while the SNr showed sparse staining, demonstrating the connectome alone is insufficient to explain LP spread (Henrich, *et al.*, 2020). The SNr contains PNNs while the superior colliculus does not (Bertolotto, *et al.*, 1996). This indicates that the PNN could be a factor governing LP spread. In agreement with this, we have shown that there is segregation between PNN rich areas and Lewy rich areas, most notably in the SN and Am, but we observed limited segregation between PNNs and LP containing neurons in the Tc indicating other factors are involved in LP spread. In agreement with the literature, LP was found in deeper layers and PNNs in superficial layers (Braak, *et al.*, 2003). The central Am nucleus is severely affected in PD while the PNN rich, lateral nuclei remains unaffected. The basolateral nucleus, which has a lower PNN density, is mildly affected in PD (Braak, *et al.*, 1994; Harding, *et al.*, 2002; Pantazopoulos, *et al.*, 2008a). The SNr, despite its close proximity to the severely affected SNc and connections to

the PPN, remains sparsely affected by LP (Hardman, *et al.*, 1996; Henrich, *et al.*, 2020). Other PNN rich regions, e.g. the red nucleus, cerebellum and parts of the basal ganglia, are also spared in PD (Carulli, *et al.*, 2006; Brückner, *et al.*, 2008; Rácz, *et al.*, 2016; Braak, *et al.*, 2003; Erskine, *et al.*, 2018). This segregation could arise due to PNN presence, the connectome or from differing  $\alpha$ SYN expression. The strength of the contribution of these factors must be compared. A PFF injection model would be best suited as ECM digestion by ChABC, connectome mapping and  $\alpha$ SYN expression could be performed and measured simultaneously. In AD, another prion-like disease, segregation of PNN rich and pathology rich areas is seen in the neocortex (Brückner, *et al.*, 1999; Morawski, *et al.*, 2010b; Morawski, *et al.*, 2012b). This indicates a proof of principle in prion-like neurodegenerative diseases.

The PNN and ECM could modulate  $\alpha$ SYN spread through several mechanisms. As discussed, the PNN could provide a barrier against  $\alpha$ SYN uptake, as shown in chapter 4. The ECM act as a barrier, limiting extracellular  $\alpha$ SYN aggregates diffusion. However in the latter case it has been shown that extracellular  $\alpha$ SYN aggregates can catalyze destruction of ECM-HA via microglia (Soria, *et al.*, 2020). Despite this, no disruption of PNNs was observed (Soria, *et al.*, 2020). This may be due to the different structure of the PNN compared to the loose ECM. The PNN is a cross-linked structure which may prevent microglia-mediated degradation. However, microglia have been found to degrade and remodel the PNN (Stamenkovic, *et al.*, 2017; Crapser, *et al.*, 2020). The results from this study provide preliminary evidence that the PNN could modulate Lewy spread but the hypothesis must be directly tested if the PNN is to be firmly established as a factor LP development.

#### **5.4.6 Conclusions and Further directions**

In this pilot study we investigated whether PNN populations were spared in PD. We have shown, in multiple brain areas, that despite neighbouring LP, PNN populations are unaffected in PD and PNN neurons do not present with LBs. This demonstrates the PNN could be a factor underlying neuronal resistance in PD. In some brain regions we also observed segregation of PNN rich and Lewy rich areas indicating the PNN could be a modulating factor in LP spread. The aim of this chapter was to investigate whether the PNN is a neuroprotective structure in PD; this study establishes the proof of principle by showing that PNN populations are unaltered in Lewy affected regions. This study should be followed up to determine the contribution of the PNN compared to other factors governing neuronal resistance and Lewy spread.

## Chapter 6 General discussion and future perspectives

### 6.1 Introduction

This thesis investigated the hypothesis: does the PNN protect neurons from  $\alpha$ SYN internalisation and pathology development in PD? Investigating this would establish whether the PNN was neuroprotective in PD. In pursuit of this, an *in vitro* neuronal culture model was established which accurately replicated PNNs as seen in the adult CNS. This model reproduced mature PNNs in both their morphology and heterogeneity. Using this model, we discovered that the PNN protects neurons from pathogenic  $\alpha$ SYN by reducing internalisation and phosphorylated aggregate development. Degradation of the PNN ablated the effect demonstrating it was PNN-dependent. PNN GAGs, CS-E and HS, were found to interact with monomeric and oligomeric  $\alpha$ SYN, revealing a putative mechanism for the neuroprotective phenomenon. To demonstrate the disease relevance of this neuroprotective mechanism we investigated PNN populations in PD and NDC brains. PNN densities were spared in all Lewy affected regions and Lewy bearing PNN neurons were not observed indicating PNN populations could be resistant to PD pathophysiology. Together this thesis has provided the first evidence to establish the PNN as a neuroprotective structure for  $\alpha$ SYN pathology in PD.

LP develops in CNS regions in a progressive manner, exhibiting both temporal and spatial conservation. Misfolded  $\alpha$ SYN has been shown to act as a prion-like agent, seeding the spread of the pathology via the connectome. However, not all connected regions or all neurons within an affected region develop LP or die off. This has led to the concept of differential neuronal vulnerability. Neuronal subtypes have different vulnerabilities to LP and  $\alpha$ SYN seeding. This vulnerability arises from the interaction of cell-autonomous and extracellular factors. Mechanistically,  $\alpha$ SYN transmission has been shown to occur both synaptically and through the extracellular space. The local release and diffusion of  $\alpha$ SYN in the extracellular space should show no bias between uptake between neuronal subtypes, unlike synaptic transmission which spreads through the connectome. Despite this, neighbouring neurons often fail to develop LP. For example, the SNc region shows severe LP and neuronal loss but the neighbouring SNr is spared. The reasons for this bias are not yet fully resolved. In AD, another prion-like disease, the PNN has been identified as a barrier to pathogenic tau internalisation. Therefore, the aim of this project was to investigate whether the PNN provides a similar neuroprotective role within PD.

## 6.2 Establishment of a mature PNN *in vitro* culture

In chapter 3 we successfully established an *in vitro* PNN culture that accurately replicated mature PNN morphology and heterogeneity. PNN cultures have been established by 4 other groups but this is the first time PNN heterogeneity *in vitro* has been demonstrated and PNN maturation examined. Of the groups, two use mouse hippocampal neurons and the other two utilise rat cortical neurons (Miyata, *et al.*, 2005; Dityatev, *et al.*, 2007; Giamanco, *et al.*, 2010; Geissler, *et al.*, 2013). The timeline of PNN development differs between the groups and may be explained by species or regional differences. Hippocampal mouse cultures demonstrate reticular PNNs around DIV21 while cortical rat cultures remain punctate, in agreement with our results. It is likely this difference arises from the species difference. Comparison of PNN maturation in the mouse cortex reveals that PNNs are reticular by DIV21, though they do continue to increase in intensity and contiguity (Ueno, *et al.*, 2017b; Sigal, *et al.*, 2019). The extended time frame needed for rat PNN maturation is a drawback of the work, though one advantage is the clear development process, which has yet to be characterised in mouse cultures. While PNNs have been characterised *in vitro* previously this is the first-time quantification of the culture has been performed. This has allowed the extent of heterogeneity to be examined. It also provides a useful baseline in understand how a treatment may affect PNN populations. This culture can be used in tracking PNN development which has great utility for understanding this process and learning how to manipulate it.

Specific roles for PNN components have been identified and discussed in chapter 3. Briefly bcan and ncan may have complimentary roles in synapse stabilisation. However, despite this we failed to observe segregation of PNN components into microdomains but instead saw a near complete colocalisation. This conflict should be investigated by examining the PNN with super-resolution techniques. The diffraction limit is a limiting factor in resolving PNN structure. However, great strides have been made in super-resolution techniques. Expansion microscopy is one such technique that holds great promise and should be employed in resolving PNN organisation and reconciling the lack apparent lack of segregation.

During development we identified a WFA positive/acan negative PNN population, indicating a different CSPG predominated during PNN development. A similar phenomenon was noted for the Cat-315 antibody which identifies the HNK-1 epitope on acan in the mature CNS (Matthews, *et al.*, 2002; Miyata, *et al.*, 2018). However, examination of Cat-315 reactivity in during PNN development *in vivo* and *in vitro* discovered it was instead bore by pcan (Dino,

*et al.*, 2006). It is not known which CSPG bears the WFA-epitope in development but pericellular ncan and pcan expression are high during PNN development *in vitro* (Miyata, *et al.*, 2005; Hayashi, *et al.*, 2005). This question should be resolved in our culture as it would improve our understanding of the PNN development is a necessary step towards identifying how PNN composition affects function.

### **6.3 The PNN reduces pathogenic $\alpha$ SYN internalisation and p- $\alpha$ SYN pathology development**

$\alpha$ SYN seeding has been studied in detail *in vitro* and the results from chapter 4 build on this. Our approach differed from the literature as we did not aim to investigate how  $\alpha$ SYN internalisation occurs but how its entry may be blocked. Examining the neuroprotective role of the PNN in PD builds on an existing body of literature which has demonstrated a neuroprotective role against ROS and in AD. This work sought to establish a link between the two areas by investigating a role for the PNN in neuronal resistance. Identifying neuronal resistance is a novel approach in PD, preventing direct comparison with the literature. Chapter 4 demonstrated the PNN reduces seeding in HEK cells and reduced oligomer internalisation and p- $\alpha$ SYN pathology development in neurons. However, we did not directly show the PNN acting as a barrier. The PNN has been shown to reduce oligomeric tau internalisation. Though they showed an increase in tau positive PNN neurons after 24hours which may be indicative of a slowing of uptake rather than a block (Suttkus, *et al.*, 2016b). We also observed  $\alpha$ SYN internalisation in PNN neurons at 24hours. Based on the results of chapter 4 alone it cannot be discerned whether the PNN blocked or slowed uptake. Indeed, even the significant increase in the internalisation and p- $\alpha$ SYN pathology after PNN degradation is consistent with either a slowing or a blocking effect. Fortunately, our work in chapter 5 does allow us to discern between them as we failed to detect any LP positive PNN neurons, indicating the PNN blocks  $\alpha$ SYN internalisation rather than slows it. A future experiment utilising live cell imaging and fluorescently labelled  $\alpha$ SYN could prove directly if the PNN acts as barrier.

Suttkus *et al.* (2016b) showed colocalization between the PNN and oligomeric tau after 4 hours of incubation. We did not observe colocalization at 24hours despite showing  $\alpha$ SYN/PNN glycan binding. The 24 hour time frame was chosen because  $\alpha$ SYN species are completely internalised by this point ( Lee *et al.*, 2008). The main aim of this study was to determine whether the PNN prevented oligomeric internalisation and subsequent seeding, not whether the

PNN colocalised with  $\alpha$ SYN. However now this has been established this should be rectified and colocalization should be investigated after a shorter period of incubation.

One unifying factor in protein-mediated  $\alpha$ SYN internalisation is that all identified proteins are glycoproteins bearing HS (Holmes, *et al.*, 2013; Mao, *et al.*, 2016; Ihse, *et al.*, 2017; Hudák, *et al.*, 2019). Based on this it is perhaps not surprising we identified a PNN GAG chelation effect. The interaction between  $\alpha$ SYN species and CS-E has not been previously identified. The presence of other CS subtypes, CS-A and DS, have been shown to affect  $\alpha$ SYN aggregation propensity and seeding capacity but neither directly interacted with  $\alpha$ SYN, as determined by NMR, in agreement with our results (Mehra, *et al.*, 2018). The effects observed in this study are most likely due to a molecular crowding phenomenon (Ray, *et al.*, 2020). As discussed, we cannot rule out a general electrostatic interaction due to the heterogeneity of the GAG source material, but we consider it unlikely as there was no interaction between CS-D and  $\alpha$ SYN species despite having the same charge ratio as CS-E. This argues for a specific interaction between CS-E and  $\alpha$ SYN but it should be confirmed using synthetic disaccharides. This would also have the advantage of revealing the minimum binding unit (Sugiyama, *et al.*, 2008; Djerbal, *et al.*, 2019; Nadanaka, *et al.*, 2020).

Chapter 4 has made the first step in establishing the PNN as a neuroprotective barrier in PD by establishing it as a neuronal resistance factor. However, there are some limitations to the study. A direct resistance phenotype for PNN neurons against p- $\alpha$ SYN could not be established due to the lack of somatic pathology. However, we rectified this by confirming the sparing of PNN populations in PD brains in the subsequent chapter. ChABC treatment also removes the loose ECM as well as the PNN raising the possibility of a role for the loose ECM. Soria *et al.* (2020) showed that the loose ECM is not spared in a model of synucleinopathy due to microglia-mediated degradation, making a loose ECM contribution less likely but as our culture did not contain microglia it cannot be ruled out.

We have demonstrated a neuroprotective role for the PNN against free  $\alpha$ SYN in the extracellular milieu, a key mechanism of spread in PD (Lee, *et al.*, 2014; Jiang, *et al.*, 2017). However, as mentioned in chapters 4 and 5, the connectome and synaptic transmission is another key mechanism of spread. We have not demonstrated whether the PNN protects neurons from synaptic transmission of  $\alpha$ SYN. The PNN is a key part of the tetrapartite synapse and surrounds the synaptic cleft, enhancing synaptic signalling (Dityatev and

Rusakov, 2011). However, while it surrounds the cleft it is usually excluded from it (one exception are the Calyx of Held synapses) and thus would not be able to act as a barrier against  $\alpha$ SYN transmission (Lendvai, *et al.*, 2013; Blosa, *et al.*, 2015). Our study does not address this question, but a future study must. Cell culture in microfluidic chambers allows synaptic  $\alpha$ SYN transmission to be interrogated *in vitro* (Gribaudo, *et al.*, 2019). We suggest this be combined with our neuronal culture to investigate the role of the PNN in synaptic transmission of  $\alpha$ SYN.

#### **6.4 PNN populations are unaffected in PD**

This study was designed as a proof of principle experiment to establish the relevance of the PNN-mediated neuroprotective phenomenon demonstrated in the previous chapter. We have shown that PNN populations are spared in multiple LP affected areas. The regions investigated develop LP at different time points during PD and thus allowed us to investigate whether the PNN was neuroprotective for a limited time i.e., before extensive cell death and microgliosis. As PNN populations were unaffected in AON and SN we concluded the PNN is protective throughout the PD time course. The aim of this chapter was to establish the PNN as a neuroprotective factor underlying neuronal resistance to LP. This had not been investigated before. Also, data of PNN populations in the human brain is sparse so our results help to fill this gap. However, this current study is underpowered due to the small cohort. While this is sufficient to establish a proof of principle to warrant further research it should be kept in mind when drawing conclusions. A follow-up study should be performed to increase the cohort number and rectify the non-specific neuronal stain used.

Many factors govern neuronal vulnerability in PD and we have established the PNN as one of them. However, it is possible that the presence of a PNN is incidental to determining neuronal susceptibility and not casual. In this case, the PNN would be segregating with other vulnerability/resistance factors not investigated by this study, e.g., arborisation degree,  $\alpha$ SYN or CaBP expression. We showed in chapter 4 that PNN degradation was sufficient to remove the neuroprotective phenotype but other factors could still be at work. CaBPs are expressed by interneurons and can be used to broadly classify interneuron subtypes (Mayer, *et al.*, 2018). PV interneurons are the predominant subtype of PNN neurons in the CNS and thus PV expression could be a confounding factor. PV expression in PD has been investigated and presents a complex picture. In the AON, an PV positive cell density increased 3-fold while a decrease was seen in the amygdala (50%) and SNr (10%) (Hardman, *et al.*,

1996; Flores-Cuadrado, *et al.*, 2017; Ubeda-Bañon, *et al.*, 2017). In the SNr, no cell loss was seen indicating it was the PV immunoreactivity that was lost. PV expression is dynamic and changes with the network state (Donato, *et al.*, 2013). It is likely the conflicting expression changes between regions reflects an alteration in the neuronal networks as they compensate for dysfunction and cell loss. In the Hc PV expression negatively correlated with  $\alpha$ SYN pathology, but a high proportion of PV cells colocalised with  $\alpha$ SYN pathology (Flores-Cuadrado, *et al.*, 2016). Compared to other CaBP interneurons, PV positive interneurons showed the highest proportion of  $\alpha$ SYN pathology demonstrating they are not protected from LP. PV neurons themselves are not a homogenous population but differ in neuropeptide expression and arborisation (Markram, *et al.*, 2004). PNN neurons are only a subset of PV interneurons and could account for LP resistant PV population. This should be examined through co-staining of post-mortem tissue. Neuronal susceptibility is the product of multiple cellular factors and no single factor is sufficient to cause LP. We have revealed that the PNN is a factor underlying neuronal resistance. Indeed, we have demonstrated the introduction of a PNN in a HEK cell line reduces  $\alpha$ SYN seeding. This, and other results in chapter 4, give a strong indication the PNN is not an incidental factor but this cannot be ruled out conclusively. Future studies should investigate this interplay to give insight into the strength of contribution of a PNN and solidify its role as a factor of neuronal resistance in PD.

## 6.5 Mechanism for PNN neuroprotection in PD

During this project, we have shown the PNN reduces pathogenic  $\alpha$ SYN internalisation and p- $\alpha$ SYN pathology development. Removal of the PNN destroys neuronal resistance, increasing internalisation and pathology development. PNN populations are unaffected in PD, by either LP or neuronal loss, demonstrating that the neuroprotection phenomenon observed *in vitro* is conserved in the human disease. Furthermore, we have highlighted that PNN GAGs can bind to monomeric and oligomeric  $\alpha$ SYN, hinting at a possible chelation mechanism underlying PNN neuroprotection. In this section, we will bring these results together to postulate a mechanism for PNN neuroprotection in PD and how the PNN fits into wider PD pathophysiology.

Pathogenic  $\alpha$ SYN is released into the extracellular space upon neuronal death or as part of compensation mechanism by neurons to decrease cellular  $\alpha$ SYN load (Lee, *et al.*, 2005; Danzer, *et al.*, 2012; Jiang, *et al.*, 2017). Once in the extracellular space it is either taken up by neighbouring cells or is degraded by extracellular proteases. In PD, only neurons go on to develop LP while glia degrade the pathogenic  $\alpha$ SYN. Several neuronal internalisation mechanisms

have been identified for  $\alpha$ SYN species (discussed in greater detail in chapter 1 and 4) but all require access to the membrane. Once internalised a proportion of the  $\alpha$ SYN escapes from the endo-lysosomal system, gaining access to the cytoplasm where it then recruits naive  $\alpha$ SYN. The PNN is a dense pericellular barrier that can prevent membrane access. We propose the PNN protects neurons by denying  $\alpha$ SYN access to the cell membrane, thereby blocking internalisation. We have shown that oligomeric  $\alpha$ SYN internalisation is greatly reduced in PNN neurons and p- $\alpha$ SYN pathology induction by PFF is also reduced. This demonstrates that the PNN plays a neuroprotective role against oligomer and fibrillar  $\alpha$ SYN.

The PNN can block  $\alpha$ SYN internalisation by two mechanisms. Firstly, we propose that the interposition of the dense, polyanionic barrier denies  $\alpha$ SYN access by preventing diffusion. Although the pore size of the PNN has not been directly investigated it can be extrapolated from the literature. Diffuse pericellular nets show a molecular sieving effect, halting 40 nm particles from reaching the cell surface (Chang, *et al.*, 2016; Scrimgeour, *et al.*, 2017). The PNN is thinner than the pericellular nets but is a denser, highly aggregated structure. The PNN-HEK cell coat can only be removed by washing with high concentrations of detergent while the diffuse pericellular net can be removed by washing with high salt (Kwok, *et al.*, 2010). The PNN is expected to be denser than the PNN-HEK counterpart as it contains crosslinkers such as TnR and Sema3a (Morawski, *et al.*, 2014; Dick, *et al.*, 2013). The presence of these crosslinkers is further expected to reduce pore size and diffusion through the PNN. Pathogenic  $\alpha$ SYN species used in this study are larger than 40 nm and therefore should be excluded. PFFs are elongated structures with a narrow diameter but their rigid nature most likely prevents their diffusion through the PNN (Fig. 30). Monomeric  $\alpha$ SYN is smaller than oligomeric species and highly flexible, so it is unlikely diffusion of monomeric  $\alpha$ SYN is hindered.

Secondly, we have highlighted that PNN GAGs, HS and CS-E can bind to oligomeric and monomeric  $\alpha$ SYN species. We suggest that PNN GAGs can chelate  $\alpha$ SYN, trapping it on the PNN surface. However, this raises the question: how long is  $\alpha$ SYN trapped? The  $K_D$  for the interactions is in the micromolar range, a similar range to other GAG interactions. This binding is relatively weak when compared to other PNN binding molecules, e.g. Sema3a and Otx2, signifying the interaction is not especially long-lived. However, the high GAG density within the PNN and the multiple binding sites per chain mean the  $\alpha$ SYN/GAG interaction must be considered in terms of avidity: while any single interaction is short lived, the sum of all interactions could lead to  $\alpha$ SYN persisting on the PNN. Experimentally we did not observe  $\alpha$ SYN binding to the

PNN though this is likely due to late time frame used (24 hours), indicating that PNN-mediated chelation of  $\alpha$ SYN is shorter than 24 hours. Both mechanisms work synergistically to reduce  $\alpha$ SYN membrane access. Furthermore, it will prolong the time  $\alpha$ SYN spends in the ECS, increasing the chance of degradation (Fig. 30). Chelation of  $\alpha$ SYN in the ECS has already been shown to reduce pathology development and improve behavioural outcomes in an animal model (Tran, *et al.*, 2014) However, this neuroprotective mechanism has several implications that will be addressed in the next section.

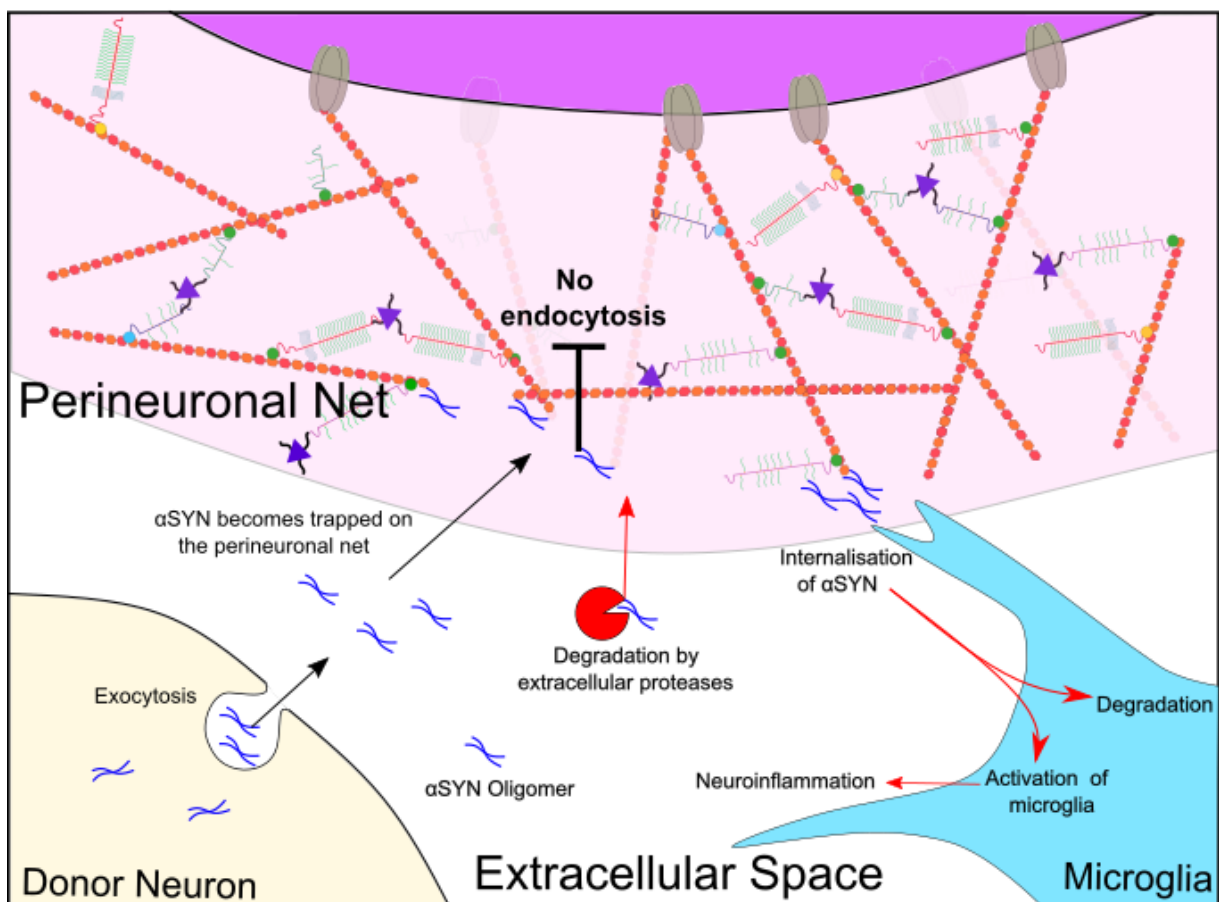


**Figure 30: Proposed mechanism of PNN in PD pathophysiology**

Pathogenic  $\alpha$ SYN is released into the extracellular space where it is then taken up by neighbouring neurons, seeding further pathology. Neurons with a PNN are protected as  $\alpha$ SYN cannot diffuse through the PNN. This prolongs the time  $\alpha$ SYN spends in the extracellular space, increasing the likelihood of degradation by microglia and extracellular proteases.

## 6.6 Implications and future directions

We have posited a mechanism to explain the PNN resistance phenomenon in PD. The creation of any theory raises further questions which must be answered to determine if the hypothesis is true.

In the last section, we briefly touched on how long  $\alpha$ SYN stays on the PNN but a further question that must be asked is what is the fate of PNN-bound  $\alpha$ SYN? There are several possible fates. First, it most likely diffuses away due to the weak binding. A second fate could be further aggregation. The binding of  $\alpha$ SYN to anionic vesicles potentiates their aggregation by increasing the nucleation rate by three orders of magnitude. It does this by raising the local concentration of the  $\alpha$ SYN through chelation and by perhaps favouring nucleation-prone conformations (Galvagnion, *et al.*, 2015). The PNN could operate in the same manner.  $\alpha$ SYN/GAG  $K_D$  is 10fold weaker than published  $\alpha$ SYN/lipid  $K_D$ . However, for this effect to occur, there must be a sufficient concentration of free  $\alpha$ SYN in the ECS. To our knowledge, the extracellular concentration of CNS  $\alpha$ SYN in PD or in physiological conditions has not been measured. This should be addressed to resolve whether the PNN could act as a pro-aggregation surface. A third fate for PNN bound  $\alpha$ SYN is degradation. Degradation can occur via several routes: extracellular proteases, microglia, or astrocytes (Fig. 30). Internalisation by glia is a double-edged sword as it leads to  $\alpha$ SYN degradation but also gliosis (Fellner, *et al.*, 2013; Rannikko, *et al.*, 2015; Kim, *et al.*, 2013; Kim, *et al.*, 2016; Zhang, *et al.*, 2005). However, potentiating  $\alpha$ SYN degradation by microglia via antibody administration has shown benefit, reducing pathology development and improving behavioural outcomes (Tran, *et al.*, 2014).

Internalisation of  $\alpha$ SYN by glia, especially microglia can cause neuroinflammation, contributing to neuronal dysfunction and disease progression (Zhang, *et al.*, 2005; Booth, *et al.*, 2017). By chelating  $\alpha$ SYN on its surface the PNN could potentiate gliosis by acting as an antigen presenting surface, a similar principle has been shown for astrocytes (Rostami, *et al.*, 2020). Microglial activation in PD is complex and dynamic. Microglial activation is a broad term and can pivot the microglia towards a harmful or neuroprotective state. This complexity arises from the diverse ligand milieu microglia are exposed to during PD progression, the composition of which will change during the disease time course. This is seen in the variation of inflammation state between brain regions (López González, *et al.*, 2016). During PD progression there are multiple sources of microglial activation,  $\alpha$ SYN, neuronal death, reactive astrocytes, cytokines etc, which occur at different time points in PD progression (Dijkstra, *et al.*, 2014). This discussion will focus on the direct effects of microglial activation by  $\alpha$ SYN as this pertains to the PNN.

Internalisation of  $\alpha$ SYN by microglia can occur via binding to CD36, TL4 or TL2 (Lee, *et al.*, 2008b; Kim, *et al.*, 2013; Fellner, *et al.*, 2013; Rannikko, *et al.*, 2015; Kim, *et al.*, 2016). This leads to their polarisation to an inflammatory

phenotype and ROS production, resulting in neuronal toxicity (Zhang, *et al.*, 2005; Kim, *et al.*, 2013; Hoffmann, *et al.*, 2016; Kim, *et al.*, 2016). However, a neuroprotective role has also been identified (Choi, *et al.*, 2020). Incorporating microglia into the PNN neuroprotection mechanism (Fig. 30) raises two implications that must be addressed: (1) are the PNN neurons spared from microglial-mediated toxicity and (2) does the PNN exacerbate microgliosis and neuronal dysfunction in the local area.

There are conflicting reports regarding the interaction between PNNs and microglia. Physiologically, microglia have been shown to remodel the PNN during learning, facilitating plasticity (Stamenkovic, *et al.*, 2017; Nguyen, *et al.*, 2020). In disease and stress conditions the PNN has been shown to be both vulnerable and resistant. Microglial activation by trimethyltin did not affect PNN ensheathed neurons while LPS administration caused a decrease (Schüppel, *et al.*, 2002; Crapser, *et al.*, 2020). It is well-documented that the PNN protects neurons from ROS-mediated toxicity, a key mechanism in microglial-mediated neuronal toxicity (Morawski, *et al.*, 2010a; Suttkus, *et al.*, 2014). PNNs are lost early in prion disease, followed by subsequent PV cell loss (Belichenko, *et al.*, 1999; Franklin, *et al.*, 2008). PNN loss was also observed in a ALS mouse model (Forostyak, *et al.*, 2020). In AD, PNNs densities are unchanged across multiple brain regions and mouse models but one group showed a loss in the middle frontal gyrus and in a mouse model (Brückner, *et al.*, 1999; Morawski, *et al.*, 2010a; Morawski, *et al.*, 2012b; Lendvai, *et al.*, 2013; Crapser, *et al.*, 2020; Reid, *et al.*, 2021). Our results have shown in PD, a sparing of PNN populations in multiple brain region, which would not be expected if they were vulnerable to microglia-mediated toxicity.

How can these conflicting results be reconciled? One explanation is the degree of inflammation. Both prion disease and AD have higher levels of inflammation compared to PD, as measured by gene expression changes (López González, *et al.*, 2016). In AD, the level of inflammation changes between regions and stage of disease progression, this could account for the conflicting sparing and destruction of PNNs reported in AD (López-González, *et al.*, 2015). We have identified and discussed PNN heterogeneity during this work, another explanation for differing reports of PNN resistance could be due to the heterogeneity of the PNNs themselves as PNNs differ in composition and thickness (Smith, *et al.*, 2015; Ueno, *et al.*, 2018a). However, differential PNN vulnerability has yet to be shown. We did not find any regional differences in PNN vulnerability in PD brains and comparison of PNN knock-out animals did not show any difference in resistance to ROS (Suttkus, *et al.*, 2014). In summary, while it is possible the PNN can be degraded by microglia in PD, no

supporting evidence has been discovered to support the assumption. Differing PNN vulnerability could be tested in our PNN culture by comparing resistance of immature PNNs to mature PNNs.

Does the PNN induce local microgliosis, creating a more toxic environment for neighbouring, PNN negative neurons? Our results did not investigate this due to the non-specificity of our neuronal stain. If this is the case, then we would expect to see an increase in microglia density around PNNs and increased neuronal loss in PNN rich areas. This should be investigated in a future study through immunohistochemical staining.

Discussed briefly earlier in this chapter was the question of how  $\alpha$ SYN synaptic transmission interacts with PNN neuroprotection. This is a limitation of the work but should be addressed in future studies through *in vitro* culture and *in vivo* injection models. Currently, reconciling synaptic transmission and PNN neuroprotection would go beyond the experimental data. The segregation observed in the PD brain and in the pattern of spreading in a PPN injection model (discussed in chapter 5) hint that reconciliation is possible but direct evidence is needed (Henrich, *et al.*, 2020). As mentioned, the PNN is but one factor underlying neuronal resistance and vulnerability in PD, it is likely that it is the interaction of the PNN with other factors that dictate vulnerability to  $\alpha$ SYN transmission.

## Chapter 7 Conclusions

The overall aim of this study was to investigate a putative neuroprotective role of the PNN in PD. To this end an *in vitro* PNN culture was established which accurately replicated mature PNNs as they would appear in the aged CNS.  $\alpha$ SYN was purified for use in this study and two distinct aggregated species were created and characterised (oligomers and PFF).

The PNN culture created in this study also modelled PNN maturation and heterogeneity as seen *in vivo*. These were characterised using quantitative methods to understand the PNN population as a whole. As the PNN population matured and aged the predominant morphology transitioned from a punctate to a reticular morphology. A population of early mature PNNs were identified that were biochemically and morphologically distinct from the remaining PNN population, this hints that different maturation mechanisms control PNN development in different sub-populations. Acan was the principal PNN CSPG in the mature culture but not during PNN maturation. Use of this model will give further insight into mechanisms governing PNN maturation and functions arising from PNN composition.

The presence of a PNN reduced internalisation of  $\alpha$ SYN oligomers by two-thirds in PNN neurons compared to neurons lacking a PNN. Degradation of the PNN was sufficient to ablate this resistance. The introduction of a PNN-like coat on the surface of HEK cells is sufficient to reduce oligomer uptake and seeding. The PNN and loose ECM were also shown to negatively regulate p- $\alpha$ SYN pathology development as ChABC prior to exposure with PFF, significantly increased the extent of pathology development. PNN GAGs, CS-E and HS, were found to interact with monomeric and oligomeric  $\alpha$ SYN, raising the possibility of a chelation mechanism by the PNN. PNN populations were spared in PD patient brains, validating the resistance effect established *in vitro*. PNN densities were unchanged compared to NDC and no LP was detected in PNN neurons, corroborating our *in vitro* findings. We also observed the segregation of LP and areas of high PNN and loose ECM density, raising the possibility that the ECM is a factor governing LP spread in PD.

Together these results establish the PNN as a neuroprotective barrier in PD by preventing neuronal uptake of pathogenic  $\alpha$ SYN and subsequent LP development. This identifies the PNN as a neuronal resistance factor contributing to the selective neuronal vulnerability and the pattern of LP spread seen in PD. This work has highlighted the importance of the ECM, specifically the PNN, in PD pathophysiology by establishing it as a factor governing selective neuronal resistance in PD.

## Chapter 8 References

- Abeliovich, A., Schmitz, Y., Fariñas, I., Choi-Lundberg, D., Ho, W.-H., Castillo, P.E., Shinsky, N., Verdugo, J.M.G., Armanini, M., Ryan, A., Hynes, M., Phillips, H., Sulzer, D. and Rosenthal, A. 2000. Mice Lacking  $\alpha$ -Synuclein Display Functional Deficits in the Nigrostriatal Dopamine System. *Neuron*. **25**(1), pp.239–252.
- Abounit, S., Bousset, L., Loria, F., Zhu, S., de Chaumont, F., Pieri, L., Olivio-Marin, J., Melki, R. and Zurzolo, C. 2016. Tunneling nanotubes spread fibrillar  $\alpha$ -synuclein by intercellular trafficking of lysosomes. *The EMBO Journal*. **35**(19), pp.2120–2138.
- Adams, I., Brauer, K., Areèlin, C., Härtig, W., Fine, A., Mader, M., Arendt, T. and Brückner, G. 2001. Perineuronal Nets In The Rhesus Monkey And Human Basal Forebrain Including Basal Ganglia. *Neuroscience*. **108**(2), pp.285–298.
- Adler, C.H., Beach, T.G., Zhang, N., Shill, H.A., Driver-Dunckley, E., Caviness, J.N., Mehta, S.H., Sabbagh, M.N., Serrano, G.E., Sue, L.I., Belden, C.M., Powell, J., Jacobson, S.A., Zamrini, E., Shprecher, D., Davis, K.J., Dugger, B.N. and Hentz, J.G. 2019. Unified Staging System for Lewy Body Disorders: Clinicopathologic Correlations and Comparison to Braak Staging. *Journal of Neuropathology & Experimental Neurology*. **78**(10), pp.891–899.
- Afitska, K., Fucikova, A., Shvadchak, V. V. and Yushchenko, D.A. 2019.  $\alpha$ -Synuclein aggregation at low concentrations. *Biochimica et Biophysica Acta - Proteins and Proteomics*. **1867**(7–8), pp.701–709.
- Alabi, A.A. and Tsien, R.W. 2013. Perspectives on kiss-and-run: Role in exocytosis, endocytosis, and neurotransmission. *Annual Review of Physiology*. **75**, pp.393–422.
- Alam, P., Bousset, L., Melki, R. and Otzen, D.E. 2019.  $\alpha$ -Synuclein Oligomers and Fibrils: a Spectrum of Species, a Spectrum of Toxicities. *Journal of Neurochemistry*. **150**(5), pp.522–534.
- Alamri, Y.A. 2015. Mental health and Parkinson's disease: from the cradle to the grave. *British Journal of General Practice*. **65**(634), pp.258–259.
- Alegre-Abarrategui, J., Brimblecombe, K.R., Roberts, R.F., Velentza-Almpani, E., Tilley, B.S., Bengoa-Vergniory, N. and Proukakis, C. 2019. Selective

vulnerability in  $\alpha$ -synucleinopathies. *Acta Neuropathologica*. **138**(5), pp.681–704.

- Alpár, A., Gärtner, U., Härtig, W. and Brückner, G. 2006. Distribution of pyramidal cells associated with perineuronal nets in the neocortex of rat. *Brain Research*. **1120**(1), pp.13–22.
- Anderegg, A., Poulin, J.-F. and Awatramani, R. 2015. Molecular Heterogeneity of Midbrain Dopaminergic Neurons – Moving Toward Single Cell Resolution. *FEBS Letters*. **589**(24), pp.3714–3726.
- Anderson, J.P., Walker, D.E., Goldstein, J.M., De Laat, R., Banducci, K., Caccavello, R.J., Barbour, R., Huang, J., Kling, K., Lee, M.K., Diep, L., Keim, P.S., Shen, X., Chataway, T., Schlossmacher, M.G., Seubert, P., Schenk, D., Sinha, S., Gai, W.-P. and Chilcote, T.J. 2006. Phosphorylation of Ser-129 is the dominant pathological modification of  $\alpha$ -synuclein in familial and sporadic lewy body disease. *Journal of Biological Chemistry*. **281**(40), pp.29739–29752.
- Aspberg, A., Miura, R., Bourdoulous, S., Shimonaka, M., Heinegård, D., Schachner, M., Ruoslahti, E. and Yamaguchi, Y. 1997. The C-type lectin domains of lecticans, a family of aggregating chondroitin sulfate proteoglycans, bind tenascin-R by protein-protein interactions independent of carbohydrate moiety. *Proceedings of the National Academy of Sciences of the United States of America*. **94**(19), pp.10116–21.
- Aspberg, A. 1995. The versican C-type lectin domain recognizes the adhesion protein tenascin-R. *Proceedings of the National Academy of Sciences of the United States of America*. **92**(November), pp.10590–10594.
- Atias, M., Tevet, Y., Sun, J., Stavsky, A., Tal, S., Kahn, J., Roy, S. and Gitler, D. 2019. Synapsins regulate  $\alpha$ -synuclein functions. *Proceedings of the National Academy of Sciences of the United States of America*. **166**(23), pp.11116–11118.
- Attems, J. and Jellinger, K.A. 2008. The dorsal motor nucleus of the vagus is not an obligatory trigger site of parkinson's disease. *Neuropathology and Applied Neurobiology*. **34**(4), pp.466–467.
- Aulić, S., Masperone, L., Narkiewicz, J., Isopi, E., Bistaffa, E., Ambrosetti, E., Pastore, B., De Cecco, E., Scaini, D., Zago, P., Moda, F., Tagliavini, F. and Legname, G. 2017.  $\alpha$ -Synuclein Amyloids Hijack Prion Protein to Gain Cell

- Entry, Facilitate Cell-to-Cell Spreading and Block Prion Replication. *Scientific Reports*. **7**(1), pp.1–12.
- El Ayachi, I., Fernandez, C., Baeza, N., De Paula, A.M., Pesheva, P. and Figarella-Branger, D. 2011. Spatiotemporal distribution of tenascin-R in the developing human cerebral cortex parallels neuronal migration. *The Journal of comparative neurology*. **519**(12), pp.2379–89.
- Baba, M., Nakajo, S., Tu, P.H., Tomita, T., Nakaya, K., Lee, V.M.Y., Trojanowski, J.Q. and Iwatsubo, T. 1998. Aggregation of  $\alpha$ -synuclein in Lewy bodies of sporadic Parkinson's disease and dementia with Lewy bodies. *American Journal of Pathology*. **152**(4), pp.879–884.
- Baig, S., Wilcock, G.K. and Love, S. 2005. Loss of perineuronal net N-acetylgalactosamine in Alzheimer's disease. *Acta Neuropathologica*. **110**(4), pp.393–401.
- Balmer, T.S. 2016. Perineuronal Nets Enhance the Excitability of Fast-Spiking Neurons. *eNeuro*. **3**(4), pp.e0112-16.2016.
- Banerjee, S.B., Gutzeit, V.A., Baman, J., Aoued, H.S., Doshi, N.K., Liu, R.C. and Ressler, K.J. 2017. Perineuronal Nets in the Adult Sensory Cortex Are Necessary for Fear Learning. *Neuron*. **95**(1), pp.169-179.e3.
- Bantle, C.M., Phillips, A.T., Smeyne, R.J., Rocha, S.M., Olson, K.E. and Tjalkens, R.B. 2019. Infection with mosquito-borne alphavirus induces selective loss of dopaminergic neurons, neuroinflammation and widespread protein aggregation. *npj Parkinson's Disease*. **5**(1), pp.1–15.
- Beach, T.G., Adler, C.H., Lue, L.F., Sue, L.I., Bachalakuri, J., Henry-Watson, J., Sasse, J., Boyer, S., Shirohi, S., Brooks, R., Eschbacher, J., White, C.L., Akiyama, H., Caviness, J., Shill, H.A., Connor, D.J., Sabbagh, M.N. and Walker, D.G. 2009. Unified staging system for Lewy body disorders: Correlation with nigrostriatal degeneration, cognitive impairment and motor dysfunction. *Acta Neuropathologica*. **117**(6), pp.613–634.
- Bekku, Y., Vargova, L., Goto, Y., Vorisek, I., Dmytrenko, L., Narasaki, M., Ohtsuka, A., Fassler, R., Ninomiya, Y., Sykova, E. and Oohashi, T. 2010. Bral1: Its Role in Diffusion Barrier Formation and Conduction Velocity in the CNS. *Journal of Neuroscience*. **30**(8), pp.3113–3123.
- Bekku, Y., Saito, M., Moser, M., Fuchigami, M., Maehara, A., Nakayama, M., Kusachi, S., Ninomiya, Y. and Oohashi, T. 2012. Bral2 is indispensable for

the proper localization of brevican and the structural integrity of the perineuronal net in the brainstem and cerebellum. *Journal of Comparative Neurology*. **520**(8), pp.1721–1736.

Bekku, Y., Rauch, U., Ninomiya, Y. and Oohashi, T. 2009. Brevican distinctively assembles extracellular components at the large diameter nodes of Ranvier in the CNS. *Journal of Neurochemistry*. **108**(5), pp.1266–1276.

Bekku, Y., Su, W.D., Hirakawa, S., Fässler, R., Ohtsuka, A., Kang, J.S., Sanders, J., Murakami, T., Ninomiya, Y. and Oohashi, T. 2003. Molecular cloning of Bral2, a novel brain-specific link protein, and immunohistochemical colocalization with brevican in perineuronal nets. *Molecular and Cellular Neuroscience*. **24**(1), pp.148–159.

Bekku, Y. and Oohashi, T. 2011. Neurocan contributes to the molecular heterogeneity of the perinodal ECM. *Archives of Histology and Cytology*. **73**(2), pp.95–102.

Belaidi, A.A. and Bush, A.I. 2016. Iron neurochemistry in Alzheimer's disease and Parkinson's disease: targets for therapeutics. *Journal of Neurochemistry*. **139**, pp.179–197.

Belichenko, P. V., Miklossy, J., Belser, B., Budka, H. and Celio, M.R. 1999. Early destruction of the extracellular matrix around parvalbumin-immunoreactive interneurons in Creutzfeldt-Jakob disease. *Neurobiol Dis*. **6**(4), pp.269–79.

Van de Berg, W.D.J., Hepp, D.H., Dijkstra, A.A., Rozemuller, J.A.M., Berendse, H.W. and Foncke, E. 2012. Patterns of alpha-synuclein pathology in incidental cases and clinical subtypes of Parkinson's disease. *Parkinsonism and Related Disorders*. **18**(SUPPL. 1), pp.S28–S30.

Van Den Berge, N., Ferreira, N., Gram, H., Mikkelsen, T.W., Alstrup, A.K.O., Casadei, N., Tsung-Pin, P., Riess, O., Nyengaard, J.R., Tamgüney, G., Jensen, P.H. and Borghammer, P. 2019. Evidence for bidirectional and trans-synaptic parasymphathetic and symphathetic propagation of alpha-synuclein in rats. *Acta Neuropathologica*.

Bernard, C. and Prochiantz, A. 2016. Otx2-PNN Interaction to Regulate Cortical Plasticity. *Neural Plasticity*. **2016**.

Bertolotto, A., Manzardo, E. and Guglielmone, R. 1996. Immunohistochemical mapping of perineuronal nets containing chondroitin unsulfate proteoglycan

- in the rat central nervous system. *Cell and Tissue Research*. **283**(2), pp.283–295.
- Beurdeley, M., Spatazza, J., Lee, H.H.C., Sugiyama, S., Bernard, C., Di Nardo, A.A., Hensch, T.K. and Prochiantz, A. 2012. Otx2 Binding to Perineuronal Nets Persistently Regulates Plasticity in the Mature Visual Cortex. *Journal of Neuroscience*. **32**(27), pp.9429–9437.
- Bieri, G., Gitler, A.D. and Brahic, M. 2017. Internalization, axonal transport and release of fibrillar forms of alpha-synuclein. *Neurobiology of Disease*.
- Binolfi, A., Rasia, R.M., Bertocini, C.W., Ceolin, M., Zweckstetter, M., Griesinger, C., Jovin, T.M. and Fernández, C.O. 2006. Interaction of  $\alpha$ -synuclein with divalent metal ions reveals key differences: A link between structure, binding specificity and fibrillation enhancement. *Journal of the American Chemical Society*. **128**(30), pp.9893–9901.
- Blosa, M., Sonntag, M., Jäger, C., Weigel, S., Seeger, J., Frischknecht, R., Seidenbecher, C.I., Matthews, R.T., Arendt, T., Rübsamen, R. and Morawski, M. 2015. The extracellular matrix molecule brevican is an integral component of the machinery mediating fast synaptic transmission at the calyx of Held. *The Journal of Physiology*. **593**(19), pp.4341–4360.
- Blosa, M., Sonntag, M., Brückner, G., Jäger, C., Seeger, G., Matthews, R.T., Rübsamen, R., Arendt, T. and Morawski, M. 2013. Unique features of extracellular matrix in the mouse medial nucleus of trapezoid body - Implications for physiological functions. *Neuroscience*. **228**, pp.215–234.
- Booth, H.D.E., Hirst, W.D. and Wade-Martins, R. 2017. The Role of Astrocyte Dysfunction in Parkinson's Disease Pathogenesis. *Trends in Neurosciences*. **40**(6), pp.358–370.
- Bousset, L., Pieri, L., Ruiz-Arlandis, G., Gath, J., Jensen, P.H., Habenstein, B., Madiona, K., Olieric, V., Böckmann, A., Meier, B.H. and Melki, R. 2013. Structural and functional characterization of two alpha-synuclein strains. *Nature Communications*. **4**.
- Braak, H., Braak, E., Yilmazer, D., de Vos, R.A.I., Jansen, E.N.H., Bohl, J. and Jellinger, K. 1994. Amygdala pathology in Parkinson's disease. *Acta Neuropathologica*. **88**(6), pp.493–500.
- Braak, H., Rüb, U., Jansen Steur, E.N.H., Del Tredici, K. and De Vos, R.A.I. 2005. Cognitive status correlates with neuropathologic stage in Parkinson

- disease. *Neurology*. **64**(8), pp.1404–1410.
- Braak, H., Ghebremedhin, E., Rüb, U., Bratzke, H. and Del Tredici, K. 2004. Stages in the development of Parkinson's disease-related pathology. *Cell and Tissue Research*. **318**(1), pp.121–134.
- Braak, H., Del Tredici, K., Rüb, U., De Vos, R.A.I., Jansen Steur, E.N.H. and Braak, E. 2003. Staging of brain pathology related to sporadic Parkinson's disease. *Neurobiology of Aging*. **24**(2), pp.197–211.
- Braak, H., Bohl, J.R., Müller, C.M., Rüb, U., de Vos, R.A.I. and Del Tredici, K. 2006. Stanley Fahn Lecture 2005: The staging procedure for the inclusion body pathology associated with sporadic Parkinson's disease reconsidered. *Movement Disorders*. **21**(12), pp.2042–2051.
- Braak, H. and Del Tredici, K. 2017. Neuropathological Staging of Brain Pathology in Sporadic Parkinson's disease: Separating the Wheat from the Chaff. *Journal of Parkinson's Disease*. **7**(s1), pp.S73–S87.
- Braidy, N., Gai, W.P., Xu, Y.H., Sachdev, P., Guillemin, G.J., Jiang, X.M., Ballard, J.W.O., Horan, M.P., Fang, Z.M., Chong, B.H. and Chan, D.K.Y. 2013. Uptake and mitochondrial dysfunction of alpha-synuclein in human astrocytes, cortical neurons and fibroblasts. *Translational Neurodegeneration*. **2**(1), pp.1–9.
- Brakebusch, C., Seidenbecher, C.I., Asztely, F., Rauch, U., Matthies, H., Meyer, H., Krug, M., Böckers, T.M., Zhou, X., Kreutz, M.R., Montag, D., Gundelfinger, E.D. and Fässler, R. 2002a. Brevican-Deficient Mice Display Impaired Hippocampal CA1 Long-Term Potentiation but Show No Obvious Deficits in Learning and Memory. *Molecular and Cellular Biology*. **22**(21), pp.7417–7427.
- Brakebusch, C., Seidenbecher, C.I., Asztely, F., Rauch, U., Matthies, H., Meyer, H., Krug, M., Bo, T.M., Zhou, X., Kreutz, M.R., Montag, D., Gundelfinger, E.D. and Fassler, R. 2002b. Brevican-Deficient Mice Display Impaired Hippocampal CA1 Long-Term Potentiation but Show No Obvious Deficits in Learning and Memory. *Molecular and Cellular Biology*. **22**(21), pp.7417–7427.
- Braun, A.R., Lacy, M.M., Ducas, V.C., Rhoades, E. and Sachs, J.N. 2014. Alpha-Synuclein-Induced Membrane Remodeling Is Driven By Binding Affinity, Partition Depth, and Interleaflet Order Asymmetry. *Journal of the*

- American Chemical Society*. **136**(28), pp.9962–9972.
- Braun, A.R., Sevcsik, E., Chin, P., Rhoades, E., Tristram-Nagle, S. and Sachs, J.N. 2012. Alpha-Synuclein Induces Both Positive Mean Curvature and Negative Gaussian Curvature in Membranes. *Journal of the American Chemical Society*. **134**(5), pp.2613–2620.
- Brown, T.P. 2017. Pure autonomic failure. *Practical Neurology*. **17**(5), pp.341–348.
- Brückner, G., Morawski, M. and Arendt, T. 2008. Aggrecan-based extracellular matrix is an integral part of the human basal ganglia circuit. *Neuroscience*. **151**(2), pp.489–504.
- Brückner, G., Hausen, D., Härtig, W., Drlicek, M., Arendt, T. and Brauer, K. 1999. Cortical areas abundant in extracellular matrix chondroitin sulphate proteoglycans are less affected by cytoskeletal changes in Alzheimer's disease. *Neuroscience*. **92**(3), pp.791–805.
- Brückner, G., Kacza, J. and Grosche, J. 2004. Perineuronal nets characterized by vital labelling, confocal and electron microscopy in organotypic slice cultures of rat parietal cortex and hippocampus. *Journal of Molecular Histology*. **35**, pp.115–122.
- Brückner, G., Grosche, J., Schmidt, S., Härtig, W., Margolis, R.U., Delpech, B., Seidenbecher, C.I., Czaniera, R. and Schachner, M. 2000. Postnatal development of perineuronal nets in wild-type mice and in a mutant deficient in tenascin-R. *Journal of Comparative Neurology*. **428**(4), pp.616–629.
- Brundin, P. and Melki, R. 2017. Prying into the Prion Hypothesis for Parkinson's Disease. *The Journal of Neuroscience*. **37**(41), pp.9808–9818.
- Buell, A.K., Galvagnion, C., Gaspar, R., Sparr, E., Vendruscolo, M., Knowles, T.P.J., Linse, S. and Dobson, C.M. 2014. Solution conditions determine the relative importance of nucleation and growth processes in alpha-synuclein aggregation. *Proceedings of the National Academy of Sciences*. **111**(21), pp.7671–7676.
- Bukalo, O., Schachner, M. and Dityatev, A. 2001. Modification of Extracellular Matrix By Enzymatic Removal of Chondroitin Sulfate And By Lack of Tenascin-R Differentially Affects Several Forms of Synaptic Plasticity In The Hippocampus. *Neuroscience*. **104**(2), pp.359–369.

- Burré, J., Sharma, M. and Südhof, T.C. 2014.  $\alpha$ -Synuclein assembles into higher-order multimers upon membrane binding to promote SNARE complex formation. *Proceedings of the National Academy of Sciences of the United States of America*. **111**(40), pp.E4274–E4283.
- Burré, J., Sharma, M., Tsetsenis, T., Buchman, V.L., Etherton, M.R. and Südhof, T.C. 2010.  $\alpha$ -Synuclein promotes SNARE-complex assembly in vivo and in vitro. *Science*. **329**(5999), pp.1663–1667.
- Busch, D.J., Oliphint, P.A., Walsh, R.B., Banks, S.M.L., Woods, W.S., George, J.M. and Morgan, J.R. 2014. Acute increase of  $\alpha$ -synuclein inhibits synaptic vesicle recycling evoked during intense stimulation. *Molecular Biology of the Cell*. **25**(24), pp.3926–3941.
- Cabin, D.E., Shimazu, K., Murphy, D., Cole, N.B., Gottschalk, W., McIlwain, K.L., Orrison, B., Chen, A., Ellis, C.E., Paylor, R., Lu, B. and Nussbaum, R.L. 2002. Synaptic vesicle depletion correlates with attenuated synaptic responses to prolonged repetitive stimulation in mice lacking  $\alpha$ -synuclein. *Journal of Neuroscience*. **22**(20), pp.8797–8807.
- Cabungcal, J.H., Steullet, P., Morishita, H., Kraftsik, R., Cuenod, M., Hensch, T.K. and Do, K.Q. 2013. Perineuronal nets protect fast-spiking interneurons against oxidative stress. *Proceedings of the National Academy of Sciences*. **110**(22), pp.9130–9135.
- Campbell, B.C.V., McLean, C.A., Culvenor, J.G., Gai, W.P., Blumbergs, P.C., Jäkälä, P., Beyreuther, K., Masters, C.L. and Li, Q.X. 2001. The solubility of  $\alpha$ -synuclein in multiple system atrophy differs from that of dementia with Lewy bodies and Parkinson's disease. *Journal of Neurochemistry*. **76**(1), pp.87–96.
- Cappai, R., Leck, S., Tew, D.J., Williamson, N.A., Smith, D.P., Galatis, D., Sharples, R.A., Curtain, C.C., Ali, F.E., Cherny, R.A., Culvenor, J.G., Bottomley, S.P., Masters, C.L., Barnham, K.J. and Hill, A.F. 2005. Dopamine promotes Alpha-synuclein aggregation into SDS-resistant soluble oligomers via a distinct folding pathway. *FASEB*. **1**(1), pp.1–19.
- Carulli, D., Pizzorusso, T., Kwok, J.C.F., Putignano, E., Poli, A., Forostyak, S., Andrews, M.R., Deepa, S.S., Glant, T.T. and Fawcett, J.W. 2010. Animals lacking link protein have attenuated perineuronal nets and persistent plasticity. *Brain*. **133**(8), pp.2331–2347.

- Carulli, D., Broersen, R., de Winter, F., Muir, E.M., Meškovic, M., de Waal, M., de Vries, S., Boele, H.J., Canto, C.B., de Zeeuw, C.I. and Verhaagen, J. 2020. Cerebellar plasticity and associative memories are controlled by perineuronal nets. *Proceedings of the National Academy of Sciences of the United States of America*. **117**(12), pp.6855–6865.
- Carulli, D., Rhodes, K.E., Brown, D.J., Bonnert, T.P., Pollack, S.J., Oliver, K., Strata, P. and Fawcett, J.W. 2006. Composition of perineuronal nets in the adult rat cerebellum and the cellular origin of their components. *Journal of Comparative Neurology*. **494**(4), pp.559–577.
- Carulli, D., Foscarin, S., Faralli, A., Pajaj, E. and Rossi, F. 2013. Modulation of semaphorin3A in perineuronal nets during structural plasticity in the adult cerebellum. *Molecular and Cellular Neuroscience*. **57**, pp.10–22.
- Carulli, D., Rhodes, K.E. and Fawcett, J.W. 2007. Upregulation of Aggrecan, Link Protein 1, and Hyaluronan Synthases during Formation of Perineuronal Nets in the Rat Cerebellum. *J Comp Neurol*. **502**(2), pp.275–290.
- Celej, M.S., Sarroukh, R., Goormaghtigh, E., Fidelio, G.D., Ruyschaert, J.M. and Raussens, V. 2012. Toxic prefibrillar  $\alpha$ -synuclein amyloid oligomers adopt a distinctive antiparallel  $\beta$ -sheet structure. *Biochemical Journal*. **443**(3), pp.719–726.
- Celio, M.R. and Chiquet-Ehrismann, R. 1993. 'Perineuronal nets' around cortical interneurons expressing parvalbumin are rich in tenascin. *Neuroscience Letters*. **162**(1–2), pp.137–140.
- Chandra, S.S., Gallardo, G., Fernández-Chacón, R., Schlüter, O.M. and Südhof, T.C. 2005.  $\alpha$ -Synuclein cooperates with CSP $\alpha$  in preventing neurodegeneration. *Cell*. **123**(3), pp.383–396.
- Chang, M.C., Park, J.M., Pelkey, K.A., Grabenstatter, H.L., Xu, D., Linden, D.J., Sutula, T.P., McBain, C.J. and Worley, P.F. 2010. Narp regulates homeostatic scaling of excitatory synapses on parvalbumin-expressing interneurons. *Nature Neuroscience*. **13**(9), pp.1090–1097.
- Chang, P.S., McLane, L.T., Fogg, R., Scrimgeour, J., Temenoff, J.S., Granqvist, A. and Curtis, J.E. 2016. Cell Surface Access Is Modulated by Tethered Bottlebrush Proteoglycans. *Biophysical Journal*. **110**(12), pp.2739–2750.
- Choi, I., Zhang, Y., Seegobin, S.P., Pruvost, M., Wang, Q., Purtell, K., Zhang,

- B. and Yue, Z. 2020. Microglia clear neuron-released  $\alpha$ -synuclein via selective autophagy and prevent neurodegeneration. *Nature Communications*. **11**(1).
- Coelho-Cerqueira, E., Carmo-Gonçalves, P., Sá Pinheiro, A., Cortines, J. and Follmer, C. 2013.  $\alpha$ -Synuclein as an intrinsically disordered monomer - Fact or artefact? *FEBS Journal*. **280**(19), pp.4915–4927.
- Conway, K.A., Harper, J.D. and Lansbury, P.T. 1998. Accelerated in vitro fibril formation by a mutant  $\alpha$ -synuclein linked to early-onset Parkinson disease. *Nature Medicine*. **4**(11), pp.1318–1320.
- Conway, K.A., Lee, S.J., Rochet, J.C., Ding, T.T., Harper, J.D., Williamson, R.E. and Lansbury, P.T. 2000. Accelerated oligomerization by Parkinson's disease linked alpha-synuclein mutants. *Annals of the New York Academy of Sciences*. **920**(617), pp.42–45.
- Cornez, G., Jonckers, E., Ter Haar, S.M., Van Der Linden, A., Cornil, C.A. and Balthazart, J. 2018. Timing of perineuronal net development in the zebra finch song control system correlates with developmental song learning. *Proceedings of the Royal Society B: Biological Sciences*. **285**(1883).
- Courte, J., Bousset, L., Boxberg, Y. Von, Catherine, V., Melki, R. and Peyrin, J.-M. 2020. The expression level of alpha- synuclein in different neuronal populations is the primary determinant of its prion-like seeding. *Scientific Reports*. **10**(1), pp.1–13.
- Crapser, J.D., Spangenberg, E.E., Barahona, R.A., Arreola, M.A., Hohsfield, L.A. and Green, K.N. 2020. Microglia facilitate loss of perineuronal nets in the Alzheimer's disease brain. *EBioMedicine*. **58**.
- Crowther, R.A., Daniel, S.E. and Goedert, M. 2000. Characterisation of isolated  $\alpha$ -synuclein filaments from substantia nigra of Parkinson's disease brain. *Neuroscience Letters*. **292**(2), pp.128–130.
- Crowther, R.A., Jakes, R., Spillantini, M.G. and Goedert, M. 1998. Synthetic filaments assembled from C-terminally truncated  $\alpha$ -synuclein. *FEBS Letters*. **436**, pp.309–312.
- Danzer, K.M., Haasen, D., Karow, A.R., Moussaud, S., Habeeb, M., Giese, A., Kretzschmar, H., Hengerer, B. and Kostka, M. 2007. Different Species of Alpha-Synuclein Oligomers Induce Calcium Influx and Seeding. *Journal of Neuroscience*. **27**(34), pp.9220–9232.

- Danzer, K.M., Kranich, L.R., Ruf, W.P., Cagsal-Getkin, O., Winslow, A.R., Zhu, L., Vanderburg, C.R. and McLean, P.J. 2012. Exosomal cell-to-cell transmission of alpha synuclein oligomers. *Molecular Neurodegeneration*. **7**(1), p.42.
- Danzer, K.M., Krebs, S.K., Wolff, M., Birk, G. and Hengerer, B. 2009. Seeding induced by  $\alpha$ -synuclein oligomers provides evidence for spreading of  $\alpha$ -synuclein pathology. *Journal of Neurochemistry*. **111**(1), pp.192–203.
- Darios, F., Ruipérez, V., López, I., Villanueva, J., Gutierrez, L.M. and Davletov, B. 2010.  $\alpha$ -Synuclein sequesters arachidonic acid to modulate SNARE-mediated exocytosis. *EMBO Reports*. **11**(7), pp.528–533.
- Davidson, W.S., Jonas, A., Clayton, D.F. and George, J.M. 1998. Stabilization of alpha-synuclein secondary structure upon binding to synthetic membranes. *The Journal of biological chemistry*. **273**(16), pp.9443–9.
- Deas, E., Cremades, N., Angelova, P.R., Ludtmann, M.H.R., Yao, Z., Chen, S., Horrocks, M.H., Banushi, B., Little, D., Devine, M.J., Gissen, P., Klenerman, D., Dobson, C.M., Wood, N.W., Gandhi, S. and Abramov, A.Y. 2016. Alpha-Synuclein Oligomers Interact with Metal Ions to Induce Oxidative Stress and Neuronal Death in Parkinson's Disease. *Antioxidants & Redox Signaling*. **24**(7), pp.376–391.
- Deepa, S.S., Carulli, D., Galtrey, C.M., Rhodes, K.E., Fukuda, J., Mikami, T., Sugahara, K. and Fawcett, J.W. 2006. Composition of perineuronal net extracellular matrix in rat brain: A different disaccharide composition for the net-associated proteoglycans. *Journal of Biological Chemistry*. **281**(26), pp.17789–17800.
- Delenclos, M., Trendafilova, T., Mahesh, D., Baine, A.T., Moussaud, S., Yan, I.K., Patel, T. and McLean, P.J. 2017. Investigation of endocytic pathways for the internalization of exosome-associated oligomeric alpha-synuclein. *Frontiers in Neuroscience*. **11**(MAR), pp.1–10.
- Desplats, P., Lee, H., Bae, E., Patrick, C., Rockenstein, E., Crews, L. and Spencer, B. 2009. Inclusion formation and neuronal cell death through neuron-to-neuron transmission of Alpha-synuclein. *Proceedings of the National Academy of Sciences*. **106**(31), pp.13010–13015.
- Dexter, D.T. and Jenner, P. 2013. Parkinson disease: from pathology to molecular disease mechanisms. *Free Radical Biology and Medicine*. **62**,

pp.132–144.

- Diao, J., Burré, J., Vivona, S., Cipriano, D.J., Sharma, M., Kyoung, M., Südhof, T.C. and Brunger, A.T. 2013. Native  $\alpha$ -synuclein induces clustering of synaptic-vesicle mimics via binding to phospholipids and synaptobrevin-2/VAMP2. *eLife*. **2**, pp.1–17.
- Dick, G., Liktan, C., Alves, J.N., Ehlert, E.M.E., Miller, G.M., Hsieh-Wilson, L.C., Sugahara, K., Oosterhof, A., Van Kuppevelt, T.H., Verhaagen, J., Fawcett, J.W. and Kwok, J.C.F. 2013. Semaphorin 3A binds to the perineuronal nets via chondroitin sulfate type E motifs in rodent brains. *Journal of Biological Chemistry*. **288**(38), pp.27384–27395.
- Dickson, D.W., Uchikado, H., Fujishiro, H. and Tsuboi, Y. 2010. Evidence in Favor of Braak Staging of Parkinson's Disease. *Movement Disorders*. **25**(SUPPL. 1), pp.78–82.
- Dietrichs, E. and Odin, P. 2017. Algorithms for the treatment of motor problems in Parkinson's disease. *Acta Neurologica Scandinavica*. **136**(5), pp.378–385.
- Dijkstra, A.A., Voorn, P., Berendse, H.W., Groenewegen, H.J., Rozemuller, A.J.M. and van de Berg, W.D.J. 2014. Stage-dependent nigral neuronal loss in incidental Lewy body and parkinson's disease. *Movement Disorders*. **29**(10), pp.1244–1251.
- Ding, T.T., Lee, S.J., Rochet, J.C. and Lansbury, P.T. 2002. Annular  $\alpha$ -synuclein protofibrils are produced when spherical protofibrils are incubated in solution or bound to brain-derived membranes. *Biochemistry*. **41**(32), pp.10209–10217.
- Dino, M.R., Harroch, S., Hockfield, S. and Matthews, R.T. 2006. Monoclonal antibody Cat-315 detects a glycoform of receptor protein tyrosine phosphatase beta/phosphacan early in CNS development that localizes to extrasynaptic sites prior to synapse formation. *Neuroscience*. **142**(4), pp.1055–1069.
- Dityatev, A., Brückner, G., Dityateva, G., Grosche, J., Kleene, R. and Schachner, M. 2007. Activity-Dependent Formation and Functions of Chondroitin Sulfate-Rich Extracellular Matrix of Perineuronal Nets. *Developmental Neurobiology*. **73**(8), pp.609–620.
- Dityatev, A. and Rusakov, D.A. 2011. Molecular signals of plasticity at the

- tetrapartite synapse. *Current Opinion in Neurobiology*. **21**(2), pp.353–359.
- Djeral, L., Lortat-Jacob, H. and Kwok, J.C.F. 2017. Chondroitin sulfates and their binding molecules in the central nervous system. *Glycoconjugate Journal*. **34**(3), pp.363–376.
- Djeral, L., Vivès, R.R., Lopin-Bon, C., Richter, R.P., Kwok, J.C.F. and Lortat-Jacob, H. 2019. Semaphorin 3A binding to chondroitin sulfate E enhances the biological activity of the protein, and cross- links and rigidifies glycosaminoglycan matrices. *BiRxiv*.
- Donato, F., Rompani, S.B. and Caroni, P. 2013. Parvalbumin-expressing basket-cell network plasticity induced by experience regulates adult learning. *Nature*. **504**(7479), pp.272–276.
- Doty, R.L., Deems, D.A. and Stellar, S. 1988. Olfactory Dysfunction in Parkinsonism: A General Deficit Unrelated to Neurologic Signs, Disease Stage, or Disease Duration. *Neurology*. **38**(8), pp.1237–1244.
- Dou, C.-L. and Levine, J.M. 1995. Differential Effects of Glycosaminoglycans Laminin and LI Substrates on Neurite Growth on. *Journal of Neuroscience*. **15**(12), pp.8053–8066.
- Dours-Zimmermann, M.T., Maurer, K., Rauch, U., Stoffel, W., Fassler, R. and Zimmermann, D.R. 2009. Versican V2 Assembles the Extracellular Matrix Surrounding the Nodes of Ranvier in the CNS. *Journal of Neuroscience*. **29**(24), pp.7731–7742.
- Du, H.-N., Tang, L., Luo, X.-Y., Li, H.-T., Hu, J., Zhou, J.-W. and Hu, H.-Y. 2003. A Peptide Motif Consisting of Glycine, Alanine, and Valine Is Required for the Fibrillization and Cytotoxicity of Human Alpha-Synuclein. *Biochemistry*. **42**, pp.8870–8878.
- Duce, J.A., Wong, B.X.W., Durham, H., Devedjian, J.-C., Smith, D.P. and Devos, D. 2017. Post translational changes to  $\alpha$ -synuclein control iron and dopamine trafficking; a concept for neuron vulnerability in Parkinson's disease. *Molecular Neurodegeneration*. **12**(45), pp.1–12.
- Duda, J., Pötschke, C. and Liss, B. 2016. Converging roles of ion channels, calcium, metabolic stress, and activity pattern of Substantia nigra dopaminergic neurons in health and Parkinson's disease. *Journal of Neurochemistry*. **139**, pp.156–178.
- Edamatsu, M., Miyano, R., Fujikawa, A., Fujii, F., Hori, T., Sakaba, T. and

- Oohashi, T. 2018. Hapln4/Bral2 is a selective regulator for formation and transmission of GABAergic synapses between Purkinje and deep cerebellar nuclei neurons. *Journal of Neurochemistry*. **147**(6), pp.748–763.
- Edwards, J.A., Risch, M. and Hoke, K.L. 2020. Dynamics of perineuronal nets over amphibian metamorphosis. *Journal of Comparative Neurology*. (September 2020), pp.1768–1778.
- Eill, G.J., Sinha, A., Morawski, M., Viapiano, M.S. and Matthews, R.T. 2020. The protein tyrosine phosphatase RPTP $\xi$ /phosphacan is critical for perineuronal net structure. *Journal of Biological Chemistry*. **295**(4), pp.955–968.
- Elstner, M., Müller, S.K., Leidolt, L., Laub, C., Krieg, L., Schlaudraff, F., Liss, B., Morris, C., Turnbull, D.M., Masliah, E., Prokisch, H. and Klopstock, T. 2011. Neuromelanin, neurotransmitter status and brainstem location determine the differential vulnerability of catecholaminergic neurons to mitochondrial DNA deletions. *Molecular Brain*. **4**(1), p.43.
- Emmanouilidou, E., Melachroinou, K., Roumeliotis, T., Garbis, S.D., Ntzouni, M., Margaritis, L.H., Stefanis, L. and Vekrellis, K. 2010. Cell-Produced Alpha-Synuclein Is Secreted in a Calcium-Dependent Manner by Exosomes and Impacts Neuronal Survival. *Neurobiology of Disease*. **30**(20), pp.6838–6851.
- Erskine, D., Patterson, L., Alexandris, A., Hanson, P.S., McKeith, I.G., Attems, J. and Morris, C.M. 2018. Regional levels of physiological  $\alpha$ -synuclein are directly associated with Lewy body pathology. *Acta Neuropathologica*. **135**(1), pp.153–154.
- Fahn, S. 2008. The history of dopamine and levodopa in the treatment of Parkinson's disease. *Movement Disorders*. **23**(SUPPL. 3).
- Fairfoul, G., McGuire, L.I., Pal, S., Ironside, J.W., Neumann, J., Christie, S., Joachim, C., Esiri, M., Evetts, S.G., Rolinski, M., Baig, F., Ruffmann, C., Wade-Martins, R., Hu, M.T.M., Parkkinen, L. and Green, A.J.E. 2016. Alpha-synuclein RT-QuIC in the CSF of patients with alpha-synucleinopathies. *Annals of Clinical and Translational Neurology*. **3**(10), pp.812–818.
- Faralli, A., Dagna, F., Albera, A., Bekku, Y., Oohashi, T., Albera, R., Rossi, F. and Carulli, D. 2016. Modifications of perineuronal nets and remodelling of

- excitatory and inhibitory afferents during vestibular compensation in the adult mouse. *Brain Structure and Function*. **221**(6), pp.3193–3209.
- Fauvet, B., Mbefo, M.K., Fares, M.B., Desobry, C., Michael, S., Ardah, M.T., Tsika, E., Coune, P., Prudent, M., Lion, N., Eliezer, D., Moore, D.J., Schneider, B.L., Aebischer, P., El-Agnaf, O.M., Masliah, E. and Lashuel, H.A. 2012.  $\alpha$ -Synuclein in central nervous system and from erythrocytes, mammalian cells, and *Escherichia coli* exists predominantly as disordered monomer. *Journal of Biological Chemistry*. **287**(19), pp.15345–15364.
- Favuzzi, E., Marques-Smith, A., Deogracias, R., Winterflood, C.M., Sánchez-Aguilera, A., Mantoan, L., Maeso, P., Fernandes, C., Ewers, H. and Rico, B. 2017. Activity-Dependent Gating of Parvalbumin Interneuron Function by the Perineuronal Net Protein Brevican. *Neuron*. **95**(3), pp.639-655.e10.
- Fawcett, J.W., Oohashi, T. and Pizzorusso, T. 2019. The roles of perineuronal nets and the perinodal extracellular matrix in neuronal function. *Nature Reviews Neuroscience*. **20**(August), pp.451–465.
- Feigin, V.L., Nichols, E., Alam, T., Bannick, M.S., Vos, T., et al. 2019. Global, regional, and national burden of neurological disorders, 1990–2016: a systematic analysis for the Global Burden of Disease Study 2016. *The Lancet Neurology*. **18**(5), pp.459–480.
- Fellner, L., Irschick, R., Schanda, K., Reindl, M., Klimaschewski, L., Poewe, W., Wenning, G.K. and Stefanova, N. 2013. Toll-like receptor 4 is required for  $\alpha$ -synuclein dependent activation of microglia and astroglia. *Glia*. **61**(3), pp.349–360.
- Filsy, S., Flavin, W.P., Iqbal, S., Pacelli, C., Renganathan, S.D.S., Trudeau, L.É., Campbell, E.M., Fraser, P.E. and Tandon, A. 2016. Effects of serine 129 phosphorylation on Alpha-synuclein aggregation, membrane association, and internalization. *Journal of Biological Chemistry*. **291**(9), pp.4374–4385.
- Flavin, W.P., Bousset, L., Green, Z.C., Chu, Y., Skarpathiotis, S., Chaney, M.J., Kordower, J.H., Melki, R. and Campbell, E.M. 2017. Endocytic vesicle rupture is a conserved mechanism of cellular invasion by amyloid proteins. *Acta Neuropathologica*. **134**(4), pp.629–653.
- Flores-Cuadrado, A., Ubeda-Bañon, I., Saiz-Sanchez, D., de la Rosa-Prieto, C. and Martinez-Marcos, A. 2016. Hippocampal  $\alpha$ -synuclein and interneurons

in Parkinson's disease: Data from human and mouse models. *Movement Disorders*. **31**(7), pp.979–988.

Flores-Cuadrado, A., Ubeda-Bañon, I., Saiz-Sanchez, D. and Martinez-Marcos, A. 2017.  $\alpha$ -synucleinopathy in the human amygdala in Parkinson disease: Differential vulnerability of somatostatin- and parvalbumin-expressing neurons. *Journal of Neuropathology and Experimental Neurology*. **76**(9), pp.754–758.

Forostyak, S., Forostyak, O., Kwok, J.C.F., Romanyuk, N., Rehorova, M., Kriska, J., Dayanithi, G., Raha-Chowdhury, R., Jendelova, P., Anderova, M., Fawcett, J.W. and Sykova, E. 2020. Transplantation of neural precursors derived from induced pluripotent cells preserve perineuronal nets and stimulate neural plasticity in ALS rats. *International Journal of Molecular Sciences*. **21**(24), pp.1–25.

Fortin, D.L., Troyer, M.D., Nakamura, K., Kubo, S.I., Anthony, M.D. and Edwards, R.H. 2004. Lipid rafts mediate the synaptic localization of  $\alpha$ -synuclein. *Journal of Neuroscience*. **24**(30), pp.6715–6723.

Foscarin, S., Raha-Chowdhury, R., Fawcett, J.W. and Kwok, J.C.F. 2017. Brain ageing changes proteoglycan sulfation, rendering perineuronal nets more inhibitory. *Aging*. **9**(6), pp.1607–1622.

Franklin, S.L., Love, S., Greene, J.R.T. and Betmouni, S. 2008. Loss of perineuronal net in ME7 prion disease. *Journal of Neuropathology and Experimental Neurology*. **67**(3), pp.189–199.

Freeman, D., Cedillos, R., Choyke, S., Lukic, Z., McGuire, K., Marvin, S., Burrage, A.M., Sudholt, S., Rana, A., O'Connor, C., Wiethoff, C.M. and Campbell, E.M. 2013. Alpha-Synuclein Induces Lysosomal Rupture and Cathepsin Dependent Reactive Oxygen Species Following Endocytosis. *PLoS ONE*. **8**(4).

Freeze, B., Acosta, D., Pandya, S., Zhao, Y. and Raj, A. 2018. Regional expression of genes mediating trans-synaptic alpha-synuclein transfer predicts regional atrophy in Parkinson disease. *NeuroImage: Clinical*. **18**(November 2017), pp.456–466.

Frischknecht, R., Heine, M., Perrais, D., Seidenbecher, C.I., Choquet, D. and Gundelfinger, E.D. 2009. Brain extracellular matrix affects AMPA receptor lateral mobility and short-term synaptic plasticity. *Nature Neuroscience*.

15(3), pp.94–95.

- Fujiwara, H., Hasegawa, M., Dohmae, N., Kawashima, A., Masliah, E., Goldberg, M.S., Shen, J., Takio, K. and Iwatsubo, T. 2002. A-Synuclein Is Phosphorylated in Synucleinopathy Lesions. *Nature Cell Biology*. **4**(2), pp.160–164.
- Fusco, G., Chen, S.W., Williamson, P.T.F., Cascella, R., Perni, M., Jarvis, J.A., Cecchi, C., Vendruscolo, M., Chiti, F., Cremades, N., Ying, L., Dobson, C.M. and De Simone, A. 2017. Structural basis of membrane disruption and cellular toxicity by  $\alpha$ -synuclein oligomers. *Science*. **358**(6369), pp.1440–1443.
- Fusco, G., Pape, T., Stephens, A.D., Mahou, P., Costa, A.R., Kaminski, C.F., Kaminski Schierle, G.S., Vendruscolo, M., Veglia, G., Dobson, C.M. and De Simone, A. 2016. Structural basis of synaptic vesicle assembly promoted by  $\alpha$ -synuclein. *Nature Communications*. **7**.
- Galtrey, C.M., Kwok, J.C.F., Carulli, D., Rhodes, K.E. and Fawcett, J.W. 2008. Distribution and synthesis of extracellular matrix proteoglycans, hyaluronan, link proteins and tenascin-R in the rat spinal cord. *European Journal of Neuroscience*. **27**(6), pp.1373–1390.
- Galtrey, C.M. and Fawcett, J.W. 2007. The role of chondroitin sulfate proteoglycans in regeneration and plasticity in the central nervous system. *Brain Research Reviews*. **54**(1), pp.1–18.
- Galvagnion, C., Buell, A.K., Meisl, G., Michaels, T.C.T., Vendruscolo, M., Knowles, T.P.J. and Dobson, C.M. 2015. Lipid vesicles trigger  $\alpha$ -synuclein aggregation by stimulating primary nucleation. *Nature Chemical Biology*. **11**(3), pp.229–234.
- Gama, C.I., Tully, S.E., Sotogaku, N., Clark, P.M., Rawat, M., Vaidehi, N., Goddard, W.A., Nishi, A. and Hsieh-Wilson, L.C. 2006. Sulfation patterns of glycosaminoglycans encode molecular recognition and activity. *Nature Chemical Biology*. **2**(9), pp.467–473.
- Gao, R., Wang, M., Lin, J., Hu, L., Li, Z., Chen, C. and Yuan, L. 2018. Spatiotemporal expression patterns of chondroitin sulfate proteoglycan mRNAs in the developing rat brain. *NeuroReport*. **29**(7), pp.517–523.
- Gaspar, R., Meisl, G., Buell, A.K., Young, L., Kaminski, C.F., Knowles, T.P.J., Sparr, E. and Linse, S. 2017. Secondary nucleation of monomers on fibril

surface dominates  $\alpha$ -synuclein aggregation and provides autocatalytic amyloid amplification. *Quarterly Reviews of Biophysics*. **50**.

Geissler, M., Gottschling, C., Aguado, A., Rauch, U., Wetzel, C.H., Hatt, H. and Faissner, A. 2013. Primary Hippocampal Neurons, Which Lack Four Crucial Extracellular Matrix Molecules, Display Abnormalities of Synaptic Structure and Function and Severe Deficits in Perineuronal Net Formation. *Journal of Neuroscience*. **33**(18), pp.7742–7755.

George, J.M., Jin, H., Woods, W.S. and Clayton, D.F. 1995. Characterization of a novel protein regulated during the critical period for song learning in the zebra finch. *Neuron*. **15**(2), pp.361–372.

Gervais-Bernard, H., Xie-Brustolin, J., Mertens, P., Polo, G., Klinger, H., Adamec, D., Broussolle, E. and Thobois, S. 2009. Bilateral subthalamic nucleus stimulation in advanced Parkinson's disease: Five year follow-up. *Journal of Neurology*. **256**(2), pp.225–233.

Geut, H., Hepp, D.H., Foncke, E., Berendse, H.W., Rozemuller, J.M., Huitinga, I. and Van de Berg, W.D.J. 2020. Neuropathological correlates of parkinsonian disorders in a large Dutch autopsy series. *Acta Neuropathologica Communications*. **8**(1), pp.1–14.

Giamanco, K.A., Morawski, M. and Matthews, R.T. 2010. Perineuronal net formation and structure in aggrecan knockout mice. *Neuroscience*. **170**(4), pp.1314–1327.

Giamanco, K.A. and Matthews, R.T. 2012. Deconstructing the perineuronal net: cellular contributions and molecular composition of the neuronal extracellular matrix. *Neuroscience*. **218**, pp.367–384.

Giasson, B.I., Murray, I. V, Trojanowski, J.Q. and Lee, V.M.Y. 2001. A hydrophobic stretch of 12 amino acid residues in the middle of alpha-synuclein is essential for filament assembly. *The Journal of biological chemistry*. **276**(4), pp.2380–6.

Giguère, N., Nanni, S.B. and Trudeau, L.E. 2018. On cell loss and selective vulnerability of neuronal populations in Parkinson's disease. *Frontiers in Neurology*. **9**(JUN).

Goetz, C.G. 2011. The history of Parkinson's disease: Early clinical descriptions and neurological therapies. *Cold Spring Harbor Perspectives in Medicine*. **1**(1).

- González, N., Arcos-López, T., König, A., Quintanar, L., Menacho Márquez, M., Outeiro, T.F. and Fernández, C.O. 2019. Effects of alpha-synuclein post-translational modifications on metal binding. *Journal of Neurochemistry*. **150**(5), pp.507–521.
- Gottschling, C., Wegrzyn, D., Denecke, B. and Faissner, A. 2019. Elimination of the four extracellular matrix molecules tenascin-C, tenascin-R, brevican and neurocan alters the ratio of excitatory and inhibitory synapses. *Scientific Reports*. **9**(1), pp.1–17.
- Graham, J.M. and Sagar, H.J. 1999. A data-driven approach to the study of heterogeneity in idiopathic Parkinson's disease: Identification of three distinct subtypes. *Movement Disorders*. **14**(1), pp.10–20.
- Greffard, S., Verny, M., Bonnet, A.M., Seilhean, D., Hauw, J.J. and Duyckaerts, C. 2010. A stable proportion of Lewy body bearing neurons in the substantia nigra suggests a model in which the Lewy body causes neuronal death. *Neurobiology of Aging*. **31**(1), pp.99–103.
- Gribaudo, S., Tixador, P., Bousset, L., Fenyi, A., Lino, P., Melki, R., Peyrin, J.-M. and Perrier, A.L. 2019. Propagation of  $\alpha$ -Synuclein Strains within Human Reconstructed Neuronal Network. *Stem Cell Reports*. **12**(2018), pp.230–244.
- Gu, Y., Huang, S., Chang, M.C., Worley, P., Kirkwood, A. and Quinlan, E.M. 2013. Obligatory role for the immediate early gene NARP in critical period plasticity. *Neuron*. **79**(2), pp.335–346.
- Guerrero-Ferreira, R., Taylor, N.M.I., Mona, D., Ringler, P., Lauer, M.E., Riek, R., Britschgi, M. and Stahlberg, H. 2018. Cryo-EM structure of alpha-synuclein fibrils. *eLife*. **7**(e36402).
- Guerrero-Ferreira, R., Taylor, N.M.I., Arteni, A.A., Kumari, P., Mona, D., Ringler, P., Britschgi, M., Lauer, M.E., Makky, A., Verasdock, J., Riek, R., Melki, R., Meier, B.H., Böckmann, A., Bousset, L. and Stahlberg, H. 2019. Two new polymorphic structures of human full-length alpha-synuclein fibrils solved by cryo-electron microscopy. *eLife*. **8**, pp.1–24.
- Guimarães, A., Zaremba, S. and Hockfield, S. 1990. Molecular and morphological changes in the cat lateral geniculate nucleus and visual cortex induced by visual deprivation are revealed by monoclonal antibodies Cat-304 and Cat-301. *Journal of Neuroscience*. **10**(9), pp.3014–3024.

- Gustafsson, G., Lööv, C., Persson, E., Lázaro, D.F., Takeda, S., Bergström, J., Erlandsson, A., Sehlin, D., Balaj, L., György, B., Hallbeck, M., Outeiro, T.F., Breakefield, X.O., Hyman, B.T. and Ingelsson, M. 2018. Secretion and Uptake of  $\alpha$ -Synuclein Via Extracellular Vesicles in Cultured Cells. *Cellular and Molecular Neurobiology*. **38**(8), pp.1539–1550.
- Halliday, G.M., Hely, M., Reid, W. and Morris, J. 2008. The progression of pathology in longitudinally followed patients with Parkinson's disease. *Acta Neuropathologica*. **115**(4), pp.409–415.
- Halliday, G.M. and Stevens, C.H. 2011. Glia: Initiators and progressors of pathology in Parkinson's disease. *Movement Disorders*. **26**(1), pp.6–17.
- Han, H., Weinreb, P.H. and Lansbury, P.T. 1995. The core Alzheimer's peptide NAC forms amyloid fibrils which seed and are seeded by  $\beta$ -amyloid: is NAC a common trigger or target in neurodegenerative disease? *Chemistry and Biology*. **2**(3), pp.163–169.
- Harding, A.J., Stimson, E., Henderson, J.M. and Halliday, G.M. 2002. Clinical correlates of selective pathology in the amygdala of patients with Parkinson's disease. *Brain*. **125**(11), pp.2431–2445.
- Hardman, C.D., McRitchie, D.A., Halliday, G.M., Cartwright, H.R. and Morris, J.G.L. 1996. Substantia Nigra Pars Reticulata Neurons in Parkinson's Disease. *Neurodegeneration*. **5**(1), pp.49–55.
- Hasegawa, M., Fujiwara, H., Nonaka, T., Wakabayashi, K., Takahashi, H., Lee, V.M.Y., Trojanowski, J.Q., Mann, D. and Iwatsubo, T. 2002. Phosphorylated  $\alpha$ -synuclein is ubiquitinated in  $\alpha$ -synucleinopathy lesions. *Journal of Biological Chemistry*. **277**(50), pp.49071–49076.
- Haunsø, A., Ibrahim, M., Bartsch, U., Letiembre, M., Celio, M.R. and Menoud, P.A. 2000. Morphology of perineuronal nets in tenascin-R and parvalbumin single and double knockout mice. *Brain Research*. **864**(1), pp.142–145.
- Hausen, D., Brückner, G., Drlicek, M., Härtig, W., Brauer, K. and Bigl, V. 1996. Pyramidal cells ensheathed by perineuronal nets in human motor and somatosensory cortex. *NeuroReport*. **7**, pp.1725–1729.
- Hayashi, N., Miyata, S., Yamada, M., Kamei, K. and Oohira, A. 2005. Neuronal expression of the chondroitin sulfate proteoglycans receptor-type protein-tyrosine phosphatase  $\beta$  and phosphacan. *Neuroscience*. **131**(2), pp.331–348.

- Henderson, M.X., Cornblath, E.J., Darwich, A., Zhang, B., Brown, H., Gathagan, R.J., Sandler, R.M., Bassett, D.S., Trojanowski, J.Q. and Lee, V.M.Y. 2019. Spread of  $\alpha$ -synuclein pathology through the brain connectome is modulated by selective vulnerability and predicted by network analysis. *Nature Neuroscience*. **22**(8), pp.1248–1257.
- Henrich, M.T., Geibl, F.F., Lakshminarasimhan, H., Stegmann, A., Giasson, B.I., Mao, X., Dawson, V.L., Dawson, T.M., Oertel, W.H. and Surmeier, D.J. 2020. Determinants of seeding and spreading of  $\alpha$ -synuclein pathology in the brain. *Science advances*. **6**(46), pp.1–17.
- Hickey, M.G., Demaerschalk, B.M., Caselli, R.J., Parish, J.M. and Wingerchuk, D.M. 2007. “Idiopathic” Rapid-Eye-Movement (REM) Sleep Behavior Disorder Is Associated With Future Development of Neurodegenerative Diseases. *The Neurologist*. **13**(2).
- Hirakawa, S., Oohashi, T., Su, W.D., Yoshioka, H., Murakami, T., Arata, J. and Ninomiya, Y. 2000. The brain link protein-1 (BRAL1): cDNA cloning, genomic structure, and characterization as a novel link protein expressed in adult brain. *Biochem Biophys Res Commun*. **276**(3), pp.982–989.
- Hirsch, E.C., Graybiel, A.M., Duyckaerts, C. and Javoy-Agid, F. 1987. Neuronal loss in the pedunculo-pontine tegmental nucleus in Parkinson disease and in progressive supranuclear palsy. *Proceedings of the National Academy of Sciences of the United States of America*. **84**(16), pp.5976–5980.
- Hirsch, E.C. 1992. Why are nigral catecholaminergic neurons more vulnerable than other cells in Parkinson’s disease? *Annals of Neurology*. **32**(1 S), pp.S88–S93.
- Hodnik, V. and Anderluh, G. 2010. Capture of Intact Liposomes on Biacore Sensor Chips for Protein--Membrane Interaction Studies *In: N. J. MOL and M. J. E. FISCHER, eds. Surface Plasmon Resonance: Methods and Protocols* [online]. Totowa, NJ: Humana Press, pp. 201–211.
- Hoffmann, A., Ettle, B., Bruno, A., Kulinich, A., Hoffmann, A.C., von Wittgenstein, J., Winkler, J., Xiang, W. and Schlachetzki, J.C.M. 2016. Alpha-synuclein activates BV2 microglia dependent on its aggregation state. *Biochemical and Biophysical Research Communications*. **479**(4), pp.881–886.
- Hoffmann, C., Sansevrino, R., Morabito, G., Logan, C., Vabulas, R.M., Ulusoy,

- A., Ganzella, M. and Milovanovic, D. 2021. Synapsin Condensates Recruit alpha-Synuclein. *Journal of Molecular Biology*. **433**(12), p.166961.
- Holmes, B.B., DeVos, S.L., Kfoury, N., Li, M., Jacks, R., Yanamandra, K., Ouidja, M.O., Brodsky, F.M., Marasa, J., Bagchi, D.P., Kotzbauer, P.T., Miller, T.M., Papy-Garcia, D. and Diamond, M.I. 2013. Heparan sulfate proteoglycans mediate internalization and propagation of specific proteopathic seeds. *Proceedings of the National Academy of Sciences*. **110**(33), pp.E3138–E3147.
- Horii-Hayashi, N., Sasagawa, T., Matsunaga, W. and Nishi, M. 2015. Development and Structural Variety of the Chondroitin Sulfate Proteoglycans-Contained Extracellular Matrix in the Mouse Brain. *Neural Plasticity*. **2015**.
- Hou, X., Yoshioka, N., Tsukano, H., Sakai, A., Miyata, S., Watanabe, Y., Yanagawa, Y., Sakimura, K., Takeuchi, K., Kitagawa, H., Hensch, T.K., Shibuki, K., Igarashi, M. and Sugiyama, S. 2017. Chondroitin Sulfate Is Required for Onset and Offset of Critical Period Plasticity in Visual Cortex. *Scientific Reports*. **7**(1), pp.1–17.
- Howlett, D.R., Whitfield, D., Johnson, M., Attems, J., O'Brien, J.T., Aarsland, D., Lai, M.K.P., Lee, J.H., Chen, C., Ballard, C., Hortobágyi, T. and Francis, P.T. 2015. Regional Multiple Pathology Scores Are Associated with Cognitive Decline in Lewy Body Dementias. *Brain pathology (Zurich, Switzerland)*. **25**(4), pp.401–408.
- Huang, C., Ren, G., Zhou, H. and Wang, C.C. 2005. A new method for purification of recombinant human  $\alpha$ -synuclein in *Escherichia coli*. *Protein Expression and Purification*. **42**(1), pp.173–177.
- Huang, M., Wang, B., Li, X., Fu, C., Wang, C. and Kang, X. 2019.  $\alpha$ -Synuclein: A multifunctional player in exocytosis, endocytosis, and vesicle recycling. *Frontiers in Neuroscience*. **13**(JAN), pp.1–8.
- Huang, Z.J., Kirkwood, A., Pizzorusso, T., Porciatti, V., Morales, B., Bear, M.F., Maffei, L. and Tonegawa, S. 1999. BDNF regulates the maturation of inhibition and the critical period of plasticity in mouse visual cortex. *Cell*. **98**(6), pp.739–755.
- Hudák, A., Kusz, E., Domonkos, I., Jósvay, K., Kodamullil, A.T., Szilák, L., Hofmann-Apitius, M. and Letoha, T. 2019. Contribution of syndecans to

- cellular uptake and fibrillation of  $\alpha$ -synuclein and tau. *Scientific Reports*. **9**(1), pp.1–19.
- Hughes, A.J., Daniel, S.E., Kilford, L. and Lees, A.J. 1992. Accuracy of clinical diagnosis of idiopathic Parkinson's disease: A clinico-pathological study of 100 cases. *Journal of Neurology Neurosurgery and Psychiatry*. **55**(3), pp.181–184.
- Huisman, E., Uylings, H.B.M. and Hoogland, P. V. 2004. A 100% increase of dopaminergic cells in the olfactory bulb may explain hyposmia in parkinson's disease. *Movement Disorders*. **19**(6), pp.687–692.
- Huisman, E., Uylings, H.B.M. and Hoogland, P. V. 2008. Gender-related changes in increase of dopaminergic neurons in the olfactory bulb of Parkinson's disease patients. *Movement Disorders*. **23**(10), pp.1407–1413.
- Hunyadi, A., Gaál, B., Matesz, C., Meszar, Z., Morawski, M., Reimann, K., Lendvai, D., Alpar, A., Wéber, I. and Rácz, É. 2020. Distribution and classification of the extracellular matrix in the olfactory bulb. *Brain Structure and Function*. **225**(1), pp.321–344.
- Ihse, E., Yamakado, H., Van Wijk, X.M., Lawrence, R., Esko, J.D. and Masliah, E. 2017. Cellular internalization of alpha-synuclein aggregates by cell surface heparan sulfate depends on aggregate conformation and cell type. *Scientific Reports*. **7**(1), pp.1–10.
- Ikenoue, T., Lee, Y.H., Kardos, J., Saiki, M., Yagi, H., Kawata, Y. and Goto, Y. 2014. Cold denaturation of  $\alpha$ -synuclein amyloid fibrils. *Angewandte Chemie - International Edition*. **53**(30), pp.7799–7804.
- Ilijina, M., Garcia, G.A., Horrocks, M.H., Tosatto, L., Choi, M.L., Ganzinger, K.A., Abramov, A.Y., Gandhi, S., Wood, N.W., Cremades, N., Dobson, C.M., Knowles, T.P.J. and Klenerman, D. 2016. Kinetic model of the aggregation of alpha-synuclein provides insights into prion-like spreading. *Proceedings of the National Academy of Sciences of the United States of America*. **113**(9), pp.1206–1215.
- Illes-Toth, E., Ramos, M.R., Cappai, R., Dalton, C.F. and Smith, D.P. 2015. Distinct higher-order  $\alpha$ -synuclein oligomers induce intracellular aggregation. *Biochem. J*. **468**, pp.485–493.
- Imai, T. 2014. Construction of functional neuronal circuitry in the olfactory bulb. *Seminars in Cell and Developmental Biology*. **35**, pp.180–188.

- Iranzo, A., Fernández-Arcos, A., Tolosa, E., Serradell, M., Molinuevo, J.L., Valldeoriola, F., Gelpi, E., Vilaseca, I., Sánchez-Valle, R., Lladó, A., Gaig, C. and Santamaría, J. 2014. Neurodegenerative disorder risk in idiopathic REM sleep behavior disorder: Study in 174 patients. *PLoS ONE*. **9**(2).
- Irvine, S.F. and Kwok, J.C.F. 2018. Perineuronal nets in spinal motoneurons: Chondroitin sulphate proteoglycan around alpha motoneurons. *International Journal of Molecular Sciences*. **19**(4).
- Itano, N., Sawai, T., Yoshida, M., Lenas, P., Yamada, Y., Imagawa, M., Shinomura, T., Hamaguchi, M., Yoshida, Y., Ohnuki, Y., Miyauchi, S., Spicer, A.P., McDonald, J.W. and Kimata, K. 1999. Three isoforms of mammalian hyaluronan synthases have distinct enzymatic properties. *The Journal of biological chemistry*. **274**(35), pp.25085–92.
- Jackson, J., Papadopulos, A., Meunier, F.A., McCluskey, A., Robinson, P.J. and Keating, D.J. 2015. Small molecules demonstrate the role of dynamin as a bi-directional regulator of the exocytosis fusion pore and vesicle release. *Molecular Psychiatry*. **20**(7), pp.810–819.
- Jain, M.K., Singh, P., Roy, S. and Bhat, R. 2018. Comparative Analysis of the Conformation, Aggregation, Interaction, and Fibril Morphologies of Human  $\alpha$ -,  $\beta$ -, and  $\gamma$ -Synuclein Proteins. *Biochemistry*. **57**(26), pp.3830–3848.
- Jakes, R., Spillantini, M.G. and Goedert, M. 1994. Identification of two distinct synucleins from human brain. *FEBS Letters*. **345**(1), pp.27–32.
- Jankovic, J. 2008. Parkinson's disease: Clinical features and diagnosis. *Journal of Neurology, Neurosurgery and Psychiatry*. **79**(4), pp.368–376.
- Jankovic, J., McDermott, M., Carter, J., Gauthier, S., Goetz, C., Golbe, L., Huber, S., Koller, W., Olanow, C. and Shoulson, I. 1990. Variable expression of Parkinson's disease: a base-line analysis of the DATATOP cohort. The Parkinson Study Group. *Neurology*. **40**(10), pp.1529–1534.
- Jellinger, K.A. 2018. *Dementia with Lewy bodies and Parkinson's disease-dementia: current concepts and controversies* [online]. Springer Vienna.
- Jiang, P., Gan, M., Yen, S.-H., McLean, P.J. and Dickson, D.W. 2017. Impaired endo-lysosomal membrane integrity accelerates the seeding progression of  $\alpha$ -synuclein aggregates. *Scientific Reports*. **7**(1), p.7690.
- Joelving, F.C., Billeskov, R., Christensen, J.R., West, M. and Pakkenberg, B. 2006. Hippocampal neuron and glial cell numbers in Parkinson's disease—

- A stereological study. *Hippocampus*. **1031**, pp.1026–1031.
- John, N., Krügel, H., Frischknecht, R., Smalla, K.H., Schultz, C., Kreutz, M.R., Gundelfinger, E.D. and Seidenbecher, C.I. 2006. Brevican-containing perineuronal nets of extracellular matrix in dissociated hippocampal primary cultures. *Molecular and Cellular Neuroscience*. **31**(4), pp.774–784.
- Jost, W.H. and Eckardt, V.F. 2003. Constipation in idiopathic Parkinson's disease. *Scandinavian Journal of Gastroenterology*. **38**(7), pp.681–686.
- Kalaitzakis, M.E., Graeber, M.B., Gentleman, S.M. and Pearce, R.K.B. 2008. The dorsal motor nucleus of the vagus is not an obligatory trigger site of Parkinson's disease: A critical analysis of  $\alpha$ -synuclein staging. *Neuropathology and Applied Neurobiology*. **34**(3), pp.284–295.
- Kalb, R.G. and Hockfield, S. 1990. Induction of a Neuronal Proteoglycan by the NMDA Receptor in the Developing Spinal Cord. *Science*. **250**, pp.294–296.
- Kalia, L. V. and Lang, A.E. 2015. Parkinson's disease. *The Lancet*. **386**(9996), pp.896–912.
- Kalia, L. V. and Lang, A.E. 2016. Parkinson disease in 2015: Evolving basic, pathological and clinical concepts in PD. *Nature Reviews Neurology*. **12**(2), pp.65–66.
- Kang, L., Moriarty, G.M., Woods, L.A., Ashcroft, A.E., Radford, S.E. and Baum, J. 2012. N-terminal acetylation of  $\alpha$ -synuclein induces increased transient helical propensity and decreased aggregation rates in the intrinsically disordered monomer. *Protein Science*. **21**(7), pp.911–917.
- Karpowicz, R.J., Haney, C.M., Mihaila, T.S., Sandler, R.M., Petersson, E.J. and Lee, V.M.Y. 2017. Selective imaging of internalized proteopathic alpha-synuclein seeds in primary neurons reveals mechanistic insight into transmission of synucleinopathies. *Journal of Biological Chemistry*. **292**(32), pp.13482–13497.
- Kempster, P.A., O'Sullivan, S.S., Holton, J.L., Revesz, T. and Lees, A.J. 2010. Relationships between age and late progression of Parkinson's disease: A clinico-pathological study. *Brain*. **133**(6), pp.1755–1762.
- Kim, C., Ho, D.-H., Suk, J.-E., You, S., Michael, S., Kang, J., Lee, S.J., Masliah, E., Hwang, D., Lee, H. and Lee, S.J. 2013. Neuron-released oligomeric  $\alpha$ -synuclein is an endogenous agonist of TLR2 for paracrine activation of microglia. *Nature Communications*. **4**, pp.1512–1562.

- Kim, C., Lee, H., Masliah, E. and Lee, S.J. 2016. Non-cell-autonomous Neurotoxicity of  $\alpha$ -synuclein through microglial toll-like receptor 2. *Experimental Neurobiology*. **25**(3), pp.113–119.
- Kingsbury, A.E., Bandopadhyay, R., Silveira-Moriyama, L., Ayling, H., Kallis, C., Sterlacci, W., Maeir, H., Poewe, W. and Lees, A.J. 2010. Brain stem pathology in Parkinson's disease: An evaluation of the Braak staging model. *Movement Disorders*. **25**(15), pp.2508–2515.
- Kitagawa, H., Tsutsumi, K., Tone, Y. and Sugahara, K. 1997. Developmental regulation of the sulfation profile of chondroitin sulfate chains in the chicken embryo brain. *Journal of Biological Chemistry*. **272**(50), pp.31377–31381.
- Knowles, T.P.J., Fitzpatrick, A.W., Meehan, S., Mott, H.R., Vendruscolo, M., Dobson, C.M. and Welland, M.E. 2007. Role of intermolecular forces in defining material properties of protein nanofibrils. *Science*. **318**(5858), pp.1900–1903.
- Kobayashi, K., Emson, P.C. and Mountjoy, C.Q. 1989. Vicia villosa lectin-positive neurones in human cerebral cortex. Loss in Alzheimer-type dementia. *Brain Research*. **498**(1), pp.170–174.
- Köppe, G., Brückner, G., Brauer, K., Härtig, W. and Bigl, V. 1997. Developmental patterns of proteoglycan-containing extracellular matrix in perineuronal nets and neuropil of the postnatal rat brain. *Cell and Tissue Research*. **288**(1), pp.33–41.
- Kordower, J.H., Chu, Y., Hauser, R.A., Freeman, T.B. and Olanow, C.W. 2008. Lewy body-like pathology in long-term embryonic nigral transplants in Parkinson's disease. *Nature Medicine*. **14**(5), pp.504–506.
- Koros, C., Simitsi, A. and Stefanis, L. 2017. Genetics of Parkinson's Disease: Genotype–Phenotype Correlations *In: International Review of Neurobiology* [online]. Elsevier Inc., pp. 197–231.
- Kuan, W.L., Stott, K., He, X., Wood, T.C., Yang, S., Kwok, J.C.F., Hall, K., Zhao, Y., Tietz, O., Aigbirhio, F.I., Vernon, A.C. and Barker, R.A. 2019. Systemic  $\alpha$ -synuclein injection triggers selective neuronal pathology as seen in patients with Parkinson's disease. *Molecular Psychiatry*.
- Kuusisto, E., Parkkinen, L. and Alafuzoff, I. 2003. Morphogenesis of Lewy Bodies: Dissimilar Incorporation of  $\alpha$ -Synuclein, Ubiquitin, and p62. *Journal of Neuropathology and Experimental Neurology*. **62**(12), pp.1241–1253.

- Kuzuhara, S., Mori, H., Izumiyama, N., Yoshimura, M. and Ihara, Y. 1988. Lewy bodies are ubiquitinated. *Acta Neuropathologica*. **75**(4), pp.345–353.
- Kwok, J.C.F., Carulli, D. and Fawcett, J.W. 2010. In vitro modeling of perineuronal nets: Hyaluronan synthase and link protein are necessary for their formation and integrity. *Journal of Neurochemistry*. **114**(5), pp.1447–1459.
- Lander, C., Kind, P., Maleski, M. and Hockfield, S. 1997. A family of activity-dependent neuronal cell-surface chondroitin sulfate proteoglycans in cat visual cortex. *Journal of Neuroscience*. **17**(6), pp.1928–1939.
- Larsen, K.E., Schmitz, Y., Troyer, M.D., Mosharov, E., Dietrich, P., Quazi, A.Z., Savalle, M., Nemani, V.M., Chaudhry, F.A., Edwards, R.H., Stefanis, L. and Sulzer, D. 2006.  $\alpha$ -Synuclein Overexpression in PC12 and Chromaffin Cells Impairs Catecholamine Release by Interfering with a Late Step in Exocytosis. *Journal of Neuroscience*. **26**(46), pp.11915–11922.
- Lashuel, H.A., Petre, B.M., Wall, J., Simon, M., Nowak, R.J., Walz, T. and Lansbury, P.T. 2002. Alpha-Synuclein, Especially the Parkinson's Disease-Associated Mutants, Forms Pore-Like Annular and Tubular Protofibrils. *Journal of Molecular Biology*. **322**(5), pp.1089–1102.
- Lashuel, H.A. and Grillo-Bosch, D. 2005. In vitro preparation of prefibrillar intermediates of amyloid- $\beta$  and  $\alpha$ -synuclein. *Methods in molecular biology (Clifton, N.J.)*. **299**, pp.19–33.
- Lautenschläger, J., Kaminski, C.F. and Kaminski Schierle, G.S. 2017. Alpha-Synuclein - Regulator of Exocytosis, Endocytosis, or Both? *Trends in Cell Biology*. **27**(7), pp.468–479.
- Lautenschläger, J., Stephens, A.D., Fusco, G., Ströhl, F., Curry, N., Zacharopoulou, M., Michel, C.H., Laine, R., Nespovitaya, N., Fantham, M., Pinotsi, D., Zago, W., Fraser, P.E., Tandon, A., St George-Hyslop, P., Rees, E., Phillips, J.J., De Simone, A., Kaminski, C.F. and Schierle, G.S.K. 2018. C-terminal calcium binding of  $\alpha$ -synuclein modulates synaptic vesicle interaction. *Nature Communications*. **9**(1).
- Lebouvier, T., Chaumette, T., Damier, P., Coron, E., Touchefeu, Y., Vrignaud, S., Naveilhan, P., Galmiche, J.P., Bruley des Varannes, S., Derkinderen, P. and Neunlist, M. 2008. Pathological lesions in colonic biopsies during Parkinson's disease. *Gut*. **57**(12), pp.1741–1743.

- Lee, B.R. and Kamitani, T. 2011. Improved immunodetection of endogenous Alpha-synuclein. *PLoS ONE*. **6**(8).
- Lee, H.-J., Suk, J.-E., Bae, E.-J., Lee, J.-H., Paik, S.R. and Lee, S.-J. 2008a. Assembly-dependent endocytosis and clearance of extracellular Alpha-synuclein. *The international journal of biochemistry & cell biology*. **40**, pp.1835–1849.
- Lee, H., Cho, E.D., Lee, K.W., Kim, J.H., Cho, S.G. and Lee, S.J. 2013. Autophagic failure promotes the exocytosis and intercellular transfer of  $\alpha$ -synuclein. *Experimental and Molecular Medicine*. **45**(5), pp.1–9.
- Lee, H., Suk, J.E., Bae, E.J. and Lee, S.J. 2008b. Clearance and deposition of extracellular  $\alpha$ -synuclein aggregates in microglia. *Biochemical and Biophysical Research Communications*. **372**(3), pp.423–428.
- Lee, H., Patel, S. and Lee, S.-J. 2005. Intravesicular Localization and Exocytosis of Alpha-Synuclein and its Aggregates. *Journal of Neuroscience*. **25**(25), pp.6016–6024.
- Lee, H.J., Bae, E.J. and Lee, S.J. 2014. Extracellular  $\alpha$ -synuclein-a novel and crucial factor in Lewy body diseases. *Nature Reviews Neurology*. **10**(2), pp.92–98.
- Lendvai, D., Morawski, M., Négyessy, L., Gáti, G., Jäger, C., Baksa, G., Glasz, T., Attems, J., Tanila, H., Arendt, T., Harkany, T. and Alpár, A. 2013. Neurochemical mapping of the human hippocampus reveals perisynaptic matrix around functional synapses in Alzheimer's disease. *Acta Neuropathologica*. **125**(2), pp.215–229.
- Lewis, S.J.G., Foltynie, T., Blackwell, A.D., Bobbins, T.W., Owen, A.M. and Barker, R.A. 2005. Heterogeneity of Parkinson's disease in the early clinical stages using a data driven approach. *Journal of Neurology, Neurosurgery and Psychiatry*. **76**(3), pp.343–348.
- Li, J.Y., Englund, E., Holton, J.L., Soulet, D., Hagell, P., Lees, A.J., Lashley, T., Quinn, N.P., Rehncrona, S., Björklund, A., Widner, H., Revesz, T., Lindvall, O. and Brundin, P. 2008. Lewy bodies in grafted neurons in subjects with Parkinson's disease suggest host-to-graft disease propagation. *Nature Medicine*. **14**(5), pp.501–503.
- Li, W., West, N., Colla, E., Pletnikova, O., Troncoso, J.C., Marsh, L., Dawson, T.M., Jäkälä, P., Hartmann, T., Price, D.L. and Lee, M.K. 2005.

- Aggregation promoting C-terminal truncation of  $\alpha$ -synuclein is a normal cellular process and is enhanced by the familial Parkinson's disease-linked mutations. *Proceedings of the National Academy of Sciences of the United States of America*. **102**(6), pp.2162–2167.
- Lill, C.M. 2016. Genetics of Parkinson's disease. *Molecular and Cellular Probes*. **30**(6), pp.386–396.
- Lipachev, N., Arnst, N., Melnikova, A., Jääliñoja, H., Kochneva, A., Zhigalov, A., Kuleskaya, N., Aganov, A. V., Mavlikeev, M., Rauvala, H., Kiyasov, A.P. and Paveliev, M. 2019. Quantitative changes in perineuronal nets in development and posttraumatic condition. *Journal of Molecular Histology*. **50**(3), pp.203–216.
- Lodato, S., Rouaux, C., Quast, K.B., Jantrachotechatchawan, C., Studer, M., Hensch, T.K. and Arlotta, P. 2011. Excitatory Projection Neuron Subtypes Control the Distribution of Local Inhibitory Interneurons in the Cerebral Cortex. *Neuron*. **69**(4), pp.763–779.
- Loers, G., Liao, Y., Hu, C., Xue, W., Shen, H., Zhao, W. and Schachner, M. 2019. Identification and characterization of synthetic chondroitin-4-sulfate binding peptides in neuronal functions. *Scientific Reports*. (November 2018), pp.1–11.
- Logan, T., Bendor, J., Toupin, C., Thorn, K. and Edwards, R.H. 2017.  $\alpha$ -Synuclein promotes dilation of the exocytotic fusion pore. *Nature Neuroscience*. **20**(5), pp.681–689.
- Lohmann, S., Bernis, M.E., Tachu, B.J., Ziemiński, A., Grigoletto, J. and Tamgüney, G. 2019. Oral and intravenous transmission of  $\alpha$ -synuclein fibrils to mice. *Acta Neuropathologica*. **138**(4), pp.515–533.
- López-González, I., Schlüter, A., Aso, E., Garcia-Esparcia, P., Ansoleaga, B., Llorens, F., Carmona, M., Moreno, J., Fusó, A., Portero-Otin, M., Pamplona, R., Pujol, A. and Ferrer, I. 2015. Neuroinflammatory signals in Alzheimer disease and APP/PS1 transgenic mice: Correlations with plaques, tangles, and oligomeric species. *Journal of Neuropathology and Experimental Neurology*. **74**(4), pp.319–344.
- López González, I., Garcia-Esparcia, P., Llorens, F. and Ferrer, I. 2016. Genetic and transcriptomic profiles of inflammation in neurodegenerative diseases: Alzheimer, Parkinson, Creutzfeldt-Jakob and Tauopathies. *International*

*Journal of Molecular Sciences.* **17**(2), pp.1–23.

- Lorenzen, N., Nielsen, S.B., Yoshimura, Y., Vad, B.S., Andersen, C.B., Betzer, C., Kaspersen, J.D., Christiansen, G., Pedersen, J.S., Jensen, P.H., Mulder, F.A.A. and Otzen, D.E. 2014. How epigallocatechin gallate can inhibit  $\alpha$ -synuclein oligomer toxicity in vitro. *Journal of Biological Chemistry.* **289**(31), pp.21299–21310.
- Low, V., Ben-Shlomo, Y., Coward, E., Fletcher, S., Walker, R.W. and Clarke, C.E. 2015. Measuring the burden and mortality of hospitalisation in Parkinson's disease: A cross-sectional analysis of the English Hospital Episodes Statistics database 2009–2013. *Parkinsonism & Related Disorders.* **21**(5), pp.449–454.
- Lucas, H.R. and Lee, J.C. 2011. Copper(ii) enhances membrane-bound  $\alpha$ -synuclein helix formation. *Metallomics.* **3**(3), pp.280–283.
- Luk, K.C., Covell, D.J., Kehm, V.M., Zhang, B., Song, I.Y., Byrne, M.D., Pitkin, R.M., Decker, S.C., Trojanowski, J.Q. and Lee, V.M.Y. 2016. Molecular and Biological Compatibility with Host Alpha-Synuclein Influences Fibril Pathogenicity. *Cell Reports.* **16**(12), pp.3373–3387.
- Luk, K.C., Kehm, V., Carroll, J., Zhang, B., Brien, P.O., Trojanowski, J.Q. and Lee, V.M.Y. 2012. Pathological  $\alpha$ -Synuclein Transmission Initiates Parkinson-like Neurodegeneration in Nontransgenic Mice. *Science.* **338**(November), pp.949–954.
- Lundell, A., Olin, A.I., Mörgelin, M., Al-Karadaghi, S., Aspberg, A. and Logan, D.T. 2004. Structural basis for interactions between tenascins and lectican C-type lectin domains: Evidence for a crosslinking role for tenascins. *Structure.* **12**(8), pp.1495–1506.
- Mahul-Mellier, A.-L., Burtscher, J., Maharjan, N., Weerens, L., Croisier, M., Kuttler, F., Leleu, M., Knott, G. and Lashuel, H.A. 2020. The process of Lewy body formation, rather than simply alpha-synuclein fibrillization, is one of the major driver of neurodegeneration in synucleinopathies. *Proceedings of the National Academy of Sciences.* **117**(9), pp.4971–4982.
- Makky, A., Bousset, L., Polesel-Maris, J. and Melki, R. 2016. Nanomechanical properties of distinct fibrillar polymorphs of the protein  $\alpha$ -synuclein. *Scientific Reports.* **6**, pp.1–10.
- Maltsev, A.S., Ying, J. and Bax, A. 2012. Impact of N-terminal acetylation of  $\alpha$ -

- synuclein on its random coil and lipid binding properties. *Biochemistry*. **51**(25), pp.5004–5013.
- Mao, X., Tianhao Ou, M., Karuppagounder, S.S., Kam, T.-I., Yin, X., Xiong, Y., Ge, P., Umanah, G.E., Brahmachari, S., Shin, J.-H., Kang, H.C., Lam, S., Keiler, J.A., Tyson, J., Kim, D., Panicker, N., Yun, S.P., Workman, C.J., Vignali, D.A.A., Dawson, V.L., Ko, H.S. and Dawson, T.M. 2016. Pathological  $\alpha$ -synuclein transmission initiated by binding lymphocyte-activation gene 3. *Science*. **353**(6307), pp.1–33.
- Markopoulou, K., Dickson, D.W., McComb, R.D., Wszolek, Z.K., Katechalidou, L., Avery, L., Stansbury, M.S. and Chase, B.A. 2008. Clinical, neuropathological and genotypic variability in SNCA A53T familial Parkinson's disease. *Acta Neuropathologica*. **116**(1), pp.25–35.
- Markram, H., Toledo-Rodriguez, M., Wang, Y., Gupta, A., Silberberg, G. and Wu, C. 2004. Interneurons of the neocortical inhibitory system. *Nature Reviews Neuroscience*. **5**(10), pp.793–807.
- Maroteaux, L., Campanelli, J. and Scheller, R.H. 1988. Synuclein: a neuron-specific protein localized to the nucleus and presynaptic nerve terminal. *Journal of Neuroscience*. **8**(8), pp.2804–2815.
- Maroteaux, L. and Scheller, R.H. 1991. The rat brain synucleins; family of proteins transiently associated with neuronal membrane. *Molecular Brain Research*. **11**(3–4), pp.335–343.
- Mason, R.J., Paskins, A.R., Dalton, C.F. and Smith, D.P. 2016. Copper Binding and Subsequent Aggregation of  $\alpha$ -Synuclein Are Modulated by N-Terminal Acetylation and Ablated by the H50Q Missense Mutation. *Biochemistry*. **55**, pp.4737–4741.
- Masuda-Suzukake, M., Nonaka, T., Hosokawa, M., Kubo, M., Shimosawa, A., Akiyama, H. and Hasegawa, M. 2014. Pathological alpha-synuclein propagates through neural networks. *Acta Neuropathologica Communications*. **2**(1), p.88.
- Matthews, R.T., Kelly, G.M., Zerillo, C. a, Gray, G., Tiemeyer, M. and Hockfield, S. 2002. Aggrecan glycoforms contribute to the molecular heterogeneity of perineuronal nets. *The Journal of neuroscience : the official journal of the Society for Neuroscience*. **22**(17), pp.7536–7547.
- Mauney, S.A., Athanas, K.M., Pantazopoulos, H., Shaskan, N., Passeri, E.,

- Berretta, S. and Woo, T.U.W. 2013. Developmental pattern of perineuronal nets in the human prefrontal cortex and their deficit in schizophrenia. *Biological Psychiatry*. **74**(6), pp.427–435.
- Maureen E. Taylor, Kurt Drickamer, Ronald L. Schnaar, Marilyn E. Etzler, and A.V. 2015. Discovery and Classification of Glycan-Binding Proteins *In: A. VARKI et al., eds. Essentials of Glycobiology*. New York: Cold Spring Harbor Laboratory Press, pp. 375–386.
- Mayer, C., Hafemeister, C., Bandler, R.C., Machold, R., Batista Brito, R., Jaglin, X., Allaway, K., Butler, A., Fishell, G. and Satija, R. 2018. Developmental diversification of cortical inhibitory interneurons. *Nature*. **555**(7697), pp.457–462.
- McRae, P.A., Rocco, M.M., Kelly, G., Brumberg, J.C. and Matthews, R.T. 2007. Sensory Deprivation Alters Aggrecan and Perineuronal Net Expression in the Mouse Barrel Cortex. *Journal of Neuroscience*. **27**(20), pp.5405–5413.
- Mehra, S., Ghosh, D., Kumar, R., Mondal, M., Gadhe, L.G., Das, S., Anoop, A., Jha, N.N., Jacob, R.S., Chatterjee, D., Ray, S., Singh, N., Kumar, A. and Maji, S.K. 2018. Glycosaminoglycans have variable effects on  $\alpha$ -synuclein aggregation and differentially affect the activities of the resulting amyloid fibrils. *Journal of Biological Chemistry*. **293**(34), pp.12975–12991.
- Mezias, C., Rey, N.L., Brundin, P. and Raj, A. 2020. Neural connectivity predicts spreading of alpha-synuclein pathology in fibril-injected mouse models: Involvement of retrograde and anterograde axonal propagation. *Neurobiology of Disease*. **134**(June 2019), p.104623.
- Middleton, E.R. and Rhoades, E. 2010. Effects of curvature and composition on  $\alpha$ -synuclein binding to lipid vesicles. *Biophysical Journal*. **99**(7), pp.2279–2288.
- Mikami, T. and Kitagawa, H. 2013. Biosynthesis and function of chondroitin sulfate. *Biochimica et Biophysica Acta - General Subjects*. **1830**(10), pp.4719–4733.
- Milev, P., Chiba, A., Häring, M., Rauvala, H., Schachner, M., Ranscht, B., Margolis, R.K. and Margolis, R.U. 1998. High affinity binding and overlapping localization of neurocan and phosphacan/protein-tyrosine phosphatase- $\zeta/\beta$  with tenascin-R, amphoterin, and the heparin-binding growth-associated molecule. *Journal of Biological Chemistry*. **273**(12),

pp.6998–7005.

- Miotto, M.C., Pavese, M.D., Quintanar, L., Zweckstetter, M., Griesinger, C. and Fernández, C.O. 2017. Bioinorganic Chemistry of Parkinson's Disease: Affinity and Structural Features of Cu(I) Binding to the Full-Length  $\beta$ -Synuclein Protein. *Inorganic Chemistry*. **56**(17), pp.10387–10395.
- Miotto, M.C., Valiente-Gabioud, A.A., Rossetti, G., Zweckstetter, M., Carloni, P., Selenko, P., Griesinger, C., Binolfi, A. and Fernández, C.O. 2015. Copper Binding to the N-Terminally Acetylated, Naturally Occurring Form of Alpha-Synuclein Induces Local Helical Folding. *Journal of the American Chemical Society*. **137**(20), pp.6444–6447.
- Miyata, S., Nishimura, Y., Hayashi, N. and Oohira, A. 2005. Construction of perineuronal net-like structure by cortical neurons in culture. *Neuroscience*. **136**(1), pp.95–104.
- Miyata, S., Nishimura, Y. and Nakashima, T. 2007. Perineuronal nets protect against amyloid  $\beta$ -protein neurotoxicity in cultured cortical neurons. *Brain Research*. **1150**(1), pp.200–206.
- Miyata, S., Komatsu, Y., Yoshimura, Y., Taya, C. and Kitagawa, H. 2012. Persistent cortical plasticity by upregulation of chondroitin 6-sulfation. *Nature Neuroscience*. **15**.
- Miyata, S., Nadanaka, S., Igarashi, M. and Kitagawa, H. 2018. Structural Variation of Chondroitin Sulfate Chains Contributes to the Molecular Heterogeneity of Perineuronal Nets. *Frontiers in Integrative Neuroscience*. **12**, p.3.
- Miyata, S. and Kitagawa, H. 2016. Chondroitin 6-Sulfation Regulates Perineuronal Net Formation by Controlling the Stability of Aggrecan. *Neural Plasticity*. **2016**, pp.7–9.
- Monderer, R. and Thorpy, M. 2009. Sleep Disorders and Daytime Sleepiness in Parkinson's Disease. *Current Neurology and Neuroscience Reports*. **9**(2), pp.173–180.
- Morawski, M., Brückner, G., Jäger, C., Seeger, G., Matthews, R.T. and Arendt, T. 2012a. Involvement of perineuronal and perisynaptic extracellular matrix in Alzheimer's disease neuropathology. *Brain Pathology*. **22**(4), pp.547–561.
- Morawski, M., Brückner, G., Jäger, C., Seeger, G., Matthews, R.T. and Arendt,

- T. 2012b. Involvement of Perineuronal and Perisynaptic Extracellular Matrix in Alzheimer's Disease Neuropathology. *Brain Pathology*. **22**(4), pp.547–561.
- Morawski, M., Reinert, T., Meyer-Klaucke, W., Wagner, F.E., Tröger, W., Reinert, A., Jäger, C., Brückner, G. and Arendt, T. 2015. Ion exchanger in the brain: Quantitative analysis of perineuronally fixed anionic binding sites suggests diffusion barriers with ion sorting properties. *Scientific Reports*. **5**(1), p.16471.
- Morawski, M., Brückner, G., Jäger, C., Seeger, G. and Arendt, T. 2010a. Neurons associated with aggrecan-based perineuronal nets are protected against tau pathology in subcortical regions in Alzheimer's disease. *Neuroscience*. **169**(3), pp.1347–1363.
- Morawski, M., Pavlica, S., Seeger, G., Grosche, J., Kouznetsova, E., Schliebs, R., Brückner, G. and Arendt, T. 2010b. Perineuronal nets are largely unaffected in Alzheimer model Tg2576 mice. *Neurobiology of Aging*. **31**(7), pp.1254–1256.
- Morawski, M., Dityatev, A., Hartlage-Rü Bsamén, M., Blosa, M., Holzer, M., Flach, K., Pavlica, S., Dityateva, G., Grosche, J., Brückner, G. and Schachner, M. 2014. Tenascin-R promotes assembly of the extracellular matrix of perineuronal nets via clustering of aggrecan. *Philosophical Transactions of the Royal Society B: Biological Sciences*. **369**(1654), pp.20140046–20140046.
- Morawski, M., Reinert, T., Brückner, G., Wagner, F.E., Arendt, T. and Tröger, W. 2005. The binding of iron to perineuronal nets: A combined nuclear microscopy and Mossbauer study. *Hyperfine Interactions*. **159**(1–4), pp.285–291.
- Mori, F., Tanji, K., Zhang, H., Kakita, A., Takahashi, H. and Wakabayashi, K. 2008.  $\alpha$ -Synuclein pathology in the neostriatum in Parkinson's disease. *Acta Neuropathologica*. **115**(4), pp.453–459.
- Mosharov, E. V., Larsen, K.E., Kanter, E., Phillips, K.A., Wilson, K., Schmitz, Y., Krantz, D.E., Kobayashi, K., Edwards, R.H. and Sulzer, D. 2009. Interplay between Cytosolic Dopamine, Calcium, and  $\alpha$ -Synuclein Causes Selective Death of Substantia Nigra Neurons. *Neuron*. **62**(2), pp.218–229.
- Mueller, A.L., Davis, A., Sovich, S., Carlson, S.S. and Robinson, F.R. 2016.

Distribution of N-Acetylgalactosamine-Positive Perineuronal Nets in the Macaque Brain : Anatomy and Implications. . **2016**.

- Mundiñano, I.C., Caballero, M.C., Ordóñez, C., Hernandez, M., DiCaudo, C., Marcilla, I., Erro, M.E., Tuñon, M.T. and Luquin, M.R. 2011. Increased dopaminergic cells and protein aggregates in the olfactory bulb of patients with neurodegenerative disorders. *Acta Neuropathologica*. **122**(1), pp.61–74.
- Murphy, D.D., Rueter, S.M., Trojanowski, J.Q. and Lee, V.M.Y. 2000. Synucleins are developmentally expressed, and  $\alpha$ -synuclein regulates the size of the presynaptic vesicular pool in primary hippocampal neurons. *Journal of Neuroscience*. **20**(9), pp.3214–3220.
- Nadanaka, S., Miyata, S., Yaqiang, B., Tamura, J.I., Habuchi, O. and Kitagawa, H. 2020. Reconsideration of the semaphorin-3a binding motif found in chondroitin sulfate using galnac4s-6st-knockout mice. *Biomolecules*. **10**(11), pp.1–16.
- Nakamura, K., Nemani, V.M., Azarbal, F., Skibinski, G., Levy, J.M., Egami, K., Munishkina, L., Zhang, J., Gardner, B., Wakabayashi, J., Sesaki, H., Cheng, Y., Finkbeiner, S., Nussbaum, R.L., Masliah, E. and Edwards, R.H. 2011. Direct membrane association drives mitochondrial fission by the Parkinson disease-associated protein  $\alpha$ -synuclein. *Journal of Biological Chemistry*. **286**(23), pp.20710–20726.
- Näsström, T., Fagerqvist, T., Barbu, M., Karlsson, M., Nikolajeff, F., Kasrayan, A., Ekberg, M., Lannfelt, L., Ingelsson, M. and Bergström, J. 2011. The lipid peroxidation products 4-oxo-2-nonenal and 4-hydroxy-2-nonenal promote the formation of  $\alpha$ -synuclein oligomers with distinct biochemical, morphological, and functional properties. *Free Radical Biology and Medicine*. **50**(3), pp.428–437.
- Nemani, V.M., Lu, W., Berge, V., Nakamura, K., Onoa, B., Lee, M.K., Chaudhry, F.A., Nicoll, R.A. and Edwards, R.H. 2010. Increased Expression of  $\alpha$ -Synuclein Reduces Neurotransmitter Release by Inhibiting Synaptic Vesicle Reclustering after Endocytosis. *Neuron*. **65**(1), pp.66–79.
- Nguyen, P.T., Dorman, L.C., Pan, S., Vainchtein, I.D., Han, R.T., Nakao-Inoue, H., Taloma, S.E., Barron, J.J., Molofsky, A.B., Kheirbek, M.A. and Molofsky, A. V. 2020. Microglial Remodeling of the Extracellular Matrix

Promotes Synapse Plasticity. *Cell*. **182**(2), pp.388-403.e15.

Nijhuis, F.A.P., Esselink, R., Bie, R.M.A. De and Groenewoud, H. 2021.

Translating Evidence to Advanced Parkinson ' s Disease Patients : A Systematic Review and Meta-Analysis. . **2**, pp.1–16.

Nikonenko, A., Schmidt, S., Skibo, G., Brückner, G. and Schachner, M. 2003.

Tenascin-R-deficient mice show structural alterations of symmetric perisomatic synapses in the CA1 region of the hippocampus. *Journal of Comparative Neurology*. **456**(4), pp.338–349.

Ninkina, N., Papachroni, K., Robertson, D.C., Schmidt, O., Delaney, L., O'Neill,

F., Court, F., Rosenthal, A., Fleetwood-Walker, S.M., Davies, A.M. and

Buchman, V.L. 2003. Neurons Expressing the Highest Levels of  $\gamma$ -Synuclein Are Unaffected by Targeted Inactivation of the Gene. *Molecular and Cellular Biology*. **23**(22), pp.8233–8245.

Odekerken, V.J.J., van Laar, T., Staal, M.J., Mosch, A., Hoffmann, C.F.E.,

Nijssen, P.C.G., Beute, G.N., van Vugt, J.P.P., Lenders, M.W.P.M.,

Contarino, M.F., Mink, M.S.J., Bour, L.J., van den Munckhof, P., Schmand, B.A., de Haan, R.J., Schuurman, P.R. and de Bie, R.M.A. 2013.

Subthalamic nucleus versus globus pallidus bilateral deep brain stimulation for advanced Parkinson's disease (NSTAPS study): A randomised controlled trial. *The Lancet Neurology*. **12**(1), pp.37–44.

Office for National Statistics 2014. *2014-based National Population Projections Lifetable* [online].

Ohama, E. and Ikuta, F. 1976. Parkinson's disease: Distribution of Lewy bodies

and monoamine neuron system. *Acta Neuropathologica*. **34**(4), pp.311–319.

Olanow, C.W. 1996. Selegiline: Current perspectives on issues related to

neuroprotection and mortality. *Neurology*. **47**(6 SUPPL. 3).

Oliveira, M.A.P., Arreckx, S., Di Monte, D., Preciat, G.A., Ulusoy, A. and

Fleming, R.M.T. 2019. The connectome is necessary but not sufficient for the spread of alpha -synuclein pathology in rats. *bioRxiv*, pp.1–62.

Oohashi, T., Hirakawa, S., Bekku, Y., Rauch, U., Zimmermann, D.R., Su, W.D.,

Ohtsuka, A., Murakami, T. and Ninomiya, Y. 2002. Bral1, a brain-specific

link protein, colocalizing with the versican V2 isoform at the nodes of Ranvier in developing and adult mouse central nervous systems. *Molecular*

- and Cellular Neuroscience*. **19**(1), pp.43–57.
- Osterberg, V.R., Spinelli, K.J., Weston, L.J., Luk, K.C., Woltjer, R.L. and Unni, V.K. 2015. Progressive Aggregation of Alpha-Synuclein and Selective Degeneration of Lewy Inclusion-Bearing Neurons in a Mouse Model of Parkinsonism. *Cell Reports*. **10**(8), pp.1252–1260.
- Ouberai, M.M., Wang, J., Swann, M.J., Galvagnion, C., Guilliams, T., Dobson, C.M. and Welland, M.E. 2013.  $\alpha$ -Synuclein senses lipid packing defects and induces lateral expansion of lipids leading to membrane remodeling. *Journal of Biological Chemistry*. **288**(29), pp.20883–20895.
- Pacelli, C., Giguère, N., Bourque, M.J., Lévesque, M., Slack, R.S. and Trudeau, L.É. 2015. Elevated Mitochondrial Bioenergetics and Axonal Arborization Size Are Key Contributors to the Vulnerability of Dopamine Neurons. *Current Biology*. **25**(18), pp.2349–2360.
- Pampalakis, G., Sykioti, V.-S., Ximerakis, M., Stefanakou-Kalakou, I., Melki, R., Vekrellis, K., Sotiropoulou, G., Pampalakis, G., Sykioti, V.-S., Ximerakis, M., Stefanakou-Kalakou, I., Melki, R., Vekrellis, K. and Sotiropoulou, G. 2016. KLK6 proteolysis is implicated in the turnover and uptake of extracellular alpha-synuclein species. *Oncotarget*. **5**(0), pp.14502–14515.
- Pantazopoulos, H., Woo, T.-U.W., Lim, M.P., Lange, N. and Berretta, S. 2008a. Extracellular Matrix-Glial Abnormalities in the Amygdala and Entorhinal Cortex of Subjects Diagnosed With Schizophrenia. *Archives General Psychiatry*. **67**(2), pp.155–166.
- Pantazopoulos, H., Murray, E.A. and Berretta, S. 2008b. Total number, distribution, and phenotype of cells expressing chondroitin sulfate proteoglycans in the normal human amygdala. *Brain Research*. **1207**, pp.84–95.
- Parashos, S.A., Maraganore, D.M., O'Brien, P.C. and Rocca, W.A. 2002. Medical Services Utilization and Prognosis in Parkinson Disease: A Population-Based Study. *Mayo Clinic Proceedings*. **77**(9), pp.918–925.
- Parkinson's UK 2017. *The cost of Parkinson's: the financial impact of living with the condition* [online].
- Parkinson's UK 2018. *The incidence and prevalence of Parkinson's in the UK*.
- Parkkinen, L., Pirttilä, T. and Alafuzoff, I. 2008. Applicability of current staging/categorization of  $\alpha$ -synuclein pathology and their clinical relevance.

*Acta Neuropathologica*. **115**(4), pp.399–407.

- Parkkinen, L., O'Sullivan, S.S., Collins, C., Petrie, A., Holton, J.L., Revesz, T. and Lees, A.J. 2011. Disentangling the Relationship between Lewy bodies and nigral neuronal loss in Parkinson's disease. *Journal of Parkinson's Disease*. **1**(3), pp.277–286.
- Parkkinen, L., Soininen, H. and Alafuzoff, I. 2003. Regional distribution of  $\alpha$ -synuclein pathology in unimpaired aging and Alzheimer disease. *Journal of Neuropathology and Experimental Neurology*. **62**(4), pp.363–367.
- Parkkinen, L., Kauppinen, T., Pirttilä, T., Autere, J.M. and Alafuzoff, I. 2005.  $\alpha$ -Synuclein Pathology Does Not Predict Extrapyrarnidal Symptoms or Dementia. *Annals of Neurology*. **57**(1), pp.82–91.
- Patterson, J.R., Polinski, N.K., Duffy, M.F., Kemp, C.J., Luk, K.C., Volpicelli-Daley, L.A., Kanaan, N.M. and Sortwell, C.E. 2019. Generation of Alpha-Synuclein Preformed Fibrils from Monomers and Use In Vivo. *Journal of visualized experiments : JoVE*. (148), pp.1–10.
- Pearce, R.K.B., Hawkes, C.H. and Daniel, S.E. 1995. The anterior olfactory nucleus in Parkinson's disease. *Movement Disorders*. **10**(3), pp.283–287.
- Pedersen, K.M., Marner, L., Pakkenberg, H. and Pakkenberg, B. 2005. No global loss of neocortical neurons in Parkinson's disease: A quantitative stereological study. *Movement Disorders*. **20**(2), pp.164–171.
- Peelaerts, W., Bousset, L., Van Der Perren, A., Moskites, A., Pulizzi, R., Giugliano, M., Van Den Haute, C., Melki, R. and Baekelandt, V. 2015.  $\alpha$ -Synuclein strains cause distinct synucleinopathies after local and systemic administration. *Nature*. **522**(7556), pp.340–344.
- Perlmutter, J.D., Braun, A.R. and Sachs, J.N. 2009. Curvature dynamics of alpha-Synuclein familial Parkinson disease mutants. Molecular simulations of the Micelle-and Bilayer-bound forms. *Journal of Biological Chemistry*. **284**(11), pp.7177–7189.
- Van der Perren, A., Gelders, G., Fenyi, A., Bousset, L., Brito, F., Peelaerts, W., Van den Haute, C., Gentleman, S.M., Melki, R. and Baekelandt, V. 2020. The structural differences between patient-derived  $\alpha$ -synuclein strains dictate characteristics of Parkinson's disease, multiple system atrophy and dementia with Lewy bodies. *Acta Neuropathologica*. **139**(6), pp.977–1000.
- Perrin, R.J., Woods, W.S., Clayton, D.F. and George, J.M. 2001. Exposure to

- Long Chain Polyunsaturated Fatty Acids Triggers Rapid Multimerization of Synucleins. *Journal of Biological Chemistry*. **276**(45), pp.41958–41962.
- Pieri, L., Madiona, K. and Melki, R. 2016. Structural and functional properties of prefibrillar  $\alpha$ -synuclein oligomers. *Scientific Reports*. **6**(April), pp.1–15.
- Pizzorusso, T., Medini, P., Berardi, N., Chierzi, S., Fawcett, J.W. and Maffei, L. 2002. Reactivation of Ocular Dominance Plasticity in the Adult Visual Cortex. *Science*. **298**(5596), pp.1248–1251.
- Pizzorusso, T., Medini, P., Landi, S., Baldini, S., Berardi, N. and Maffei, L. 2006. Structural and functional recovery from early monocular deprivation in adult rats. *Proceedings of the National Academy of Sciences of the United States of America*. **103**(22), pp.8517–8522.
- Poewe, W., Seppi, K., Tanner, C.M., Halliday, G.M., Brundin, P., Volkman, J., Schrag, A.E. and Lang, A.E. 2017. Parkinson disease. *Nature Reviews Disease Primers*. **3**, pp.1–21.
- Pont-Sunyer, C., Hotter, A., Gaig, C., Seppi, K., Compta, Y., Katzenschlager, R., Mas, N., Hofeneder, D., Brücke, T., Bayés, A., Wenzel, K., Infante, J., Zach, H., Pirker, W., Posada, I.J., Álvarez, R., Ispierto, L., De Fàbregues, O., Callén, A., Palasí, A., Aguilar, M., Martí, M.J., Valdeoriola, F., Salamero, M., Poewe, W. and Tolosa, E. 2015. The onset of nonmotor symptoms in parkinson's disease (the ONSET PD study). *Movement Disorders*. **30**(2), pp.229–237.
- Popelář, J., Gómez, M.D., Lindovský, J., Rybalko, N., Burianová, J., Oohashi, T. and Syka, J. 2017. The absence of brain-specific link protein Bral2 in perineuronal nets hampers auditory temporal resolution and neural adaptation in mice. *Physiological research*.
- Pranke, I.M., Morello, V., Bigay, J., Gibson, K., Verbavatz, J.M., Antony, B. and Jackson, C.L. 2011.  $\alpha$ -Synuclein and ALPS motifs are membrane curvature sensors whose contrasting chemistry mediates selective vesicle binding. *Journal of Cell Biology*. **194**(1), pp.89–103.
- Rácz, E., Gaál, B. and Matesz, C. 2016. Heterogeneous expression of extracellular matrix molecules in the red nucleus of the rat. *Neuroscience*. **322**, pp.1–17.
- Rajiah, K., Maharajan, M.K., Yeen, S.J. and Lew, S. 2017. Quality of Life and Caregivers' Burden of Parkinson's Disease. *Neuroepidemiology*. **48**(3–4),

pp.131–137.

- Rajput, A.H. and Rozdilsky, B. 1976. Dysautonomia in Parkinsonism: A clinicopathological study. *Journal of Neurology, Neurosurgery and Psychiatry*. **39**(11), pp.1092–1100.
- Rankin-Gee, E.K., McRae, P.A., Baranov, E., Rogers, S., Wandrey, L. and Porter, B.E. 2015. Perineuronal net degradation in epilepsy. *Epilepsia*. **56**(7), pp.1124–1133.
- Rannikko, E.H., Weber, S.S. and Kahle, P.J. 2015. Exogenous  $\alpha$ -synuclein induces toll-like receptor 4 dependent inflammatory responses in astrocytes. *BMC Neuroscience*. **16**(1), pp.1–11.
- Rauch, U., Zhou, X.-H. and Roos, G. 2005. Extracellular matrix alterations in brains lacking four of its components. *Biochemical and Biophysical Research Communications*. **328**(2), pp.608–617.
- Ray, S., Singh, N., Kumar, R., Patel, K., Pandey, S., Datta, D., Mahato, J., Panigrahi, R., Navalkar, A., Mehra, S., Gadhe, L.G., Chatterjee, D., Sawner, A.S., Maiti, S., Bhatia, S., Gerez, J.A., Chowdhury, A., Kumar, A., Padinhateeri, R., Riek, R., Krishnamoorthy, G. and Maji, S.K. 2020.  $\alpha$ -Synuclein aggregation nucleates through liquid–liquid phase separation. *Nature Chemistry*, pp.1–12.
- Reha, R.K., Dias, B.G., Nelson, C.A., Kaufer, D., Werker, J.F., Kolbh, B., Levine, J.D. and Hensch, T.K. 2020. Critical period regulation across multiple timescales. *Proceedings of the National Academy of Sciences of the United States of America*. **117**(38), pp.23242–23251.
- Reid, H.M.O., Chen-Mack, N., Snowden, T. and Christie, B.R. 2021. Understanding Changes in Hippocampal Interneurons Subtypes in the Pathogenesis of Alzheimer’s Disease: A Systematic Review. *Brain Connectivity*. **11**(3), pp.159–179.
- Rendón-Ochoa, E.A., Hernández-Flores, T., Avilés-Rosas, V.H., Cáceres-Chávez, V.A., Duhne, M., Laville, A., Tapia, D., Galarraga, E. and Bargas, J. 2018. Calcium currents in striatal fast-spiking interneurons: Dopaminergic modulation of Ca V 1 channels. *BMC Neuroscience*. **19**(1), pp.1–14.
- Rey, N.L., Petit, G.H., Bousset, L., Melki, R. and Brundin, P. 2013. Transfer of human  $\alpha$ -synuclein from the olfactory bulb to interconnected brain regions

- in mice. *Acta Neuropathologica*. **126**(4), pp.555–573.
- Rey, N.L., Steiner, J.A., Maroof, N., Luk, K.C., Madaj, Z., Trojanowski, J.Q., Lee, V.M.Y. and Brundin, P. 2016. Widespread transneuronal propagation of  $\alpha$ -synucleinopathy triggered in olfactory bulb mimics prodromal Parkinson's disease. *The Journal of Experimental Medicine*. **213**(9), pp.1759–1778.
- Rey, N.L., Bousset, L., George, S., Madaj, Z., Meyerdirk, L., Schulz, E., Steiner, J.A., Melki, R. and Brundin, P. 2019.  $\alpha$ -Synuclein conformational strains spread, seed and target neuronal cells differentially after injection into the olfactory bulb. *Acta Neuropathologica Communications*. **7**(1), pp.1–18.
- Reyes, J.F., Sackmann, C., Hoffmann, A., Svenningsson, P., Winkler, J., Ingelsson, M. and Hallbeck, M. 2019. Binding of  $\alpha$ -synuclein oligomers to Cx32 facilitates protein uptake and transfer in neurons and oligodendrocytes. *Acta Neuropathologica*. **138**(1), pp.23–47.
- Richter, R.P., Baranova, N.S., Day, A.J. and Kwok, J.C.F. 2018. Glycosaminoglycans in extracellular matrix organisation: are concepts from soft matter physics key to understanding the formation of perineuronal nets? *Current opinion in structural biology*. **50**, pp.65–74.
- del Rio, J., de Lecea, L., Ferrer, I. and Soriano, E. 1994. The development of parvalbumin-immunoreactivity in the neocortex of the mouse. *Developmental Brain Research*. **81**(2), pp.247–259.
- Robertson, D.C., Schmidt, O., Ninkina, N., Jones, P.A., Sharkey, J. and Buchman, V.L. 2004. Developmental loss and resistance to MPTP toxicity of dopaminergic neurones in substantia nigra pars compacta of  $\gamma$ -synuclein,  $\alpha$ -synuclein and double  $\alpha/\gamma$ -synuclein null mutant mice. *Journal of Neurochemistry*. **89**(5), pp.1126–1136.
- Rogers, S.L., Rankin-Gee, E., Risbud, R.M., Porter, B.E. and Marsh, E.D. 2018. Normal Development of the Perineuronal Net in Humans; In Patients with and without Epilepsy. *Neuroscience*. **384**, pp.350–360.
- Rossi, M., Candelise, N., Baiardi, S., Capellari, S., Giannini, G., Orrù, C.D., Antelmi, E., Mamma, A., Hughson, A.G., Calandra-Buonaura, G., Ladogana, A., Plazzi, G., Cortelli, P., Caughey, B. and Parchi, P. 2020. Ultrasensitive RT-QuIC assay with high sensitivity and specificity for Lewy body-associated synucleinopathies. *Acta Neuropathologica*. **140**(1), pp.49–

62.

- Rostami, J., Fotaki, G., Sirois, J., Mzezewa, R., Bergström, J., Essand, M., Healy, L. and Erlandsson, A. 2020. Astrocytes have the capacity to act as antigen-presenting cells in the Parkinson's disease brain. *Journal of neuroinflammation*. **17**(1), p.119.
- Rowlands, D., Lensjø, K.K., Dinh, T., Yang, S., Andrews, M.R., Hafting, T., Fyhn, M., Fawcett, J.W. and Dick, G. 2018. Aggrecan directs extracellular matrix-mediated neuronal plasticity. *Journal of Neuroscience*. **38**(47), pp.10102–10113.
- Roy, S. and Wolman, L. 1969. Ultrastructural observations in Parkinsonism. *The Journal of Pathology*. **99**(1), pp.39–44.
- Rubinstein, M. and Colby, R.H. 2003. *Polymer physics* [online]. Oxford: Oxford University Press.
- Runfola, M., De Simone, A., Vendruscolo, M., Dobson, C.M. and Fusco, G. 2020. The N-terminal Acetylation of  $\alpha$ -Synuclein Changes the Affinity for Lipid Membranes but not the Structural Properties of the Bound State. *Scientific Reports*. **10**(1), pp.1–10.
- Sacino, A.N., Brooks, M., McGarvey, N.H., McKinney, A.B., Thomas, M.A., Levites, Y., Ran, Y., Golde, T.E. and Giasson, B.I. 2014. Induction of CNS  $\alpha$ -synuclein pathology by fibrillar and non-amyloidogenic recombinant  $\alpha$ -synuclein. *Acta Neuropathologica Communications*. **2**(1), p.1.
- Saghatelian, A.K., Dityatev, A., Schmidt, S., Schuster, T., Bartsch, U. and Schachner, M. 2001. Reduced perisomatic inhibition, increased excitatory transmission, and impaired long-term potentiation in mice deficient for the extracellular matrix glycoprotein tenascin-R. *Molecular and Cellular Neuroscience*. **17**(1), pp.226–240.
- Scheiber, I.F., Mercer, J.F.B. and Dringen, R. 2014. Metabolism and functions of copper in brain. *Progress in Neurobiology*. **116**, pp.33–57.
- Schmidt, S., Arendt, T., Morawski, M. and Sonntag, M. 2020. Neurocan Contributes to Perineuronal Net Development. *Neuroscience*. **442**, pp.69–86.
- Schrag, A., Horsfall, L., Walters, K., Noyce, A. and Petersen, I. 2015. Prediagnostic presentations of Parkinson's disease in primary care: A case-control study. *The Lancet Neurology*. **14**(1), pp.57–64.

- Schuck, P. and Zhao, H. 2001. The Role of Mass Transport Limitation and Surface Heterogeneity in the Biophysical Characterization of Macromolecular Binding Processes by SPR Biosensing *In*: N. J. DE MOL and M. J. E. FISCHER, eds. *Surface Plasmon Resonance: Methods & Protocols*. New York: Humana Press, pp. 15–54.
- Schüppel, K., Brauer, K., Härtig, W., Grosche, J., Earley, B., Leonard, B.E. and Brückner, G. 2002. Perineuronal nets of extracellular matrix around hippocampal interneurons resist destruction by activated microglia in trimethyltin-treated rats. *Brain Research*. **958**(2), pp.448–453.
- Schweitzer, B., Singh, J., Fejtova, A., Groc, L., Heine, M. and Frischknecht, R. 2017. Hyaluronic acid based extracellular matrix regulates surface expression of GluN2B containing NMDA receptors. *Scientific Reports*. **7**(1), pp.1–9.
- Scott, D.A. and Roy, S. 2012.  $\alpha$ -Synuclein inhibits intersynaptic vesicle mobility and maintains recycling-pool homeostasis. *Journal of Neuroscience*. **32**(30), pp.10129–10135.
- Scrimgeour, J., McLane, L.T., Chang, P.S. and Curtis, J.E. 2017. Single-Molecule Imaging of Proteoglycans in the Pericellular Matrix. *Biophysical Journal*. **113**(11), pp.2316–2320.
- Shahmoradian, S.H., Lewis, A.J., Genoud, C., Hench, J., Moors, T.E., Navarro, P.P., Castaño-Díez, D., Schweighauser, G., Graff-Meyer, A., Goldie, K.N., Sütterlin, R., Huisman, E., Ingrassia, A., Gier, Y. de, Rozemuller, A.J.M., Wang, J., Paepe, A. De, Erny, J., Staempfli, A., Hoernschemeyer, J., Großerüschkamp, F., Niedieker, D., El-Mashtoly, S.F., Quadri, M., Van IJcken, W.F.J., Bonifati, V., Gerwert, K., Bohrmann, B., Frank, S., Britschgi, M., Stahlberg, H., Van de Berg, W.D.J. and Lauer, M.E. 2019. Lewy pathology in Parkinson's disease consists of crowded organelles and lipid membranes. *Nature Neuroscience*. **22**(7), pp.1099–1109.
- Sharma, M., Burré, J. and Südhof, T.C. 2011. CSP $\alpha$  promotes SNARE-complex assembly by chaperoning SNAP-25 during synaptic activity. *Nature Cell Biology*. **13**(1), pp.30–39.
- Shimozawa, A., Ono, M., Takahara, D., Tarutani, A., Imura, S., Masuda-Suzukake, M., Higuchi, M., Yanai, K., Hisanaga, S.I. and Hasegawa, M. 2017. Propagation of pathological  $\alpha$ -synuclein in marmoset brain. *Acta*

*neuropathologica communications*. **5**(1), p.12.

- Shrivastava, A.N., Redeker, V., Fritz, N., Pieri, L., Almeida, L.G., Spolidoro, M., Liebmann, T., Bousset, L., Renner, M., Léna, C., Aperia, A., Melki, R. and Triller, A. 2015.  $\alpha$ -synuclein assemblies sequester neuronal  $\alpha$ 3-Na<sup>+</sup>/K<sup>+</sup>-ATPase and impair Na<sup>+</sup> gradient. *EMBO Journal*. **34**(19), pp.2408–2423.
- Siebert, J.R., Stelzner, D.J. and Osterhout, D.J. 2011. Chondroitinase treatment following spinal contusion injury increases migration of oligodendrocyte progenitor cells. *Experimental Neurology*. **231**(1), pp.19–29.
- Sigal, Y.M., Bae, H., Bogart, L.J., Hensch, T.K. and Zhuang, X. 2019. Structural maturation of cortical perineuronal nets and their perforating synapses revealed by superresolution imaging. *Proceedings of the National Academy of Sciences of the United States of America*. **116**(14), pp.7071–7076.
- Smith, C.C., Mauricio, R., Nobre, L., Marsh, B., Wüst, R.C.I., Rossiter, H.B. and Ichiyama, R.M. 2015. Differential regulation of perineuronal nets in the brain and spinal cord with exercise training. *Brain Research Bulletin*. **111**, pp.20–26.
- Smith, D.P., Tew, D.J., Hill, A.F., Bottomley, S.P., Masters, C.L., Barnham, K.J., Cappai, R., Colin Masters, X.L., Barnham, K.J. and Cappai, R. 2008. Formation of a high affinity lipid-binding intermediate during the early aggregation phase of  $\alpha$ -synuclein. *Biochemistry*. **47**(5), pp.1425–1434.
- Sorg, B.A., Berretta, S., Blacktop, J.M., Fawcett, J.W., Kitagawa, H., Kwok, J.C.F. and Miquel, M. 2016. Casting a Wide Net: Role of Perineuronal Nets in Neural Plasticity. *The Journal of Neuroscience*. **36**(45), pp.11459–11468.
- Soria, F.N., Paviolo, C., Doudnikoff, E., Arotcarena, M.L., Lee, A., Danné, N., Mandal, A.K., Gosset, P., Dehay, B., Groc, L., Cognet, L. and Bezard, E. 2020. Synucleinopathy alters nanoscale organization and diffusion in the brain extracellular space through hyaluronan remodeling. *Nature Communications*. **11**(1).
- Sorrentino, Z.A., Vijayaraghavan, N., Gorion, K.M., Riffe, C.J., Strang, K.H., Caldwell, J. and Giasson, B.I. 2018. Physiological C-terminal truncation of  $\alpha$ -synuclein potentiates the prion-like formation of pathological inclusions. *Journal of Biological Chemistry*. **293**(49), pp.18914–18932.
- Spatazza, J., Lee, H.H.C., DiNardo, A.A., Tibaldi, L., Joliot, A., Hensch, T.K. and Prochiantz, A. 2013. Choroid-Plexus-Derived Otx2 Homeoprotein

- Constrains Adult Cortical Plasticity. *Cell Reports*. **3**(6), pp.1815–1823.
- Spicer, A.P., Joo, A. and Bowling, R.A. 2003. A hyaluronan binding link protein gene family whose members are physically linked adjacent to chondroitin sulfate proteoglycan core protein genes. The missing links. *Journal of Biological Chemistry*. **278**(23), pp.21083–21091.
- Spillantini, M.G., Crowther, R.A., Jakes, R., Cairns, N.J., Lantos, P.L. and Michel, G. 1998a. Filamentous  $\alpha$ -synuclein inclusions link multiple system atrophy with Parkinson's disease and dementia with Lewy bodies. *Neuroscience Letters*. **251**(3), pp.205–208.
- Spillantini, M.G., Crowther, R.A., Jakes, R., Hasegawa, M. and Goedert, M. 1998b.  $\alpha$ -Synuclein in filamentous inclusions of Lewy bodies from Parkinson's disease and dementia with Lewy bodies. *Proceedings of the National Academy of Sciences*. **95**(11), pp.6469–6473.
- Spillantini, M.G., Schmidt, M.L., Lee, V.M.Y., Trojanowski, J.Q., Jakes, R. and Goedert, M. 1997.  $\alpha$ -Synuclein in Lewy bodies. *Nature*. **388**(6645), pp.839–840.
- Staal, R.G.W., Mosharov, E. V. and Sulzer, D. 2004. Dopamine neurons release transmitter via a flickering fusion pore. *Nature Neuroscience*. **7**(4), pp.341–346.
- Stamenkovic, V., Stamenkovic, S., Jaworski, T., Gawlak, M., Jovanovic, M., Jakovcevski, I., Wilczynski, G.M., Kaczmarek, L., Schachner, M., Radenovic, L. and Andjus, P.R. 2017. The extracellular matrix glycoprotein tenascin-C and matrix metalloproteinases modify cerebellar structural plasticity by exposure to an enriched environment. *Brain Structure and Function*. **222**(1), pp.393–415.
- Stokholm, M.G., Danielsen, E.H., Hamilton-Dutoit, S.J. and Borghammer, P. 2016. Pathological  $\alpha$ -synuclein in gastrointestinal tissues from prodromal Parkinson disease patients. *Annals of Neurology*. **79**(6), pp.940–949.
- Stopschinski, B.E., Holmes, B.B., Miller, G.M., Manon, V.A., Vaquer-Alicea, J., Prueitt, W.L., Hsieh-Wilson, L.C. and Diamond, M.I. 2018a. Specific glycosaminoglycan chain length and sulfation patterns are required for cell uptake of tau versus alpha-synuclein and beta-amyloid aggregates. *Journal of Biological Chemistry*. **293**(27), pp.10826–10840.
- Stopschinski, B.E., Holmes, B.B., Miller, G.M., Manon, V.A., Vaquer-Alicea, J.,

- Prueitt, W.L., Hsieh-Wilson, L.C. and Diamond, M.I. 2018b. Specific glycosaminoglycan chain length and sulfation patterns are required for cell uptake of tau vs.  $\alpha$ -synuclein and  $\beta$ -amyloid aggregates. *Journal of Biological Chemistry*. **293**, p.jbc.RA117.000378.
- Storey, A. 2018. *Living longer - how our population is changing and why it matters*.
- Sucha, P., Chmelova, M., Kamenicka, M., Bochín, M., Oohashi, T. and Vargova, L. 2020. The Effect of Hapln4 Link Protein Deficiency on Extracellular Space Diffusion Parameters and Perineuronal Nets in the Auditory System During Aging. *Neurochemical Research*. **45**(1), pp.68–82.
- Sugiyama, S., Di Nardo, A.A., Aizawa, S., Matsuo, I., Volovitch, M., Prochiantz, A. and Hensch, T.K. 2008. Experience-Dependent Transfer of Otx2 Homeoprotein into the Visual Cortex Activates Postnatal Plasticity. *Cell*. **134**(3), pp.508–520.
- Sulzer, D. and Edwards, R.H. 2019. The physiological role of  $\alpha$ -synuclein and its relationship to Parkinson's Disease. *Journal of Neurochemistry*. **150**(5), pp.475–486.
- Sun, J., Wang, L., Bao, H., Premi, S., Das, U., Chapman, E.R. and Roy, S. 2019. Functional cooperation of  $\alpha$ -synuclein and VAMP2 in synaptic vesicle recycling. *Proceedings of the National Academy of Sciences of the United States of America*. **166**(23), pp.11113–11115.
- Sung, J.Y., Kim, J., Paik, S.R., Park, J.H., Ahn, Y.S. and Chung, K.C. 2001. Induction of Neuronal Cell Death by Rab5A-dependent Endocytosis of Alpha-Synuclein. *Journal of Biological Chemistry*. **276**(29), pp.27441–27448.
- Surguchov, A. 2008. Chapter 6 Molecular and Cellular Biology of Synucleins. *International Review of Cell and Molecular Biology*. **270**(C), pp.225–317.
- Surmeier, D.J., Obeso, J.A. and Halliday, G.M. 2017a. Parkinson's Disease Is Not Simply a Prion Disorder. *The Journal of Neuroscience*. **37**(41), pp.9799–9807.
- Surmeier, D.J., Obeso, J.A. and Halliday, G.M. 2017b. Selective neuronal vulnerability in Parkinson disease. *Nature Reviews Neuroscience*. **18**(2), pp.101–113.
- Suttkus, A., Rohn, S., Weigel, S., Glöckner, P., Arendt, T. and Morawski, M.

2014. Aggrecan, link protein and tenascin-R are essential components of the perineuronal net to protect neurons against iron-induced oxidative stress. *Cell Death and Disease*. **5**(3), p.e1119.
- Suttkus, A., Morawski, M. and Arendt, T. 2016a. Protective Properties of Neural Extracellular Matrix. *Molecular Neurobiology*. **53**(1), pp.73–82.
- Suttkus, A., Holzer, M., Morawski, M. and Arendt, T. 2016b. The neuronal extracellular matrix restricts distribution and internalization of aggregated Tau-protein. *Neuroscience*. **313**, pp.225–235.
- Sveinbjörnsdóttir, S. 2016. The clinical symptoms of Parkinson's disease. *Journal of Neurochemistry*. **139**, pp.318–324.
- Syková, E., Voříšek, I., Mazel, T., Antonova, T. and Schachner, M. 2005. Reduced extracellular space in the brain of tenascin-R- and HNK-1-sulphotransferase deficient mice. *European Journal of Neuroscience*. **22**(8), pp.1873–1880.
- Taylor-Whiteley, T.R., Le Maitre, C.L., Duce, J.A., Dalton, C.F. and Smith, D.P. 2019. Recapitulating Parkinson's disease pathology in a three-dimensional human neural cell culture model. *Disease Models & Mechanisms*. **12**, p.dmm.038042.
- Thakar, D., Migliorini, E., Coche-Guerente, L., Sadir, R., Lortat-Jacob, H., Boturyn, D., Renaudet, O., Labbe, P. and Richter, R.P. 2014. A quartz crystal microbalance method to study the terminal functionalization of glycosaminoglycans. *Chemical Communications*. **50**(96), pp.15148–15151.
- Thakur, P., Breger, L.S., Lundblad, M., Wan, O.W., Mattsson, B., Luk, K.C., Lee, V.M.Y., Trojanowski, J.Q. and Björklund, A. 2017. Modeling Parkinson's disease pathology by combination of fibril seeds and  $\alpha$ -synuclein overexpression in the rat brain. *Proceedings of the National Academy of Sciences of the United States of America*. **114**(39), pp.E8284–E8293.
- Tofaris, G.K., Layfield, R. and Spillantini, M.G. 2001.  $\alpha$ -Synuclein metabolism and aggregation is linked to ubiquitin-independent degradation by the proteasome. *FEBS Letters*. **509**(1), pp.22–26.
- Tran, H.T., Chung, C.H.Y., Iba, M., Zhang, B., Trojanowski, J.Q., Luk, K.C. and Lee, V.M.Y. 2014.  $\alpha$ -Synuclein Immunotherapy Blocks Uptake and Templated Propagation of Misfolded  $\alpha$ -Synuclein and Neurodegeneration.

*Cell Reports*. **7**(6), pp.2054–2065.

- Tsuboi, Y., Uchikado, H. and Dickson, D.W. 2007. Neuropathology of Parkinson's disease dementia and dementia with Lewy bodies with reference to striatal pathology. *Parkinsonism & related disorders*. **13 Suppl 3**, pp.S221-4.
- Turnbull, K., Caslake, R., Macleod, A., Ives, N., Stowe, R. and Counsell, C. 2005. Monoamine oxidase B inhibitors for early Parkinson's disease. *Cochrane Database of Systematic Reviews*.
- Tysnes, O.B. and Storstein, A. 2017. Epidemiology of Parkinson's disease. *Journal of Neural Transmission*. **124**(8), pp.901–905.
- Ubeda-Bañon, I., Flores-Cuadrado, A., Saiz-Sanchez, D. and Martinez-Marcos, A. 2017. Differential Effects of Parkinson's Disease on Interneuron Subtypes within the Human Anterior Olfactory Nucleus. *Frontiers in Neuroanatomy*. **11**(December), pp.1–9.
- Ueda, K., Fukushima, H., Masliah, E., Xia, Y.U., Iwai, A., Yoshimoto, M., Otero, D.A.C., Kondo, J., Ihara, Y. and Saitoh, T. 1993. Molecular cloning of cDNA encoding an unrecognized component of amyloid in Alzheimer disease (neurodegeneration/chaperone/amyloid P/A4 protein/neuritic plaque). *Proc. Natl. Acad. Sci. USA*. **90**(December), pp.11282–11286.
- Ueno, H., Takao, K., Suemitsu, S., Murakami, S., Kitamura, N., Wani, K., Okamoto, M., Aoki, S. and Ishihara, T. 2018a. Age-dependent and region-specific alteration of parvalbumin neurons and perineuronal nets in the mouse cerebral cortex. *Neurochemistry International*. **112**, pp.59–70.
- Ueno, H., Suemitsu, S., Murakami, S., Kitamura, N., Wani, K., Matsumoto, Y., Aoki, S., Okamoto, M. and Ishihara, T. 2018b. Hyaluronic acid is present on specific perineuronal nets in the mouse cerebral cortex. *Brain Research*. **1698**(June), pp.139–150.
- Ueno, H., Suemitsu, S., Okamoto, M., Matsumoto, Y. and Ishihara, T. 2017a. Parvalbumin neurons and perineuronal nets in the mouse prefrontal cortex. *Neuroscience*. **343**, pp.115–127.
- Ueno, H., Suemitsu, S., Okamoto, M., Matsumoto, Y. and Ishihara, T. 2017b. Sensory experience-dependent formation of perineuronal nets and expression of Cat-315 immunoreactive components in the mouse somatosensory cortex. *Neuroscience*. **355**, pp.161–174.

- Ulmer, T.S., Bax, A., Cole, N.B. and Nussbaum, R.L. 2005. Structure and dynamics of micelle-bound human  $\alpha$ -synuclein. *Journal of Biological Chemistry*. **280**(10), pp.9595–9603.
- Uversky, V.N., Li, J. and Fink, A.L. 2001. Metal-triggered structural transformations, aggregation, and fibrillation of human  $\alpha$ -synuclein: A possible molecular link between parkinson's disease and heavy metal exposure. *Journal of Biological Chemistry*. **276**(47), pp.44284–44296.
- Van't Spijker, H.M., Rowlands, D., Rossier, J., Haenzi, B., Fawcett, J.W. and Kwok, J.C.F. 2019. Neuronal Pentraxin 2 Binds PNNs and Enhances PNN Formation. *Neural Plasticity*. **2019**.
- Van't Spijker, H.M. and Kwok, J.C.F. 2017. A Sweet Talk: The Molecular Systems of Perineuronal Nets in Controlling Neuronal Communication. *Frontiers in Integrative Neuroscience*. **11**(December), pp.1–10.
- Do Van, B., Gouel, F., Jonneaux, A., Timmerman, K., Gelé, P., Pétrault, M., Bastide, M., Laloux, C., Moreau, C., Bordet, R., Devos, D. and Devedjian, J.-C. 2016. Ferroptosis, a newly characterized form of cell death in Parkinson's disease that is regulated by PKC. *Neurobiology of Disease*. **94**, pp.169–178.
- Vargas, K.J., Schrod, N., Davis, T., Fernandez-Busnadiego, R., Taguchi, Y. V., Laugks, U., Lucic, V. and Chandra, S.S. 2017. Synucleins Have Multiple Effects on Presynaptic Architecture. *Cell Reports*. **18**(1), pp.161–173.
- Vargas, K.J., Makani, S., Davis, T., Westphal, C.H., Castillo, P.E. and Chandra, S.S. 2014. Synucleins regulate the kinetics of synaptic vesicle endocytosis. *Journal of Neuroscience*. **34**(28), pp.9364–9376.
- Virmani, T., Moskowitz, C.B., Vonsattel, J.P. and Fahn, S. 2015. Clinicopathological characteristics of freezing of gait in autopsy-confirmed Parkinson's disease. *Movement Disorders*. **30**(14), pp.1874–1884.
- Vo, T., Carulli, D., Ehlert, E.M.E., Kwok, J.C.F., Dick, G., Mecollari, V., Moloney, E.B., Neufeld, G., de Winter, F., Fawcett, J.W. and Verhaagen, J. 2013. The chemorepulsive axon guidance protein semaphorin3A is a constituent of perineuronal nets in the adult rodent brain. *Molecular and Cellular Neuroscience*. **56**, pp.186–200.
- Volpicelli-Daley, L.A., Luk, K.C. and Lee, V.M.Y. 2014. Addition of exogenous  $\alpha$ -synuclein preformed fibrils to primary neuronal cultures to seed recruitment

of endogenous  $\alpha$ -synuclein to Lewy body and Lewy neurite-like aggregates. *Nature Protocols*. **9**(9), pp.2135–2146.

- Volpicelli-Daley, L.A., Luk, K.C., Patel, T.P., Tanik, S.A., Riddle, D.M., Stieber, A., Meaney, D.F., Trojanowski, J.Q. and Lee, V.M.Y. 2011. Exogenous Alpha-Synuclein Fibrils Induce Lewy Body Pathology Leading to Synaptic Dysfunction and Neuron Death. *Neuron*. **72**(1), pp.57–71.
- Volpicelli-Daley, L.A., Abdelmotilib, H., Liu, Z., Stoyka, L., Daher, J.P.L., Milnerwood, A.J., Unni, V.K., Hirst, W.D., Yue, Z., Zhao, H.T., Fraser, K.B., Kennedy, R.E. and West, A.B. 2016. G2019S-LRRK2 Expression Augments Alpha-Synuclein Sequestration into Inclusions in Neurons. *Journal of Neuroscience*. **36**(28), pp.7415–7427.
- Wakabayashi, K., Matsumoto, K., Takayama, K., Yoshimoto, M. and Takahashi, H. 1997. NACP, a presynaptic protein, immunoreactivity in Lewy bodies in Parkinson's disease. *Neuroscience Letters*. **239**(1), pp.45–48.
- Wakabayashi, K., Tanji, K., Mori, F. and Takahashi, H. 2007. The Lewy body in Parkinson's disease: Molecules implicated in the formation and degradation of  $\alpha$ -synuclein aggregates. *Neuropathology*. **27**(5), pp.494–506.
- Wakisaka, Y., Furuta, A., Tanizaki, Y., Kiyohara, Y., Iida, M. and Iwaki, T. 2003. Age-associated prevalence and risk factors of Lewy body pathology in a general population: The Hisayama study. *Acta Neuropathologica*. **106**(4), pp.374–382.
- Walker, L., Stefanis, L. and Attems, J. 2019. Clinical and neuropathological differences between Parkinson's disease, Parkinson's disease dementia and dementia with Lewy bodies – current issues and future directions. *Journal of Neurochemistry*. **150**(5), pp.467–474.
- Wang, H., Katagiri, Y., Mccann, T.E., Unsworth, E., Yu, Z., Tan, F., Santiago, L., Mills, E.M., Wang, Y., Aviva, J. and Geller, H.M. 2008. Chondroitin-4-sulfation negatively regulates axonal guidance and growth. *Journal of cell science*. **121**(Pt 18), pp.3083–3091.
- Wang, L., Das, U., Scott, D.A., Tang, Y., McLean, P.J. and Roy, S. 2014.  $\alpha$ -Synuclein multimers cluster synaptic vesicles and attenuate recycling. *Current Biology*. **24**(19), pp.2319–2326.
- Watanabe, H., Cheung, S.C., Itano, N., Kimata, K. and Yamada, Y. 1997. Identification of hyaluronan-binding domains of aggrecan. *Journal of*

- Biological Chemistry*. **272**(44), pp.28057–28065.
- Weber, P., Bartsch, U., Rasband, M.N., Czaniera, R., Lang, Y., Bluethmann, H., Margolis, R.U., Levinson, S.R., Shrager, P., Montag, D. and Schachner, M. 1999. Mice deficient for tenascin-R display alterations of the extracellular matrix and decreased axonal conduction velocities in the CNS. *The Journal of neuroscience : the official journal of the Society for Neuroscience*. **19**(11), pp.4245–4262.
- Wegner, F., Ha, W., Bringmann, A., Grosche, J., Wohlfarth, K., Zuschratter, W. and Brückner, G. 2003. Diffuse perineuronal nets and modified pyramidal cells immunoreactive for glutamate and the GABA A receptor  $\alpha 1$  subunit form a unique entity in rat cerebral cortex. *Experimental Neurology*. **184**, pp.705–714.
- Weinreb, P.H., Zhen, W., Poon, A.W., Conway, K.A. and Lansbury, P.T. 1996. NACP, a protein implicated in Alzheimer's disease and learning, is natively unfolded. *Biochemistry*. **35**(43), pp.13709–13715.
- WHO 2011. Global Health and Aging. *NIH Publication*. **1**(4), pp.273–277.
- Wilhelm, B.G., Mandad, S., Truckenbrodt, S., Kröhnert, K., Schäfer, C., Rammner, B., Koo, S.J., Claßen, G. a, Krauss, M., Haucke, V., Urlaub, H. and Rizzoli, S.O. 2014. Composition of isolated synaptic boutons reveals the amounts of vesicle trafficking proteins. *Science*. **344**(6187), pp.1023–1028.
- de Winter, F., Kwok, J.C.F., Fawcett, J.W., Vo, T., Carulli, D. and Verhaagen, J. 2016. The Chemorepulsive Protein Semaphorin 3A and Perineuronal Net-Mediated Plasticity. *Neural Plasticity*. **2016**.
- Wood, S.J., Wypych, J., Steavenson, S., Louis, J.C., Citron, M. and Biere, A.L. 1999. Alpha-synuclein fibrillogenesis is nucleation-dependent. Implications for the pathogenesis of Parkinson's disease. *The Journal of biological chemistry*. **274**(28), pp.19509–12.
- Xu, J.-C., Xiao, M.-F., Jakovcevski, I., Sivukhina, E., Hargus, G., Cui, Y.-F., Irintchev, A., Schachner, M. and Bernreuther, C. 2014. The extracellular matrix glycoprotein tenascin-R regulates neurogenesis during development and in the adult dentate gyrus of mice. *Journal of Cell Science*. **127**(3), pp.641–652.
- Xu, J., Wu, X.S., Sheng, J., Zhang, Z., Yue, H.Y., Sun, L., Sgobio, C., Lin, X.,

- Peng, S., Jin, Y., Gan, L., Cai, H. and Wu, L.G. 2016.  $\alpha$ -Synuclein mutation inhibits endocytosis at mammalian central nerve terminals. *Journal of Neuroscience*. **36**(16), pp.4408–4414.
- Yamada, J., Ohgomori, T. and Jinno, S. 2017. Alterations in expression of Cat-315 epitope of perineuronal nets during normal ageing, and its modulation by an open-channel NMDA receptor blocker, memantine. *Journal of Comparative Neurology*. **525**(9), p.spc1.
- Yamada, J. and Jinno, S. 2017. Molecular heterogeneity of aggrecan-based perineuronal nets around five subclasses of parvalbumin-expressing neurons in the mouse hippocampus. *Journal of Comparative Neurology*. **525**(5), pp.1234–1249.
- Yamada, T., McGeer, P.L., Baimbridge, K. and McGeer, E.G. 1990. Relative sparing in Parkinson's disease of substantia nigra dopamine neurons containing calbindin-D 28K. *Brain research*. **526**, pp.303–307.
- Yamaguchi, Y. 2000. Lecticans: organizers of the brain extracellular matrix. *Cellular and Molecular Life Sciences*. **57**(2), pp.276–289.
- Yang, N., Zhang, L. and Shen, L. 1999. The synuclein family. *Progress in Biochemistry and Biophysics*. **26**(6), p.524.
- Yang, S., Hilton, S., Alves, J.N., Saksida, L.M., Bussey, T.J., Matthews, R.T., Kitagawa, H., Spillantini, M.G., Kwok, J.C.F. and Fawcett, J.W. 2017. Antibody recognizing 4-sulfated chondroitin sulfate proteoglycans restores memory in tauopathy-induced neurodegeneration. *Neurobiology of Aging*. **59**, pp.197–209.
- Yasuhara, O., Akiyama, H., McGeer, E.G. and McGeer, P.L. 1994. Immunohistochemical localization of hyaluronic acid in rat and human brain. *Brain Research*. **635**(1–2), pp.269–282.
- Ye, Q. and Miao, Q. long 2013. Experience-dependent development of perineuronal nets and chondroitin sulfate proteoglycan receptors in mouse visual cortex. *Matrix Biology*. **32**(6), pp.352–363.
- Yoshimoto, M., Iwai, A., Kang, D., Otero, D.A.C., Xia, Y. and Saitoh, T. 1995. NACP, the precursor protein of the non-amyloid  $\beta$ /A4 protein (A $\beta$ ) component of Alzheimer disease amyloid, binds A $\beta$  and stimulates A $\beta$  aggregation. *Proceedings of the National Academy of Sciences of the United States of America*. **92**(20), pp.9141–9145.

- Zaccai, J., Brayne, C., McKeith, I., Matthews, F. and Ince, P.G. 2008. Patterns and stages of  $\alpha$ -synucleinopathy: Relevance in a population-based cohort. *Neurology*. **70**(13), pp.1042–1048.
- Zahed, H., Zuzuarregui, J.R.P., Gilron, R., Denison, T., Starr, P.A. and Little, S. 2021. The Neurophysiology of Sleep in Parkinson's Disease. *Movement Disorders*, pp.1–18.
- Zamecnik, J., Homola, A., Cicanic, M., Kuncova, K., Marusic, P., Krsek, P., Sykova, E. and Vargova, L. 2012. The extracellular matrix and diffusion barriers in focal cortical dysplasias. *European Journal of Neuroscience*. **36**(1), pp.2017–2024.
- Zarbiv, Y., Simhi-Haham, D., Israeli, E., Elhadi, S.A., Grigoletto, J. and Sharon, R. 2014. Lysine residues at the first and second KTKEGV repeats mediate  $\alpha$ -Synuclein binding to membrane phospholipids. *Neurobiology of Disease*. **70**, pp.90–98.
- Zhang, W., Wnag, T., Pei, Z., Miller, D.S., Wu, X., Block, M.L., Wilson, B., Zhang, W., Zhou, Y., Hong, J.-S. and Zhang, J. 2005. Aggregated Alpha-synuclein activates microglia: a process leading to disease progression in Parkinson's disease. *FASEB*. **19**(6), pp.533–542.
- Zhou, F.M., Wilson, C.J. and Dani, J.A. 2002. Cholinergic interneuron characteristics and nicotinic properties in the striatum. *Journal of Neurobiology*. **53**(4), pp.590–605.
- Zhou, X.-H., Brakebusch, C., Matthies, H., Oohashi, T., Hirsch, E., Moser, M., Krug, M., Seidenbecher, C.I., Boeckers, T.M., Rauch, U., Buettner, R., Gundelfinger, E.D., Fassler, R. and Fässler, R. 2001. Neurocan Is Dispensable for Brain Development. *Molecular and Cellular Biology*. **21**(17), pp.5970–5978.
- Zimmer, G., Schanuel, S.M., Bürger, S., Weth, F., Steinecke, A., Bolz, J. and Lent, R. 2010. Chondroitin sulfate acts in concert with semaphorin 3A to guide tangential migration of cortical interneurons in the ventral telencephalon. *Cerebral Cortex*. **20**(10), pp.2411–2422.